Sedimentological and Stratigraphic evolution of a muddy submarine slope succession, Karoo basin, South Africa

UNIVERSITY OF
LIVERPOOL

Thesis submitted in accordance with the
requirements of the University of Liverpool for the
degree of Doctor in Philosophy

by

Jorge de Jesus Picanço de Figueiredo

June 2009

To Leila, Rodrigo, Lucas

Manoel (in memoriam) and Jolene

Abstract

Middle and upper submarine slope successions are usually muddy, and therefore poorly exposed and rarely studied at outcrop. However, this setting is critical to understanding the timing and processes of sediment transfer from continents to the deep ocean. Here, the physical stratigraphy of an exhumed 470 m-thick, late Permian, mudstone-dominated middle to upper submarine slope succession was analysed over a 400 km^2 study area in the Laingsburg depocentre, South Africa. Five sand-prone units (Units D/E, E, F, G, and H), separated by extensive claystone units, were mapped and characterized. From Unit D/E up to Unit F, the sand prone units show an overall pattern of thickening upward, expanding southward across the slope, and stepping basinward. This stacking pattern is reversed from Unit F to the base of Unit H, above which basinward stepping is again observed. Different architectural styles of sand-prone deposits occupy predictable stratigraphic positions within the basinward stepping section, starting with distributive intraslope lobes through channel-levee complexes to entrenched slope valleys. The percentage of sandstone preserved in each unit decreases with increasing confinement through the basinward stepping section, which is related to increasing amounts of sediment bypass. The landward stepping stratigraphy is dominated by claystone units with thin distal fringes of sand-poor distributive systems. The upper basinward stepping succession (Unit H) is characterized by a distributive system linked to a shelf edge delta. Across strike distribution of sand-prone units was controlled by subtle variations in seabed relief driven by differential compaction. The resulting spatially irregular distribution of sandstones regionally highlights the need for 3-D analysis of ancient slope successions rather than relying on 2-D profiles.

Based on a synthesis of claystone thickness data, stacking patterns of the sand-prone deposits and depths of incision surfaces, a sequence hierarchy is proposed. Regionally mappable hemipelagic claystone deposits separating the sand-prone units represent shut down of sand supply to the whole slope and are interpreted as transgressive and highstand systems tract deposits. The sand-prone units are interpreted as lowstand systems tract deposits and exhibit a wide range of depositional geometries. Using this approach, eleven depositional sequences are identified, nine of which are arranged into three composite sequences (Units E, F, and G). The three composite sequences plus one individual sequence comprise a composite sequence set. The highly organised physical stratigraphic stacking suggests that glacioeustasy, during the late Permian icehouse period, was the main driving process for the analysed succession.

A smaller scale of stratigraphic organisation is present within each depositional sequence. This is defined through a hierarchy of depositional elements from individual channel-fills, through channel complexes and channel complex sets to slope valley-fills, based on dimensions, stacking patterns, and lithofacies. Mapping of seismic reflection data from a comparable slope setting, offshore Brazil, indicates that channel and channel complex-scale elements are rarely resolvable seismically, meaning that these settings are more heterogeneous than is apparent from seismic data alone. At outcrop and in seismic data the exact stratigraphic relationship between channel-fills and adjacent levees is not resolved.

The predictive models developed here can aid the identification and production of hydrocarbon reservoirs in muddy slope settings.

Acknowledgments

This project was only possible because it was built upon a solid tripod - the support I received from my employer, my supervisors, and my family. I acknowledge Petrobras (my employer) for the financial support for this project through the commitment of the Director Mr. Guilherme Estrella, and the former and current Executive Managers, Mr. Paulo M. M. Mendonça, Dr. Paulo T. M. Guimarães and Dr. Mario Carminatti. I thank my managers Mr. Paulus H. vd Ven and Mr. Otaviano Pessoa Neto for the support and encouragement I received through this project. I also thank Lucila Reis, the manager of the E&P-Exp Human Resources, and her team for their assistance with the bureaucratic issues.

The role played by my supervisors Dr. David M. Hodgson and Prof. Stephen S. Flint throughout this PhD project was crucial for its results. I am very grateful to have been advised by such experts and, more importantly, within a friendly environment. The guidance, encouragement, enthusiasm and patience (especially with my English) I received from them gave me the self-confidence to go ahead. Dave and Steve offered me not only technical support for the development of the project, but also the friendly relationship they have with their students was very helpful for me to make me feel emotionally well with my work and enjoy doing it. They also offered non-academic support when I needed it. Once more, thanks Dave and Steve for these 3.5 years of extra-work you have had with me.

The third leg of the support tripod for this project came from my family. They left behind in Brazil a comfortable life to accompany me in this endeavour and to give me the necessary material and emotional support. Leila, my wife, once more postponed her career plans to join me in this journey. My sons, Rodrigo and Lucas, left their friends and their well known environment to immerse themselves in a completely unknown world. My family did this to support me and I am indebted to them for this. All in all, despite the ups and downs, I am sure that after these 3.5 years we are taking many good things from this experience in the United Kingdom.

In the Stratigraphic Group of the DEOS of the University of Liverpool (UoL) I had the opportunity to meet people whose friendship I really enjoyed.

We shared very good moments working or having coffee/tea/beer together and also I received help from many of them. Research assistants Chris Haigh, Laura McAllister, Rebecca Harrison, Emily Parrot, Sophia Stone and Ajay Mistry many times stopped their activities to help me when I needed. It was very fruitful to have technical chats with Dr. Rufus Brunt and Dr. Claudio di Celma. I also have to say thanks to Ms Kay Lancaster for help with some thesis figures. A special thanks for my field assistants John Kavanagh, Laura McAllister and Emily Parrot. More than an assistant in two field seasons, John was a friend I made in the Department and his experience as a field geologist was important for me to re-learn many things I had forgotten about field work after 20 years working as an oil company geologist. I thank Maureen Dodd (Mo) for her friendship and for trying to make a familiar environment and my office mates Rowena Moore, Carlos Oliveira and Willem vd Merwe for the friendly environment we shared. I thank Willem for facilitating access to the field area, but also I thank the farmers for access.

I'm in debit with many people in Petrobras especially my colleagues from the Equatorial Margin Exploration team José Ferrer, Ivanise Wolff, Emilson Soares, Leila Pezzin, Rosalia Amaral and Sonia Ludovice. They provided everything I needed from Petrobras to add in this project. Especially, I have to acknowledge the geophysicist José Ferrer for help with seismic interpretation and draftsperson Leila Pezzin for finalising diagrams.

A special thanks to my referees during the application process to the UoL Prof. Werner Truckenbrodt and Dr. Marco Moraes. In fact, Marco was the person who introduced me to my supervisor Stephen Flint.

Finally, I cannot forget to thank my two Brazilian friends in Liverpool, Carlos and Gilvan and their families for their friendship. Carlos was already in Liverpool when I arrived. He opened the Liverpool doors for me and my family. His support, especially at the beginning, during those dark, cold and wet days was very important to make us feel comfortable. Gilvan, who I had not met before he arrived in Liverpool, is now a good friend. Our families enjoyed good time together.

Table of Contents

Chapter 1 - Introduction

1.1 - Aims of the Thesis

1.1.1 - The geological problem: Mud-rich submarine slopes and their sand-prone depositional systems

Models for the sedimentary processes and depositional products associated with mud-dominated submarine slope settings have evolved significantly over the last decade, mainly due to the advent of high resolution 3-D seismic datasets. These datasets have facilitated an improved understanding of the patterns of incision, deposition and remobilisation of sediment and the interaction of long-lived sediment transport conduits and their relationships with active growth and decay of seabed topography (e.g. Prather et al., 1998; Beaubouef & Friedmann, 2000; Mayall & Stewart, 2000; Kolla et al., 2001; Fonesu, 2003; Abreu et al., 2003; Adeogba, 2005; Mayall et al., 2006; Deptuck et al., 2007; Kolla et al., 2007). However, this high quality seismic data has a resolution limit, beyond which the exact nature of the sedimentary system is unknown. Outcrop studies have been carried out to help understand the distribution of erosional and depositional processes, and the architecture of preserved deposits at a sub-seismic scale (e.g. Cronin et al., 2000; Campion et al., 2000; Beaubouef, 2004; Wild et al., 2005; Shultz et al., 2005; Pickering & Corregidor, 2005; Moraes et al., 2006; Anderson et al., 2006; Kane et al., 2007). However, due to exposure limitations most outcrop observations are biased toward the sand-prone and less weathered or covered components of the stratigraphy. There remains a paucity of detailed outcrop analogues for all components of mud-rich systems.

Early stratigraphic models considered middle and upper submarine slope settings as simply zones of bypass, with coarse-grained sediment transported through the slope, to the deep basin floor (Walker, 1978; Bouma, 1979; Pickering et al. 1989; Reading & Richards, 1994; Galloway, 1998; Bouma 2000) (Fig 1.1).

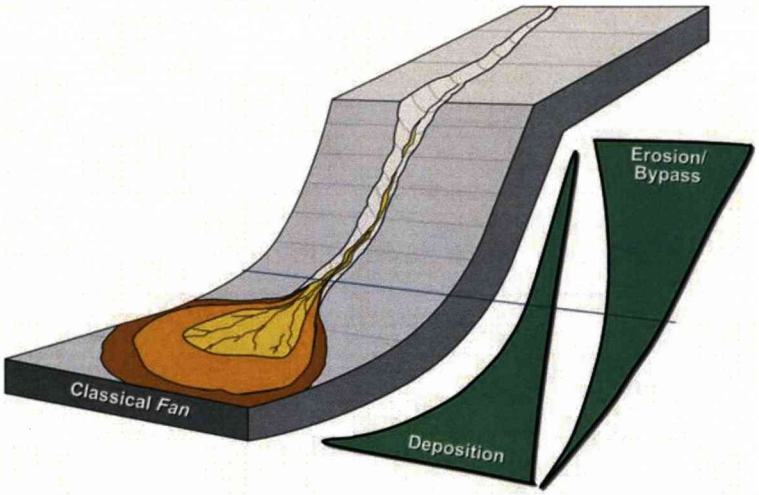

Figure 1.1 – Idealised cartoon for the classical interpretation for deep-water coarse-grained depositional systems. In this model the middle and upper submarine slope settings are zones of bypass for coarse-grained sediments to the deep basin and toe of slope (from Sprague et al., 2003).

Recently, several authors have demonstrated that the submarine slope is a complicated and dynamic setting in which usable accommodation varies in time and space, controlling the balance between deposition (storage) and bypass (routeing) of sediment (Pirmez *et al.*, 2000; Prather 2000; Prather, 2003; Sprague, 2003; Flint & Hodgson, 2005). These workers showed that a range of coarse-grained deposits with complicated spatial and temporal variations in facies, architecture and pinchout geometries can occur in mud-rich middle and upper submarine slope settings (Fig 1.2).

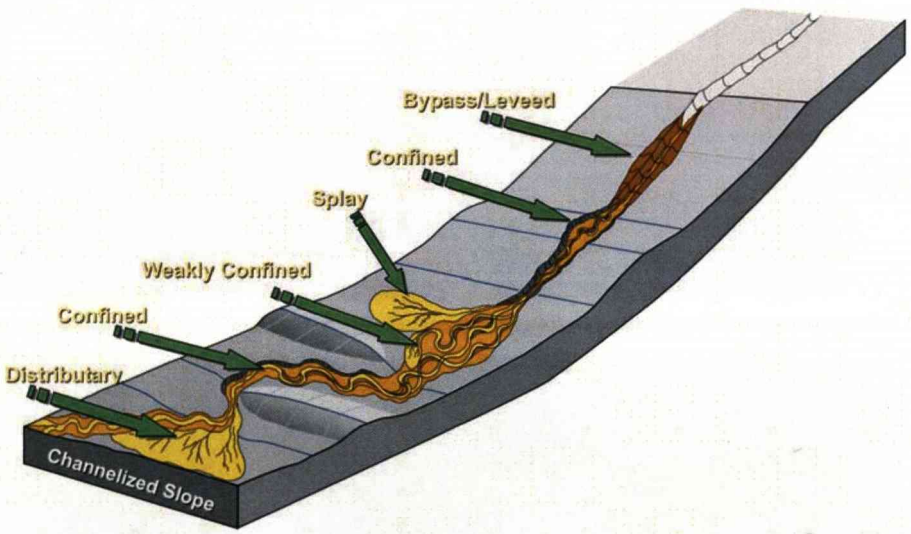

Figure 1.2 - Idealised cartoon depicting a more complex distribution of coarse-grained depositional systems on the submarine slope including the middle and upper slope settings (from Sprague et al., 2003).

1.1.2 - The scientific focus of this work

This thesis addresses the architecture and evolution of mud-rich middle and upper submarine slope settings and their sand-prone depositional systems. Models for the origin, sequence stratigraphic context and range of detailed stratigraphic architecture of coarse-grained bodies to be expected within those settings are presented and discussed.

The scientific focus of this work is based upon the following questions and testable hypotheses:

1- What range of sedimentary processes act in middle and upper submarine slope settings (beyond the shelf edge)?
Hypothesis 1: *Periods of deposition by sand-rich gravity currents alternate with dominantly hemipelagic and pelagic deposition. The sedimentary process involved in sand deposition is strongly controlled by the degree of erosional and/or depositional confinement of the flow.*

2- What does fining-upward, muddy stratigraphy represent in submarine slope settings?
Hypothesis 2: *Fining-upward stratigraphy in a slope setting can represent increased confinement and increased coarse-grained sediment bypass on the scale of observation. It may also represent long-term backstepping – how can the two interpretations be resolved?*

3- The upper and middle slope are settings where conduits for coarse-grained sediments bypass are regularly re-excavated and entrenched, however recent high resolution 3-D seismic data have suggested that a wider range of coarse grained deposits might occur in these settings. Can such deposits be also identified from outcrop dataset?
Hypothesis: Analyses of a well exposed exhumed ancient middle to upper submarine slope can resolve the range and styles of deposition.

4- What are the roles of subtle sea floor topography and the temporal evolution of the submarine slope (progradation or retrogradation) on the

control of the development of different types of sand-prone deposits on the middle and upper slope? How can subtle sea floor topography be reconstructed from outcrops in the absence of measurable onlap?
Hypothesis: The integration of lithofacies association distribution, architectural patterns and palaeoflow indicators from outcrop data should provide information on both spatial (down slope and across slope) and temporal (stratigraphic) trends that are a function of sea floor topography convolved with changes in usable accommodation and modulations in sediment supply.

5- What are the dominant depositional processes of the gravity driven flows?
Hypothesis: Where sand deposition occurs on the middle and upper slope the deposits are dominated by the Bouma sequence, representing deposition from waning single turbidity currents.

To address these questions and test the related hypotheses, an extensive field work programme was carried out on an exceptionally well exposed succession of deposits thought to represent middle to upper slope deposits, in the Upper Permian Laingsburg Formation, Ecca Group, SW Karoo basin, South Africa (Fig 1.3). In addition, a seismic dataset with geologically analogous parameters from an offshore Brazil sedimentary basin was analyzed to compare and contrast the 3D geometric aspects of the interpreted sandy bodies with those observed in the field.

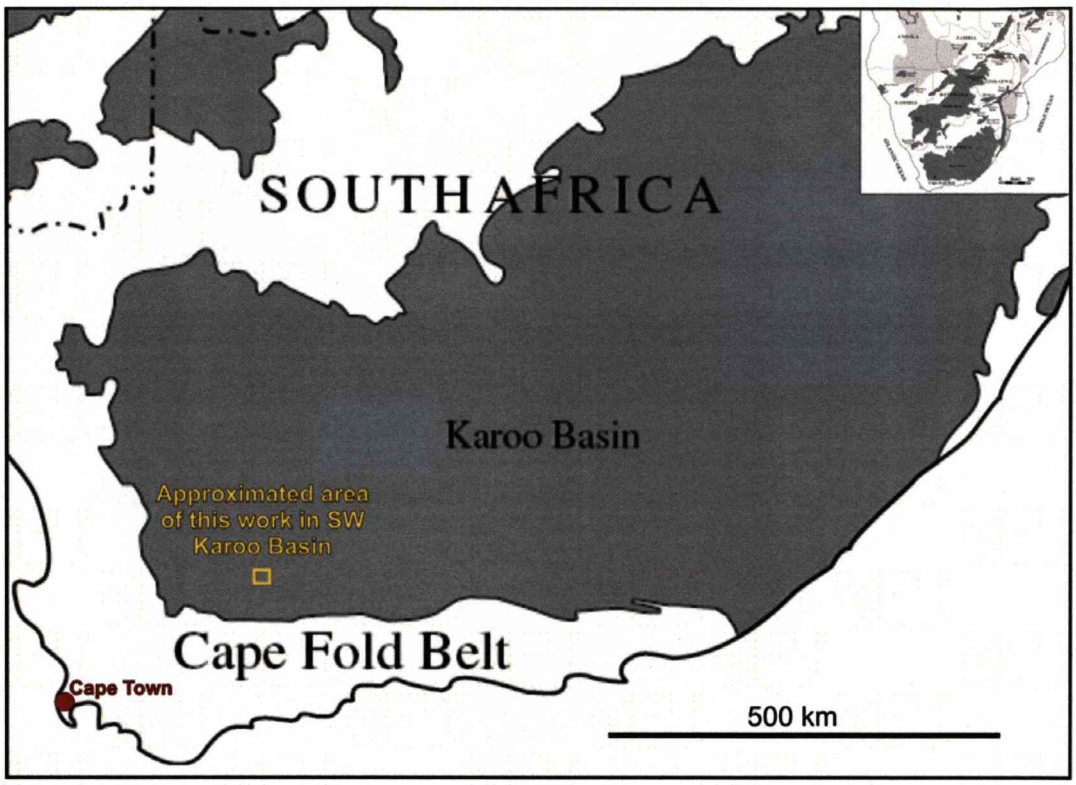

Figure 1.3 – Map of geographic location of the Karoo Basin. Inset shows Karoo Basin among other major sedimentary basins in southern Africa (modified from Catuneanu et al., 2005).

1.2 - Thesis Layout

This thesis is composed of seven chapters and four appendices. Chapter 1 presents the geological problem addressed in this research and introduces the general background to the topic and the geological and stratigraphic setting of the study area. Chapter 2 presents the description and interpretation of lithofacies and lithofacies associations identified in this work. Chapter 3 is a paper that was submitted to and accepted by the Journal of Sedimentary Research (current stage: in revision). In this paper the dynamic of development of the sand-prone depositional systems and stratigraphic evolution of the 450 m thick middle/upper submarine slope study succession is presented.

Chapter 4 breaks down a single depositional sequence into its erosional and depositional constituents and analyses their development and stratigraphic relationships. Chapter 5 presents at higher spatial resolution the development of a specific slope channel complex and its constituent

individual channels. Chapter 6 compares a seismic analogue from offshore Brazil with the examples interpreted from field work in terms of scale of the identified erosional/depositional elements, stratigraphic settings and evolution. Chapter 7 synthesises the conclusions of this work, considering their scientific relevance and practical applicability. An outline of possible further work to refine the dataset and interpretations is presented.

The four appendices present: (1) the palaeocurrent dataset; (2) key for the sedimentary logs; (3) a list of the UTM coordinates (Global Positioning System) of the bases and tops of all sections logged (also in the CD-ROM); (4) sedimentary logs (in the CD-ROM).

1.3 - Formation and evolution of mud-rich submarine slopes

1.3.1 - What is a submarine slope?

Submarine slopes were originally defined by Wagner (1900) in Bouma (1979) as *that area on the margin between the shelf break and the abyssal floor*. Later, Heezen *et al.* (1959) *in* Pickering *et al.* (1989) restricted the term to *that relatively steep (3-6°) portion of the sea floor which lies at the seaward border of the continental shelf*. Bouma (1979) defined submarine slopes as *the central part of the margin which is generally located above the transition between continental and oceanic crust*[1]. All these definitions were based on the morphology of modern continental submarine slopes and were tentatively applied to ancient systems. The upper boundary of submarine slopes, located beyond the shelf break, is the easiest geomorphic feature to recognize in modern systems. The lower boundary, in contrast, is often diffuse and not so easy to locate precisely. The angle of the submarine slope is also very variable. Shepard (1973) *in* Bouma (1979) suggested an average value of 4.17°, but this can range from gentle angles as low as 0.5° on the Amazon Fan (Damuth & Kumar, 1975) to angles as high as 45° as observed on coral islands (Fairbridge, 1966 *in* Bouma, 1979). Nittrouer *et al.* 2007 presented two cartoons depicting the configuration of active and passive

[1] This definition considers marine basins with oceanic crust. In this case should be added the term "Continental" to the submarine slope.

continental margins. In both cases, submarine continental slopes are shown as a transition from shallow to deep marine environments (Fig. 1.4).

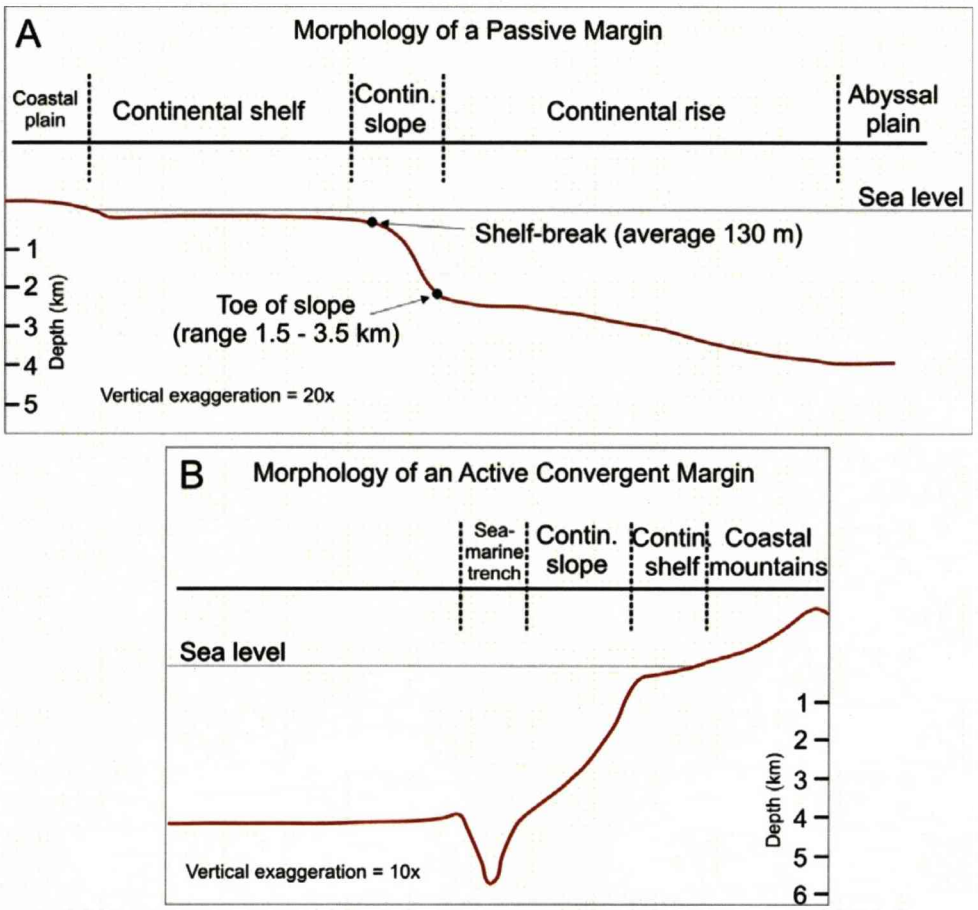

Figure 1.4 – Morphology of passive (A) and active (B) continental margins (from Brink et al., 1992 *in* Nittrouer et al., 2007) showing the continental submarine slope in both cases.

1.3.2 - Classification of submarine slopes

Initial classifications for submarine slopes were primarily based on the morphology and the tectonic setting of the present-day continental submarine margins. Dietz (1964) recognized 3 main kinds of submarine slopes whereas Emery (1977) distinguished 6 different types. Many studies on turbidite systems in deep-water, both in modern and in ancient systems, had been undertaken from the 1960s and these included models for aspects of submarine slope development (Normark, 1970; Mutti & Ricci Lucchi, 1972; Walker, 1978; Reading & Richards, 1994; Galloway, 1998). From the 1990s, however, due to the evolution of 3-D seismic acquisition/ processing/ interpretation methods, and the advent of high resolution 3-D seismic data,

the internal structure of the submarine slopes could be assessed more clearly.

The most comprehensive attempt to classify turbidite systems in deep-water environments was presented by Reading & Richards (1994). Their classification was based on sediment grain size (mud-rich, mud/sand-rich, sand-rich, and gravel-rich) and configuration of the feeder systems (point source, line source, and multipoint source). Reading and Richards (1994) proposed two matrices with 12 classes of deep-water turbidite systems for both modern and ancient systems, later summarized by Stow & Mayall (2000) in a matrix with 9 classes (Fig. 1.5). In these studies there is also a broad understanding of how submarine slopes are constructed. Nevertheless, this model still considers the middle and upper areas of mud-rich submarine slopes only as a zone of bypass for turbidity currents carrying coarse-grained sediments into the deeper basin. Hence, sandy deposition on the middle and upper mud-rich submarine slopes is not considered in the Reading & Richards (1994) model.

High resolution 3-D seismic data from marine basins do not corroborate in many instances the Reading & Richards (1994) model. Instead, these data show that the acting sedimentary processes and the resultant facies distributions are much more dynamic; e. g. on the same mud-prone slope a genetically related system can show features of both sand-rich systems (the initial linear channel pattern) and mud-rich systems (highly sinuous channel pattern) (Mayall & Stewart, 2000).

Prather (2000) and Prather (2003) developed the concept of slope-readjustment (Dailly, 1983; Ross *et al.*, 1994) based on high-resolution 3-D seismic surveys from the Gulf of Mexico, and proposed a new model for slope evolution that highlighted the importance of intra-slope topography. These authors identified 3 categories of submarine slopes, which interact with each other as end members of a tripartite system (Fig. 1.6), and control the distribution, facies and architecture of coarse-grained deposits.

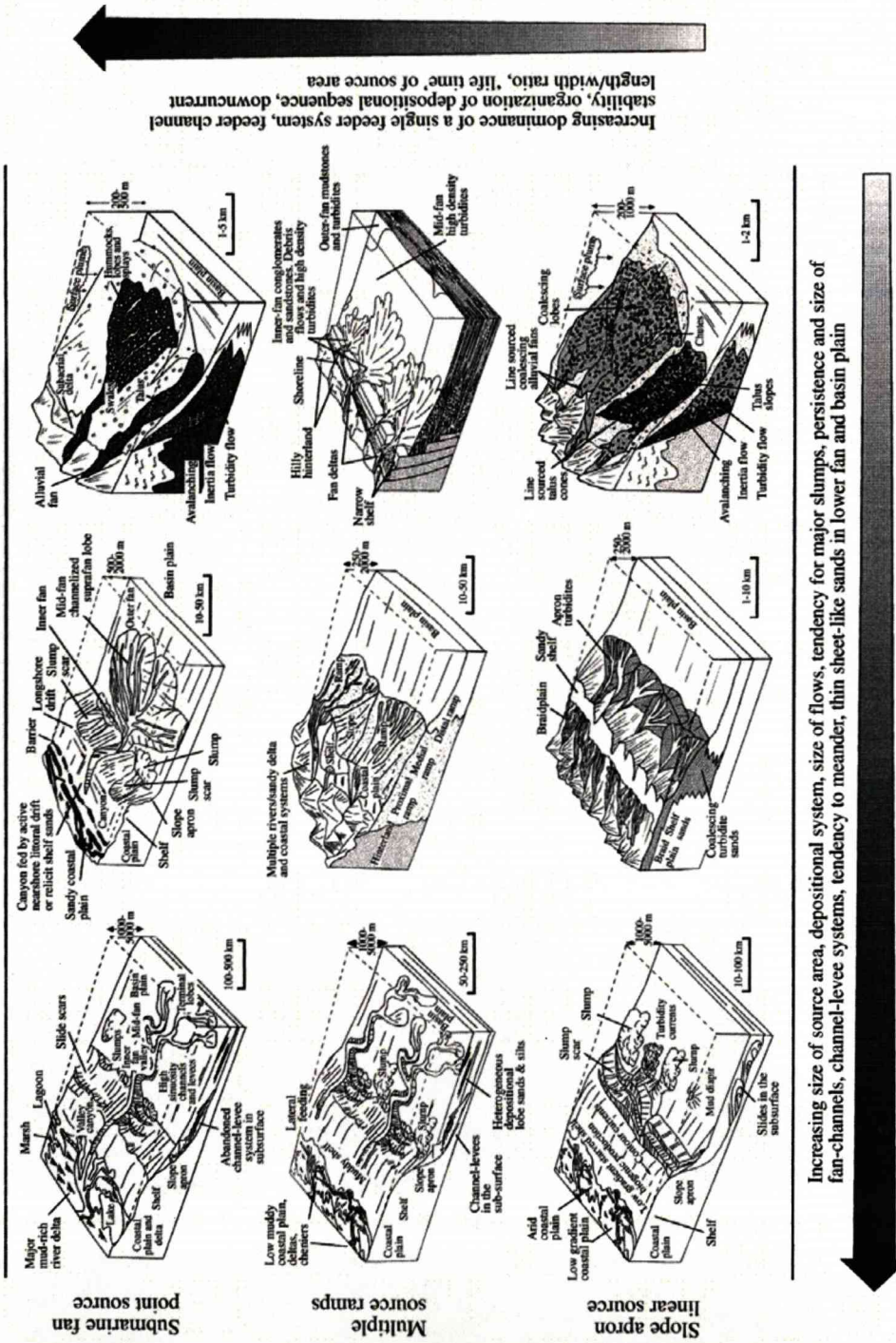

Figure 1.5 - Summary environmental models for submarine fans, ramps and slope-apron systems (from Reading & Richard, 1994 and modified by Stow & Mayall, 2000)

Graded slopes are characterized by large amounts of healed-slope accommodation at the toe of submarine slope which receives the bulk of the coarse-grained deposition. Sediment bypass characterizes the upper parts of graded slopes (Fig. 1.7). Due to the absence of ponded accommodation in many middle slope positions, healed-slope accommodation, controlled by slope angle and subtle topography, control the deposition of coarse-grained sediments in these settings. Rates of mud deposition across mid slopes play a major role in controlling slope angles. Low angle slopes occur in association with high rates of sediment flux. High rates of sediment flux result in overpressured shales with low shear strength and low stable slope angles. Faults and submarine slides caused by low, stable slope angles can create local topography which can be a site for local deposition of coarse grained sediments in middle slope positions on graded slopes systems (Prather, 2003).

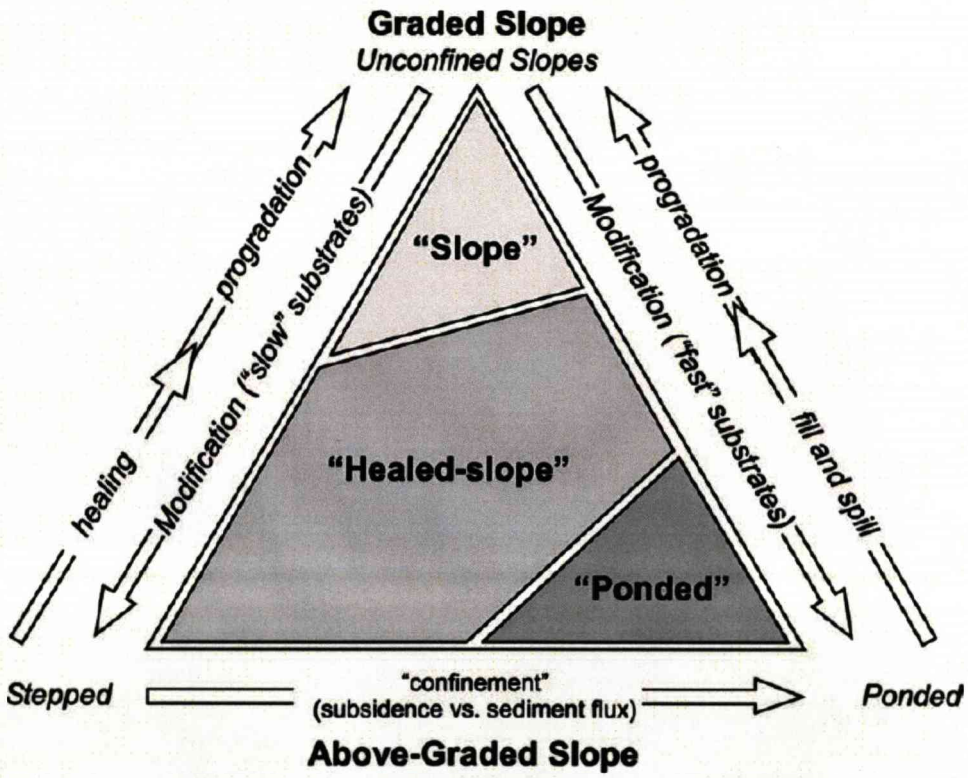

Figure 1.6 – Ternary diagram (from Prather, 2003) showing slope type end-members and key processes controlling grade to above grade slope transitions.

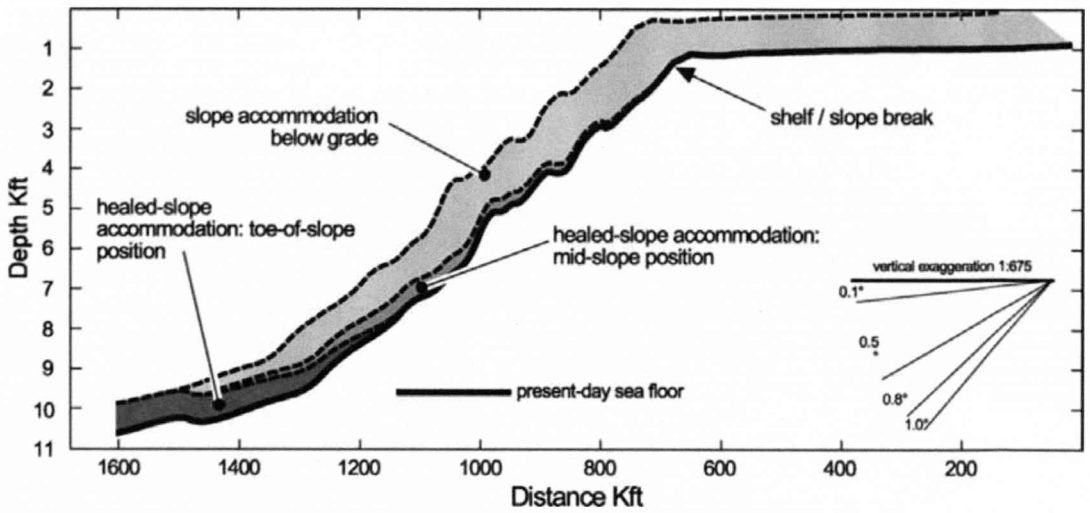

Figure 1.7 - Sea floor profile across the eastern Gulf of Mexico showing the distribution of accommodation on a graded slope profile (from Prather, 2003).

Above-grade slopes were split by Prather (2003) into 2 categories: (1) those with well-developed ponded accommodation and large amounts of mid– to upper-slope healed-slope accommodation; and (2) those with stepped profiles that lack well-developed ponded accommodation (Fig. 1.8).

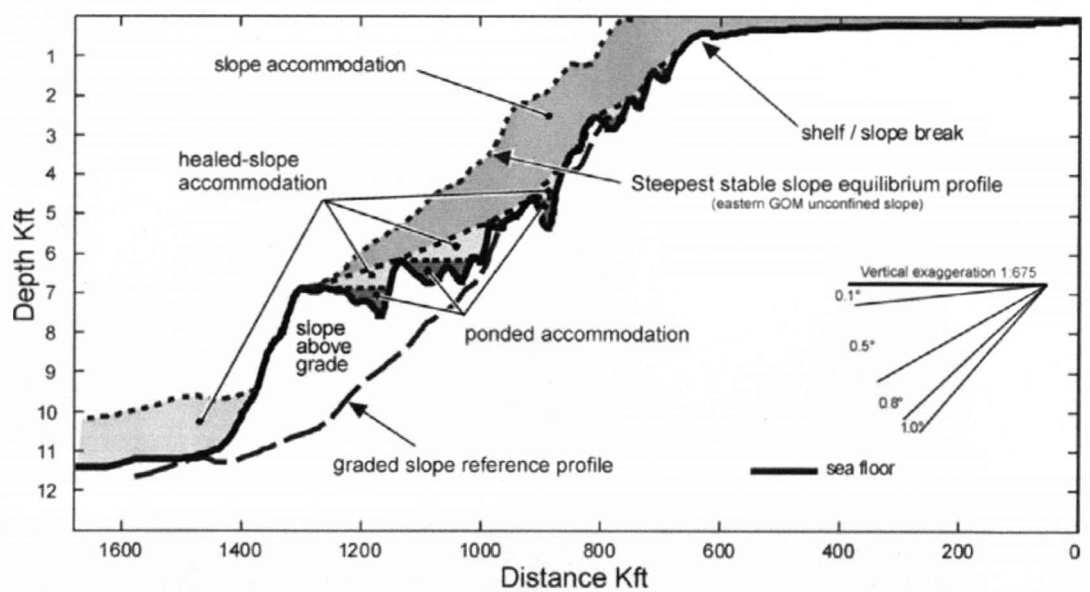

Figure 1.8 – Sea floor profile showing the distribution of accommodation on an end-member above-grade slope profile with ponded basins from the central Gulf of Mexico (from Prather, 2003).

Type 1: These kinds of slopes are developed in areas with mobile substrates caused by salt or shale movement. The development of bathymetrically restricted 'ponds' and 'corridors' on the middle and upper

slope is an ideal situation in which to trap coarse-grained sediment in these settings. The ponds are convenient receptacles for gravity flows carrying coarse-grained sediments (Beaubouef & Friedman, 2000; Prather, 2003). After the pond infills there is still a downstream step to be healed.

Type 2: Normal faults are the main driving mechanism to form above-grade slopes with stepped profiles (Moraes et al., 2000; Prather, 2003). Interconnected topographic depressions caused by normal faults form a complicated pathway for gravity flows to travel and deliver their coarse-grained content to middle and upper slope settings. In gravity gliding cells in submarine slopes the compressional end also develops topography which can divert gravity driven flows and control sand deposition (e.g. chapter 6). Differential compaction might also form steps in middle and upper slopes.

1.3.3 - How submarine slopes evolve

Variations in grain size and feeder system pattern can generate a range of submarine slope types (Reading & Richards, 1994). A focus of this project was to study the architecture and evolution of mud-rich submarine slopes and their depositional systems.

The physiography of the continental margins was addressed by Hedberg (1970), who recognised two different types of continental margins: (1) *Progradational or Graded margins*, where depositional profiles advance or prograde into the basin; and (2) *Erosional or Out-of-grade margins*, where the basin margin is oversteepened and sediments are bypassed to a base-of-slope position. (Ross *et al.*, 1994)

Progradational or Graded margins are a product of the equilibrium between the continental margins physiographic profiles and the depositional and erosional processes operating on the basin. At the scale of a continental margin each environment (shelf, slope, deep basin) is graded (or not) by its own set of erosional and depositional processes (Ross, 1990; Thorne & Swift, 1991). However, the equilibrium operating within the basin is controlled by three major factors that drive the deep-water depositional system, i.e. (1) *Regional basin tectonics*; (2) *Rate, type and source of sediment supply*; and (3) *Sea-level fluctuations* (Richards *et al.*, 1998). Variation in one or more of

these factors can perturb the graded equilibrium profile and force the submarine slope to an *out-of-grade* condition where the middle, and especially, the upper slope plus part of the shelf can be cannibalised and the eroded material deposited on the toe-of-slope and basin floor. In addition, slump scars can represent additional localised accommodation.

The literature on the subject of submarine slope development is far less extensive than that concerning delta construction (Gilbert, 1885; Gilbert 1890; Bates, 1953; Coleman *et al.*, 1983; Kenyon & Turcotte, 1985; Swift & Thorne, 1991; Syvitski *et al.* 1988; Syvitski *et al.*, 1992; Pirmez, 1998; Steel *et al.*, 2000; Steel *et al.*, 2003; Porebski & Steel, 2006); however, in terms of architectural elements, delta slopes and basin progradational slopes share a similar building block: *clinoforms*. Therefore the processes acting to build up the former can also act to construct the latter (Pirmez *et al.*,1998), mainly in those special cases (shelf edge deltas) where the delta clinoform is coincident with the slope clinoform (Steel *et al.*, 2000; Steel *et al.*, 2003; Porebski & Steel, 2006). In submarine slopes, as in delta front slopes, several processes, such as *bulk- transport* or *diffusive processes* (creeps; slides; slumps); *sediment advection;* and *gravity-driven sediment transport,* can operate to construct a *progradational* or erosional profile. These processes were modelled by different authors in different approaches to explain delta development on the continental platform. They will be used here as analogues to help the understanding of basin slope development.

Ross *et al.* (1994) modelled the development of continental submarine slopes taking into consideration the slope-readjustment concepts first addressed by Dailly (1983) and the principles introduced by Kenyon & Turcotte (1985) and Syvitsky *et al.* (1988). In their work Ross *et al.* (1994) presented a model that considered the role of changing physiography in the progradation of the continental submarine slope. In this model, change in physiography was defined as a steepening of the slope, significantly above a stable, equilibrium angle, and was distinguished from minor fluctuations in physiography produced by ongoing mass wasting and erosional processes operating under graded progradation. A significant oversteepening of the slope would lead to a long-term out-of-grade state and, as a result, to trigger long-term slope-grading process, including erosional mass wasting and

depositional processes, which produce submarine canyons and submarine fans aprons. Eventually these slope-readjustment processes would act to return the system to grade.

Physically the resultant architectural pattern of the slope-readjustment model raised by Ross *et al.* (1994) resembles the depositional sequence of Mitchum *et al.* (1977), which is an established paradigm on the development of continental margins, but the driving mechanisms are different (Fig. 1.9).

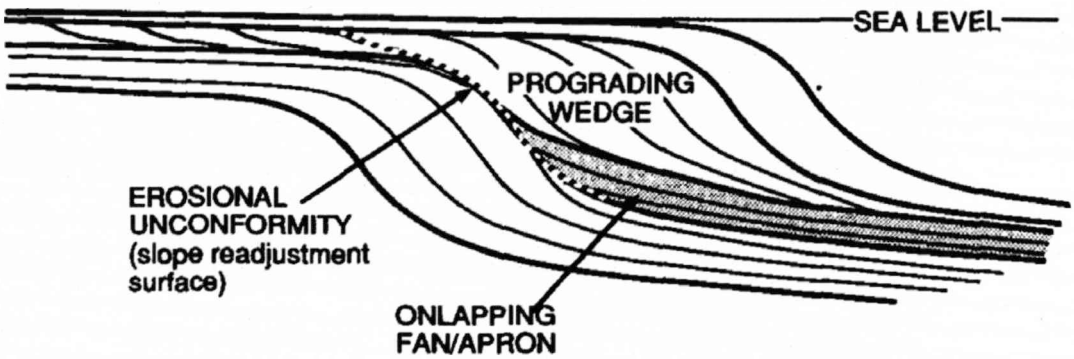

Figure 1.9 – Disconformable basin-fill geometry in slope-to-basin setting (from Ross et al., 1994).

Ross *et al.* (1994) and Pirmez *et al.* (1998) suggested that models for delta slope development can also be applied to basin slope environments. Ideal cases would be those where deltas play important roles as sediment feeders into the basin. Shelf-margin deltas are the most important factor in this scenario, however, inner- or mid-shelf deltas are also significant. Large rivers feeding mid-shelf to shelf edge deltas can deliver, in addition to episodic coarse-grained material, large amounts of fine-grained sediment into the basin as suspended load. In this case, the buoyant plume can bypass the shelf margin and hemipelagic sedimentation occurs on the submarine slope obeying the principles stated by Pirmez *et al.* (1998). This mechanism can force the progradation of the mud-rich submarine slope under graded circumstances.

An empirical approach to the study of continental submarine slopes was presented by Adams & Schlager (2000). In work encompassing 150 seismic transects of modern continental margins around the world they found that over 80% of submarine continental slopes can have their first-order profile fitted into three basic types of equations curves (Linear, Exponential,

and Gaussian) (Fig. 1.10). The linear slope profiles are the least common (12%). It is suggested that they are represented by sediments that rest at the angle of response such that entire system is in a state of "self-organized criticality" (Bak et al., 1988 *in* Adams & Schlager, 2000). Exponential slope profiles (20%) are attributed to the generalized exponential decay of sediment transport through the slope considering deterministic sedimentation under graded conditions on the slope (Adams & Schlager, 2000). The most common slope profile (50%) found was that fitted to the Gaussian curve. The authors suggest that processes acting to develop Gaussian profile continental slopes are the same as the exponential ones; however, in this case, the shelf break would be smoothed by other processes acting on it. No direct correlation was possible linking slope composition with slope profile because siliciclastic (both, sand and mud dominated), carbonate and mixed slopes were found in all categories. However, when contrasting mud and sand dominated slopes, the former have a lower slope angle than the latter.

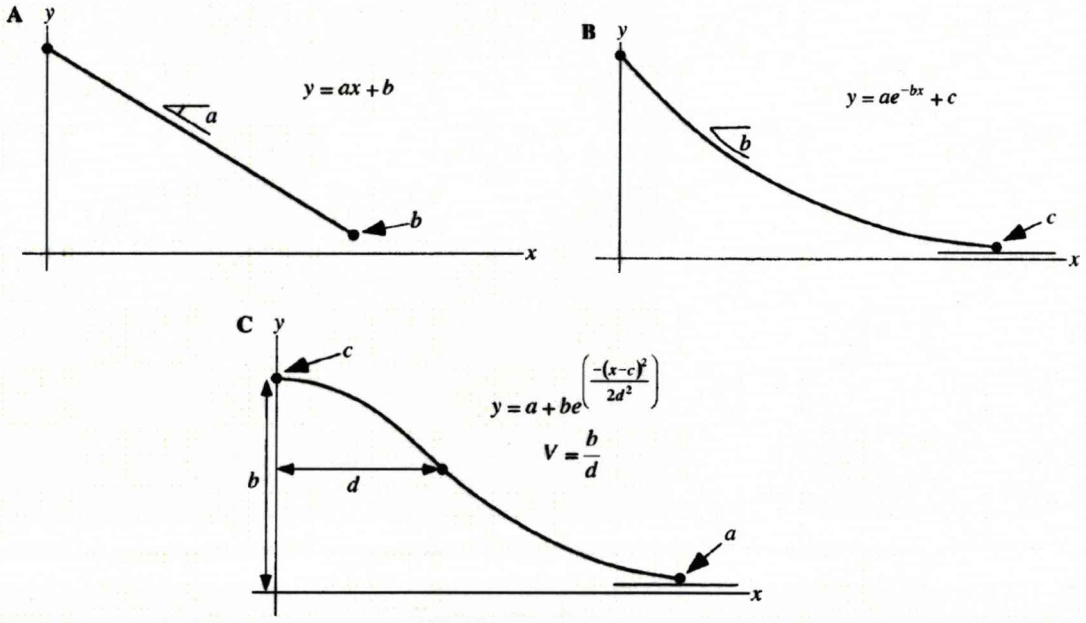

Figure 1.10 – Three slope types and their governing equations. (A) Planar morphology described by a linear equation. (B) Concave curvature described by an exponential function. (C) Sigmoidal morphology described by a Gaussian distribution (from Adams & Schlager, 2000).

Finally, an additional contribution to the understanding of slope and shelf edge evolution comes from the study of delta development according to location on the shelf (Steel *et al.*, 2000; Mellere *et al.*, 2002; Steel *et al.*,

2003; Porebski & Steel, 2006; Wild et al 2009). These authors advocate that deltas are the key element in the building of constructional shelves and shelf margins. Shelf-margin deltas, particularly those developed during falling relative sea level, can develop clinoforms of great height (hundreds of meters) and length (more than 10 km) which are deposited over the shelf margin into the deep water on the upper submarine slope (Porebski & Steel, 2006). On a graded slope these deltas play a fundamental role in slope progradation.

The variety of models and approaches used to interpret the evolution of submarine slopes include a wide range of forcing factors, however all of them can be grouped within the context of the three major driving factors suggested by Richards *et al.*, (1998), i.e. sea level fluctuation; regional basin tectonics; and rate, type and source of sediment supply, albeit it could be argued that the third is dependent on the first two. Considering the variables acting on the system it is most unlikely that two or more identical results can be produced. Nevertheless the results can be grouped by certain similarities, and so it is possible to proceed to analyse mud-dominated submarine slopes as a group where the elements share some or even many characteristics.

1.3.4 - Transmission of coarse-grained sediment through muddy slopes to the basin floor

Walker (1973) acknowledge that the first major advanced in the study of the turbidites was the recognition that sandstone graded beds, characterized by an assemblage of sedimentary structures, is a distinct lithofacies and he ascribe this discovery to a seminal paper in the history of the turbidite paradigm published by Bailey (1930). Migliorini (1943, translated by Ricci-Lucchi, 2003), after his studies in the Marmoso-arenaea Formation, Apennines, Italy, recognised the presence of coarse-grained sediments in deep-water environments and suggested that the failure of material (sliding) from the submarine slopes could mix with sea water and "*form a heavily loaded turbid plume. This flow will behave like a liquid denser than the ambient water and will proceed along the bottom up to where its slope will permit or the sediment load will be deposited along the way*".

Later, Keunen & Migliorini (1950), combining field observation with laboratory modelling (flume experiments), suggested that many graded sandstones in exhumed ancient successions could have been deposited by high-density turbidity currents. These two seminal works explained for the first time the *process* (turbidity current) and its *resultant deposit* (graded sandstones), and started a new era in studies of deep-water depositional systems.

The turbidite paradigm, later expanded to comprise gravity-driven mass-flow processes (debris-flows and slumps) as responsible for remobilisation of sediments in deep-water environments, established ***how*** coarse-grained sediments can reach deep-waters. However, the timing, or ***when*** this occurs had to wait for about 30 years to have a robust theory comprising a series of forcing factors which drive deposition in marine environments. Seismic stratigraphy (Vail & Mitchum Jr, 1977; Vail *et al.,* 1977a; b; c; Mitchum *et al.* 1977a; b; c; Todd & Mitchum Jr, 1977) and the subsequent sequence stratigraphy (Van Wagoner *et. al.,* 1988; Posamentier *et al.,* 1988; Posamentier & Allen, 1998) assert that coarse-grained deposition in shallow water occurs preferentially while relative sea level is high, due to the presence of available accommodation in proximal areas. At this time the deep-water areas are starved and receive only pelagic and hemipelagic sedimentation. At lowstand times, especially in the situation when the shelf edge is exposed, the previously deposited coarse-grained sediments on the shelf are remobilized and transported by gravity-driven processes into the deep-water environments.

These two paradigms (turbidites and seismic/sequence stratigraphy) have faced many investigations. For the turbidite paradigm one of the most debated points concerns the occurrence in the geological record of thick beds of structureless sandstones (Allen, 1991; Kneller *et al.,* 1995; Shanmugam, 2000). Sequence stratigraphy has also been tested extensively, however its proposers have emphasised that it is just "an *approach* or a way of looking at stratigraphic succession rather than a unique model or template to which all data sets must conform". (Posamentier & Allen, 1999).

One discussed point in the sequence stratigraphic paradigm is the timing of transfer of coarse sediment from the shelf to the deep-marine environment. The first concept states that it occurs during low sea level times, however a growing number of publications have demonstrated that this process also can happen during high sea level stands (Kuehl *et al.*, 1989, Weber *et al.,* 1997; Droz *et al.,* 2001; Mulder *et al.,* 2001; Covault *et al.*, 2007). It is generally understood nowadays that shelf physiography is an important variable. Narrow shelves or the presence of incised canyons on shelves can facilitate the transfer of coarse-grained sediment to deep marine environments during high sea level times.

In summary, the combination of slope physiography and the mechanisms of transferring coarse-grained sediments from shallow marine to deep-water environments discussed above play an important role in the processes of storage of these sediments in the middle and upper submarine slope settings and/or their bypass to deep basin and toe of slope. The understanding of this general geological background was crucial to the interpretation of a range of sand-prone depositional systems developed in the middle and upper submarine slope of the Laingsburg Formation, SW Karoo Basin.

1.4 - Geological Context of the Karoo Deepwater Deposits

1.4.1 - Introduction

The Palaeozoic to early Mesozoic tectono-stratigraphic development of southern Africa and specifically the Karoo basin can be related to the large scale evolution of western Gondwana. However, the detailed record for southern Africa is less complete than for South America and Antarctica, due to the major Mesozoic regional strike-slip and extensional tectonics that removed much of the late Palaeozoic record to the south of present day South Africa.

De Wit and Ransome (1992) summarised the major episodes of compression and extension that alternated along the southern margin of Gondwana as follows:

1) The Pan-Gondwanean convergence circa 650 ± 100 Ma, which is associated with the fusion of greater Gondwana (of which North America may have been part);
2) The late Proterozoic to early Palaeozoic extension circa 500 ± 100 Ma, which relates to the break-up of greater proto-Gondwana and the formation of an extensive Atlantic-type passive margin along the southern edge of Gondwana;
3) The late Palaeozoic convergence circa 300 ± 100 Ma, which is related to the assembly of Pangea and development of "Hercynian"-aged fold-thrust belts such as the Cape Fold Belt;
4) The mid- to late Mesozoic extension circa 150 ± 50 Ma, which involved the break-up of Gondwana with subsequent opening of the southern oceans.

In this geotectonic context, from the Early Ordovician to Early Jurassic, two sedimentary mega-successions separated by a major unconformity (ca. 30 Ma) were deposited in two laterally offset major sedimentary basins in southern Africa (Visser, 1987; 1997; Tankard et al., 2009) (Fig 1.11). The Cape Supergroup (Cape Basin) comprises approximately 8000 m of shallow marine, deltaic and fluvial deposits that

thicken towards the south into an east-west trending depo-axis (Rust, 1973; Broquet, 1990; Turner, 1990) and spans from the Early Ordovician to Early

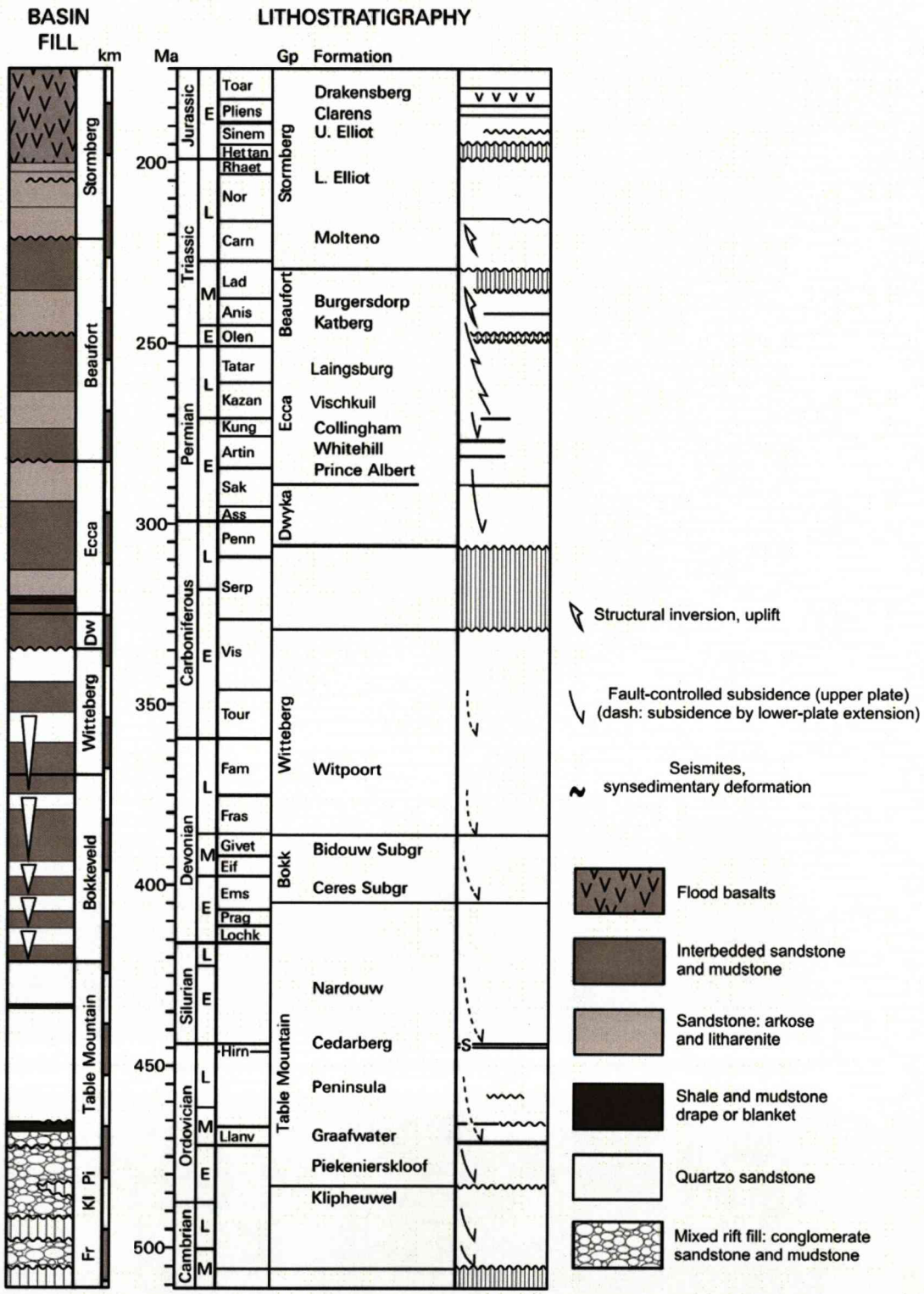

Figure 1.11 - Stratigraphic and tectonic evolution of the Cape and Karoo basins. Unconformities divide the succession into major basin stages (modified from Tankard et al., 2009).

Carboniferous (Veevers et al., 1994). Sediments of this mega-succession were derived from a cratonic source to the north and probably underwent extensive reworking by shallow-marine processes on a stable shelf to produce quartz-rich sands (Tankard et al., 1982) (Fig 1.11). The overlying Karoo Supergroup (Karoo Basin) comprises approximately 5500 m (maximum thickness) of deep marine to fluvial deposits that span from Late Carboniferous to Early Jurassic (Fig. 1.11). The ~30 Ma unconformity separating these two successions is interpreted to reflect uplift due to the mid-Carboniferous assembly of Pangea (Veevers et al., 1994).

1.4.2 – Formation and evolution of the Karoo Basin and the Cape Fold Belt

A longstanding interpretation for the formation of the Karoo and other major southern Gondwana basins (Paraná, Beacon and Bowen Basins) is that these basins developed in response to accretion tectonics along the southern margin of Gondwana during the Late Palaeozoic (Hälbich 1983; Johnson 1991; Gresse et al. 1992; Cole, 1992; De Wit and Ransome 1992; Veevers et al. 1994; Visser and Praekelt 1996; Catuneanu et al. 1998; López-Gamundí and Rossello, 1998; Faure and Cole, 1999; Catuneanu, 2004) (Fig. 1.12). Northward subduction of the Panthalassan (palaeo-Pacific Ocean) plate beneath the Gondwana plate led to the formation of a magmatic arc between the Karoo Basin and the southern margin of Gondwana (Johnson, 1991; Visser, 1993). Continued subduction resulted in northward compression and development of a fold-thrust belt inboard of the magmatic arc (Visser, 1987, Veevers et al., 1994; Visser & Praekelt, 1996) (Fig. 1.13). These and other authors (Johnson 1991; De Wit and Ransome 1992; Cole, 1992; Catuneanu et al. 1998; Catuneanu, 2004) have therefore considered that the Karoo Basin developed as a retroarc foreland basin with the fold-thrust belt (Cape Fold Belt) lying along the southern margin of the basin. However, an increasing amount of new generation data from sedimentary provenance (geochemical, petrographic and isotopic analyses) (Anderson et. al., 2004; van Lente, 2004) combined with radiometric dating of the Ecca Group (Fildani et al., 2007) have led to new interpretations that question the contemporaneity of the Cape Fold Belt with the Ecca Group.

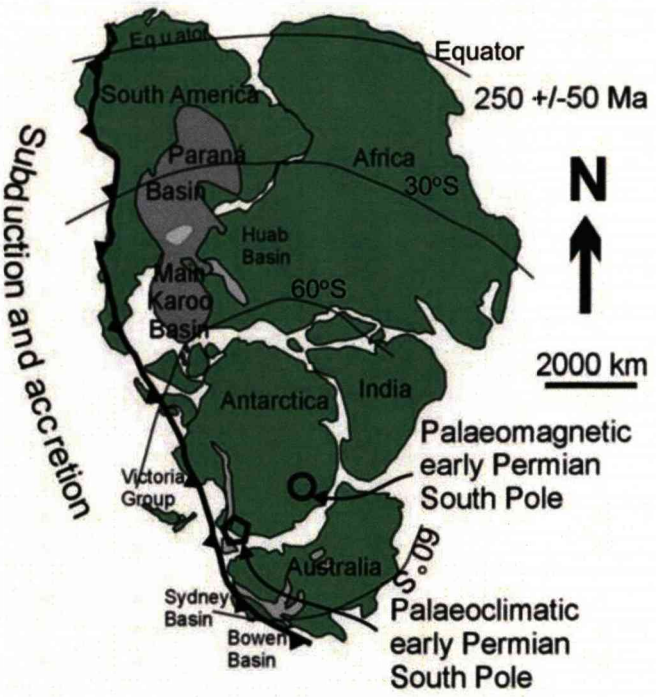

Figure 1.12 - Early Permian geodynamics of Gondwana (from Faure and Cole, 1999).

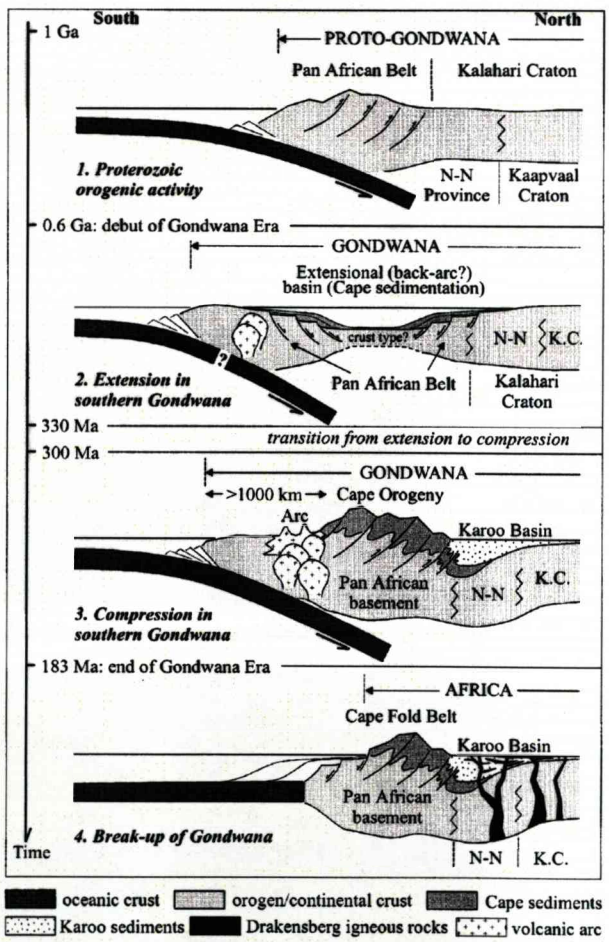

Figure 1.13 – Crustal evolution of southern Africa considering Karoo Basin as a Foreland basin in response for the uplift of the Cape Fold Belt. N-N = Namaqua-Natal mobile belt. K.C. = Kaapvaal craton (from Catuneanu et al., 1998)

Based on sedimentary provenance dataset, seismic stratigraphy, relationship of cleavage fabrics to diagenetic mineral assemblages (de Swardt & Rowsell, 1974), the Cape Fold Belt is now interpreted as Triassic in age (Tankard et al., 2009). The sedimentary provenance data (van Lente, 2004) suggest that only the upper Beaufort Group and above match with the Cape Fold Belt as a sedimentary source. This new interpretation implies that the Karoo foreland basin is younger than the Dwyka, Ecca and lower Beaufort Groups.

Tankard et al. (2009) offer an alternative interpretation for the tectonosedimentary evolution of the pre-foreland Karoo Basin (Dwyka and Ecca and lower Beaufort Groups) and also for the earlier Cape Basin. According to these authors these basins formed within the continental interior of Gondwana as a result of vertical motion of rigid blocks and intervening crustal faults. This model proposes that each basin episode records a three-stage evolution consisting of crustal uplift, fault-controlled subsidence and long periods of regional subsidence largely unaccompanied by faulting or erosional truncation. This last phase is morphologically interpreted as a sag-like basin. This model is summarised in figure 1.14 (stage F applies to the study interval presented in this thesis).

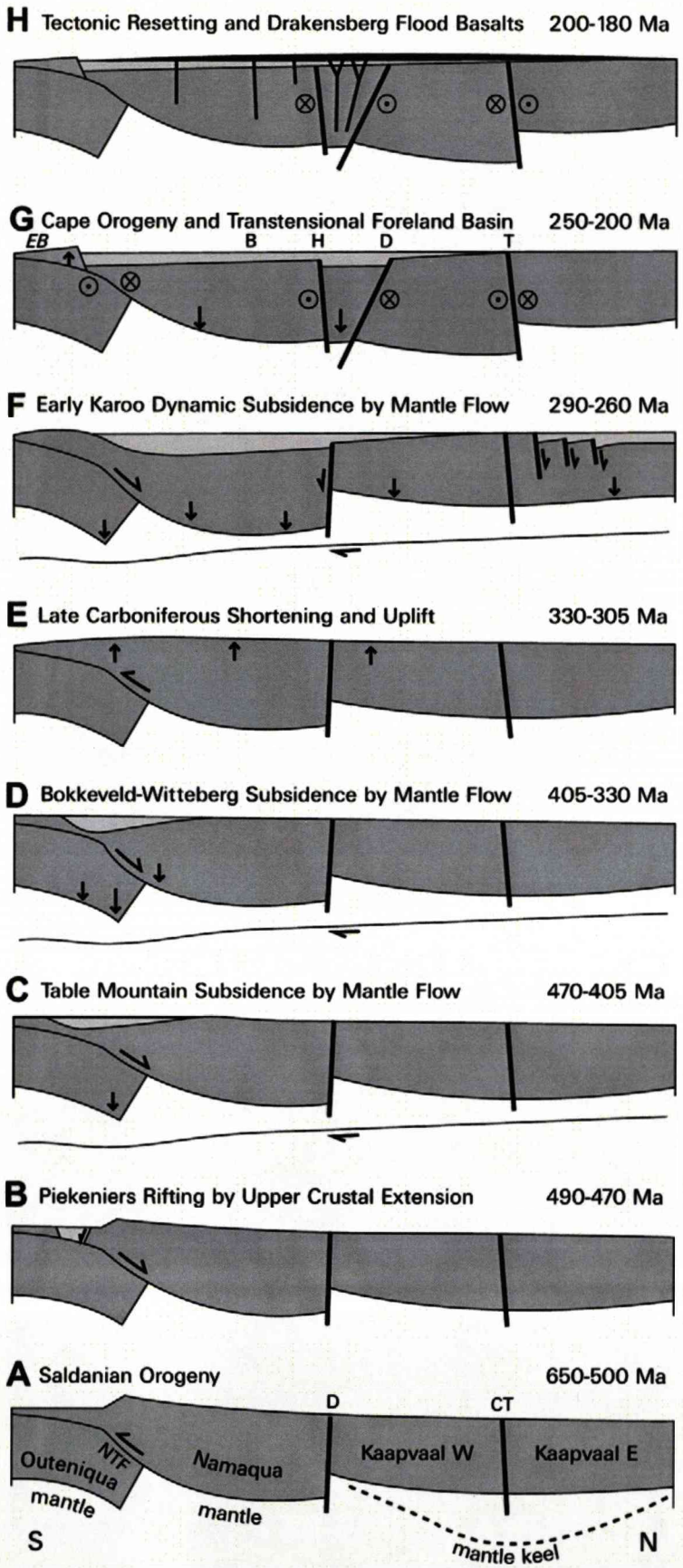

Figure 1.14 – Model evolution of Cape and Karoo Basins. (A-D) Saladian orogeny and Cape Basin. (E-F) Regional uplift and pre-Foreland Karoo Basin. (G-H) Cape Fold Belt orogeny and Foreland Karoo Basin (from Tankard et al., 2009).

1.4.3 - Permian Post-Glacial Maximum Deposits of the Karoo Supergroup

1.4.3.1 - Lower Ecca Group in the SW Karoo Basin

In the southwestern Karoo Basin, the Ecca Group comprises more than 1500 m of siliciclastic sediments, capped by the fluvial Beaufort Group (Veevers et al., 1994; Sixsmith et al., 2004; Grecula et al., 2003; this work) (Fig. 1.15). After final disintegration of the Dwyka ice sheets during Sakmarian times large parts of southwestern Gondwana were flooded and as southern Africa moved away from the paleo-pole, a thin succession of terrigenous to siliceous mudstones and siltstones, bentonites, and thin sandstones accumulated in a large, shallow, basin. The basal Prince Albert Formation has a maximum thickness of 180 m and comprises predominantly shale and cherty shale beds with inter- to supra-tidal carbonates (Visser, 1993) (Fig. 1.15). It is succeeded by black, carbonaceous shales of the Whitehill Formation (Visser, 1993) (Fig. 1.15). These initial post-glacial units are unusual in being highly condensed, yet relatively shallow water, consistent with a low subsidence rate and minimal clastic supply (no Cape Fold Belt).

Overlying the Whitehill Formation, the Collingham Formation (Fig. 1.15) is 30 – 70 m thick and is marked by an abrupt lithological change from dark carbonaceous shales to thin-bedded siliciclastic turbidites associated with an extremely high concentration of ash beds and a supply of mud (Visser, 1993). The unit thins to the east and ash density decreases in accord. Viljoen (1994) divided the Collingham into the basal Zoute Kloof and middle Buffels River Members, separated by the distinctive Matjiesfontein chert regional mark (Fig. 1.15).

1.4.3.2 - Upper Ecca Group in the SW Karoo Basin

The upper Ecca Group in the SW Karoo basin was deposited in two depocentres (Fig. 1.15). To the northwest (Tanqua depocentre) the succession comprises the Tierberg (basinal shales), Skoorsteenberg (submarine fans) and Kookfontein (slope to shelf edge) Formations. Around 100 km to the southeast, in the Laingsburg depocentre (study area of results

presented in this thesis) the upper Ecca Group comprises the Vischkuil (basin floor) and Laingsburg (submarine fan and slope succession) Formations (Fig. 1.15).

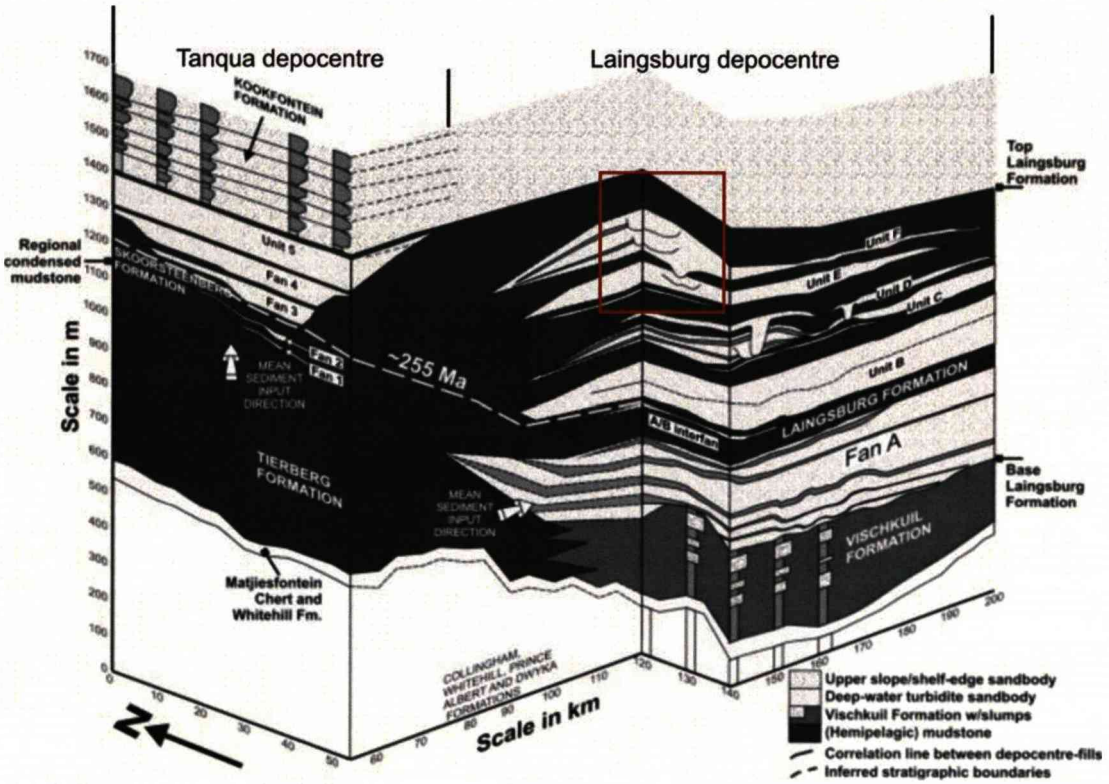

Figure 1.15 – Correlation between Laingsburg and Tanqua depocentres. The time line of ~255 Ma is based on Fildani et al. (2007). Red box illustrates the section studied in this thesis and the level of understanding of the upper Laingsburg stratigraphy at the outset of this work.

In the Laingsburg depocentre the Vischkuil Formation conformably overlies the Collingham Formation and is composed of mud-capped silty turbidites with a series of large scale zones of mass transport deposits and debrites (van der Merve et al., 2009). The ~1200 m thick Laingsburg Formation comprises the main deepwater depositional system with an upward passage from basin floor fan through a slope succession of intercalated mud-prone and sand-prone deposits to mixed wave/tide-influenced shelf edge deltas with marine trace fossils (Wickens, 1994; Sixsmith et al., 2003; Grecula et al., 2003; this work). This study addresses the upper part of the Laingsburg Formation (Fig. 1.15).

The Ecca Group is overlain by a 5000 m thick fluvial/nonmarine succession of the Beaufort Group, capped by Jurassic lavas that relate to

extensional breakup of Gondwana and opening of the South Atlantic ocean (Veevers et al., 1994)

1.5 – Methodology

This study is based largely on field work with a small, supporting study based on seismic data. The field data were acquired via a combination of logging sections, mapping of units, measurement of palaeocurrents and walking out sedimentary body geometries and key surfaces. The data collected included:

1) More than 14,000 m of logged sections. The sedimentological logging was undertaken at a cm-scale and was divided in long sections and short sections. The former aimed to constrain the stratigraphic framework of the study succession and usually covered all analysed intervals. The shorter logs were collected to characterize in detail specific deposits. The lateral distances between long logged sections varies from hundreds of metres to kilometres. The short logs are spaced between 20 m and 40 m (see Fig. 3.3). All logged sections are enclosed in the electronic version of this thesis on a CD-ROM.

2) More than 1,200 palaeocurrent measurements (appendix 1).

3) Seismic interpretation of 1 seismic horizon from a 3D high resolution project over an area of 1200 km^2 with generation of RMS amplitude maps (details in chapter 6).

The logged sections were combined with satellite images and electronic versions (ARC-GIS) of 1:30,000 conventional aerial photographs to correlate boundaries of genetic units and to constrain the large-scale architecture of the analysed stratigraphic succession. Key surfaces were walked out between logged sections in order to obtain reliable stratigraphic correlation. The products of this data integration were several regional stratigraphic panels. Across strike and down dip panels were integrated in a

fence diagram resulting in 3D physical constraint of the analysed succession over the study area.

Trends in sediment dispersal were reconstructed using measured thicknesses and palaeocurrents indicators (mainly foresets of current and climbing ripples, but also sole marks and erosive features), combined into isopach maps. Lithofacies, lithofacies association and architectural analyses were also undertaken. This interpretation combined with the trends in sediment dispersal and also with the stratigraphic framework enabled to reconstruct the depositional palaeo-environment for selected stratigraphic intervals. The combination of several depositional palaeo-environment constraints over time and space provided insights on the stratigraphic evolution of the analysed succession.

Finally, a comparison was made between the depositional environments, architecture and lithofacies distribution of some depositional bodies interpreted from the field data with the equivalent architecture derived from a 3D seismic dataset from the Amazon Fan in the Foz do Amazonas Basin, Brasil.

Chapter 2 – Lithofacies and Lithofacies associations

2.1- Introduction

The stratigraphic succession analyzed in this research comprises deposits that can be divided into two main categories; clay-prone and sand-prone deposits. Based on field observations, the sand-prone deposits are composed mainly of sandstone and siltstone, with only fine-grained and very fine-grained sandstone recognised. Intraformational conglomerates and chaotic deposits are also present. No petrographic analyses were carried out in this research, therefore the lithofacies analysis is based on field observations and descriptions, and data from the literature. Van Lente (2004) undertook petrographic analysis on six samples from the sand-prone deposits in the upper Laingsburg Formation, and using a QmFLt diagram (method after Johnson, 1976 *in* van Lente, 2004) classified these sandstones as feldspathic to lithofeldspathic. Tables 2.1a, b and c show a summary of the results presented by van Lente (2004).

The lithofacies analysis carried out in this work followed the Mutti and Ricci Lucchi (1975) approach, considering a sedimentary *facies* as a "layer or group of layers showing lithological, geometrical and sedimentological characteristics which are different from those of adjacent layers. A facies is considered to be the product of a specific depositional mechanism or several related mechanisms acting at the same time". A *facies association* is a "combination of two or more facies forming sedimentary bodies of various scales and degrees of organization". A facies association is considered to be the preserved spatial expression of a depositional environment or process". In this work the prefix *litho* is added to *facies* used by Mutti and Ricci Lucchi (1975) in order to strictly relate them to the lithological characteristics and to avoid confusion with other categories of facies (e.g. seismic facies). Based on these premises nine lithofacies were recognized, described and interpreted in this work.

Stratigraphic Unit	Detrital components						
	Quartz	Feldspar	Mica	Lithoclasts	Accessory Minerals	Matrix	Opaques
Unit E	35.78	17.77	11.36	4.37	0.55	9.00	3.18
Unit F	38.84	16.11	10.23	3.79	--	10.00	0.47

Table 2.1a – Summary of the composition (% of detrital components) of sandstones from Units E and F (modified from van Lente, 2004)

Stratigraphic Unit	Authigenic minerals				
	Quartz cement And overgrowths	Illite	Chlorite	Calcite	Mica
Unit E	6.29	5.70	0.86	5.57	2.84
Unit F	6.63	6.63	1.89	2.84	2.56

Table 2.1b – Summary of the composition (% of authigenic minerals) of sandstones from Units E and F (modified from van Lente, 2004)

Stratigraphic Unit	Texture		Rock classification
	Grain size	Sorting	
Unit E	Fine-grained	Poorly to well sorted	Feldspathic to Lithofeldspathic
Unit F	Fine-grained	Poorly to moderately sorted	Feldspathic

Table 2.1c – Summary of the texture and rock classification of sandstones from Units E and F (modified from van Lente, 2004)

2.2 - Lithofacies: description and interpretation

Lithofacies	Lithology	Outcrop expression	Description	Depositional process
L1	Claystone		Thickness - 0.5 m - 100 m. Geometry - laterally extensive sheets. Bounding surface - base: gradational; top: gradational or sharp Structures - structureless with a degree of fissility	Deposition from hemipelagic suspension fallout
L2	Siltstone		Thickness - 0.01 m - 0.1 m. Geometry - tabular or lenticular. Bounding surface - base: sharp; top: slight gradational. Depositional structures - planar-, wavy-, and ripple lamination. structureless Grading - weak normal grading. Turbidite division - Td ans Tcd.	Deposition from dilute turbidity current
L3	Current rippled sandstone		Thickness - 0.1 m - 0.3 m. Geometry - tabular at outcrop scale. Bounding surface - base: sharp; top: slight gradational. Depositional structures - current and planar ripple lamination. Erosional structures - flutes and grooves (occasionally). Grain size - very fine grained sand. Grading - weak normal grading. Turbidite division - Tcd.	Deposition from dilute turbidity current

Figure 2.1 – Table of lithofacies.

Lithofacies	Lithology	Outcrop expression	Description	Depositional process
L4a	Climbing ripple-laminated very fine-grained sandstone		Thickness - 0.1 m - 0.6 m. Geometry - tabular at outcrop scale. Bounding surface - base: sharp; top: sharp Depositional structures - climbing ripple lamination (predominant) planar lamination (occasionally) Post-depositional structures - load (occasionally). Erosional structure - flutes (rare). Grain size - very fine grained. Grading - no grading to weak normal grading. Turbidite division - Tc; Tb,c.	Rapid deposition from decelerating quasi-stead/waning high density turbidity currents.
L4b	Climbing ripple-laminated fine-grained sandstone		Thickness - 0.5 m - 1.5 m. Geometry - tabular at outcrop scale. Bounding surface - base: sharp; top: sharp Depositional structures - climbing ripple lamination Post-depositional structures - load (common). Grain size - fine grained sand. Grading - no grading. Turbidite division - Tc.	Rapid deposition from decelerating high density sustained turbidity current.
L5	Planar-laminated fine-grained sandstone		Thickness - 0.3 m - 1.2 m. Geometry - (1) tabular, mapped for hundred of metres when outside of erosive features; (2) discontinuous when inside of erosive features. Bounding surface - base: sharp or weak gradational; top: sharp Depositional structures - planar lamination, rare ripples on top. Erosional structures - scours; occasionally flutes and grooves. Grain size - fine grained sand. Grading - weak normal grading. Turbidite division - Tb; rare Tb,c..	Deposition from prolonged, quasi-steady high-density turbidity currents.

Figure 2.2 – Table of lithofacies.

Lithofacies	Lithology	Outcrop expression	Description	Depositional process
L6	Structureless fine-grained sandstone		Thickness - 0.3 m - 1.2m. Geometry - irregular; usually cut by or onlap onto erosional surfaces. Bounding surface - base: sharp; top: sharp. Depositional structures - structureless. Post-depositional structures - dewatering (rare). Erosional structures - scours, flutes and grooves. Grain size - fine grained sand. Grading - no grading. Turbidite division - Ta.	Deposition from prolonged, quasi-steady high-density turbidity currents due to non-uniformity in th flow.
L7	Mudclast comglomerate		Thickness - 0.1 m - 2.0 m. Geometry - irregular occurrence. Bounding surface - base: sharp; top: sharp. Depositional structures - structureless. Erosional structures - scours. Grading size - intraformational muddy pebbles and cobbles. Matrix - sandy Grading - no grading Turbidite division - F3 (Mutti, 1992)	Residual deposits of erosive high density turbidity currents.
L8	Chaotic (fine-grained)		Thickness - up to 5 m. Geometry - irregular occurrence. Bounding surface - base: sharp; top: sharp. Depositional structures - structureless poorly sorted. Erosional structures - not observed. Grain size - mix of sand, silt and clay size grain. Grading - no grading. Turbidite division - F1/F2(?) (Mutti, 1992).	*En masse* deposition from mass flows.

Figure 2.3 – Table of lithofacies.

Lithofacies	Lithology	Outcrop expression	Description	Depositional process
L8b	Chaotic (coarse-grained)		Thickness - base not exposed but at least 7 m. Geometry - irregular occurrence. Bounding surface - base: not observed; top: sharp. Depositional structures - structureless, poorly sorted. Erosional structures - not observed. Grain size - cobbles/boulders (up to 6m long axis) in a sand matrix. Grading - apparently inverse. Turbidite division - F1/F2(Mutti, 1992).	*En masse* deposition.
L9	Folded thin beds		Thickness - 0.3 m - 3.0 m. Geometry - irregular occurrence Bounding surface - base: sharp; top: sharp.	*En masse* deposition.

Figure 2.4 – Table of lithofacies.

2.3 - Lithofacies associations: description and interpretation

2.3.1 - Lithofacies association LA 1 - Claystone (Fig. 2.5)

Description: Dark grey claystones are the most common lithofacies association in the study area. They are composed only of lithofacies L1, but they occur in laterally extensive and regionally correlatable deposits that separate sand-prone Units and vary from 18 m to 100m in thickness. Where they separate Sub-units they are thinner than 5m. The stratigraphic bases are usually gradational and commonly difficult to identify due to the fine grained content of the upper part of the underlying sand-prone Unit or Sub-unit, and poor exposure. Their tops can be sharp, due to erosion by the overlying sand-prone Unit/Sub-unit, or transitional.

Interpretation: Deposition is interpreted to be from hemipelagic suspension fallout. Claystone units are interpreted to mark widespread and long term reduction in the supply of coarse-grained sediment to the depocentre and are used as reliable correlation markers.

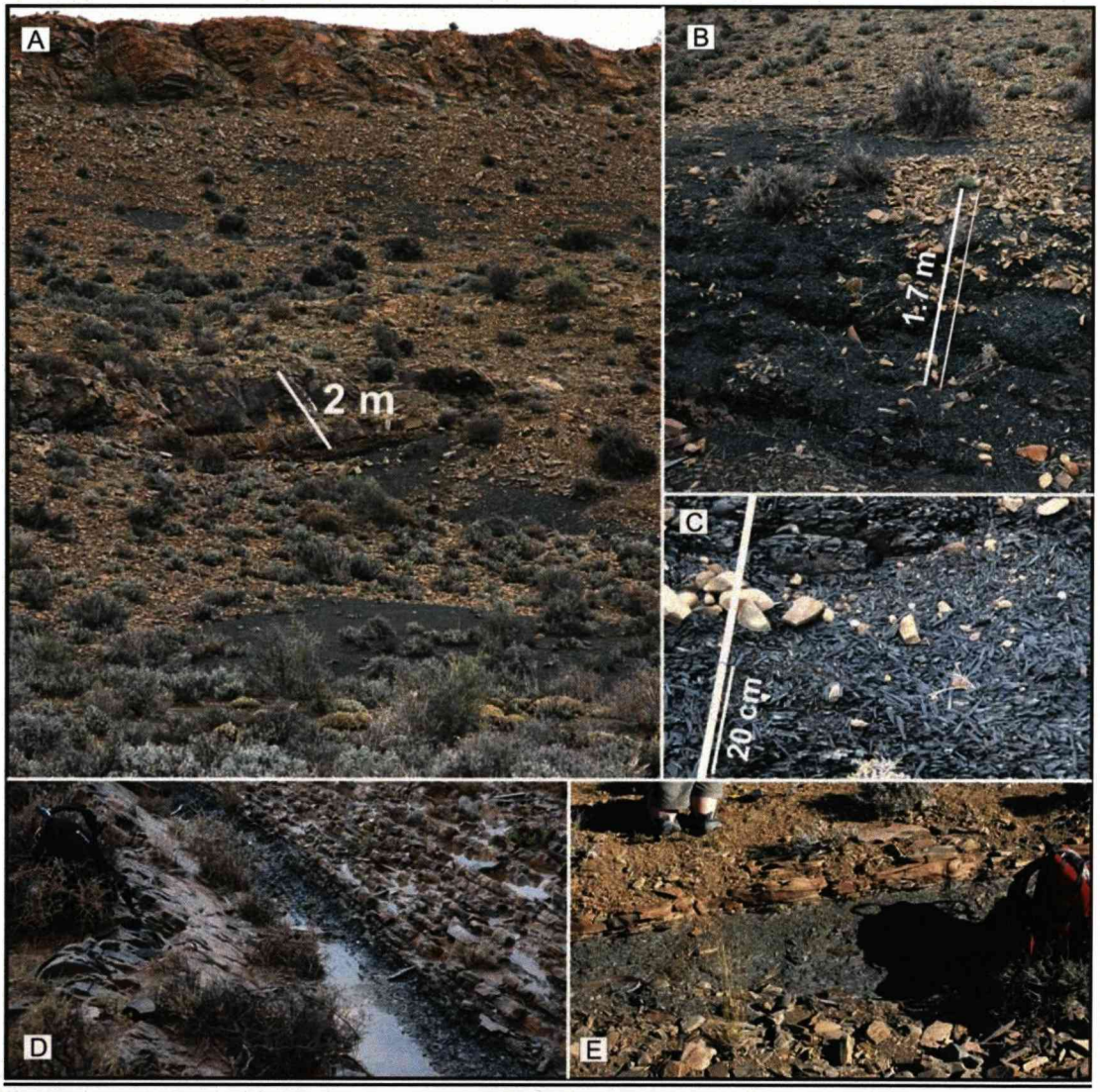

Figure 2.5 – Representative photographs showing geometric features and lithofacies details of lithofacies association LA1. Photographs A, B and C are close ups of the same inter-unit claystone between sand-prone Units D/E and E in southern flank of the Heuningberg anticline located near to log HBS 03. Photographs D and E are the lower and upper E intra-units claystone respectively. The former is located between logs HBS 02 and HBS 03 (Enclosure 2A), and the latter near to log HBS 02 to the east.

2.3.2 - Lithofacies association LA 2 – Silty heteroliths (Fig. 2.6)

Description: A common lithofacies association within sand-prone units, the silty heteroliths comprise lithofacies L2 and L3 with predominance of the first. Commonly these thin-bedded deposits occur in thick (more than 30 m) and extensive (longer than the outcrop scale) packages that are occasionally cut by incisional surface. This association can also mantle erosion surfaces where they are thinner and present irregular geometry. Their bases and tops can be both sharp and gradational. The first occurs where LA 2 is cut by or overlies incisional surfaces. The second occurs away from the erosive features, and usually transits from or into LA 4. Siltstones are planar-, wavy-, and ripple laminated showing weak normal grading and Td and Tcd division. Sandstone beds are current and planar ripple laminated, very fine grained showing weak normal grading and Tcd division.

Interpretation: The extensive deposits of LA 2 are interpreted to be the result of deposition from discrete dilute turbidity currents in depositional environments such as channel overbank or distal fringes of distributive systems and apron-like deposits. The irregular deposits appear as part of the fills of channel/channel complexes/valleys and are interpreted to be deposited either from the tails of high density turbidity currents or from dilute turbidity currents during backfill and abandonment of those depositional elements.

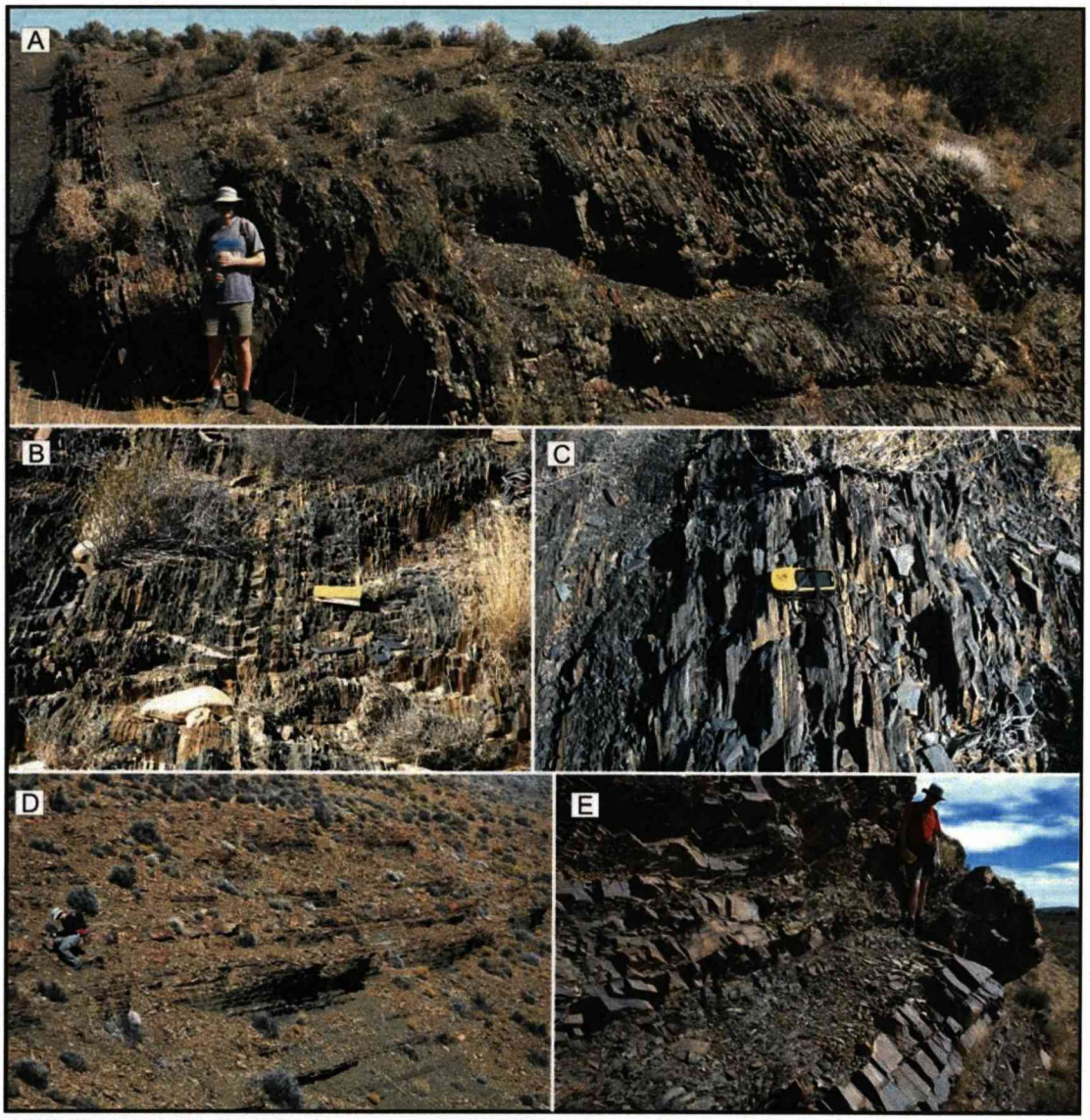

Figure 2.6 – Representative photographs showing geometric features and lithofacies details of lithofacies association LA2. Photographs A, B and C show intervals composed only by siltstone. (A) Unit G at log BVS 01 (Enclosure 3B), interpreted as distal fringes of distributive systems. (B) Sub-unit F2 at log HBN 05 (Enclosure 1B), interpreted as overbank deposits. (C) Unit D/E at log HBN 05 (Enclosure 1B), interpreted as distal fringes of distributive system. Photograph D, located near to log HNS 28 (Enclosure 2A) show thin and medium beds of sandstone intercalated with siltstone in Sub-unit F1 interpreted as fringes of distributive system. Photograph E shows siltstone overlying erosional surface that the geologist is stand on (Sub-unit E2, log HBS 10 in Enclosure 2A) within a channel.

2.3.3 - Lithofacies association LA 3 – Siltstone intercalated with laminae/very thin beds of very fine-grained sandstone (Fig. 2.7)

Description: This association is not common having localised occurrences. It is characterized by lithofacies L2 intercalated with laminae or very thin beds (<10 cm) of lithofacies L3. In LA 3, siltstones are structureless (as opposed to current and climbing ripple laminated siltstone in LA2). The very fine grained sandstones in LA 3 are thinner and do not show current or climbing ripple lamination, as in LA 2, but only planar and starved ripple lamination.

Interpretation: Lithofacies association LA 3 is interpreted to be deposited from multiple discrete dilute turbidity currents. The absence of structures in the siltstones suggests that they can also have a component of hemipelagic fallout. This lithofacies association appears locally as part of the upper portion of the fill of a major erosive feature interpreted as a slope valley.

Figure 2.7 – Representative photographs showing details of lithofacies association LA3. Photographs A, B and C are close ups of the same outcrop located in the topographic low between Units E and F on the southern flank of the Heuningberg anticline to east of the log HBS 03 (Enclosure 2A). The structureless siltstone intercalated with very fine-grained sandstone is interpreted as the backfill of the slope valley identified in the southern flank of the Heuningberg anticline.

2.3.4 - Lithofacies association LA 4 – Sandy heteroliths (Fig. 2.8)

Description: Another common lithofacies association within sand-prone units, the sandy heteroliths are composed of lithofacies L2, L3 and L4a. Like LA 2, they appear to both mantle erosion surfaces and to be cut by them. This association can occur in thick (up to 60 m) and extensive (longer than the outcrop scale) packages, or locally in irregular occurrences usually overlying erosive surfaces. LA 4 has a transitional base and top since usually it passes from or into LA 2. In cases where LA 4 is cut by or overlies erosional surfaces, tops or bases are sharp. The common sedimentary structures in the sandstone beds of this lithofacies association are climbing ripple lamination.

Interpretation: This association is interpreted to be deposited predominantly from denser flows than those in LA 2. Like LA 2 the extensive deposits are interpreted to occur in levee-overbank environments (however, in these cases, they represent more proximal deposits) and in distributive, apron-like deposits. The irregular deposits appear as part of channel, channel complex, and slope valleys fills, and in particular are related to channel margins or abandonment phase deposits.

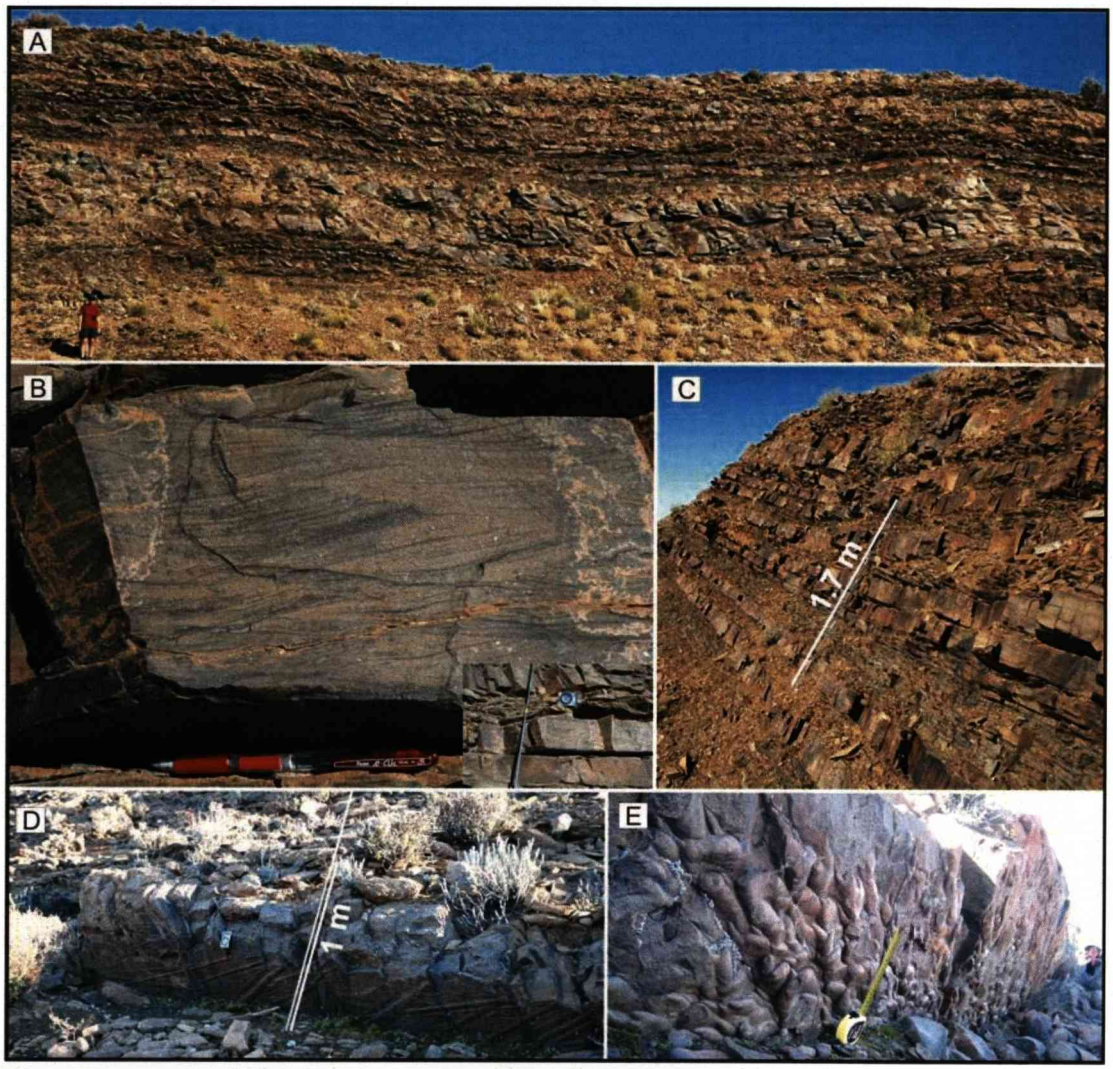

Figure 2.8 – Representative photographs of lithofacies association LA4. Photographs A, B and C are close ups of the same outcrop (Sub-unit E2) located on the southern flank of the Heuningberg anticline to the east of log HBS 09 (Enclosure 2A) to show geometric features and lithofacies details. This interval is interpreted as channel margin deposits. Photos D and E show the base of the same bed in different positions located in the southern flank of Baviaans syncline (to the east of the log BVS 01). In photo D grooves can be seen at the base of the bed while in photo E (approximately 500 m to the east -downdip- of photo D) flutes are present. The bed shown in photos D and E belongs to Sub-unit F1 and is interpreted distributive system.

2.3.5 - Lithofacies association LA 5 – Thick and very thick beds of climbing ripple laminated fine grained sandstone (Fig. 2.9)

Description: This association is not very common having a localised occurrence. It is composed mainly of lithofacies L4b, but locally, thin/medium beds (10-20 cm) of lithofacies L2 appear intercalated with lithofacies L4b. The most common occurrence is the amalgamation of thick beds of lithofacies 4b in bedsets that can reach 3 m. These bedsets can be followed for hundreds of metres to kilometres. In some locations they are cut by erosional surfaces. The bases and tops of the association are always sharp.

Interpretation: LA 5 is interpreted to form from rapidly decelerating and depositing high density sustained turbidity currents. The thick beds of lithofacies L5 represent the bulk of the sediment content in high-volume flows. The occurrence of the thin beds of lithofacies L2 represents low volume flows. The thickness of the individual beds is interpreted to be proportional to the flow volume. The depositional environment of the association is interpreted to be proximal crevasse splays/lobes in channel-levee systems.

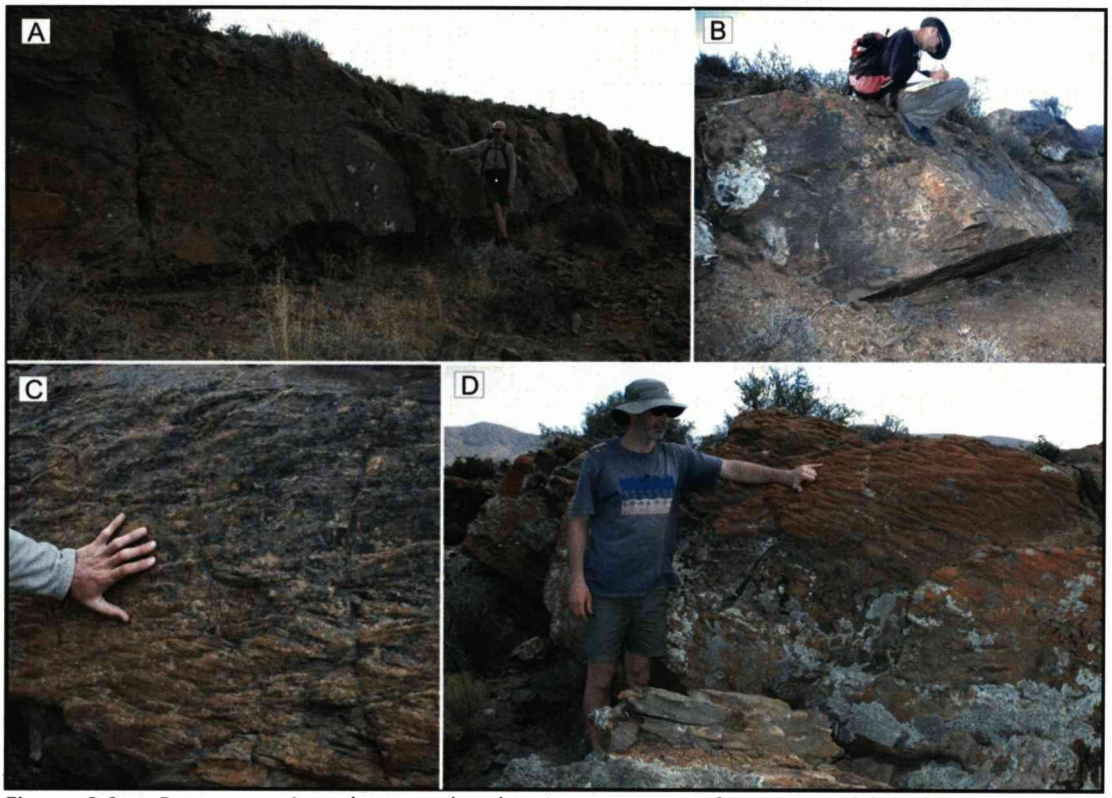

Figure 2.9 – Representative photographs showing geometric features and lithofacies details of lithofacies association LA5. Photographs A and C are close ups of the same bed. Photograph C shows the lithofacies detail of a climbing ripple laminated fine-grained sandstone bed. Photograph A shows the geometric aspect of a 2m-thick bedset formed by the amalgamation of beds like that shown in photograph C. This outcrop is located in the Zoutkloof syncline near to the log ZK 01 (Enclosure 2B) and the depicted sandy bodies belong to Sub-unit F2. Photograph B is also located in the Zoutkloof syncline (log ZK 03; Enclosure 2B) and is part of the same stratigraphic interval. This photograph shows the geometric features of a very thick single bed of climbing ripple laminated fine-grained sandstone. The sandy bodies shown in photographs A, B and C are interpreted as crevasse-splay/lobe deposits. Photograph C show a sandy body that also belongs to Sub-unit F2 but is located in the southern flank of the Baviaans syncline (between log BVS 02 and BVS 03; Enclosure 3B). This photograph shows the detail (climbing ripple lamination) of fine-grained sandstone beds also interpreted as crevasse-splay/lobe.

2.3.6 - Lithofacies association LA 6 – Planar-laminated/structureless sandstones (Fig. 2.10)

Description: The main characteristics of this association are: (1) predominance of lithofacies L5 with subordinate lithofacies L6 and L2; (2) weak transitional to sharp non-erosive base and sharp top; (3) laterally extensive exposure parallel and orthogonal to palaeoflow (hundreds of metres to kilometre), without change in geometry and slight change in lithofacies. The thick beds of lithofacies L5, and locally lithofacies L6, form bedsets (up to 5 m thick) by amalgamation or having erosive contact. However, locally they are intercalated with the thin/medium (0.1 m – 0.3 m) beds of lithofacies L2.

Interpretation: LA 6 is interpreted to be the result of deposition from prolonged, quasi-steady high-density turbidity currents (Kneller and Branney, 1995). Similar to LA 5 the occasional occurrence of the thin beds of lithofacies L2 are interpreted as the remnants (those that were not eroded by the subsequent flow) of the deposits from the flow tails. Although LA 6 presents some erosive features it is dominated by depositional characteristics. Its attributes lead to interpret distributive intraslope lobes as its depositional environment.

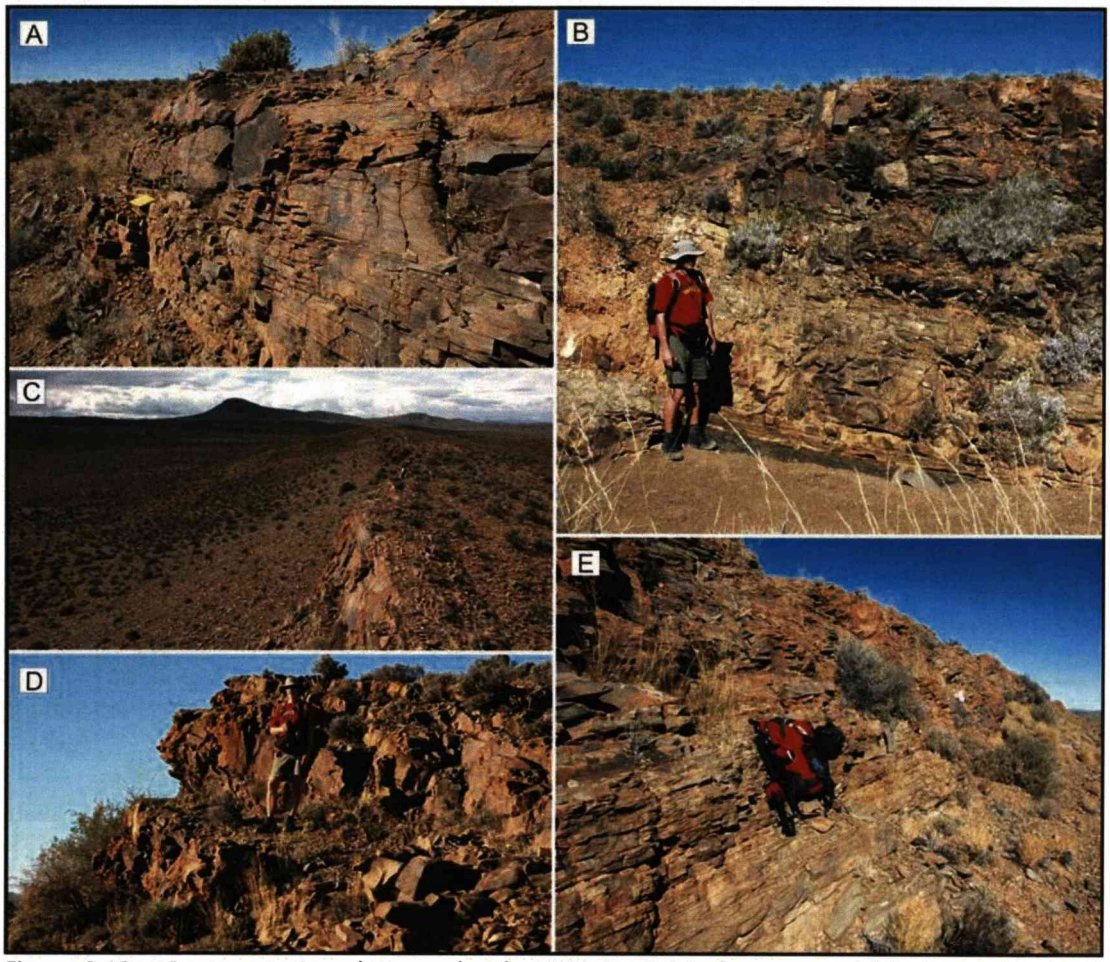

Figure 2.10 – Representative photographs showing geometric features and lithofacies details of lithofacies association LA 6. Photographs A, B, C and E are from Sub-unit E1 in the southern flank of the Heuningberg anticline (between logs HBS 02 and HBS 03; Enclosure 2A). Photographs A and B show the lithofacies details (lithofacies L5) of a bedset formed by the amalgamation/erosion of beds of planar-laminated fine-grained sandstone. Photograph A also shows an erosional surface (left) cutting down into Sub-unit E1. Photograph B shows the sharp but non-erosive base of the Sub-unit (claystone -dark grey lithology at the foot of the geologist- overlain by sandstone –lighter lithology). Photograph C shows the geometric aspect, an extensive sandbody with slight variation in lithofacies association. Photograph D is from Unit D/E in the nose of the Heuningberg anticline and shows two thick beds of sandstone (lithofacies L5) intercalated with a thin bed of siltstone (lithofacies L2). These two lithofacies compose lithofacies association LA 6.

2.3.7 - Lithofacies association LA 7 – Structureless/planar-laminated sandstones (Fig. 2.11)

Description: This association is composed predominantly of lithofacies L6, but lithofacies L5 is also present, albeit in many cases the planar lamination, characteristic of lithofacies L5, is faint showing transition from or into L6. LA 7 commonly overlies erosion surfaces. Erosive or loaded contacts between beds are common. Beds are usually grouped in bedsets that can be up to 6 m thick. Beds and bedsets are discontinuous due to (1) truncation by erosional surfaces; (2) onlap onto erosional surfaces; and (3) abrupt lithofacies changes at outcrop scale. Claystone clasts occur either isolated or concentrated in layers within beds or at tops and bases (revealed by imprints) where, in some cases, imprints of organic material are observed. Scours are common and dewatering structures are rare.

Interpretation: Lithofacies association LA 7 is interpreted to be the result of deposition from prolonged, quasi-steady high-density turbidity currents due to non-uniformity in the flow (Kneller and Branney, 1995). The intercalation between structureless and planar laminated sandstone within the individual beds suggests variation in the uniformity of the flow. The thicknesses of the individual beds do not necessarily relate to the thickness of the parent flow (Kneller and Branney, 1995) since it is interpreted that only the near bed portion of the flow is deposited while the bulk is still bypassing in a regime of sustained flows.

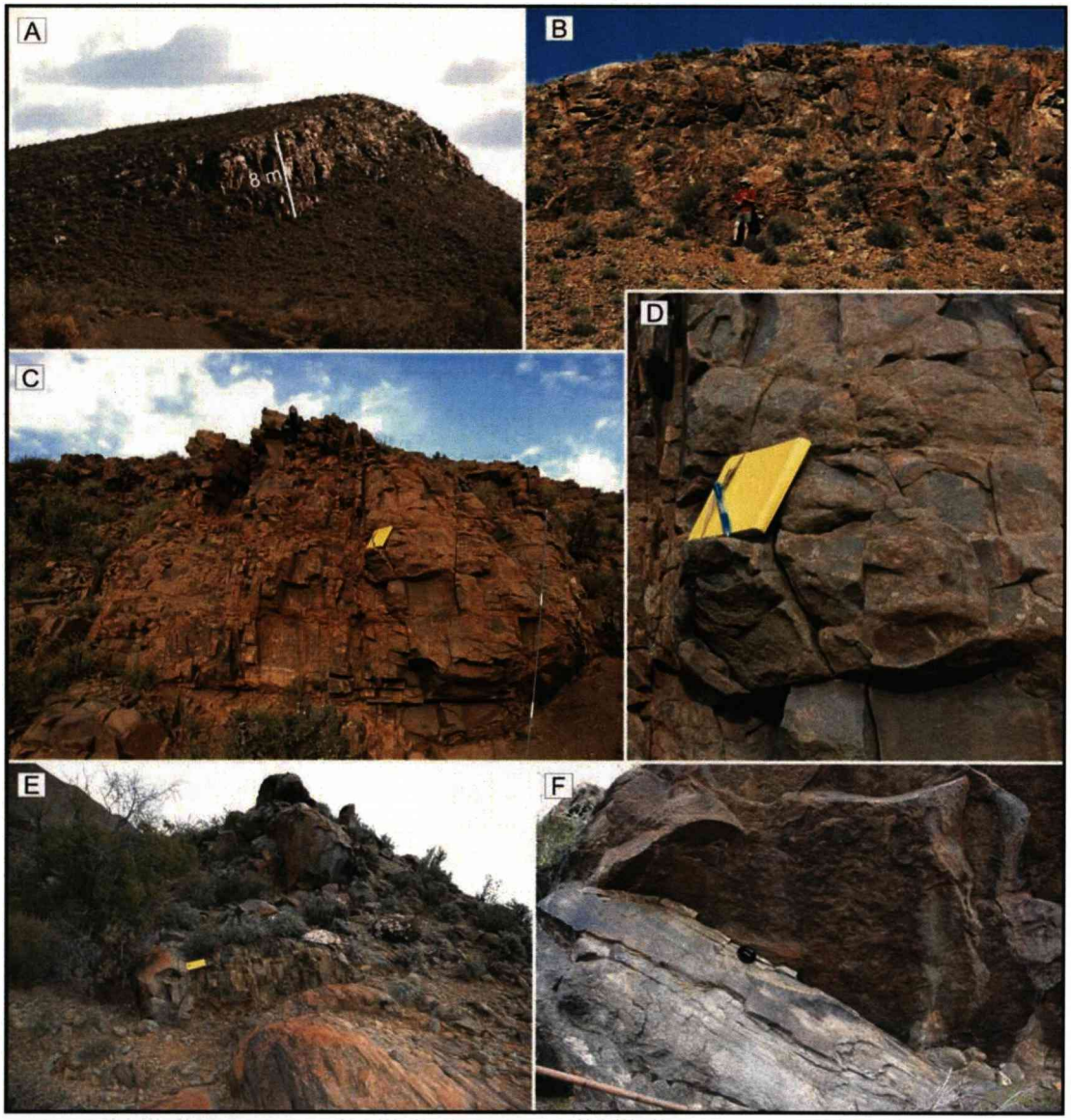

Figure 2.11 – Representative photographs showing geometric features and lithofacies details of lithofacies association LA 7. Photographs A and B are from Sub-unit E2 in the southwestern Heuningberg anticline (Doornfontein farm, near to log HBS 15; Figure 3.3 and Enclosure 2A) and show geometric aspects of the bedsets formed by amalgamation of beds of lithofacies L6. Abrupt lateral variation in lithofacies association is seen in the sandbody, which is interpreted to represent channel fill. Photographs C and D are from Sub-Unit F2 in the southwestern Heuningberg anticline (Doornfontein farm, channel complex 3, discussed in chapter 5; Figure 3.3 and Enclosure 6) showing geometric aspect (photo C) of the bedset formed by amalgamation of beds of lithofacies L6. Abrupt lateral variation in lithofacies association is seen (base of the sandbody) in the sandbody shown which is interpreted to represent channel fill. Photograph D is a detail of C to show the structureless characteristic of the lithofacies L6 that composes lithofacies association LA 7. Photographs E and F are from Sub-unit F2 in the southern flank of Baviaans syncline (east of the log BVS 01; Enclosure 3B). Photograph E show a vertical sequence of erosive base beds of lithofacies L6 and L5 (the stratigraphic way up is to the right upper corner of the photo). Photograph F is a detail of E showing the erosive contact between beds of lithofacies L5 and L6 underlying and overlying the erosional surface respectively.

2.3.8 - Lithofacies association LA 8 – Claystone clast conglomerates (Fig. 2.12)

Description: This association has localised occurrences. It is composed of lithofacies L7 and discontinuous beds of lithofacies L6, and always overlies erosion surfaces.

Interpretation: Lithofacies association LA 8 is interpreted to be the residual deposits (channel lags) of erosive high density bypassing turbidity currents. The depositional environments of this association are channel/channel complex fills where it appears in the axial portion.

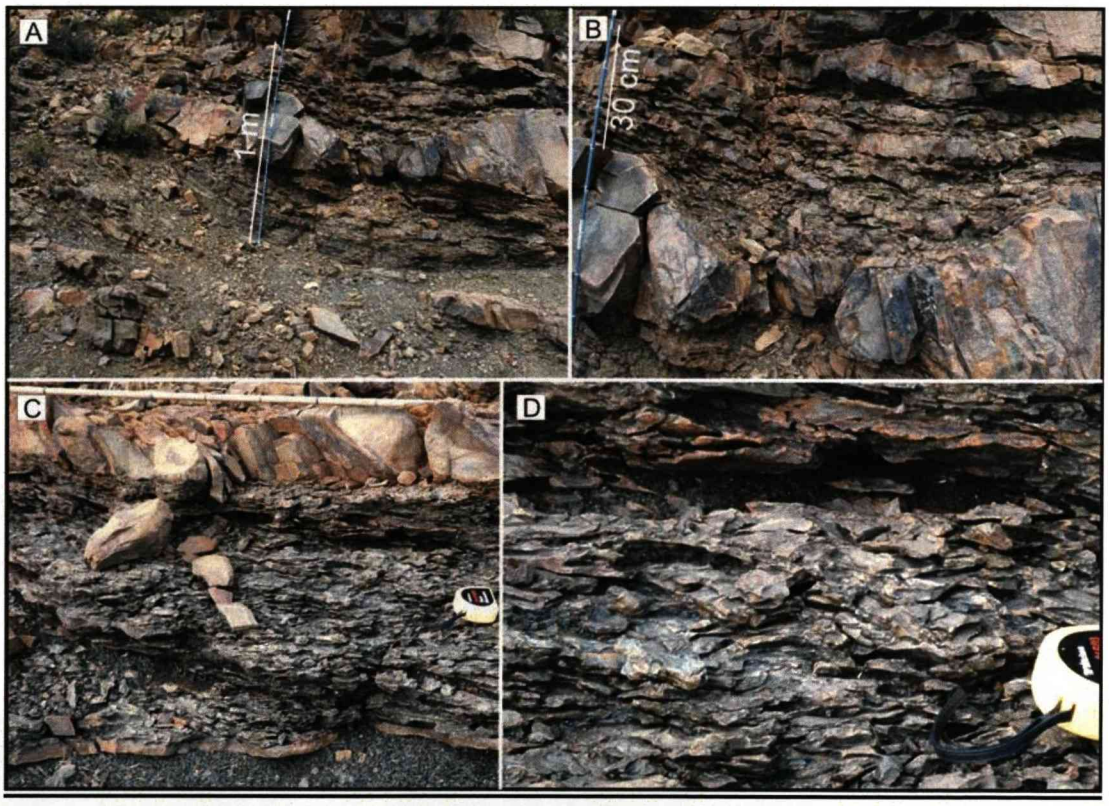

Figure 2.12 – Representative photographs showing geometric features and lithofacies details of lithofacies association LA 8. All photographs are from Sub-unit F2 in southwestern Heuningberg anticline (Doornfontein farm, channel complex 3, discussed in chapter 5; Figure 3.3 and Enclosure 6). Photograph B is a detail of A, and Photograph D a detail of C. They show the geometric aspects of the of the beds of lithofacies L7 (channel lags) that compose lithofacies association LA 8.

2.3.9 - Lithofacies association LA 9 – Chaotic deposits (Fig. 2.13)

Description: Lithofacies association 9 is composed of lithofacies 8a and 8b. At outcrop scale it is not possible to conclude whether the two lithofacies that compose this association are the result of different flows or only one flow. In lithofacies 8b large (5m diameter) intraformational clasts occur, locally with clastic injection structures. This lithofacies association is found only as the basal deposits of slope valley-fills and channel-fills.

Interpretation: LA 9 is interpreted to represent *en masse* deposition from mass flows. Its depositional environment is interpreted to be the fill of large erosive features.

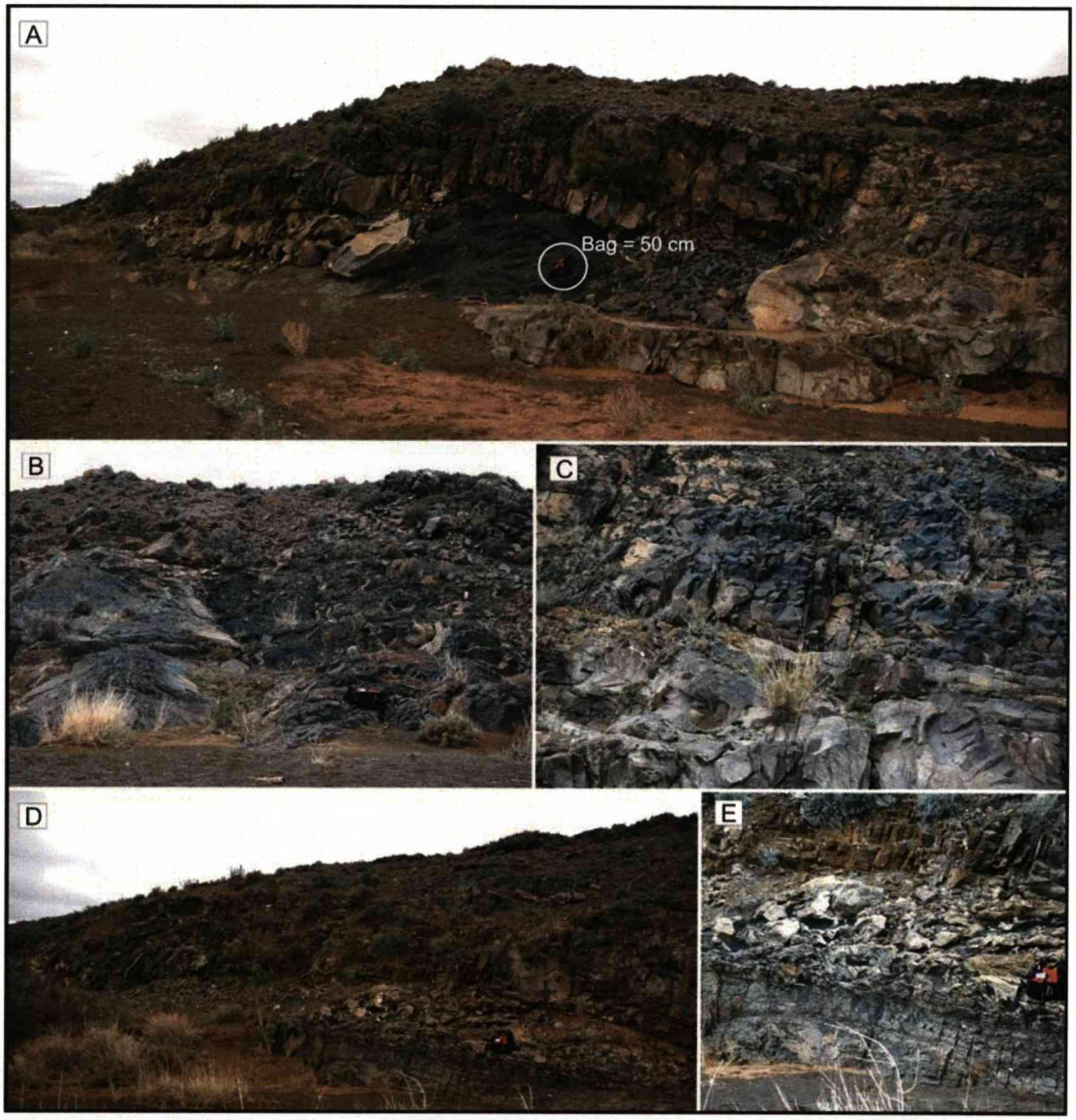

Figure 2.13 – Representative photographs showing geometric features and lithofacies details of lithofacies association LA 9. All photographs are from Sub-unit F2 in southwestern Heuningberg anticline (between logs HBS 09 and HBS 10; Enclosure 2A) showing the basal fill of a slope valley. All photos show examples of mass flow deposits composed of sandy matrix and intraformational clast of claystone. Photo A shows a large clast of claystone. Photo B, taken from few metres to right of photo A, shows another large claystone clast. Photo C shows an interval of the sandy structureless matrix without clasts. Photo D, taken from few metres to left of the photo A shows decimetre scale claystone clasts supported by the sandy matrix. In the left portion of photo D a succession of beds are seen vertically tilted. This succession is interpreted as a slide from the margin of the slope valley within the debrites. Photo E is a detail of photo D and shows below the level where the bag is placed a "smoothed" area (compared with the level just above full of clasts). This smoothed area is interpreted as a "mould" of another large claystone clast that would have been eroded.

2.3.10 - Lithofacies association LA 10 – Folded thin beds (Fig. 2.14)

Description: This lithofacies association also has localised occurrences and is composed only by lithofacies L9. This association is usually related to incisional surfaces where it mantles them, but it is also locally found outside of erosional surfaces commonly at the top or base of sand-prone Units/Sub-units.

Interpretation: Lithofacies association LA 10 is interpreted to represent *en masse* deposition from laminar mass flows (creep, slides, slumps). When related to erosional surface it is interpreted to be remobilisation of older or contemporaneous deposits outside the channel through channel margin collapse. Outside the channels, LA 10 is interpreted to be the result of small scale mass movement due to some kind of instability on the submarine slope.

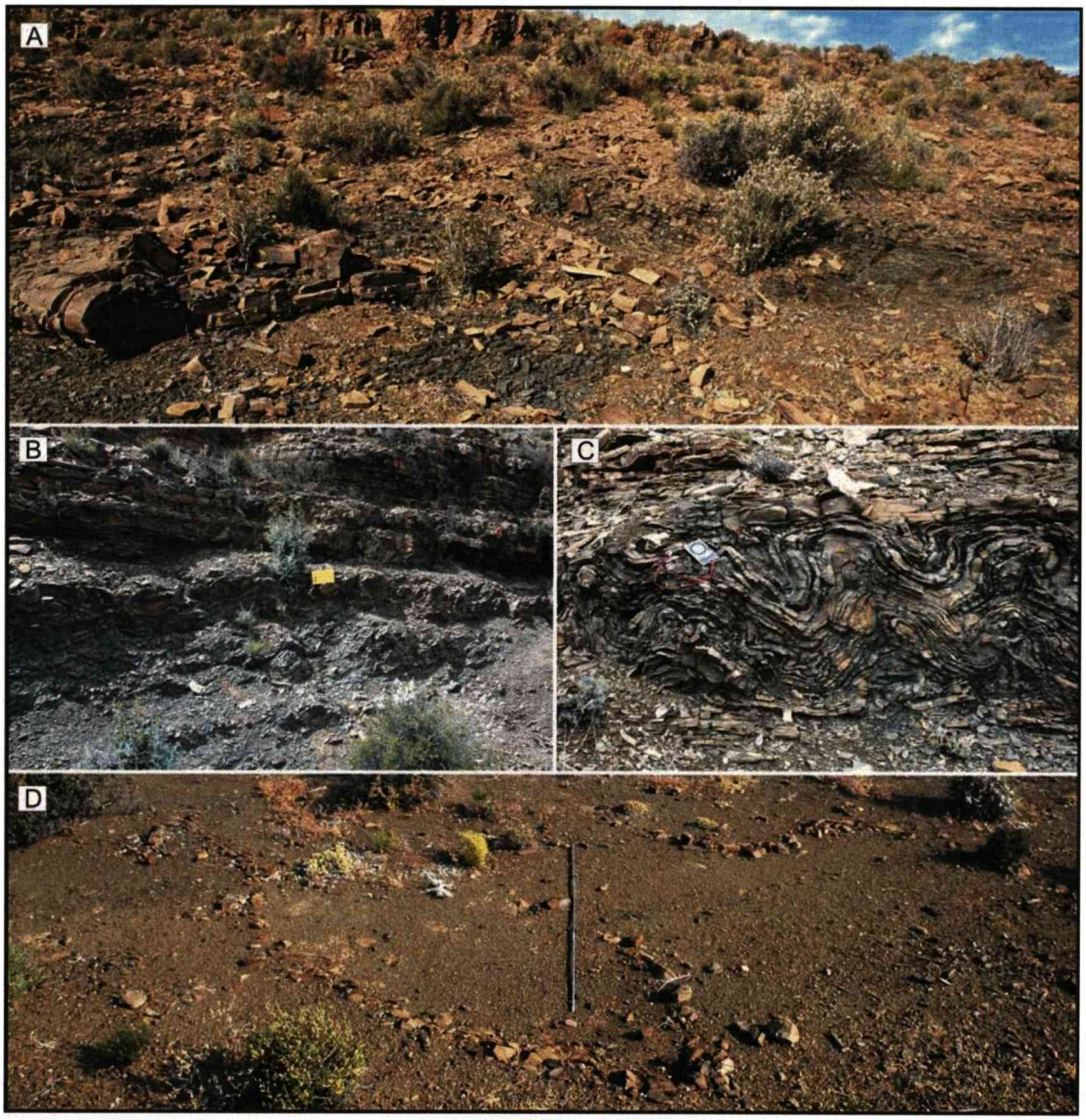

Figure 2.14 – Representative photographs showing geometric features and lithofacies details of lithofacies association LA 10. All photographs show contorted beds interpreted as slump deposits. Photograph A shows slumps as part of a channel fill overlying erosional surface (channel complex 3 discussed in chapter 5; Enclosure 6). Photograph B shows a 2 m thick slumped claystone section underlying a sand-prone unit (Sub-unit F1, log HBS 22; Enclosure 6). Photo C a 1 m thick slumped section interpreted as part of a channel margin fill. Photo D shows a contorted thin bed of sandstone involved in "mass" of claystone. This slump (~3 m thick) is at the top of a sand unit (Sub-unit E3, log HBS 15; Enclosure 2A), and is interpreted to be the result of instability on the slope after the deposition of the sand-unit.

2.4 - Lithofacies associations: representation in logged sections

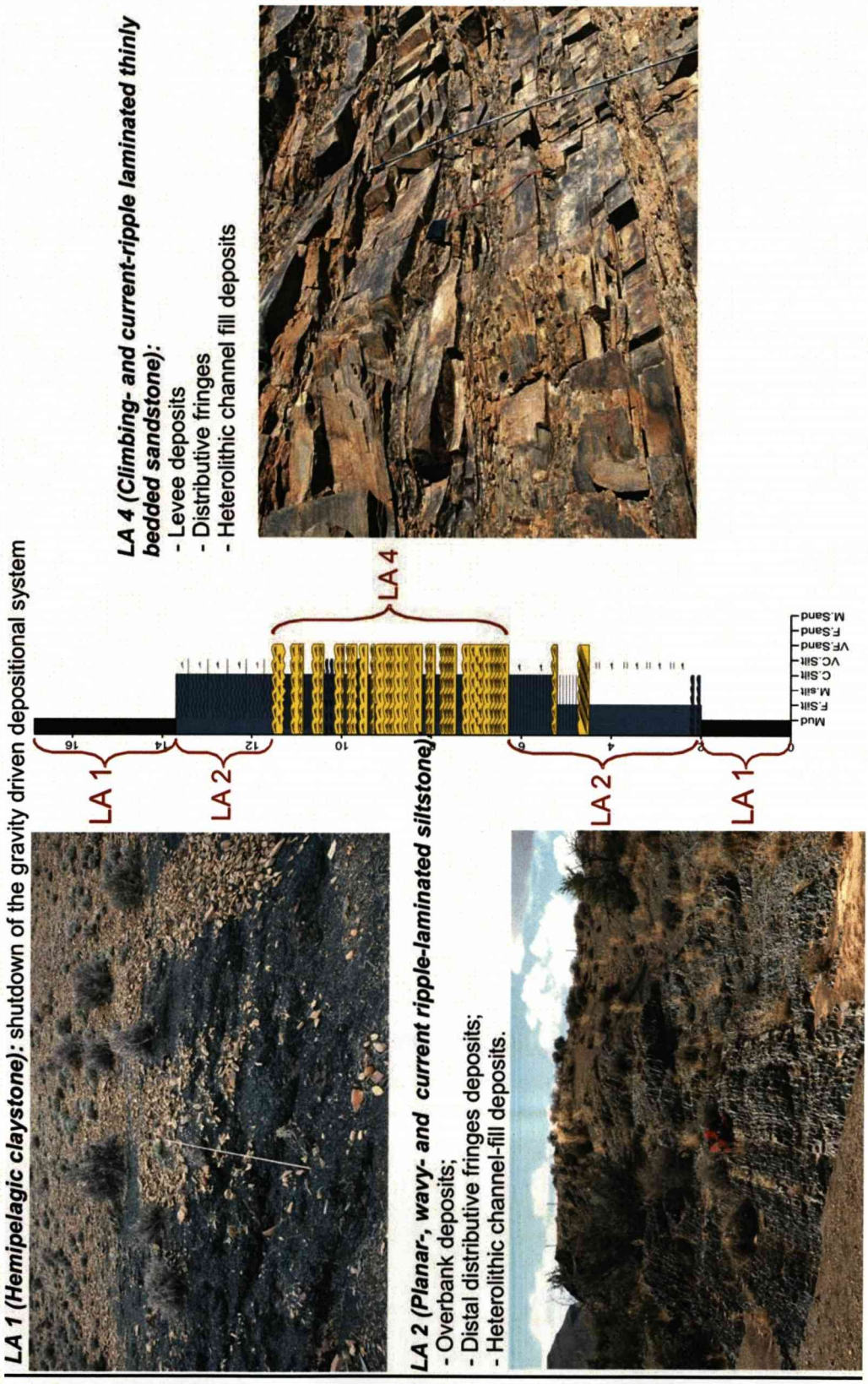

Figure 2.15 – Examples of lithofacies associations in logged sections

Figure 2.16 – Examples of lithofacies associations in logged sections

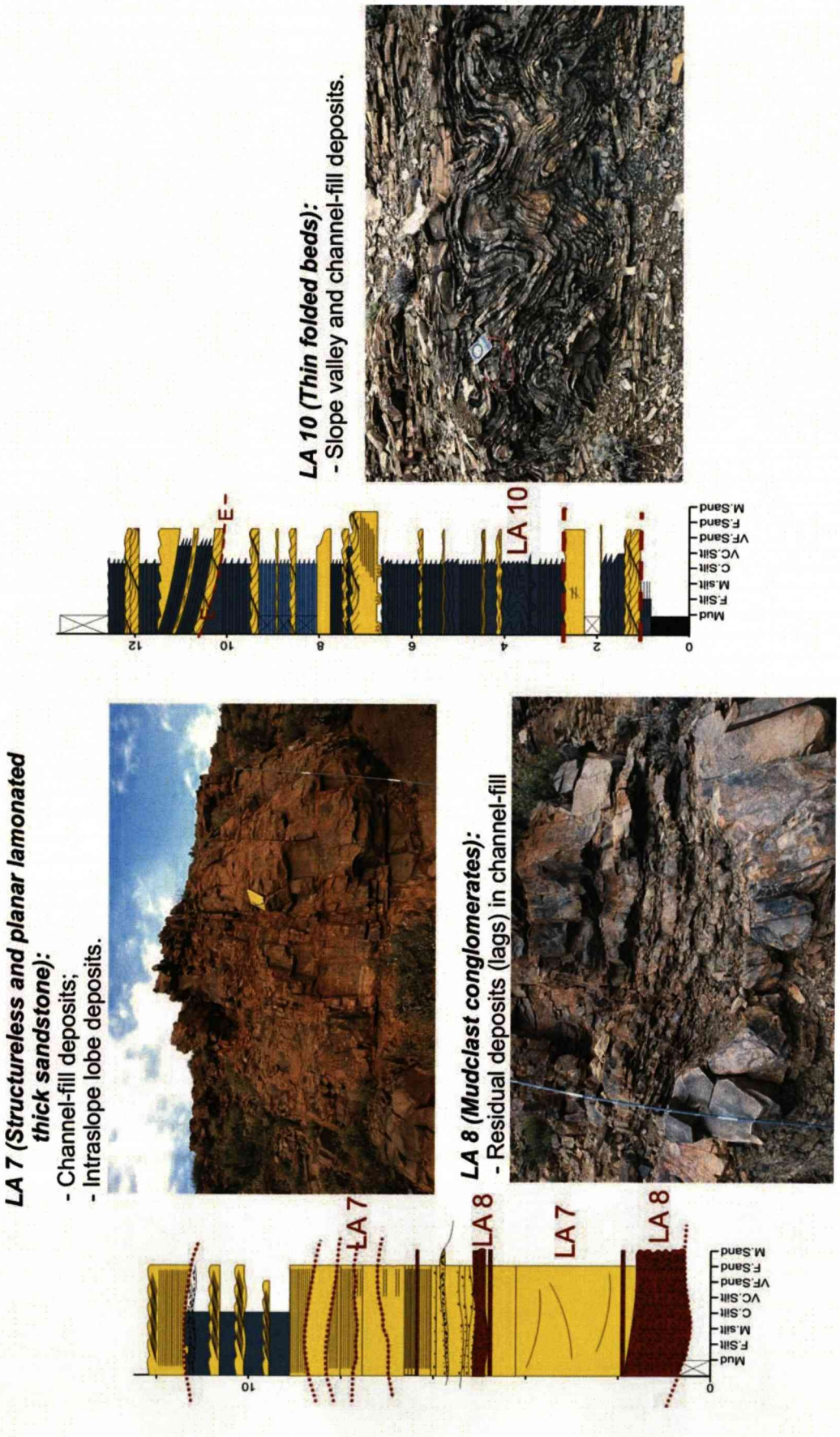

Figure 2.17 – Examples of lithofacies associations in logged sections

Chapter 3 – Depositional environments and sequence stratigraphy of an exhumed Permian mud-dominated submarine slope succession, Karoo Basin, South Africa

Explanatory statement

The bulk of this chapter is in the form of a manuscript that was submitted to and accepted by the Journal of Sedimentary Research, subject to minor revision (current stage: in revision), as allowed by University of Liverpool regulations. The manuscript is entitled Depositional environments and sequence stratigraphy of an exhumed Permian mud-dominated submarine slope succession, Karoo Basin, South Africa, by J.J.P. Figueiredo, D.M. Hodgson, S.S. Flint and J. Kavanagh. The references from the manuscript are presented together with the thesis references at the end of this volume. Some of the manuscript figures are enlarged for the thesis chapter and the figure numbers and sections are reformatted to fit thesis style. The role of each manuscript author was as follows: Jorge Figueiredo: principal investigator, 100% of data collection and interpretation, writer of the manuscript; David Hodgson: mentor, field assistance and extensive manuscript review; Stephen Flint: mentor, field assistance and extensive manuscript review; John Kavanagh: field assistance.

Abstract

The physical stratigraphy of a 470 m-thick, claystone-dominated exhumed middle to upper submarine slope succession was constrained within an area of 400 km^2 in which 5 sand-prone units were characterized (Units D/E, E, F, G, and H). Units D/E to Unit F show an overall pattern of thickening upward and basinward stepping. This stacking pattern is reversed from top Unit F to the base of Unit H, above which basinward stepping is again observed. Different architectural styles of sand-prone deposits occupy predictable stratigraphic positions within the basinward stepping section, starting with intraslope lobes through channel-levee complexes to entrenched slope valleys. Sandstone percentage is highest in the intraslope

lobes and lowest in the slope valley-fills, reflecting a change from depositional to bypass processes. The upper basinward stepping succession (Unit H) is a distributive system possibly linked to a shelf edge/upper slope delta. Across strike complexity in the distribution of sand-prone units was controlled by cross-slope topography driven by differential compaction processes. Hemipelagic claystones separating the sand-prone units represent shut down of the sand delivery to the whole slope and are interpreted as relative sea level highstand deposits. Eleven depositional sequences are identified, nine of which are arranged into three composite sequences (Units E, F, and G) that together form a composite sequence set. The three composite sequences plus one individual sequence (Unit D/E) comprise a composite sequence set. The highly organised physical stratigraphic stacking suggests that glacioeustasy, during the late Permian icehouse period, was the main driving process for the analysed succession.

3.1 - Introduction

Stratigraphic and sedimentological research on the upper reaches of mud-dominated submarine slope settings has increased in the last decade due to the advent of high resolution 3-D seismic datasets. Previously these settings were interpreted simply as zones of bypass of coarse-sediment to the deep basin floor (Walker 1978; Bouma 1979; Pickering et al. 1989; Reading and Richards 1994; Galloway 1998; Bouma 2000), but are now seen as possible sites for accumulation of sand (Prather et al. 1998; Beauboeuf and Friedmann 2000; Mayall and Stewart 2000; Kolla et al. 2001; Fonesu 2003; Abreu et al. 2003; Adeogba et al. 2005; Mayall et al. 2006; Deptuck et al. 2007; Kolla et al. 2007). Seismic datasets have a resolution limit below which the exact nature of the sedimentary system is unclear. Outcrop studies help our understanding of the distribution, architecture and depositional processes of slope sediments (e.g. Cronin et al. 2000; Campion et al. 2000; Beauboeuf 2004; Wild et al. 2005; Shultz et al. 2005; Pickering and Corregidor 2005; Anderson et al. 2006; Moraes et al. 2006; Kane et al. 2007). However, due to exposure limitations most outcrop studies have

concentrated on the coarse-grained and less weathered or covered components, which biases observation of the stratigraphic record. There remains a paucity of detailed outcrop analogues for mud-dominated slope systems. Key questions that require outcrop observations include; what is the lateral distribution of lithofacies in middle/upper slope settings? What factors control the location and timing of deposition and erosion on the middle/upper slope? What is the nature of the fill in entrenched upper slope conduits?

These questions have been addressed in exposures of the Upper Permian Laingsburg Formation of the SW Karoo basin, South Africa (Fig. 3.1), which comprises a regionally well exposed mudstone-dominated succession interpreted as a continental submarine slope setting (Grecula 2000, Grecula et al. 2003; Flint et al. 2007). Regional analyses of the succession have documented aspects of the stratigraphy (Keunen 1963; Theron 1967; Truswell and Ryan 1969, all in Wickens 1994) and detailed work has been completed on basin floor fan and base of slope deposits in the lower part of the Laingsburg Formation (Grecula 2000; Sixsmith 2000; Grecula et al. 2003; Sixsmith et al. 2004).

This paper presents for the first time a detailed, data-driven analysis of the physical stratigraphy of the upper Laingsburg Formation succession. Mapping, logging, and paleoenvironmental reconstructions have established a sequence stratigraphic framework. Controls on the timing and loci for storage and/or routeing of coarse-grained sediments through an upper and middle submarine slope setting are constrained. This was made possible by the unique characteristics of the 400 km2 study area, in which the analysed succession is well exposed on the flanks of regional post-depositional synclines and anticlines, allowing three dimensional control on the down-dip and across strike variations in lithofacies, thicknesses and key surfaces.

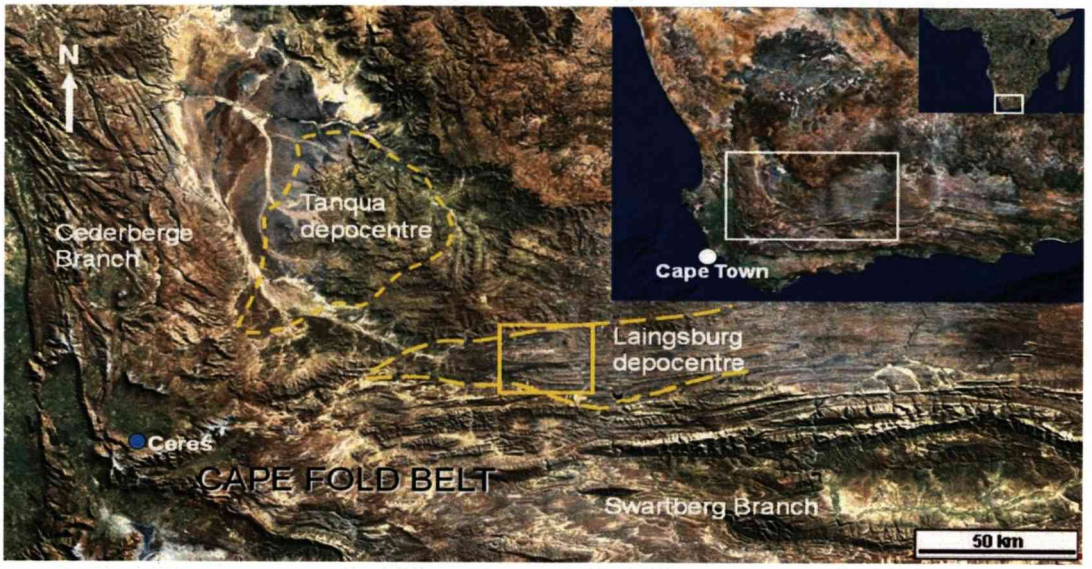

Figure 3.1 – Location map of the Laingsburg depocentre in the SW Karoo Basin, South Africa. Yellow square in Laingsburg depocentre comprises the study area in this work. This area is shown in detail in figure 3.3.

3.2 - Geological and stratigraphical setting of the Laingsburg Formation

The 1200 m thick Laingsburg Formation crops out in the SW Karoo basin, and forms part of the Ecca Group, a siliciclastic sedimentary succession underlain by glaciogenic deposits of the Dwyka Group and overlain by fluvial deposits of the Beaufort Group (Fig. 2). These 3 groups comprise the Karoo Supergroup, the late Carboniferous to late Triassic fill of the basin (Visser 1993; Veevers et al. 1994; Visser 1995). Traditionally, the Karoo basin has been interpreted as a retro-arc foreland basin (Johnson 1991; De Wit and Ransome 1992; Veevers et al. 1994; Visser and Praekelt 1996; Catuneanu et al. 1998; Catuneanu, 2004). Tankard et al. (2009) present an alternative interpretation for the tectono-sedimentary evolution of the Karoo Basin dividing it into pre-foreland phase (Dwyka, Ecca and lower Beaufort Groups) and foreland phase (upper Beaufort Group). According to these authors the pre-foreland Karoo Basin formed within the continental interior of Gondwana as a result of vertical motion of rigid blocks and intervening crustal faults, and the foreland Karoo Basin formed as a response to the uplift of the Cape Fold Belt during the early Triassic. This model is supported by provenance studies (Van Lente 2004) that suggest the Cape Fold Belt was not an emergent source area during Ecca Group time.

In the Laingsburg area Wickens (1994) recognised four regional sand-prone turbidite units overlying distal turbidites of the Vischkuil Formation and labelled them "Fans" A (base) to D (top). More recent studies interpreted Fan A (Sixsmith 2000; Sixsmith et al. 2004) and Unit B (Grecula 2000; Grecula et al. 2003) as basin floor fan and toe of slope deposits, respectively, forming the lower part of a complete deepwater basin floor to shelf succession. Units C and D have been interpreted as lower to mid slope settings by Flint et al. (2007). The 470 m thick upper Laingsburg Formation presented here is bounded at the base by Unit D and to the top by the base of the deltaic deposits (Fig. 3.2). The depositional context of the study succession is therefore middle to upper submarine slope.

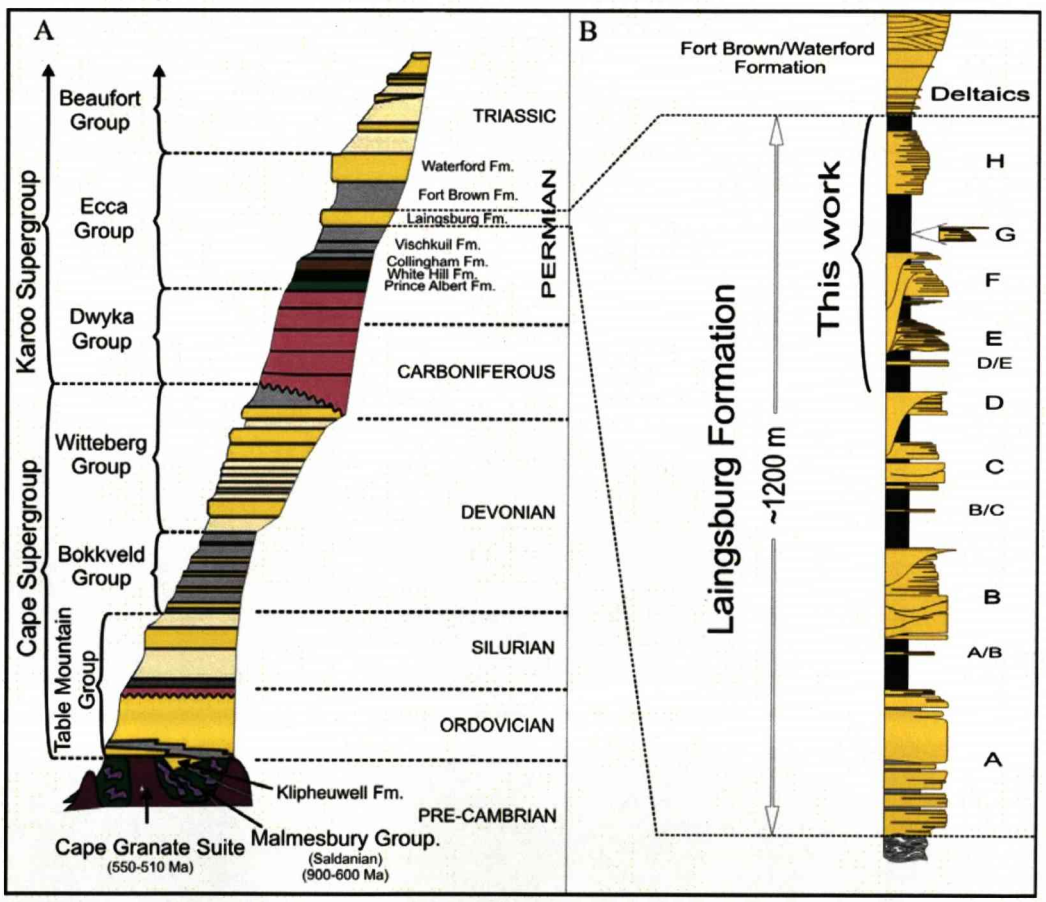

Figure 3.2 - A: regional lithostratigraphy of the Western Cape Province (modified from Wickens, 1994). B: Lithostratigraphy of the Laingsburg Formation (Data from Fan A to Unit D compiled from Sixsmith et al. (2004); Grecula et al. (2003); Flint et al. (2007). From D to the deltaic deposits: this work).

3.3 - Methodology

The study area (20 km W-E by 20 km N-S) comprises E-W trending, gently eastward plunging post-depositional folds named from the north the Heuningberg anticline (northern study area) the Zoutkloof syncline (central study area) and the Baviaans syncline (southern study area) (Fig. 3). Topographic ridges are formed by sand-prone units and the lows between them usually represent hemipelagic claystones (Wickens 1994; Grecula 2000; Grecula et al. 2003).

Aero-photographic interpretation was integrated with field-based sedimentological and stratigraphic observations, including more than 14 km of logged sections, more than 1,200 paleocurrent measurements, and mapping of sedimentary body geometries and key surfaces for 10s of km (Fig. 3). The initial objective was to establish a reliable stratigraphic framework for the 470 m thick succession between Unit D and the deltaic deposits, which was achieved by accurately measuring the thicknesses of hemipelagic claystone units and sand-prone units and walking these bodies out across the study area.

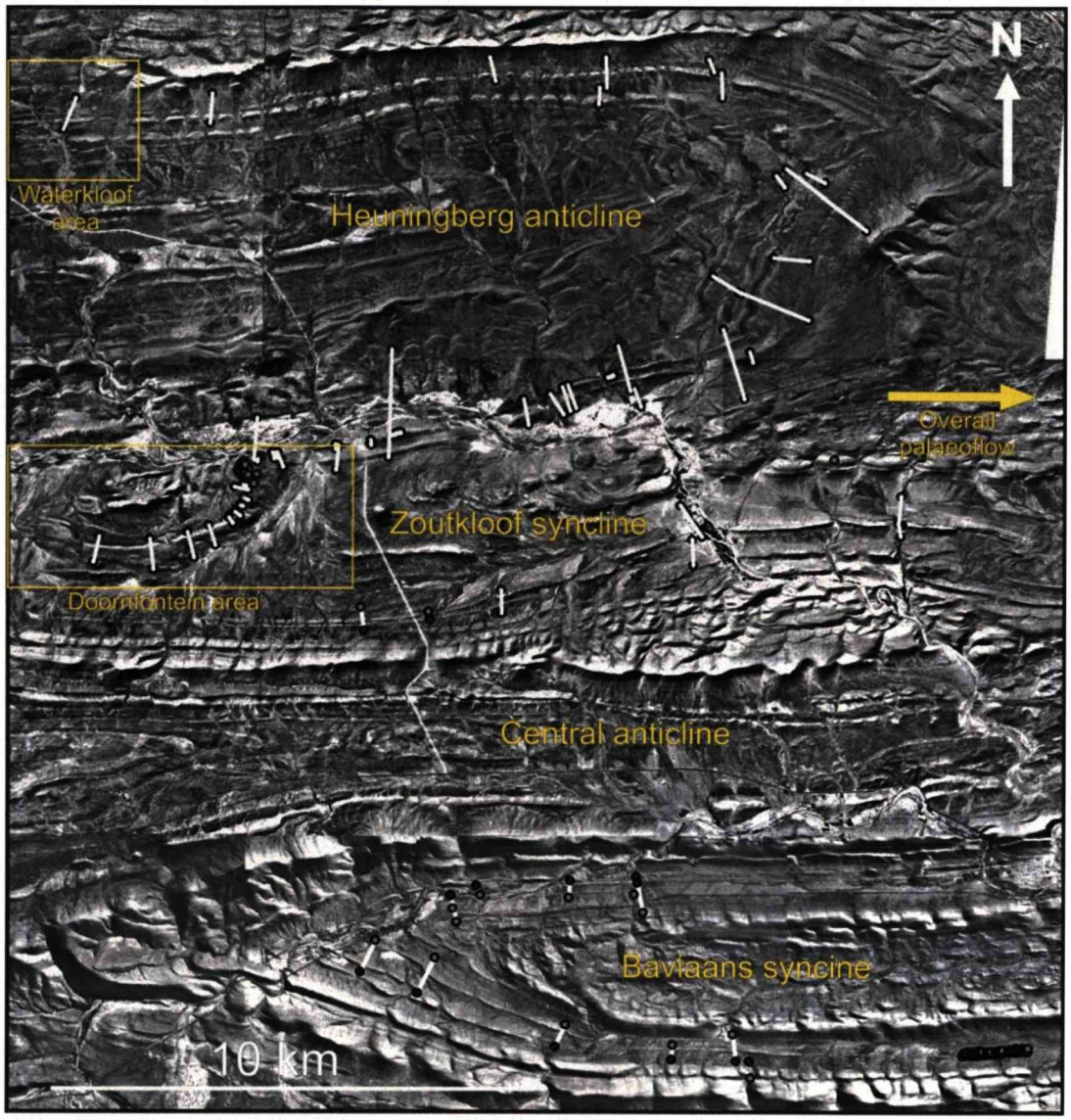

Figure 3.3 – Mosaic of aerial photos showing the study area. The area comprises approximately 400 km^2 and is the same area of the small red square in figure 3.1. Logged section tracks are depicted in whitish lines between dots that represent UTM coordinates of the base and tops of the logs. These points were plotted on the aerophotos using ARC-GIS software (Appendix 3 present a complete spreadsheet for the UTM coordinates).

3.4 - Sedimentology and depositional environments

The sand-prone units were described and interpreted according to their lithofacies and lithofacies association distributions (description and interpretation presented in chapter 2), external and internal architecture, geometries and palaeo-flow directions (Appendix 1). The results were integrated to develop a stratigraphic model for environments of deposition, and evolution of the submarine slope and relative timing of sand storage and bypass into the deeper basin.

Table 3.1 presents a classification for bed thicknesses (based on Stow 2005) referred in the text hereafter.

Centimetre	Thickness	Classification
>100	Very thick	Beds
30 – 100	Thick	
10 – 30	Medium	
3 – 10	Thin	
1 – 3	Very thin	

Table 3.1 – Bed thicknesses defined in this work, based on Stow (2005).

3.4.1 - Claystone Units

Observations: Monotonous dark grey claystone deposits of lithofacies association 1 (LA 1) separate sand-prone units and are called inter-unit claystones. Claystone units are also found within sand-prone units and these are referred to as intra-unit claystones. The inter-unit claystones range from 18 m to 110 m in thickness while the intra-unit claystones are ≤5 m thick. The cumulative thickness of claystone between top Unit D and the base of the deltaic deposits is similar across the 400 km^2 study area, ranging from 210 m in the north to 225 m in the south (this difference is within measurement error, given variable exposure and structural dip). However, as the number and stratigraphic position of the sand-prone units vary across regional depositional strike so does the number of claystone units (Table 3.2).

Interpretation: The claystone units are interpreted to be hemipelagic drapes due to the uniform fine grain size, absence of siltstone, absence of tractional sedimentary structures, and consistent thickness. The uniform

cumulative thickness of the hemipelagic claystones between northern and southern study areas provides a relative temporal framework for the sand-prone units and the intra-unit claystone allow division of the sand-prone units into mappable sub-units (see below).

Northern study area	Central study area	Southern study area
D – D/E = 45 m	*D/E not present*	*D/E not present*
D/E - E = 20 m	D – E = 60 m (cumulative)	*E not present*
E – F = 25 m	E – F = 30 m	D – F = 90 m (cumulative)
F – H = 95 m (cumulative)	F – H = 100 m (cumulative)	F – G = 40 m
G not present	*G not present*	G – H = 70 m
G – Deltaics = 20 m	G – Deltaics = 25 m	G – Deltaics = 20 m
Cumulative thickness = 205 m	Cumulative thickness = 215 m	Cumulative thickness = 220 m

Table 3.2 - Average of claystone thicknesses through the study area. Cumulative thickness means that the claystone interval represents the cumulative thickness of two or more claystone units.

3.4.2 - Sand-prone Units

Between the top of Unit D (*sensu* Grecula 2000 Grecula et al. 2003; Flint et al. 2007) and the base of the deltaic deposits, five sand-prone units are described and interpreted (Fig. 3.2). Units E and F were described briefly by Grecula (2000) but the increased stratigraphic control afforded by mapping of the claystone units here has identified three new sand-prone units informally referred to as Units D/E, G and H (Fig. 3.2; Enclosure 1A). The first (Unit D/E) lies between units D and E and is present only in the northern study area (around the Heuningberg anticline). Unit G lies above Unit F but its occurrence is restricted to the southern study area (Baviaans syncline). Unit H is the youngest newly identified unit and is present across the whole study area. Detailed mapping has also shown that Unit E is not present in the south, having been miscorrelated by previous authors with Unit F.

3.4.2.1 - Unit D/E

Observations: Unit D/E overlies a ~45 m thick claystone unit above Unit D around the Heuninberg anticline. On the southern flank and southern nose of the anticline, D/E comprises lithofacies association 6 (LA 6) with a sharp but non-erosive base and a sharp top. Its maximum thickness is ~8 m and the unit can be walked out for more than 5 km parallel to paleoflow

without changes in geometry or lithofacies (Enclosures 1A, 2A). Internally D/E is composed of 0.3 m – 1.0 m thick beds of fine-grained sandstone that amalgamate to form bedsets which commonly are separated by siltstone (<0.2 m). Bedsets have broad tabular geometries that thin gently over tens of metres. On the northern flank of the Heuningberg anticline Unit D/E is composed of LA 4, being finer grained and more thinly bedded than on the southern flank, and passes gradually westward into siltstone (LA 2), thinning to 2 m. Paleoflow indicators are to the east (Fig. 3.5; Appendix 1). The overall percentage of sandstone in Unit D/E based on data from logged sections is 90%.

Interpretation: The dominance of lithofacies association LA 6, lack of incisional surfaces, and tabular geometry support an interpretation of Unit D/E as a submarine lobe (following Prélat et al. 2009). The internal architecture with bedsets of sandstone separated by thin beds of siltstone suggests that the lobe is composed of smaller elements that are interpreted as lobe elements (Prélat et al. 2009). Lithofacies associations on the northern flank suggest a lobe fringe setting. As no evidence of younger channels was found in either lobe axis or lobe fringe areas, Unit D/E is interpreted as a terminal lobe (Figs. 3.5, 3.6). Regional control and previous work (Grecula 2000; Grecula et al. 2003; Flint et al. 2007) indicate that this distributive system occupies an intraslope rather than a basin floor setting.

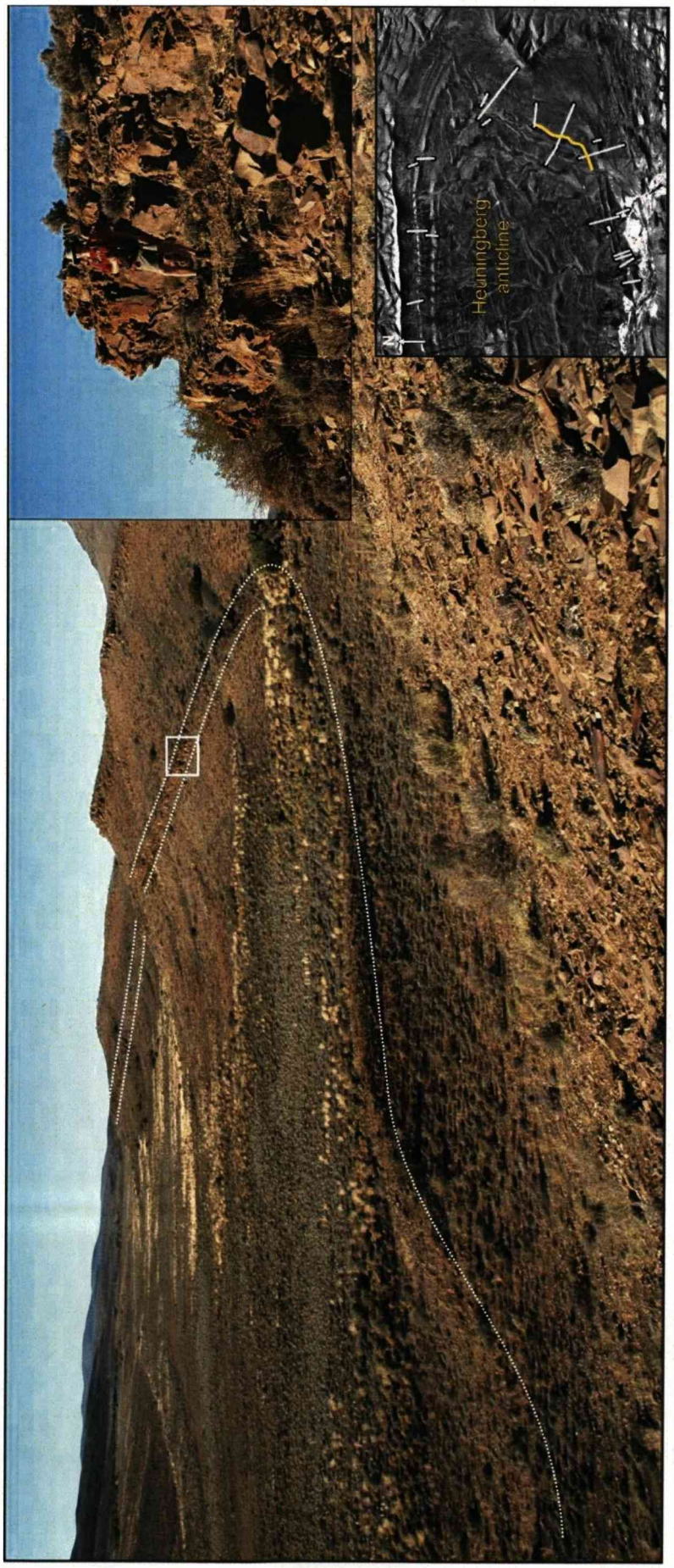

Figure 3.4 – Outcrop expression of Unit D/E. Two roughly parallel white dotted lines define the unit showing very small variation in thickness. Upper right inset shows lithofacies association LA 6 characteristic of D/E. The yellow line on the aerial photo in the lower right inset shows the position of the outcrop on the southern flank and nose of Heuningberg anticline.

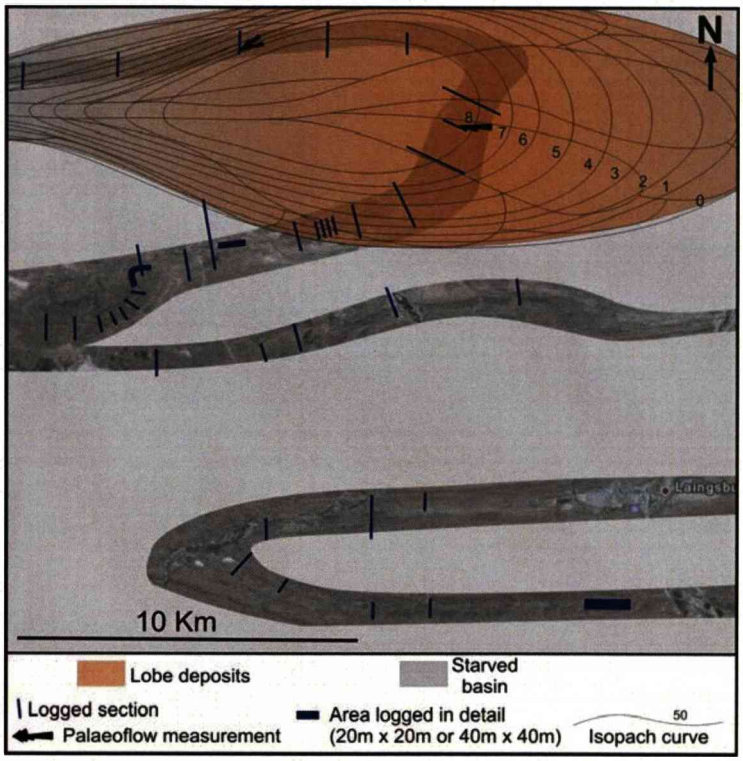

Figure 3.5 – Palaeo-environmental and isopach maps of Unit D/E, interpreted as terminal intraslope lobe. Smaller geometries within the lobe are interpreted as lobe elements.

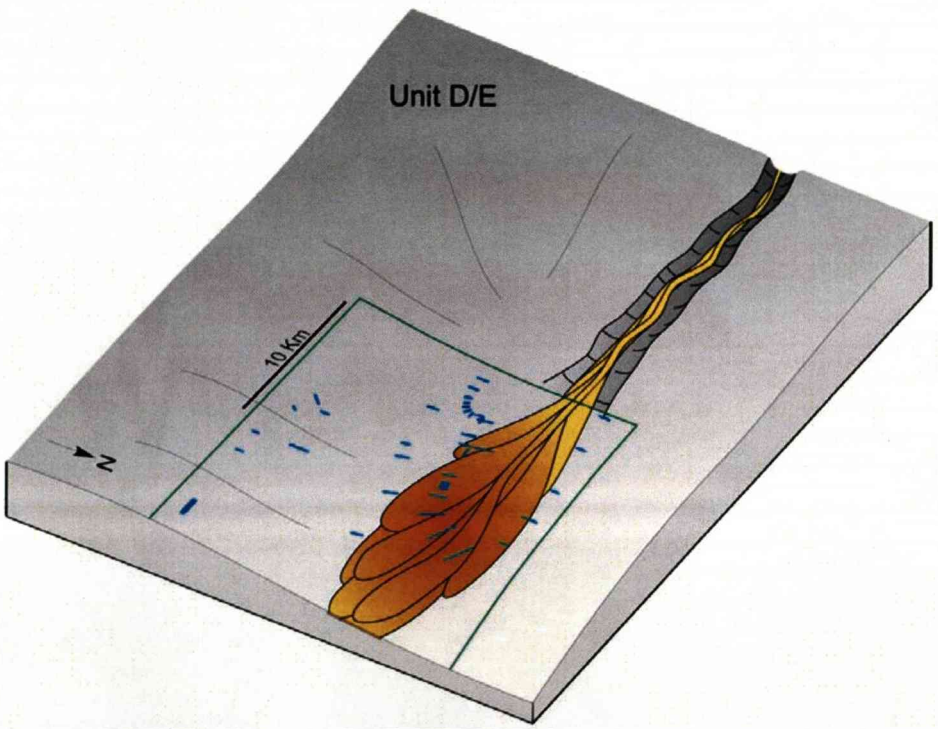

Figure 3.6 – Three dimensional reconstruction of D/E terminal intraslope lobe. Down-dip is to east. Localised north-facing slope (discussed in section 3.5.1) favours the formation of a step (local depocentre) in the slope that controlled deposition of the D/E lobe. Green square represents the analysed area and blue lines represent logged sections (these features are common to all 3D diagrams hereafter).

3.4.2.2 - Unit E

Unit E is present in the northern (Heuningberg anticline) and central (Zoutkloof syncline) study areas. In the north it overlies an 18-20 m thick inter-unit claystone above Unit D/E. In the central area, Unit E is the first sand-prone unit above Unit D; they are separated by 60-65 m of claystone (the same thickness as the combined Unit D-to-Unit D/E and Unit D/E-to-Unit E claystones in the north; table 3). Unit E thins and fines southward from 100 m on the northern flank of the Heuningberg anticline, to 40 m in the central area (Zoutkloof syncline). It is absent in the southern area (Baviaans syncline; Enclosure 1 - 4).

Around the Heuningberg anticline Unit E is divided into three sand-prone sub-units (called E1, E2 and E3; Enclosures 1A/B, 4) by two thin (~0.6 m), extensive intra-unit claystones (the lower and upper E claystones). In the Zoutkloof syncline only one internal claystone was identified which separates E into two sand-prone sub-units. These are correlated as E2 and E3 since E1 thins southward and is interpreted to have pinched out somewhere between southern Heuningberg and Zoutkloof (Enclosures 2B, 4).

E1: Observations

Sub-unit E1 is similar to D/E in geographical location, lithofacies associations distribution and geometrical characteristics (Figs. 3.7, 3.8, 3.9). However the contacts between beds are more erosive in E1 than in D/E. Also, in some locations on the nose of the Heuningberg anticline erosional surfaces cut through E1 and into the underlying inter-unit claystone (maximum incision of ~10 m), and are filled with LA 7. The fills of these erosional surfaces, like the rest of E1 in this area, are overlain by the lower E intra-unit claystone. Paleocurrents range from ENE to ESE (Fig. 3.8; Appendix 1). The overall sandstone percentage in E1 is 90%.

E1: Interpretation

Following the same principles as for Unit D/E, E1 is interpreted as a distributive lobe composed of internal lobe elements (Figs. 3.8, 3.9). The erosional features filled with LA 7 are interpreted as E1-aged channels

because the overlying lower E intra-unit claystone is not cut by them. Because of their depth of incision (deeper than the base of the Unit) it is difficult to envisage these channels as distributive channels genetically linked to the lobe and so they are interpreted as slightly younger bypass channels. This interpretation classifies E1 as a transient intra-slope lobe (e.g. Adeogba et al. 2005; Fonesu 2003), in which the channels bypass sediment through the lobe area to feed more distal sites.

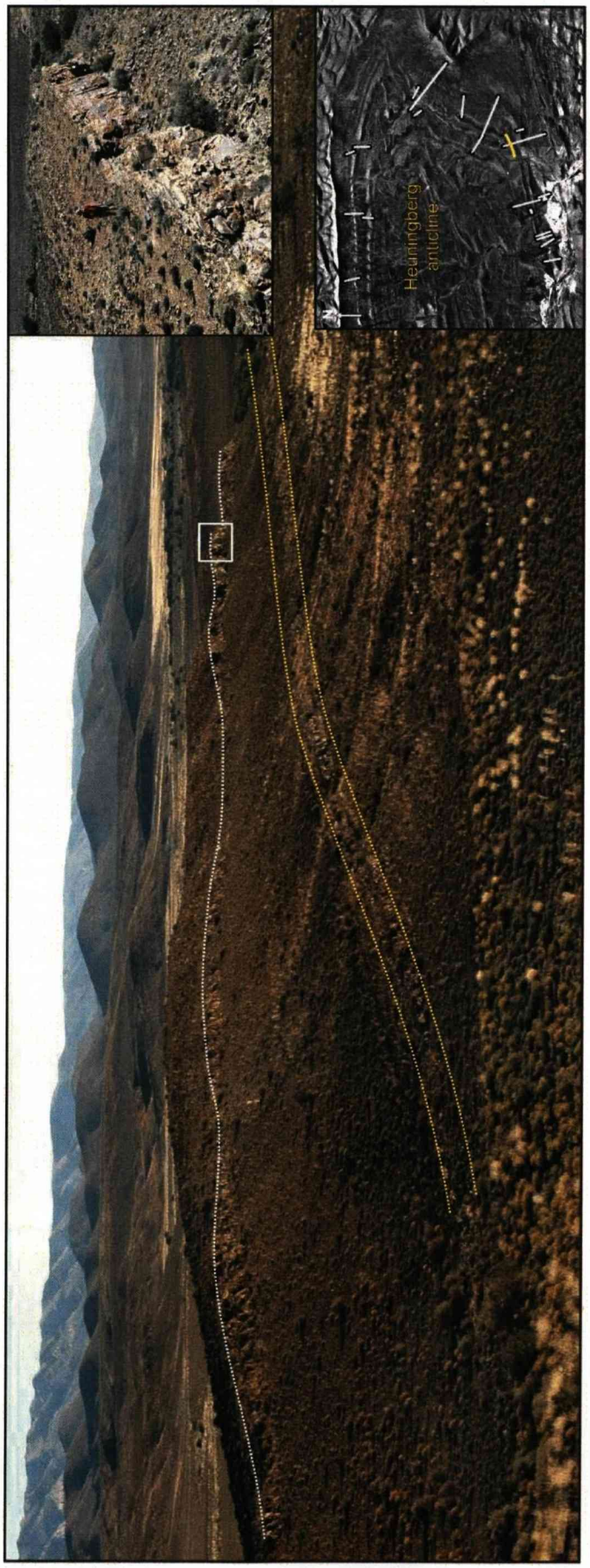

Figure 3.7 – Outcrop expression Units E1, D/E, and the intervening hemipelagic claystone. Subtle wavy white dotted line marks the top of Unit E1 that is intermittently cut by the younger Unit E2 (the lithological content of E2 in this location is predominantly LA 4). Two roughly parallel yellow dotted lines encase Unit D/E showing very small variation in thickness. Upper right inset shows lithofacies association LA 6, characteristic of E1. The yellow line on the aerial photo in the lower right inset shows the position of the outcrop on the southern flank and nose of the Heuningberg anticline. Unit E1 is separated from Unit D/E by a ~20 m thick layer of hemipelagic claystone.

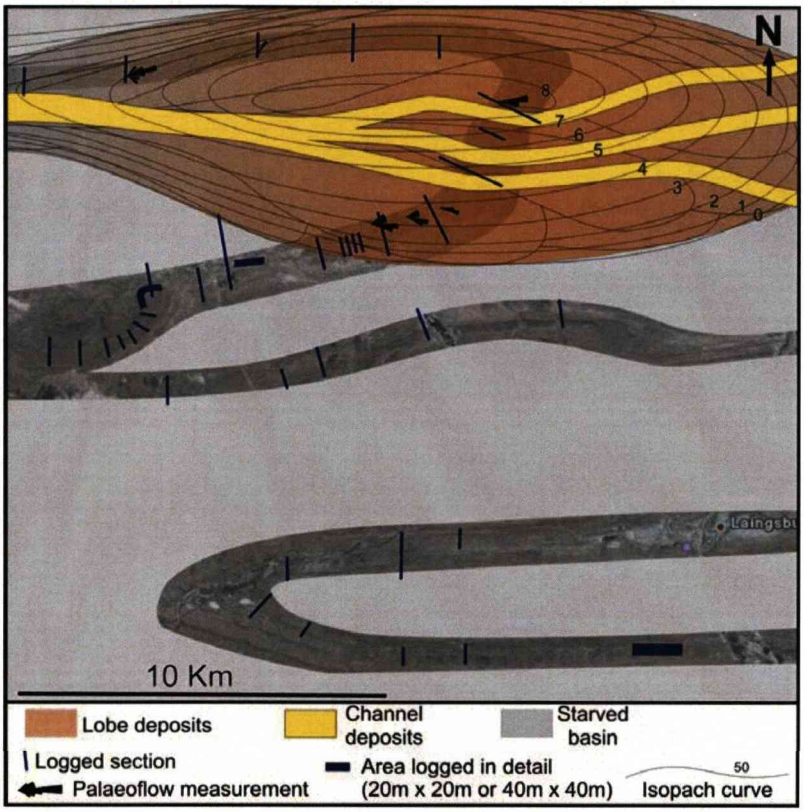

Figure 3.8 – Palaeo-environmental and isopach maps of Sub-unit E1. Due to the presence of interpreted bypass channels this Sub-unit is interpreted as a transient intraslope lobe. Smaller geometries within the lobe are interpreted as lobe elements.

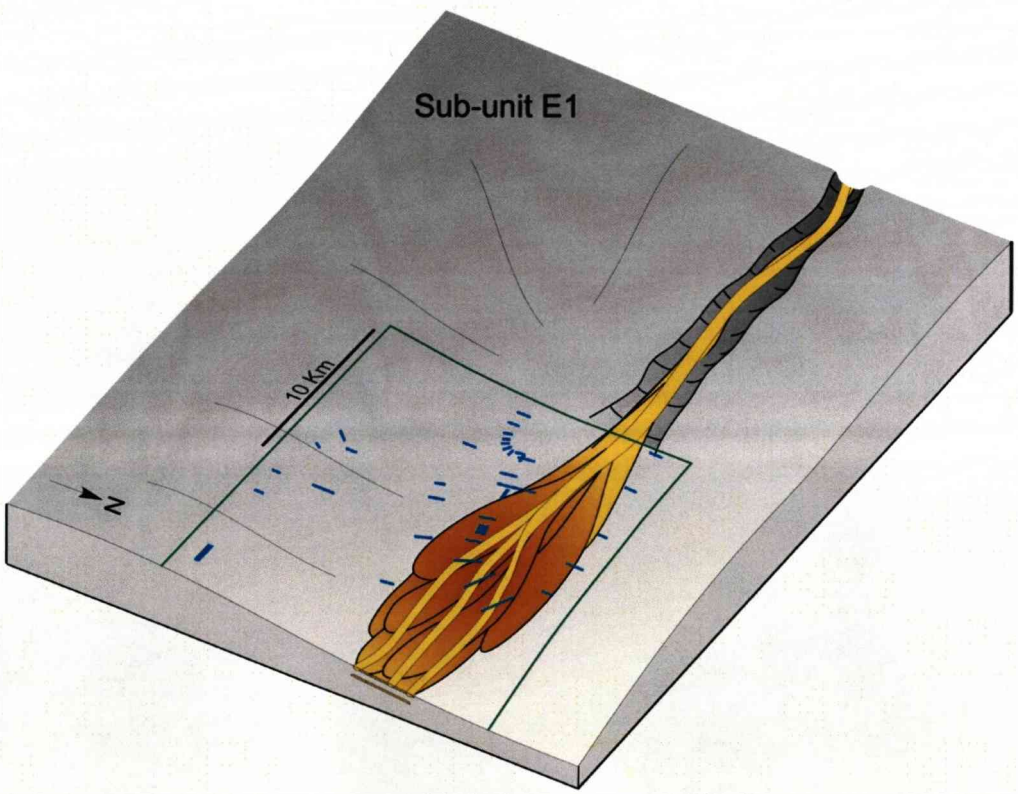

Figure 3.9 – Three dimensional reconstruction of E1 transient intraslope lobe. Similar to D/E lobe, a step in the slope (local depocentre) is interpreted to have controlled the E1 lobe deposition.

E2: Observations

In the northern and central areas E2 comprises: (1) mainly heterolithic lithofacies association LA 4 that onlaps erosional surfaces and more commonly is truncated by them; and (2) LA 7, found only overlying erosional surfaces (Enclosure 1B). Paleoflow indicators, mainly from ripple lamination, range from ENE to ESE (Fig. 3.10; Appendix 1).

Around the Heuningberg anticline E2 varies from 25-30 m thick on the northern flank to 13-24 m on the southern flank (Enclosures 1B, 2A). On the northern flank the upper E claystone is continuous but the lower E claystone is locally truncated by intra-E2 erosional surfaces that are overlain by LA 7. These erosional features appear intermittently along the northern flank and around the nose of the Heuningberg anticline (Enclosure 1B). Similar erosional features are observed in the eastern portion of the southern flank, but here they are overlain by LA 4 (Enclosure 2A).

At Doornfontein farm (Fig. 3.3) the upper E claystone is present, but the lower E claystone is absent, indicating that in this area the base of Unit E is E2 in age. Here, E2 is ~20 m thick and erosive based (log HBS10 in enclosure 2A). In the central study area (Zoutkloof syncline) the same field relations are found (i.e. E2 is the basal Sub-unit of Unit E), but here E2 is heterolithic and thins eastward from 6 m to 1 m (Enclosure 2B). The overall sandstone percentage in E2 is about 40%.

E2: Interpretation

Sub-unit E2 is markedly different from E1 and Unit D/E in terms of geographic extent, thickness, geometry of the sand-prone bodies, distribution of lithofacies associations, and dimensions of erosional features. The pattern of erosion of E2 into E1 along both flanks of the Heuningberg anticline and the palaeoflow indicators suggest two sub-parallel E-W trending channel belts (Figs. 3.10, 3.11). Delimiting the margins of the channel belts is problematic because the fills are heterolithic in places (therefore not well exposed) and the channels run sub-parallel to the flanks of the post-depositional fold.

The characteristics of the adjacent heteroliths leads to two possible interpretations: (1) distributive lobe fringes cut by younger channels; or (2)

levee-overbank deposits genetically related to the adjacent channels. The predominance of climbing ripple lamination in medium/thin beds of LA 4 suggests a high rate of deposition as commonly found in levee deposits (Posamentier and Walker 2006; Kane et al. 2007). The geometry of E2, which forms a wedge, thinning to the south, is typical of levee-overbank geometry. The bedding in the wedge fines and thins stratigraphically and in the same direction as the wedge thins. The deeper incision of the E2-channels compared to E1-channels suggests a more proximal environment. These three lines of evidence support the interpretation of a levee-overbank environment for the heteroliths adjacent to the channel-fills in E2 (Figs 3.10; 3.11).

E3: Observations

Sub-unit E3 is the thickest component of Unit E and is bounded at the base by the upper E claystone and capped by the E-F inter-unit claystone. E3 thins from ~60 m on the northern flank of the Heuningberg anticline to ~30 m in the Zoutkloof syncline and is not present in the Baviaans syncline (Enclosure 1A/B, 2A/B, 4). On the northern flank and nose of the Heuningberg anticline E3 is dominated by fining- and thinning-upward LA 4 to LA 2 deposits with no evidence of erosion (Enclosure 1B). Paleocurrents from ripple lamination range from ENE to E (Fig. 3.12; Appendix 1). On the southern flank E3 is absent for ~4.1 km due to incision on a younger erosional surface (Enclosure 2A).

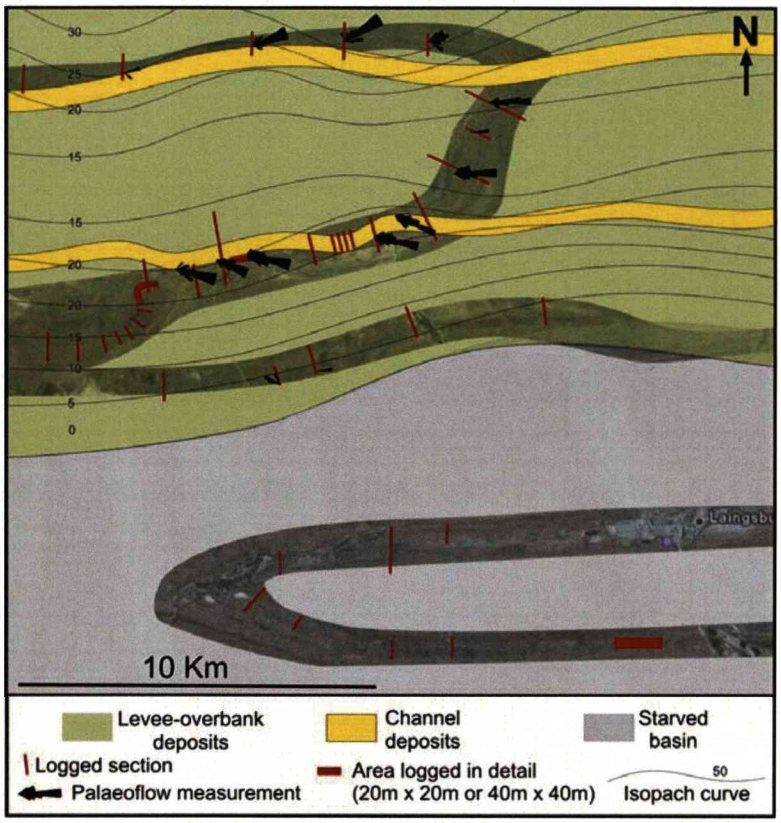

Figure 3.10 – Palaeo-environmental and isopach maps of Sub-unit E2 interpreted as channel-levee systems.

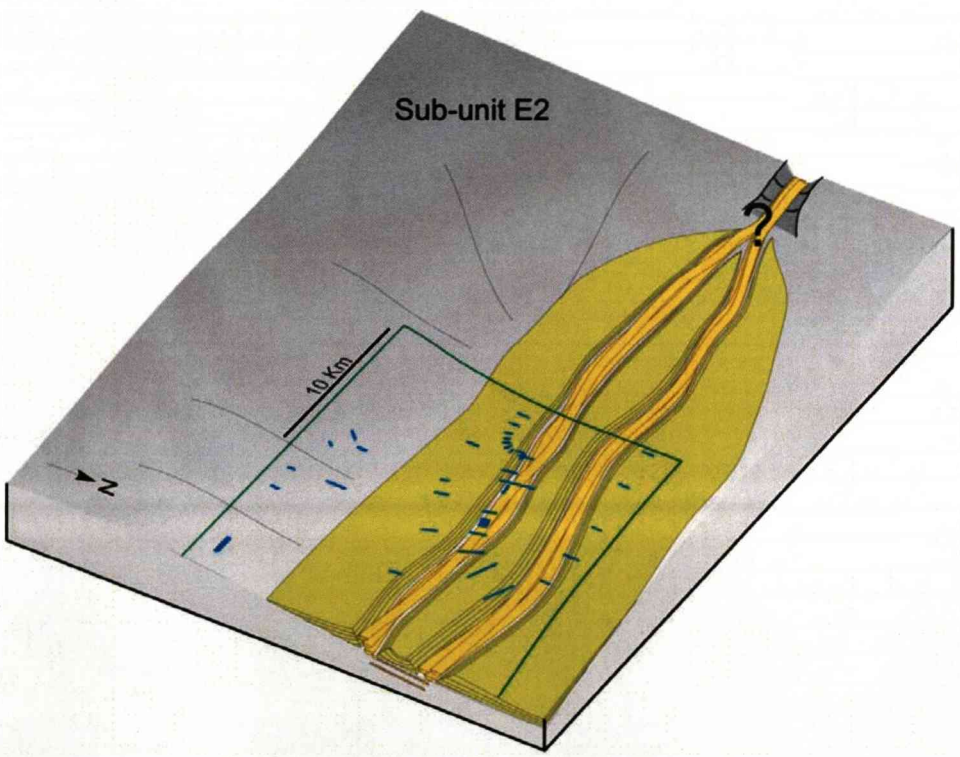

Figure 3.11 – Three dimensional reconstruction of E2 channel-levee system. E2 is not present in the southern area suggesting control of the local northern depocentre on its deposition.

On Doornfontein farm (Fig. 3.3) E3 truncates E2 and possibly E1, with a minimum incision depth of 25 m (base not exposed; log HBS15 in enclosure 2A). Paleocurrents from ripples in this area range from E to ESE (Fig. 3.12; Appendix 1). In the Zoutkloof syncline, E3 is dominated by LA 4 and LA 2, but locally, thick-bedded sandstones (LA 7) overlie erosional surfaces that cut into E2 (Enclosure 2B). Paleocurrents from flute casts and ripple lamination range from NE to SE (Fig. 3.12; Appendix 1). E3 has an overall sandstone percentage of ~30%.

E3: Interpretation

Similarly to Sub-unit E2, thick-bedded sandstones (LA 7) overlying erosional surfaces in the northern and central areas are interpreted as E-W trending slope channel-fills and the volumetrically dominant heteroliths (LA 4 and LA 2) are interpreted as adjacent levee-overbank deposits (Figs. 3.12; 3.13). The thickness and the depth of incision of E3 channels in southern Heuningberg suggest more proximal and energetic conditions than in E2.

The E3 levee forms a wedge that fines, thins and eventually pinches out to the south (Enclosure 1A). A channel cuts through almost midway across this levee wedge (southern flank of Heuningberg; Enclosure 2A), however its incisional depth is much less than the thickness of the levee deposits to the north (Enclosure 1B). A possible explanation is that the main channel system to the large levee lies in the subcrop to the north of the Heuningberg anticline and the channel in the middle of the levee-overbank wedge is a smaller crevasse channel from the main system that breached the levee up-dip from the study area (Fig. 3.13).

The overall stratigraphic organization of the sedimentary package with Unit D/E interpreted as a terminal frontal lobe and E1 as a transient lobe indicates basinward stepping of the depositional system. After deposition of D/E and E1 as intra slope lobes the available accommodation for this kind of deposits seems to have been filled, leading to the change in style of deepwater deposition to channel/levee systems. In this context Unit E is interpreted to record 3 stages of basinward stepping of a deepwater slope system: lobes with small and high aspect by-pass channels (E1); high aspect

ratio channel-levee complex (E2), low aspect ratio channel-levee or crevasse channels in levee from major channel system (E3).

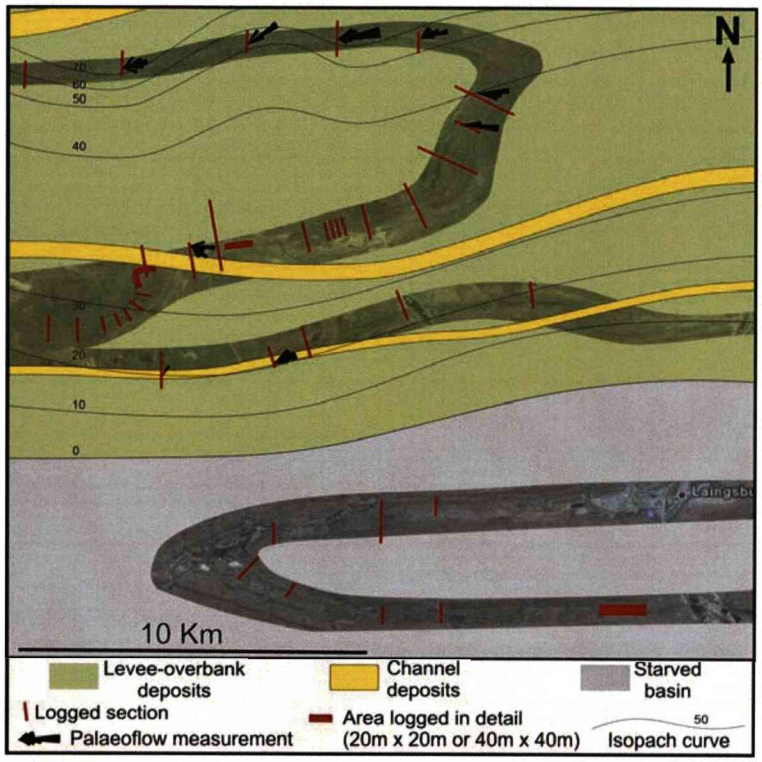

Figure 3.12 – Palaeo-environmental and isopach maps of Sub-unit E3 interpreted as channel-levee systems.

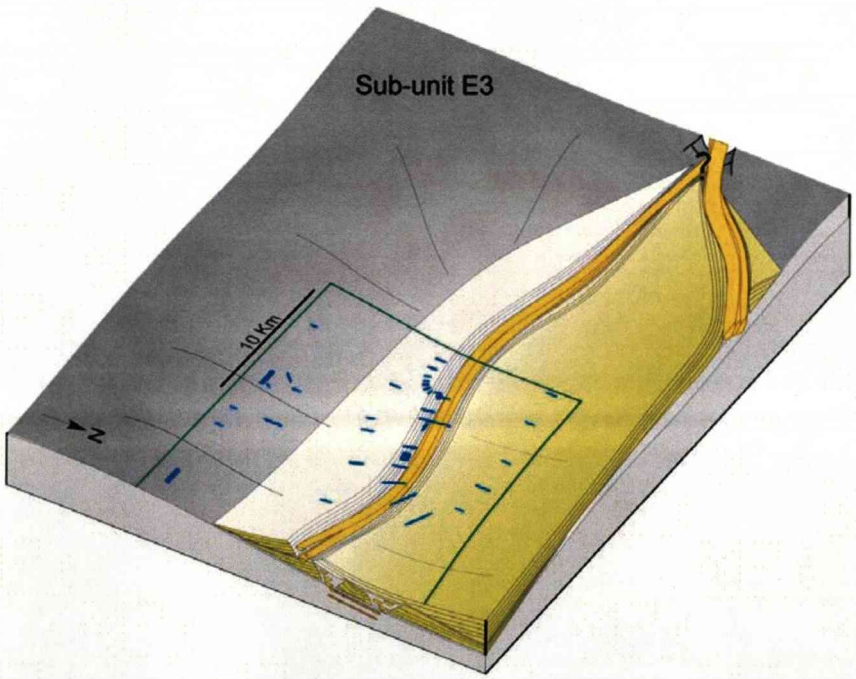

Figure 3.13 – Three dimensional reconstruction of E3 channel-levee system. The northern depocentre still controlled the deposition of E3 channel complex. It is speculated that an up-dip avulsion of the major channel in E3, which would have run (overall W-E trend) to the north of the study area (see interpretation in the text), influenced the deposition of this system.

3.4.2.3 - Unit F

In contrast to the underlying units, Unit F is identified over the entire study area (Enclosures 1- 4). Therefore, it is the third unit stratigraphically above Unit D in the north, the second in the central area, and the first in the south. The thickness of the claystone between Units E and F ranges between 26 m and 30 m around the Heuningberg anticline and the Zoutkloof syncline respectively. In the Baviaans syncline there is ~90 m of claystone between Unit D and Unit F (Table 3.2). Like Unit E, F can be divided into three sand-prone sub-units (F1, F2, and F3) separated by two intra-unit claystones comprising (LA 1) and (LA 2) (Enclosures 1 – 4).

F1: Observations

Sub-unit F1 is present over the whole area and is composed only of heterolithic lithofacies associations, predominantly LA 2 (Enclosures 1 – 4). In some locations, mainly where F1 is thicker, LA 4 is also present. In these cases LA 2 thickens and coarsens upward into LA 4. Thickness is typically less than 10 m, but in some locations (western Heuningberg; Enclosures 1B, 2A) it is ~15 m. The contact of F1 with the underlying claystone is transitional and non-erosive. Throughout the study area no erosion surfaces of F1 age were observed. Palaeocurrents from ripple lamination and flutes in the southern Baviaans syncline range from NE to ESE (Fig. 3.14; Appendix 1) but elsewhere there are very few palaeoflow indicators. The overall sandstone percentage in F1 is 10%.

F1: Interpretation

This Sub-unit is markedly different from E3 and E2. It does not present the characteristic wedge geometry of E3 and E2, but is present across the study area with subtle variation in thickness. No channels are present. The heteroliths coarsen and thicken upward, in contrast to E3 and E2. Therefore, F1 is not interpreted as levee deposits but rather as the fringes of a distributive system deposits (Figs. 3.14, 3.15).

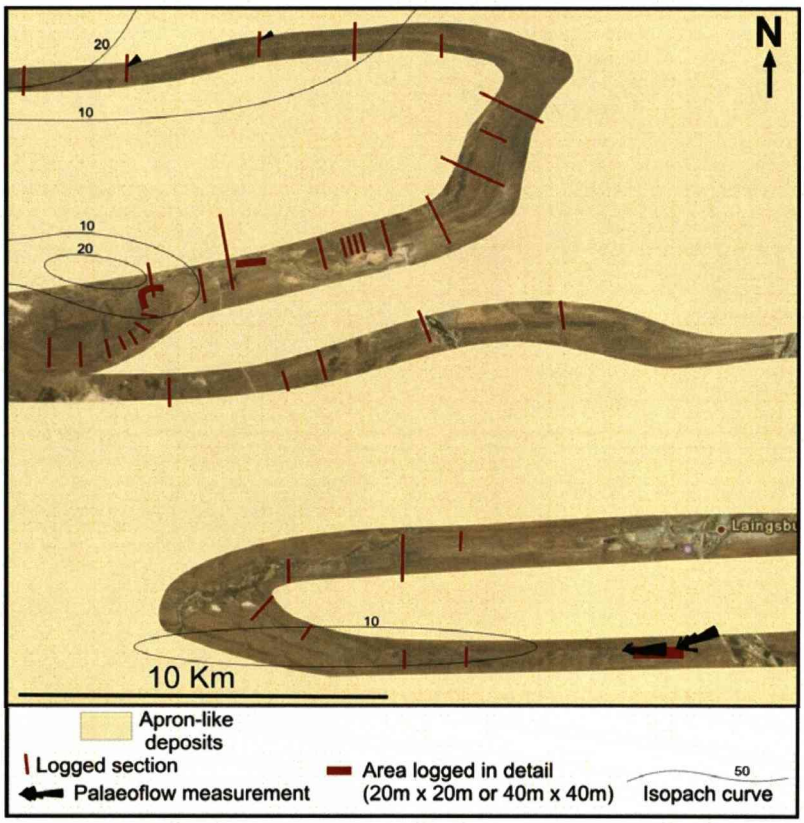

Figure 3.14 – Palaeo-environmental and isopach maps of the F1 distributive system.

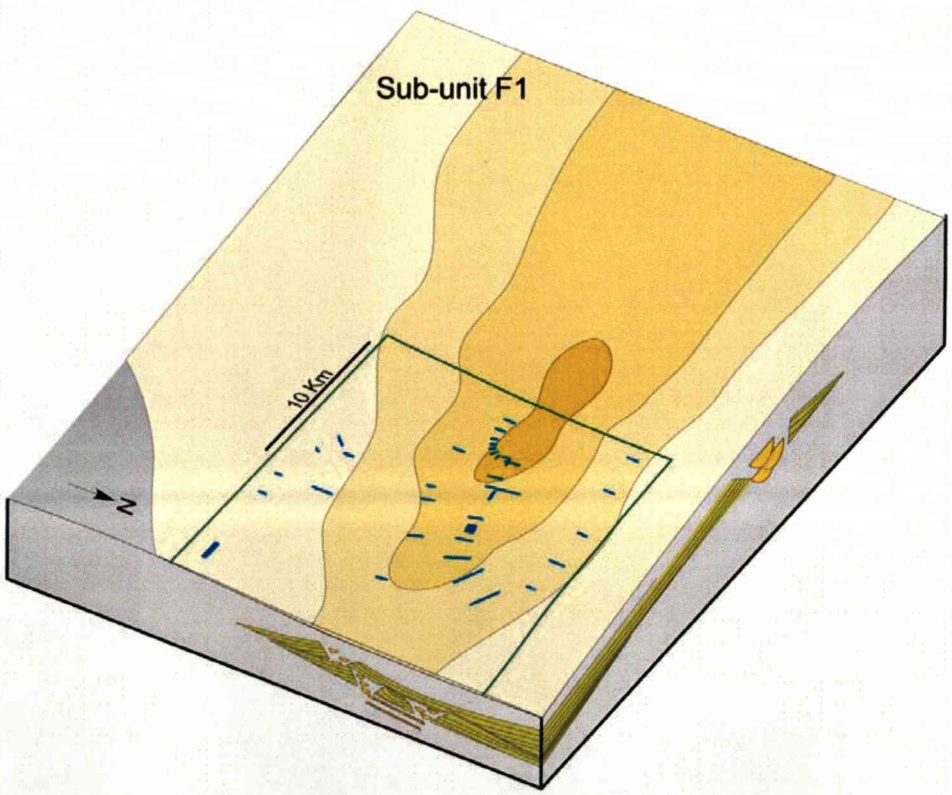

Figure 3.15 – Three dimensional reconstruction of F1 distributive system. Colour grading represents relative thickness of the unit (the darker the colour, the thicker the unit). An influence of the northern depocentre on F1 deposition is still evident but it was mapped across the whole study area.

F2: Observations

Sub-unit F2 on the northern flank and nose of the Heuningberg anticline is dominated by a 25-45 m thick package of LA 4 and LA 2 (dominant) in an overall thinning- and fining-upward pattern. No erosional surfaces are observed and palaeocurrents range from NE to ESE (Enclosure 1B, 4; Fig. 3.18; Appendix 1).

Along the southern flank of Heuningberg a surface marked by abrupt termination of lithofacies and truncation of several underlying lithostratigraphic units can be mapped. Although the surface is only directly exposed locally, mapping of overlying and underlying claystone units and sand-prone units (F1, E3, E2, E1) indicates a steep, stepped erosion surface with a flat base that cuts out ~150 m of underlying stratigraphy (to below the base of Unit E) and is 4.1 km wide (oblique dip width; Enclosures 2A, 4). The distribution of lithofacies in the fill of the erosional relief is variable (including LA 10, LA 9, LA 8, LA 7, LA 4, LA 3 and LA 2) but the dominant association is LA 3 which is found only within this F2 incisional relief (Fig. 3.16). The base of the cut is overlain by LA 10 and LA 9. These basal deposits are locally onlapped by LA 7 deposits that fine- and thin upward into LA 4 and LA 2. This succession is overlain by LA 3, which represents the bulk of the fill (Fig. 3.16). Another localised occurrence of LA 3 on Doornfontein farm (Fig. 3.3) fills a steep (>80°) erosion surface that cuts down into the E-F inter-unit claystone (Enclosures 2A, 4).

Flanking the main mapped incisional surface, F2 comprises ~60 m (log HBS02 and HBS10 in figure 3.16 and enclosures 2A and 4) of heterolithic deposits (LA 4 by LA 2) and varies in thickness from ~60 m to ~20 m over ~5 km. Palaeocurrents from ripple lamination in sandstone beds on both sides of the erosional feature are to the ESE (Fig. 3.18; Appendix 1).

In the Zoutkloof syncline, F2 comprises a basal 4 m thick succession of non-erosive LA 4 overlain by a non-erosive, but sharp based package (maximum 5 m thick) of LA 5 that is mappable for 8 km W-E. The third lithofacies association is marked by erosional surfaces overlain by LA 7 developed intermittently along the W-E outcrop belt and cutting into underlying deposits to a maximum depth of 8 m. Above these three distinctive associations, the top of F2 comprises a repetition of the basal

package, (LA 4) but in this case it thins- and fines-upward into LA 2 (Enclosure 2B). Palaeocurrents from current and climbing ripple lamination range from ENE to ESE (Fig. 3.18; Appendix 1).

On the southern flank of the Baviaans syncline F2 varies from ~40 m and ~60 m in thickness and is marked by a combination of LA 4 (predominant), LA 2, LA 7 and LA 5 (Enclosure 3B). The thickest sections are dominantly LA 4 varying upward into LA 2, with palaeocurrents from ripples to the NE (dominant) with subsidiary flows to the NW (Fig. 3.18; Appendix 1). In the thinnest sections F2 comprises a basal ~18 m thick succession of LA 7 overlying erosional surfaces that incise to a maximum depth of ~12 m. This succession is overlain by LA 4 and LA 2. Palaeocurrents from ripples in LA 4 show an ENE direction (Fig. 3.16; Appendix 1). On the northern flank of the Baviaans syncline, F2 is 25 m thick and comprised only of LA 2. Poor exposure precluded acquisition of palaeocurrents (Enclosure 3A). The percentage of sandstone in F2 is 10%.

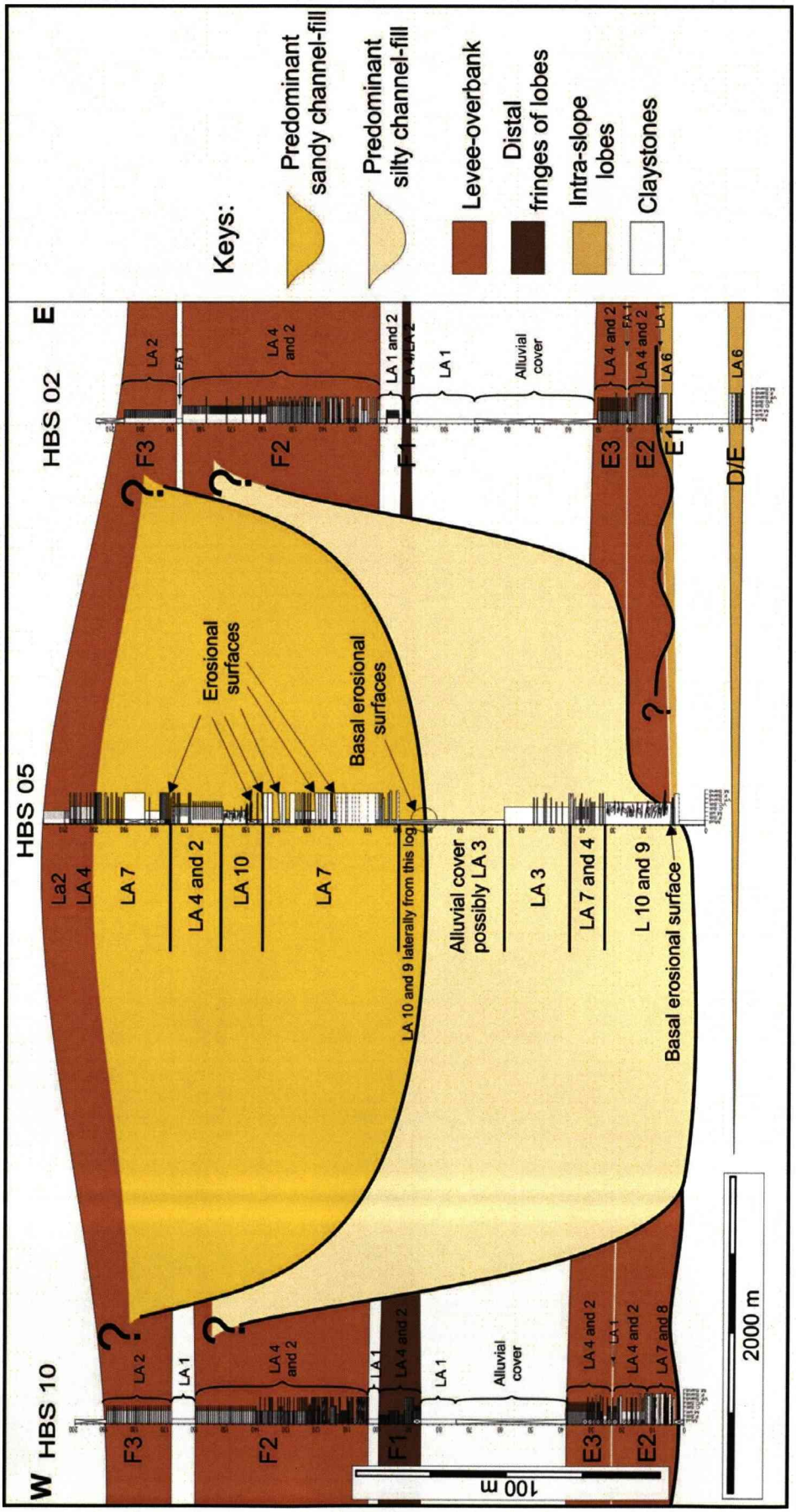

Figure 3.16 – Panel with lithofacies distribution and constraint of the main geometric features based on mapping of key surfaces and stratigraphic units, and correlation of a larger number of logs. The panel depicts a segment of the southern flank of the Heuningberg anticline with selected sedimentary log sections for reference (see enclosure 2A for regional location). All important features are indicated in the panel

F2: Interpretation

The ~150 m deep F2-aged erosional surface that cuts to a position below Unit E on the southern flank of the Heuningberg anticline is interpreted as an entrenched slope valley, being steep-sided with steps and flat based (Figs. 3.16, 3.17, 3.19; Enclosures 2A, 4). The fill of this entrenched system is variable. The basal deposits (chaotic material and folded thin beds) are interpreted as debrites and slumps that originated from the margins of the slope valley and/or from farther up-slope. These are interpreted to have been deposited during the entrenchment phase of the valley development when sediment bypass to the deeper basin was most efficient. Overlying these mass flow deposits are the first and only sand-prone deposits preserved in the whole fill that comprise channel scale features (maximum of 10 m deep). Volumetrically, the dominant lithofacies association is LA 3. These fine-grained deposits could be interpreted as either the partial backfill of the slope valley during aggradation and abandonment, or as inner levee deposits that formed during continued sediment bypass down-dip. As no adjacent channel-fills or crevasse deposits are identified, and the siltstone facies stretches across the incision surface it favours the backfill and abandonment interpretation (Fig. 3.17).

Regional distribution of lithofacies associations and erosional surfaces suggest a slightly sinuous, overall W-E trend to the slope valley-fill that obliquely intersects the WSW-ENE outcrop belt of the southern flank of Heuningberg anticline with a WNW-ESE segment of a bend (Figs. 3.17, 3.19). Up-dip from this point the valley-fill would run mostly sub-parallel to the Heuningberg anticline axis but has been all eroded. Nevertheless, a small section appears on Doornfontein farm. Down-dip the valley is interpreted to run in the subcrop through the Zoutkloof syncline or beyond the Heuningberg anticline nose (Fig. 3.18). The interpreted slight sinuous to linear trend is consistent with modern and ancient subsurface slope valleys of a similar scale (e.g. Deptuck et al. 2007).

Lateral to the major incisional surface the ~60 m succession of thin beds that thin and fine away from the incisional surface, and fine- and thin-upward are interpreted as levee-overbank deposits as previously discussed for E3 and E2 (Fig. 3.19). Flows with energy high enough to carve a slope

valley might have been large enough to spill over the confining margins and build up levee and overbank deposits (following Peakall et al. 2000). Even so, it is difficult to envisage that medium/thick beds of climbing ripple laminated sandstone in the lower part of the fining- and thinning-upward successions formed by spill out of the entrenched incision surface. Rather, the adjacent levee deposits are interpreted to be genetically related to a precursor channel-levee system active prior to the formation of the major valley system. In this model, the precursor channels have been removed by the younger slope valley system.

In the Zoutkloof syncline, thick bedded tabular deposits are interpreted as small distributary crevasse lobes that are cut by a crevasse channel. The lobes are encased in the lower part of the thin/medium interbedded succession interpreted as levee-overbank deposits to the main F2 channels to the north, therefore they are thought to be coeval to the earlier channel-levee system which was later incised out by the slope valley (Figs. 3.18, 3.19; Enclosure 2B).

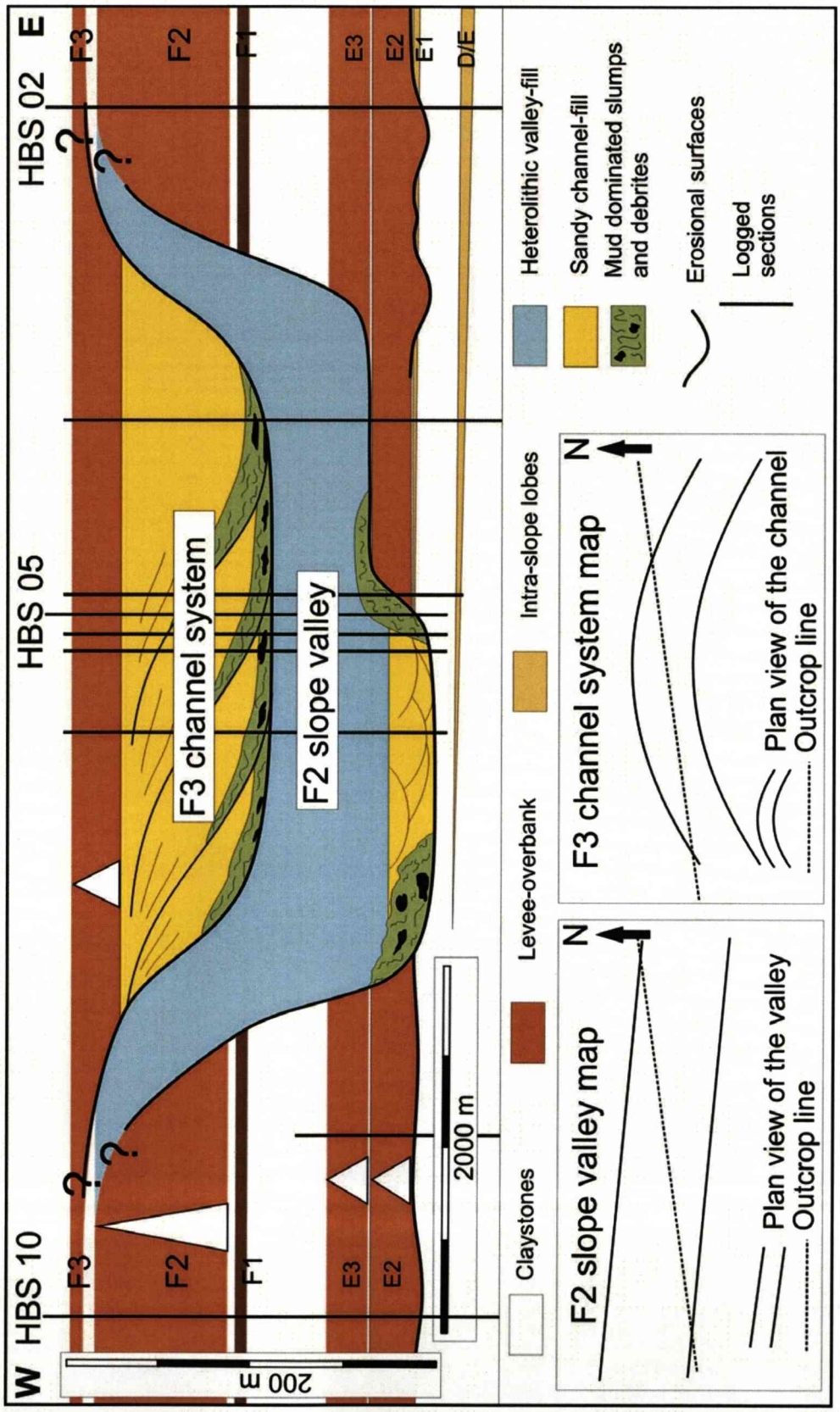

Figure 3.17 – Schematic panel presenting the interpretation for depositional environments and lithofacies distribution in the same segment shown in Figure 3.16. Below, two small schematic maps to show the interpreted plan view of the F2 and F3 erosional features in relation to the outcrop belt

On the northern flank of the Baviaans syncline F2 is dominated by ~25 m of thin and very thin beds of siltstone (LA 2), which could be interpreted as the far southerly (distal) reaches of the levees to the F2 channels in the north. However, further south, on the southern flank of the Baviaans syncline, a ~60 m thick succession of interbedded sandstones and siltstones in fining- and thinning-upward packages show NE and NW directed palaeocurrents suggesting that they are part of a levee to another feeder channel to the south of the study area. These observations are supported by the 18 m-thick, channel-fill exposed on the same southern flank of the Baviaans syncline ~4 km to the east of log BVS01 in enclosure 3B.

These lithofacies distributions, thickness trends, and palaeocurrents support a model of an overall W-E oriented channel-levee system running close to the southern flank of the Baviaans syncline. In this model, the very thin beds of siltstones on the northern flank are most likely the northern reaches of this system rather than the southern reaches of the Heuningberg system. These two distinct, broadly coeval channel-levee systems could have interfingered somewhere coincident with the present-day central anticline where the older Dwyka Group is now exposed.

In conclusion, F2 seems to comprise two separate systems. In the north an early channel-levee system was cut by a major entrenched sandstone-poor valley system. A southern, broadly coeval channel levee-system may have been abandoned as the northern system became increasingly entrenched and dominated the supply of sediment into the deeper basin.

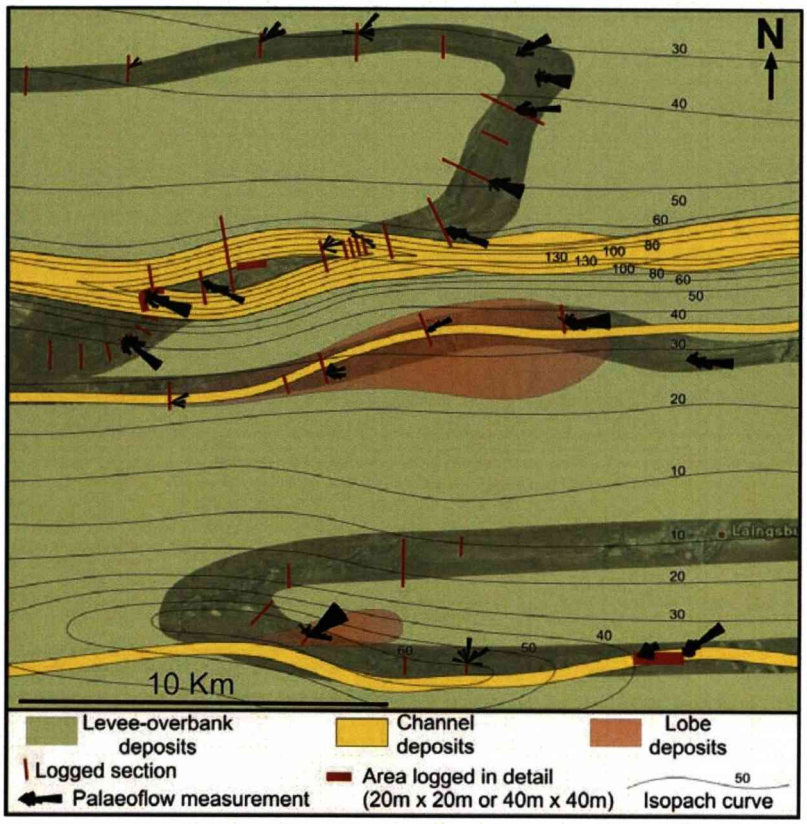

Figure 3.18 – Palaeo-environmental and isopach maps of Sub-unit F2 showing channel-levee system and slope valley (northern area); crevasse lobe and channel (central area); channel-levee system and crevasse lobe (southern area).

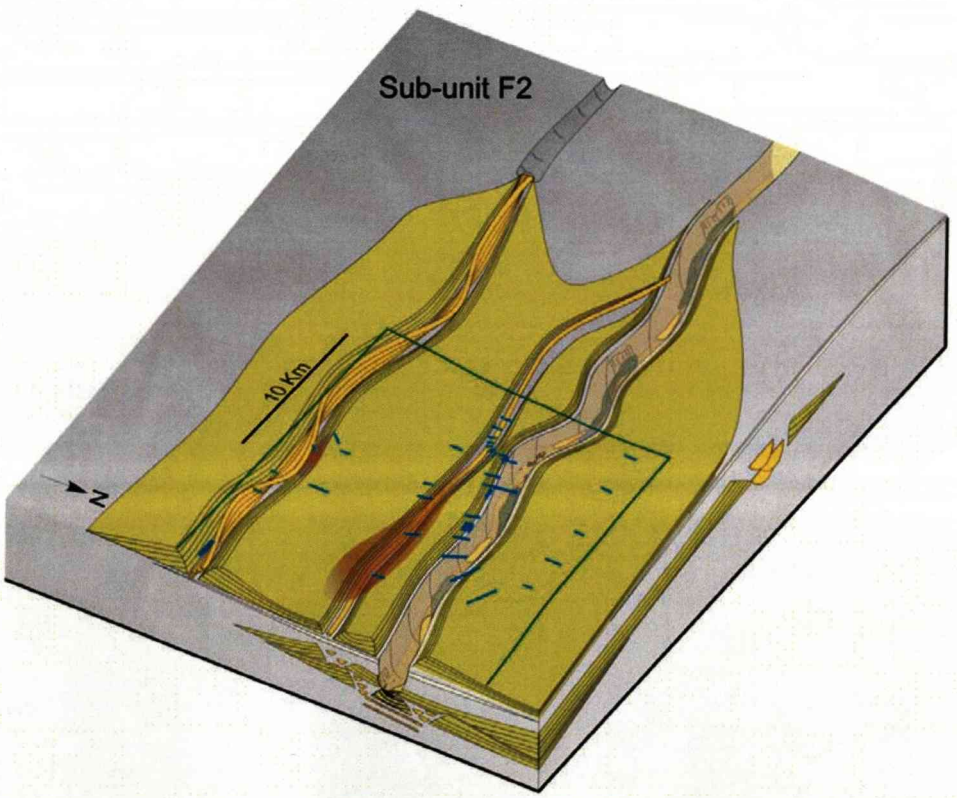

Figure 3.19 – Three dimensional reconstruction of F2 depositional systems. For depositional systems see caption and keys of figure 3.18. Sub-unit F2 does not show influence of the northern depocentre.

F3: Observations

Sub-unit F3 overlies the upper F intra-unit claystone. On the northern flank and nose of Heuningberg and in the Zoutkloof syncline F3 is dominated by regular intercalation of medium and thin beds of LA 4 and LA 2, with limited palaeocurrent measurements showing an eastward direction (Enclosures 1B, 2B; Fig. 3.20; Appendix 1). On the southern flank of Heuningberg this heterolithic association is interrupted in two locations by erosional surfaces filled by a variable range of lithofacies associations (LA 9, LA 8, LA 7, LA 4 and LA 2).

The position of the eastern incisional surfaces is coincident with the underlying F2 slope valley (logs HBS03 to HBS08 in enclosures 2A and 4; Fig. 3.16). Here the basal F3 erosional surface shows a maximum incision of ~90 m below the base of the Unit, however it is composed of multiple smaller-scale incisional surfaces which step laterally eastward (Fig. 3.17). The main F3 erosional surface is exposed in a WSW-ENE outcrop line and is highly oblique to the eastward palaeoflow (Fig. 3.17). The vertical infill of the container defined by these surfaces starts with chaotic deposits (LA 10, LA 9) overlain by a thick (maximum of ~70 m) succession of predominantly amalgamated or erosive based beds of structureless fine-grained sandstone (LA 7), which pass upward into thin beds of LA 4 and LA 2. This succession typically includes internal erosional surfaces (Fig 3.16).

The western incisional surfaces (Doornfontein farm; logs HBS11, 12 and 13 in enclosure 2A) cut ~120 m below the base of the Unit and are also characterized by a variable range of lithofacies associations (discussed in more detail in chapters 4 and 5).

Outside of these erosional surfaces F3 is dominated by LA 4 and LA 2, but localised bodies of LA 7 mantle small (~5 m deep) erosional surfaces in the central study area (Enclosures 1A/B, 2A/B, 4). The heteroliths outside of erosion surfaces in F3 are thinner than those in F2 (maximum thickness ~30 m). In the Baviaans syncline, only the lower intra-unit claystone is present in Unit F, and so F3 is absent (Enclosures 1A, 3A/B). The overall percentage of sandstone in F3 is about 50%.

F3: Interpretation

The erosional cuts along the southern flank of the Heuningberg anticline were confirmed to be F3-aged erosional surfaces by stratigraphic correlation between logged sections and mapping of the upper intra-unit claystone and overlying F-H inter-unit claystone (Enclosure 2A, 4). They are interpreted as slope channel deposits and, given the palaeocurrent directions and similar architecture of the two fills, they are likely to form part of the same slope channel system that runs with some sinuosity along the southern flank of the Heuningberg anticline. The lateral relationship between the slope channel and the adjacent medium and thin beds is not clear but following the same criteria used in the older sand-prone units these deposits are interpreted as levees (Figs. 3.20, 3.21).

The small erosional surfaces mantled by LA 7 that occur intermittently in the western Zoutkloof syncline are interpreted as marking a small W-E trending channel. The exact stratigraphic relationship of this small channel-fill with the channel complex to the north remains unclear due to exposure limitations, but it is broadly coeval. The absence of F3 in the southern study area means that the thin F3 levee system pinches out southwards somewhere between the Zoutkloof and Baviaans synclines, possibly coincident with the present day central anticline (Figs 3.20; 3.21).

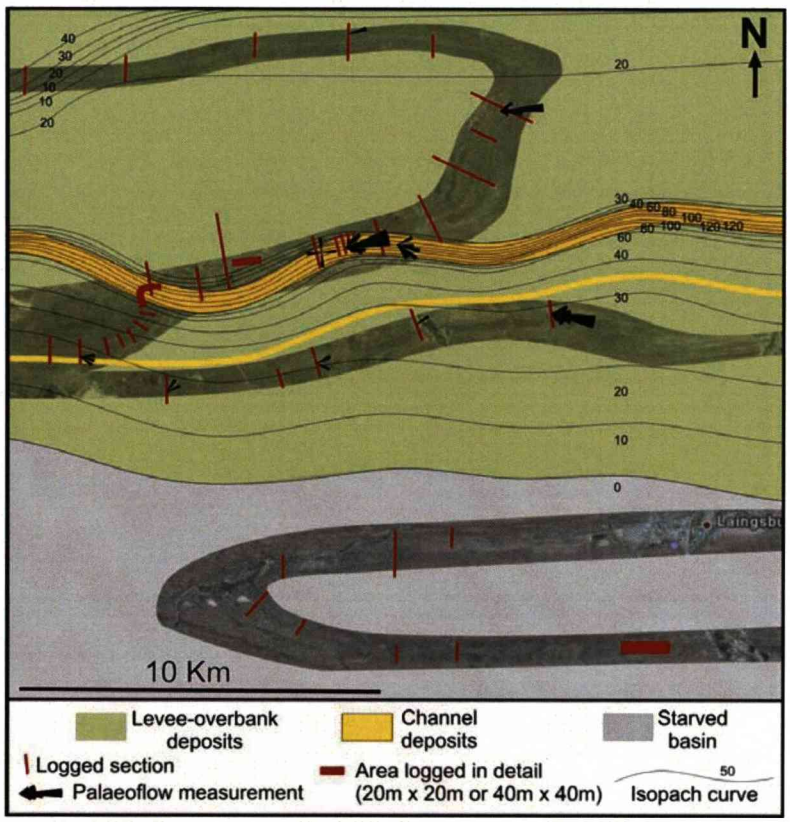

Figure 3.20 – Palaeo-environmental and isopach maps of Sub-unit F3 interpreted as channel-levee systems.

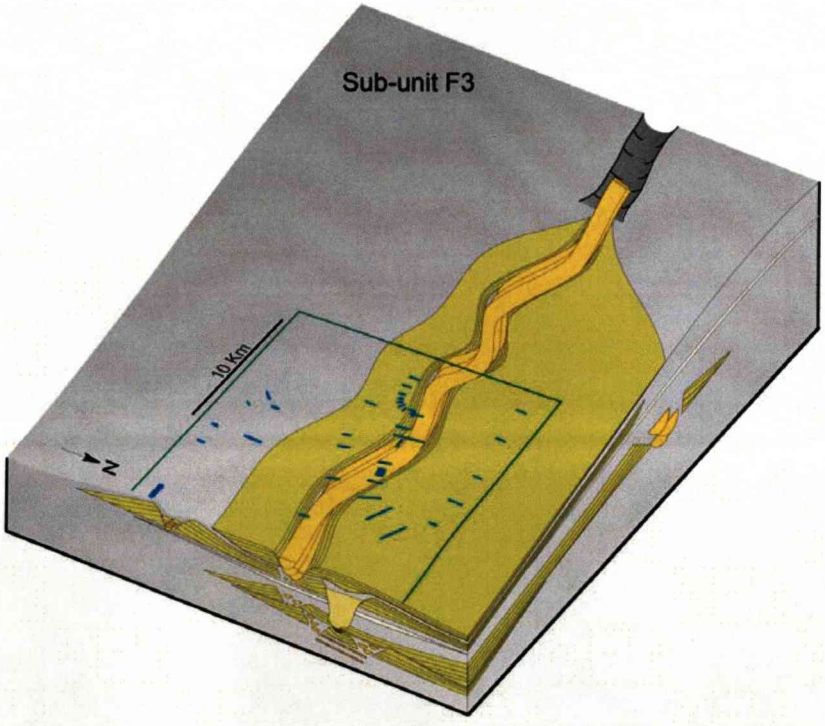

Figure 3.21 – Three dimensional reconstruction of F3 channel-levee systems. Sub-unit F3 is restricted to the northern and central areas, it seems that the F2 channel-levee system developed in the south had some influence on local palaeo-topography "pushing" F3 to the north.

3.4.2.4 - Unit G

Observations: In the northern and central study areas, the thickness of claystone above Unit F before the next sand-prone unit is ~100 m and ~110 m respectively, while in the southern area it is only 40 m. This difference indicates that an additional sand-prone unit is present only in the south (Enclosures 1 - 4). This unit has not been previously identified and hereafter is named Unit G. Like Units E and F, it can be divided into three sand-prone sub-units (henceforth labelled G1, G2 and G3) by two regionally mapped intra-unit claystones (lower and upper G claystones). In a similar style to Units E and Unit F, the thickest sub-unit in Unit G is the middle G2 (~15 m), while G1 is ~2m thick and G3 is ~3.5 m thick. The lower G claystone is 0.5 m thick and the upper G claystone is 5 m thick (Enclosure 3B). Overall, Unit G is thinner and finer grained than Unit E or Unit F. It is composed almost entirely of LA 2 thin beds that reach a maximum thickness of 25 m. No erosional surfaces have been identified in any of the sub-units. On the northern flank of the Baviaans syncline Unit G is even thinner (~15 m) and finer grained than on the southern side and the distinction of the three sub-units becomes more difficult due to the overall fine grained character (Enclosure 3A). Due to the poor exposure paleocurrent data were not acquired and the overall sandstone percentage is 5%.

Interpretation: The characteristics of Unit G indicate a purely depositional setting, with no evidence of erosion or sediment bypass (Enclosures 1 – 4). The map pattern indicates a major reduction in sand volume compared to Units F or E and an overall low energy setting. These observations suggest either a northward thinning levee to a slope channel system lying to the south of the study area, or a low energy terminal intraslope distributive system. Stratigraphically, Unit G overlies a ~40m thick claystone unit and is overlain by another regional claystone of ~70m thickness. This suggests that the whole depositional system was becoming less sand-prone. With this combination of characteristics and the overall stratigraphic setting the favoured interpretation for Unit G is a distributive

lobe fringe (Figs. 3.22; 3.23). This may be related to a large scale landward retreat of the Laingsburg delivery system, which is discussed further below.

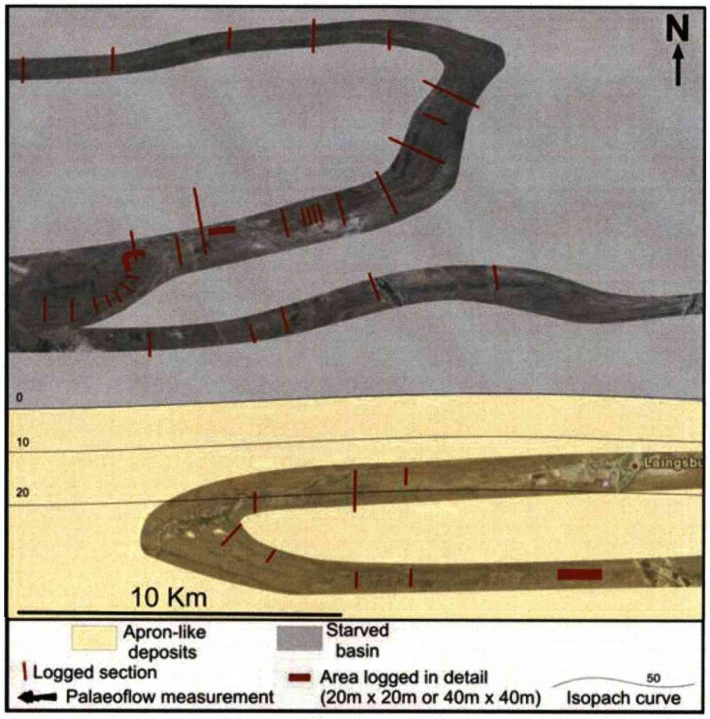

Figure 3.22 – Palaeo-environmental and isopach maps of Unit G, interpreted as a distal distributive system.

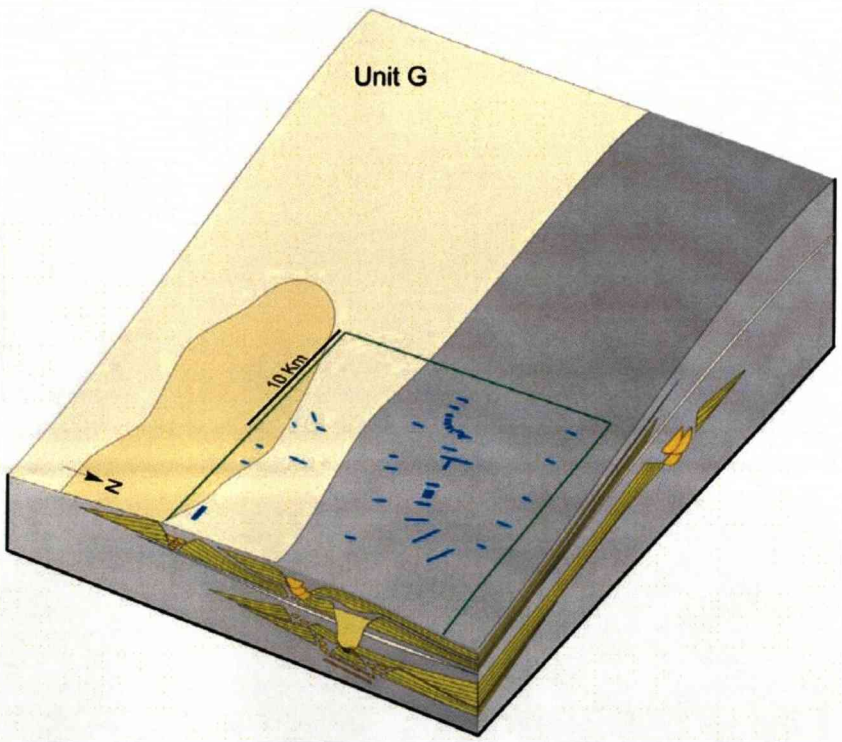

Figure 3.23 – Three dimensional reconstruction of Unit G distal distributive system. The sandy depositional system shifted to the south, relative to F3. The concentration of the underlying sandy deposits in the north is interpreted to have driven this process (see section 3.5.1 for discussion).

3.4.2.5 - Unit H

Observations: The claystone units above Unit G in the south and Unit F in the central and northern areas are ~70 m and ~100 m thick respectively. They include several metre-thick units of very thin bedded siltstone and are overlain by another newly identified sand-prone unit, hereafter called Unit H, which is developed across the whole study area and reaches a maximum thickness of ~120 m around the Zoutkloof syncline and the southern flank of the Heuningberg anticline. A slight thinning is observed northwards from the Zoutkloof syncline (from ~120 m to ~90m in ~8 km) and only siltstone is present on the northern flank of Heuningberg. Unit H wedges southward (from ~120 m to ~30 m in 9 km) and westward (from about ~120 m to ~40 m in ~8 km) (Enclosures 1 - 4). Very thin and thin beds of LA 2 form thickening- and coarsening-upward bedsets to the middle of the unit, followed by thinning- and fining-upward bedsets to the top. In the south and west, where Unit H is thinner, it is sand-prone in the upper part, with examples of bioturbation (simple horizontal burrows) and symmetrical ripples at the tops of beds. Erosional surfaces were not observed. The sandstone percentage in Unit H is about 10%.

Interpretation: Unit H is one of the thickest mapped sand-prone units, but is uniformly thin bedded, mainly siltstone with no channel features. The symmetrical ripples are interpreted as forming under oscillatory currents and, together with the onset of bioturbation, suggest shallower water conditions. Unit H is interpreted as a distal distributive system of low density turbidites, slightly reworked by oscillatory currents, possibly related to deep effects of storm events. A similar lithofacies is described by Wild et al. (2009) in the Tanqua depocentre. The stratigraphic setting with deltaic deposits above supports a distal pro-delta setting (Figs. 3.24, 3.25; Steel et al. 2000; Porębski and Steel 2003; Porębski and Steel 2006).

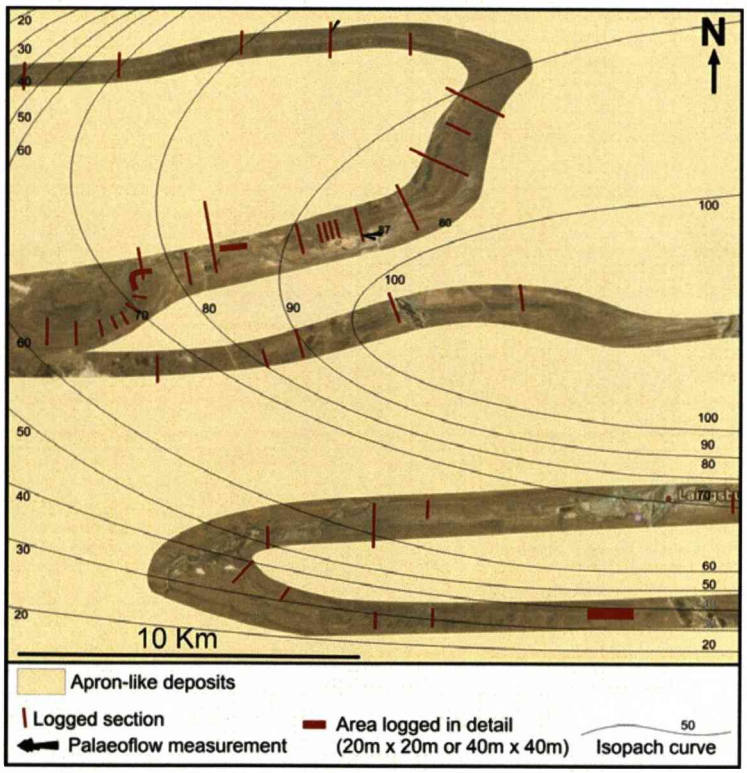

Figure 3.24 – Palaeo-environmental and isopach maps of Unit H interpreted as distributive system.

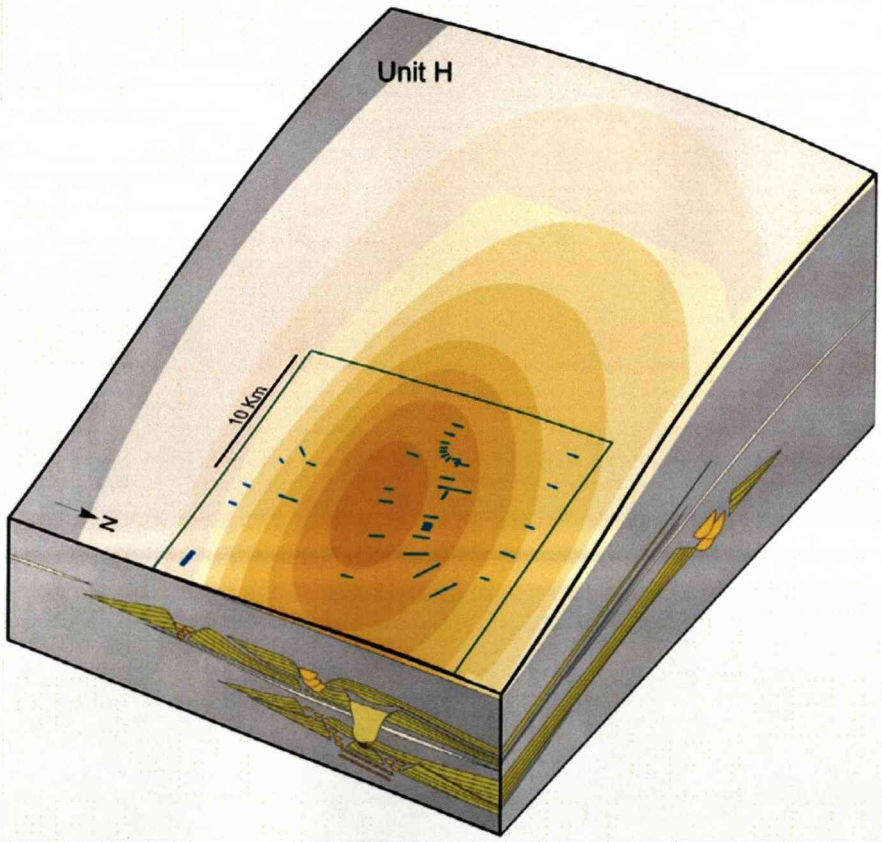

Figure 3.25 – Three dimensional reconstruction of H distributive system. Unit H in one of the thickest units of the analysed succession and was deposited throughout the study area.

3.4.2.6 - Deltaic deposits (Fort Brown/Waterford Formations): Observation and Preliminary Interpretation

A 25 m thick succession of claystone separates Unit H from the overlying succession of several hundred metres of sand-prone deposits, which exhibit a major change in sedimentary characteristics. These thickening-upward bedsets are dominated by symmetrical ripples, interpreted as wave induced ripples, and truncated low angle cross stratification, interpreted as hummocky cross stratification, plus unsorted beds and moderate bioturbation. These characteristics, plus their stratigraphic context within the whole analysed succession suggest deposition as mouth bars in a mixed influence delta. No detailed work has been carried out on this succession to date.

3.5 – Levee deposits: key characteristics

By area and volume, levees are the dominant deposits in E2, E3, F2 and F3 and provide a rare outcrop example of regionally well exposed proximal (near channel) to distal (far from channel) deposits, allowing the definite mapping of trends in lithofacies and thickness. In all examples, the key characteristics are the same, suggesting a degree of predictability. In proximal levee settings the lower portion is dominated by lithofacies association 4, with the percentage of sandstone varying between 40% and 60%. Upward, LA 4 passes into LA 2 (< 20% sandstone) in the upper proximal levee, usually through an intermediate section characterized by a mix of these two associations in which the percentage of sandstone varies from 20% to 40%. In distal settings only LA 2 is present. The transition in lithofacies associations from proximal to distal occurs in the same way as the upward transition in the proximal setting LA 4 passes through LA 4/LA 2 to LA 2. This vertical and lateral variation in lithofacies is illustrated in figure 3.26. The rate of thickness change away from the channel, 40 m in approximately 5 km, orthogonal to the paleoflow, and a typical rate of thinning of ~10 m/km is commonly observed. The constant thickness of

underlying claystone demonstrates that the levee wedges are aggradational. The lowermost component of proximal levee stratigraphy is always the sandiest and could be interpreted as early frontal lobe facies, related to the early development of the channel system.

In all examples where channel-fill deposits were interpreted as part of a channel-levee system, their basal erosion surface cuts deeper than the base of the adjacent levee. This observation suggests that, at least during their initial phase, the channels were erosionally confined. This erosional confinement varies from less than 10 m (E2) to approximately 120 m (F3) However, the depth of the erosional surface below of the base of the adjacent levee deposits is less than the total thickness of the channel-fill, indicating that the channels became confined by the levees after an initial erosional phase. Following Mutti and Normark (1987) most channel-levee systems within the study area are classified as erosional/depositional systems. The exception is the F3 channel system, where the thickness of the levees (~ 30 m maximum, but averaging 10 m) is much less than the thickness of the channel-fill deposits (~ 120 m at the thickest section). This geometry suggests that F3 was mainly erosionally confined throughout its evolution.

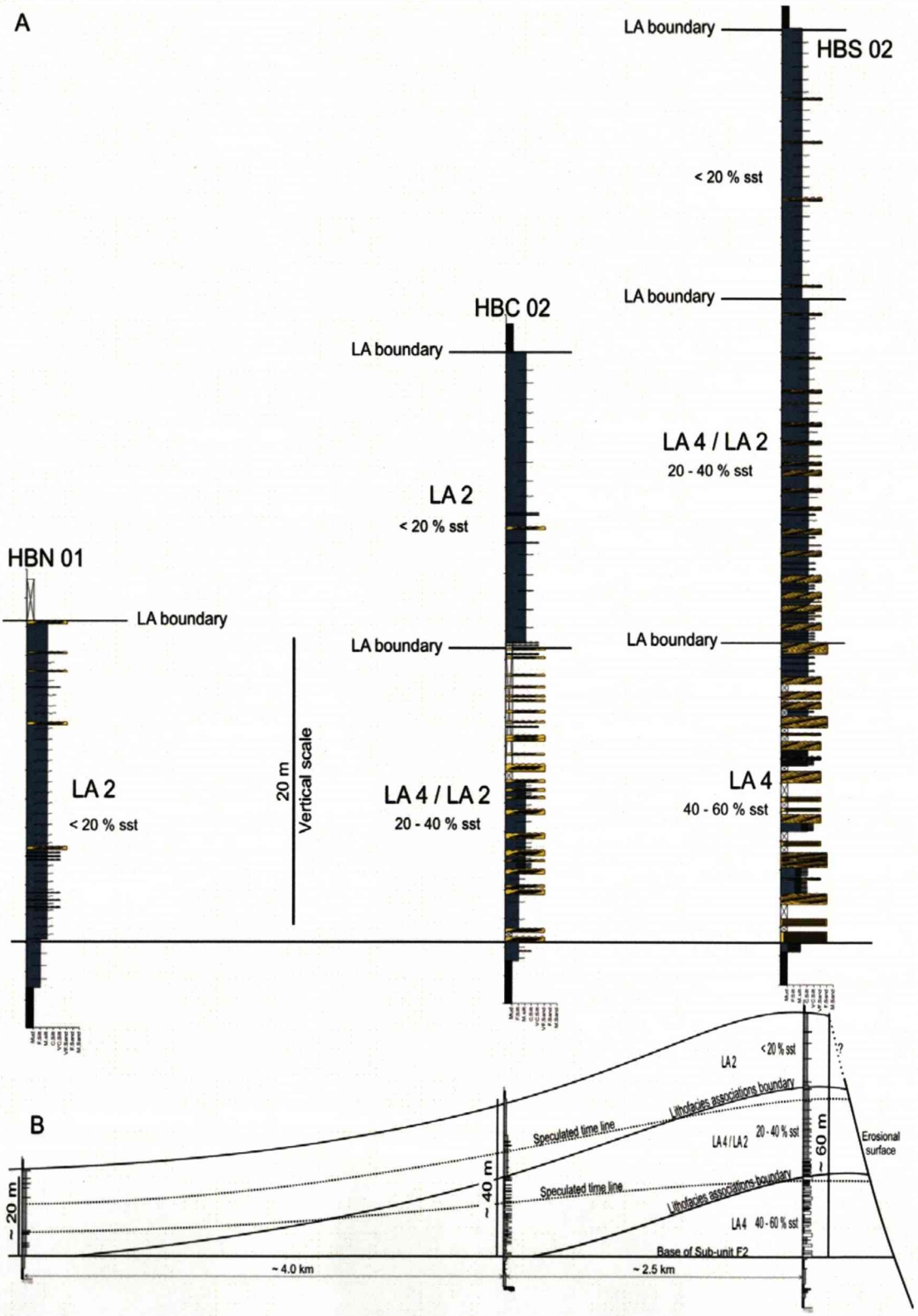

Figure 3.26 – Logged sections through a fully exposed levee succession that show the lateral and stratigraphic distribution of lithofacies associations. Log 1 is in a proximal levee setting (near channel) and log 3 in a distal levee setting (far from channel). Lateral distribution and thickness of the lithofacies associations is shown in the cross-section.

3.6 - Discussion

3.6.1 - Controls on the stacking and distribution of sand-prone units

The systematic upward change in the character of the sand-prone units from early terminal intraslope lobes with no channels, through channel-levee systems to entrenched slope valley fills is interpreted to represent basinward stepping of the submarine slope from Unit D/E to the top of Unit F2. This stratigraphic organization forms part of the long-term progradational trend from basin floor (Fan A) through toe of slope to mid and upper slope (Units B-G) to shelf edge deltaics (Fort Brown Formation).

The stacking pattern from Sub-unit F3 to the base of Unit H is aggradational to landward stepping based on the overall, regional fining-upward trend. An alternative interpretation is that all sand bypassed at this stage but across the large study area no evidence for any slope valley systems that would be required for major sediment bypass was identified. The system is interpreted to have switched back into basinward stepping with Unit H through the overlying deltaic succession. Across depositional strike, mapping shows that Unit D/E is restricted to the northern part of the study area. Unit E occurs in the northern and central areas while Unit F is present across the whole study area. Unit G occurs only in the southern area. This outcrop pattern of the successive units suggests that the locus of sand-prone deposition expanded and stepped southward across strike with time and eventually switched to the south with Unit G. This trend could be related to up-dip avulsion of the depositional system and/or due to the development of local seabed topography.

Several mechanisms can be invoked to drive the development of relief on submarine slopes including salt or clay dynamics, gravitational tectonism and emplacement of mass transport deposits (e.g. Beauboeuf and Friedman 2000; Prather 2000; Prather 2003; Pickering and Corregidor 2005; Gee and Gawthorpe 2006). No evidence of these mechanisms was identified in the study area. Active tectonism is an alternative mechanism to drive change in seabed topography during sedimentation (e.g. Hodgson and Haughton 2004). In the study area, tectonically-driven seabed deformation has been

interpreted as a control on sand distribution in the older Laingsburg Formation stratigraphy (Grecula et al. 2003, Sixsmith et al. 2004). However, evidence in this study that tectonism was not active during the upper Laingsburg Formation includes: (1) the uniform cumulative thickness of the claystones, which suggests that folding was post-depositional; (2) the Unit D/E and E1 lobes were deposited across the axis of the Heuningberg anticline; (3) slope channels follow the flanks of present day anticlines rather than the cores of synclines; (4) the distribution of the sand-prone units, from Unit D/E shows a concentration of sands in the north (expanding to the south through time) that is "out of phase" with the tectonic features observed today. In the absence of clear evidence of tectonism or diapirism, the restriction of sand-prone units to the north of the study area (units D/E, E and F) is interpreted to have been driven by differential compaction over underlying stratigraphy. Units B, C, and D are thicker and more sand-prone in the southern part of the study area (Grecula et al. 2003; Flint et al. 2007). Consequently, the coeval mud–prone succession to the north would have undergone more compaction than the sand-prone southern succession. This would create a higher gradient for up-dip channels to exploit, leading to the northern locus for deposition of Units D/E, E and F. The topography generated by compaction would form a north-dipping lateral gradient on the overall east-facing slope that would also enhance the southward thinning of these units (Figs. 3.27, 3.28).

The ~260 m thick succession between top Unit D and top Unit F contains ~170 m of sandstone in the north but only ~70 m in the south. Therefore, after Unit F time, differential compaction of this part of the slope succession is likely to have resulted in greater compaction of the mud-prone southern section, resulting in a reversal in the direction of the lateral across-slope gradient, to the south as seen by the localised deposition of Unit G in the south. Therefore, sand-prone deposition in the slope succession shifted across strike from south-to-north and back to the south through time (Figs. 3.27, 3.28). The influence of differential compaction in mud-prone submarine slope settings is well known at the scale of slope valleys (e.g. Mayall et al. 2006), and at larger-scales (e.g. Koša 2007), and is likely to occur in slope settings where narrow sand-prone channel-fills or channel-levee systems are

encased in background claystone. The depositional relief on channel-levee systems can be enhanced by differential compaction resulting in large-scale compensational stacking. There is less evidence for the impact of differential compaction at the scale of slope valleys, e.g. F2. This might be due to the underfilled nature and low sand content of the fill.

The range of architectural patterns identified in this work (lobes, channel-levee complexes and entrenched slope valleys) cannot be ascribed only to the across strike variation in sea floor topography and basinward stepping of the sandy feeder system but also requires down-dip topographic changes. The development of intraslope lobes on the middle submarine slope in Units D/E and E1 suggests the presence of a lower gradient area (a step) on the east-facing paleoslope that was progressively filled and cut through by younger channels. The step may have formed as a consequence of the change of the slope equilibrium profile (sensu Pirmez et al. 2000) caused by an unequal down dip distribution of the sand-prone deposits in the underlying succession (following Dailly 1983; Ross et al. 1994; Prather 2003). The basin floor Fan A system (Sixsmith et al. 2004) and the toe of slope deposits of Unit B (Grecula et al. 2003) may have disrupted the previous equilibrium profile of the Laingsburg slope. This could have impacted the development of the sand-prone units in the middle/upper slope succession. The absence of outcrop constraints down dip to the study area precludes confirmation of this interpretation.

In summary, the storage, bypass, and architecture of the sand-prone deposits on the middle and upper submarine slope in the Laingsburg Formation were the result of a complicated interplay between seabed topography (across strike and down-dip) and the dynamics of the feeder system.

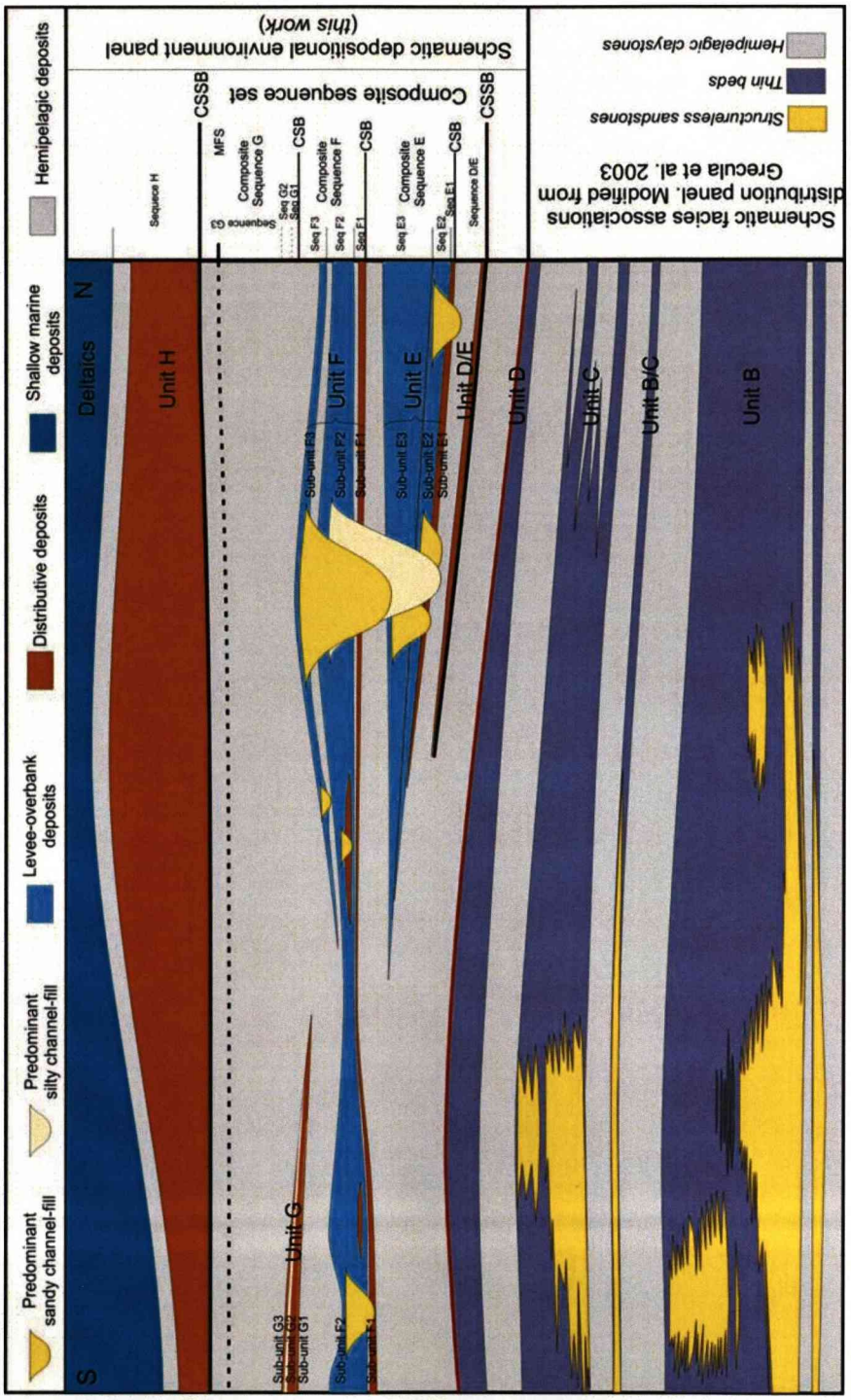

Figure 3.27 – Merged diagram showing across strike depositional environment panel from top of Unit D up to the deltaic deposits (this work), and the lithofacies associations distribution panel for the underlying succession (modified from Grecula et al. 2003). The boundary between the two panels is the top of Unit D (solid red line). The lower succession (from Unit B to Unit D) shows a preferential concentration of structureless sandstones within the sand-prone units in the south in contrast with more thin beds in the north. In the upper succession, from Unit D/E to Unit F, this trend is reversed with concentration of the sand-prone units in the north. Unit G shows a switch of sand-prone deposits back again to the south. Differential compaction (see discussion in the text) is interpreted to have controlled the distribution of the sand-prone deposits. Right column shows the sequence stratigraphy of the analysed succession (discussed in section 3.5.3).

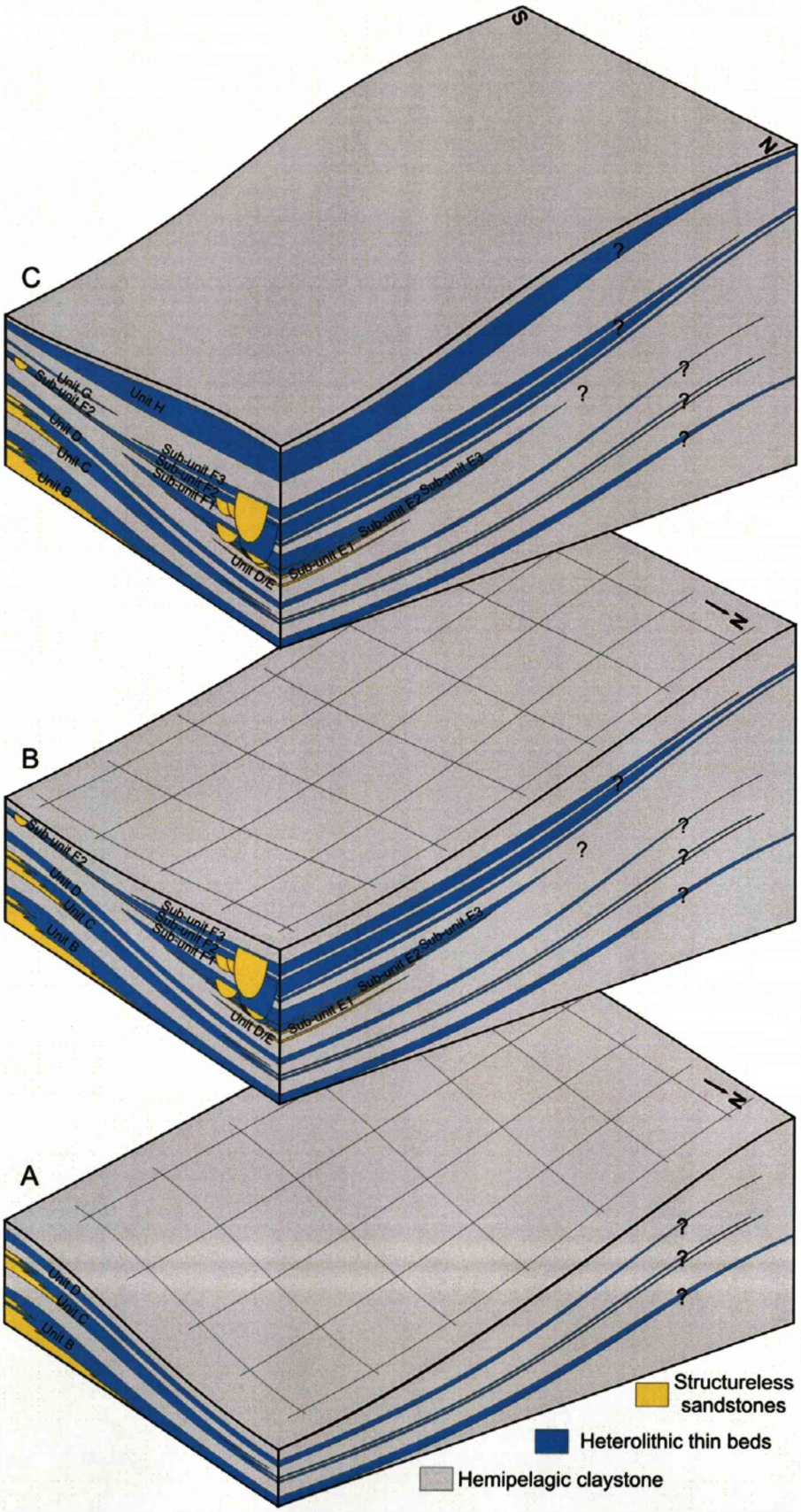

Figure 3.28 – Three dimensional reconstruction of the stratigraphic evolution of the analysed succession. (A) Reconstruction of the palaeo-topography at the time of initiation of Unit D/E based on Grecula et al. (2003). (B) Palaeo-topography at the initiation of deposition of Unit G. (C) Palaeo-topography at the top of the Unit H time (see text for discussion).

3.6.2 - Sand distribution on the mid/upper submarine slope in Laingsburg Formation

In the succession from Unit D/E to Sub-unit F2 the overall percentage of sandstone preserved in the study area decreases upwards (Fig. 3.29). In F3, after the system stopped stepping basinward and switched to aggradation the sandstone percentage increases to about 50%. Above F3, when the depositional system shows a landward stepping pattern, the ratio drops again and Unit G shows the lowest percentage of sandstone in the entire succession (5%). The system is interpreted to have switched back into basinward stepping with Unit H in which the sandstone percentage increases to 10%. In summary, the more proximal the system the lower the percentage of sandstone preserved (Fig. 3.29). This is interpreted as due to an increase in the amount of bypass with proximality.

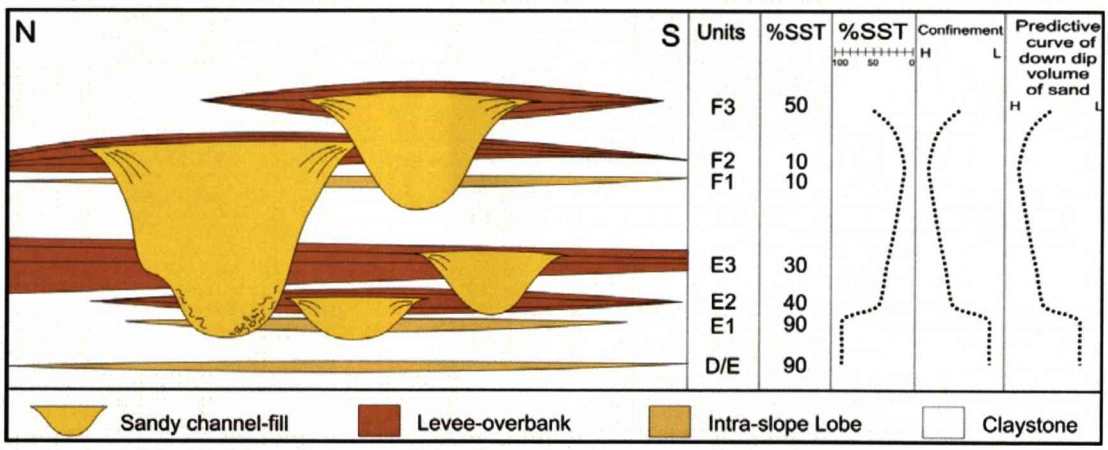

Figure 3.29 – Schematic across strike panel (based on stratigraphic panel shown in enclosure 1A) showing depositional environments of the northern area and distribution of the total percentage of sand from Unit D/E to Sub-unit F3. Right hand columns show the inverse relationship between degree of confinement and percentage of sand in the sand-prone units.

3.6.3 - Sequence stratigraphy of the Laingsburg slope succession

The limited absolute age data available at present precludes the establishment of a chronostratigraphically based sequence stratigraphic framework for the upper Laingsburg Formation. However the data set enables the establishment of a physical stratigraphy that includes a hierarchy of key surfaces that bound genetically related, regionally correlatable bodies.

Key observations include thicknesses of hemipelagic claystones, the depositional pattern of sand-prone units and the maximum depths of incision.

The physical stratigraphy presented here reveals a high degree of organization and a consistent hierarchy in the compacted thicknesses of the inter-unit claystones (Fig. 3.30). A similar organizational pattern was observed in the underlying stratigraphy (Unit C and Unit D) (Flint et al. 2007; Fig. 3.30). The base of each sand-prone unit marks an abrupt introduction of sand-grade sediment into a submarine slope environment dominated by suspension fall-out of clay grade material over at least 400 km^2. These regionally mapped surfaces, each coincident with a major increase in depositional energy and sediment grain size, are interpreted as sequence boundaries (Vail et al. 1977; Posamentier et al. 1988; Posamentier and Allen 1998). The same arguments apply when interpreting sub-units E1, E2 and E3 within Unit E; F1, F2 and F3 within Unit F; and G1, G2 and G3 within Unit G. Each of these sub-units fulfils the same criteria for a regional abrupt increase in system energy and grain size across a single mappable surface above hemipelagic claystone.

Following the methodology of Sprague et al. (2002), each sub-unit is interpreted as a lowstand systems tract to a depositional sequence and the overlying intra-unit claystone is interpreted as the transgressive and highstand systems tracts to that sequence. Units E, F and G are therefore sequence sets, each comprising three sequences (Fig. 3.30). In each case, the complete sandy unit (E, F, G) and the overlying inter-unit claystone is interpreted as a composite sequence (Mitchum and van Wagoner 1991). Units D/E and H do not appear to be composite and so are interpreted as lowstand systems tracts of single sequences (Fig. 3.30). However, it cannot be ruled out that Unit D/E represents the distal end of the most basinward developed sequence within a composite sequence that is more fully developed up-dip.

As demonstrated above from sedimentological criteria alone, the Unit D/E to F succession shows a basinward stepping stacking pattern, marked by an upward increase in depositional energy and an increasingly proximal character of depositional environments (Fig. 3.31). The maximum depth of incision recorded in the whole succession is the slope valley in F2. Above

Unit F, the system shows a backstepping trend through Unit G into the ~70m thick claystone that underlies Unit H. Integration of all these observations allows the interpretation that the sequences and composite sequences form a larger scale composite sequence set. The basal composite sequence set boundary is interpreted to be at the base of Unit D/E and the upper boundary at the base of Unit H (Fig. 3.31). This surface terminates the complete deepwater system and is probably a composite sequence set boundary but this needs substantiating through further work on the deltaic stratigraphy (Figs. 3.30, 3.31).

By definition, each depositional sequence must also contain a maximum flooding surface (MFS). Within this framework the maximum flooding surface to each sequence scale is placed within the intra-unit claystone; at composite sequence scale within the overlying inter-unit claystone; and at composite sequence set scale within the thickest claystone unit, between Units G and H (Fig. 3.30).

An alternative interpretation that the sand-prone sub-units and intra-unit claystones represent lateral switching of a system due to upstream avulsion is possible but nowhere in the regional study area do the claystones pass laterally into fringes of sand-prone sub-units. This supports the interpretation of the claystones being hemipelagic condensed transgressive/highstand deposits.

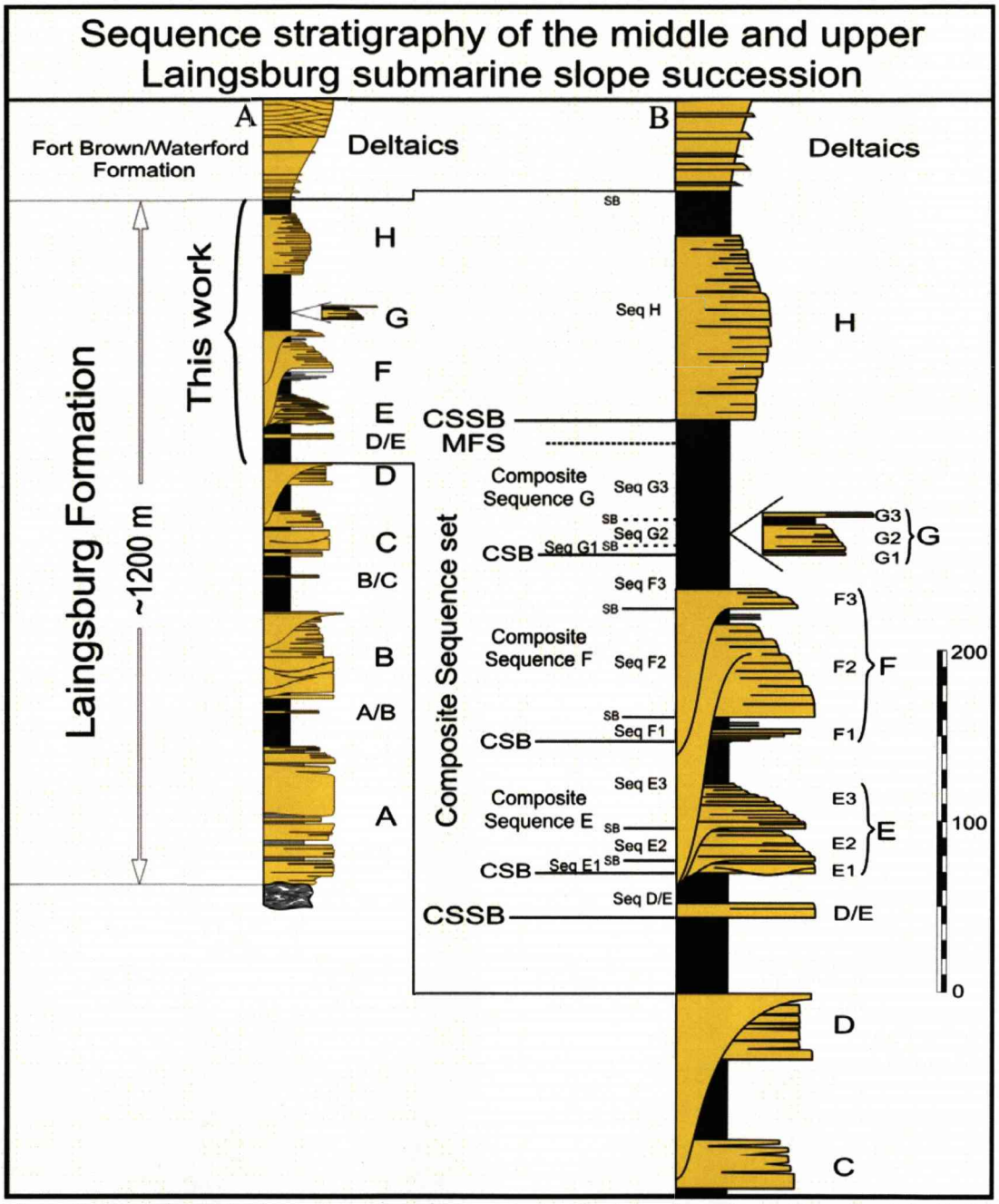

Figure 3.30 – Column A: Physical stratigraphic constraints for Laingsburg Formation. Fan A to Unit D compiled from previous work (Sixsmith et al. 2004; Grecula et al. 2003; Flint et al. 2008). Unit D to the deltaic deposits from this work. Column B: Detail of the section in this work coupled with the sequence stratigraphic interpretation considering the vertical stacking on the southern flank of the Heuningberg anticline (northern area) plus Unit G which occurs only in the southern area. Black column represents hemipelagic claystones and yellow = the sand-prone units. CSSB: Composite sequence set boundary; CSB: Composite sequence boundary; SB: Sequence Boundary; MFS: Maximum flooding surface.

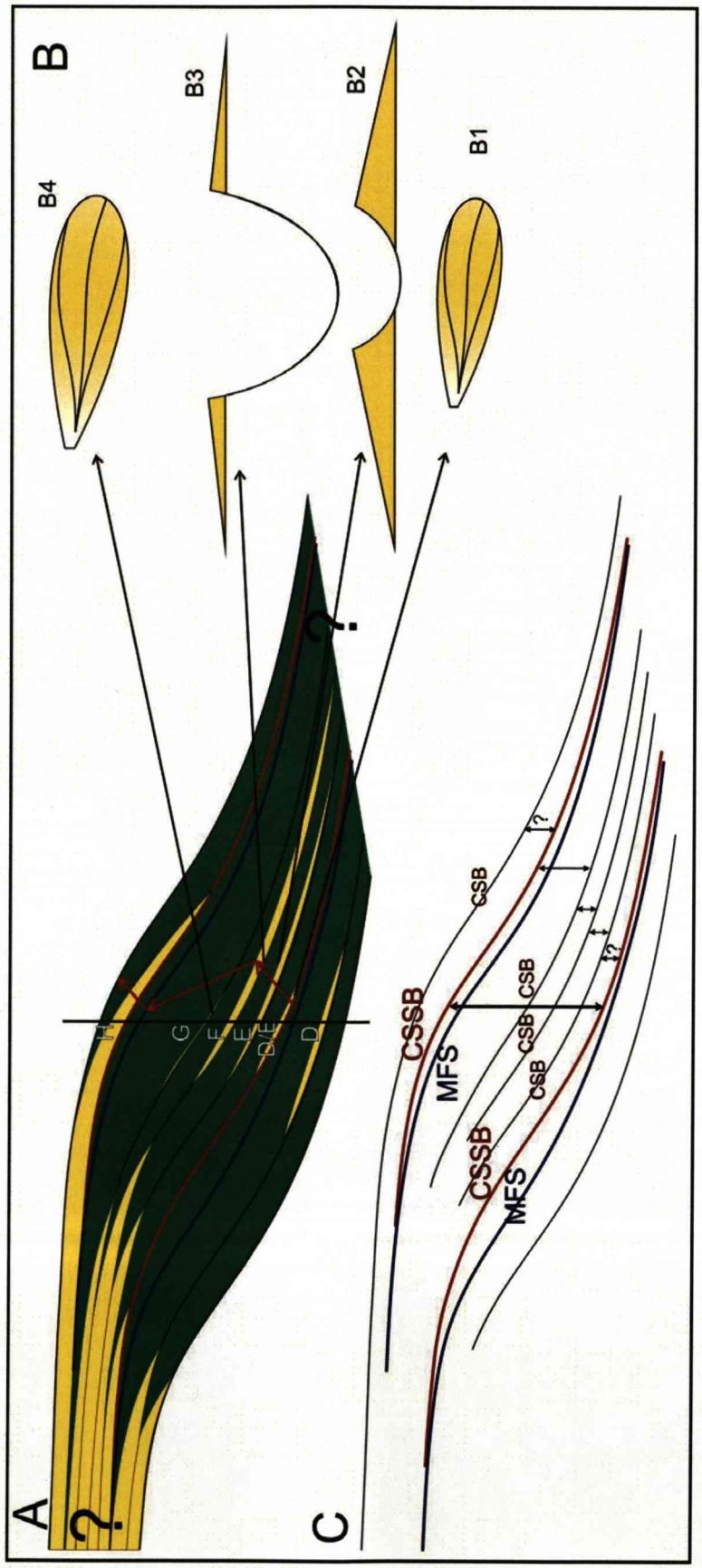

Figure 3.31 – Schematic cartoon depicting: (A) Dip profile of the slope evolution showing progradation from Unit D/E to Unit F, retrogradation from F to base of H, and then progradation again through Unit H and the overlying deltaic deposits not represented in this cartoon. (B) Basic geometries of the predominant erosional/depositional systems in each sand-prone unit: B1 and B4, distributive deposits; (B2) channel levee systems; B3 entrenched slope valley. (C) Hierarchy of the sequence stratigraphy of the analysed succession based on the profile shown in A. The individual depositional sequences are not shown due to the scale of the cartoon. There is no control on the stratigraphic constraint farther up or down dip from the 20 km lateral section studied; therefore the interpretations shown in the profile for these end members are purely speculative

3.6.4 - Controls on sequence development

Although deepwater slope successions are known to be complicated, the physical stratigraphic hierarchy and the distribution of depositional settings presented above shows a high degree of organization (Fig. 3.30). The main complexity is the across-strike changes in depositional patterns that this large scale outcrop data set has constrained (Figs. 3.27, 3.28; Enclosures 1 - 4). These data suggest that the sequence driving mechanisms must have operated on a regular timescale, delivering sediment to the submarine slope in a modulated way and storing sand-grade sediment on the coeval shelf during times of claystone deposition on the slope. As explained above, the Cape Fold Belt was not active until the Triassic and therefore active tectonism is unlikely to have been a significant driver for sequence development.

The high degree of stratigraphic organization in the Laingsburg succession is also documented in the Tanqua depocentre deposits, 100 km to the NW (Goldhammer et al. 2000; Hodgson et al. 2006) and is consistent with sediment supply being modulated by glacio-eustatic sea level cycles, astronomically induced during the Permian ice-house climatic regime (Fairbridge 1976; Herbert and Fischer, 1986; Dean and Gardner, 1986; Abbott and Carter 1994; Goldhammer et al. 1994; Matthews and Perlmutter 1994; Yang and Baumfalk 1994). Recent work has shown that the late Paleozoic glaciation persisted at least until the Capitanian (late Permian; Fielding et al. 2008a; Fielding et al. 2008b; Rygel et al. 2008), thus providing a viable glacio-eustatic driver for the cyclicity observed.

3.6.5 - Origin of the erosive features (channels, channel complexes and slope valley) identified in the study area

The origin of the erosive features on the submarine slope can be linked to a range of processes, some of which may be related to relative sea-level change and others that are not. Pratson et al. (2007) and references therein present alternative possibilities such as earthquakes and spring sapping for the initiation and development of erosive features on submarine

slopes. These processes are largely independent of the sequence stratigraphic evolution and in many cases are localised on the middle and lower submarine slope. Twichell et al. (2009) showed how submarine landslides caused by processes such as those proposed by Pratson et al. (2007) can scour the continental margin on a regional scale. In this work however, the evidence leads to a different interpretation than those above.

As previously demonstrated the stratigraphy of the analysed succession shows a high degree of organisation. All major erosive features identified in the study area (mainly in Units E and F) are genetically related to the sand-prone units. In all cases the incisional surfaces that cut out clay-prone units have been mapped and shown to link to a sand-prone unit. An important observation is that the initial deposits of both Units E and F (sub-units E1 and F1) are not erosive, but are depositional distributive systems. All erosive features are linked to sub-units E2, E3, F2 and F3. This organised pattern suggests that the control on the development of the channels and slope valley is unlikely to be related to random (in space and time) failure processes but rather to the feeder system up dip of the study area. In fact, throughout the whole dataset, only in one location are mass movement deposits (slumps) that are not related to a sand-prone unit (E/F inter-unit claystone in Jakkarlsfontein farm). In this case they are of small scale (< 3 m thick) and do not involve sand deposition.

Based on these lines of evidence the major erosional features (channel, channel complexes and slope valley) identified in this work are interpreted to be controlled by the stratigraphic evolution of the depositional succession. In this interpretation, relative sea-level fall drove the incision processes. Moreover, the three-dimensional exposure of the outcrop belts around anticlines and synclines afforded a good control on the planform geometry of these features revealing that they are all slightly sinuous W-E oriented channels and a slope valley, rather than the fill of slump scars.

3.6.6 - The possibility of sediment transfer to deep-water during relative sea level highstand

The principles of seismic stratigraphy (Vail & Mitchum Jr, 1977; Vail *et al.,* 1977a; b; c; Mitchum *et al.* 1977a; b; c; Todd & Mitchum Jr, 1977) and the subsequent sequence stratigraphy (Van Wagoner *et. al.,* 1988; Posamentier *et al.,* 1988; Posamentier & Allen, 1998) assert that coarse-grained deposition in shallow water occurs preferentially while relative sea level is high, due to the presence of available accommodation in proximal areas. At this time the deep-water areas are starved and receive only pelagic and hemipelagic material. At lowstand times, especially in the situation when the shelf edge is subaerially exposed, the previously deposited coarse-grained sediments on the shelf are remobilized and transported by gravity-driven processes into deep-water environments. However a growing number of publications have demonstrated that this process also can happen during high sea level stands (Kuehl *et al.*, 1989, Weber *et al.,* 1997; Droz *et al.,* 2001; Mulder *et al.,* 2001; Covault *et al.*, 2007). It is generally understood nowadays that shelf physiography is an important variable. Narrow shelves or the presence of incised canyons on shelves can facilitate the transfer of coarse-grained sediment to deep marine environments during high sea level times.

These data provide new insights on the stratigraphic evolution of deep-marine depositional successions in the sense that sediment can also be transferred to deep-water during highstands, but only if the shelf physiography provides a mechanism to effectively narrow the shelf width, which arguably is then mimicking the 'typical' LST situation. These particular cases represent exemptions rather than general rules. In the case study, the shallow marine deposits coeval to the analysed succession are not present due post-depositional uplift of the Cape Fold Belt and therefore erosional removal of the up-dip section. Therefore, no interpretation is possible regarding to the particular characteristics of the shelf during the time of the deposition of the Laingsburg Formation. Consequently, the interpretation assumed in this work for the stratigraphic development of the succession is based on the general principles stated by the sequence stratigraphy

paradigm according to which the transfer of coarse-grained sediments to deep-water occur preferentially during lowstands.

3.7 - Conclusions

The upper Laingsburg Formation provides a 400 km^2 window into the stratigraphic evolution of a 470 m thick mid/upper submarine slope succession at a resolution higher than provided by seismic datasets. The across-slope distribution of sand-prone units is complicated by topographic effects that are related here to differential compaction of underlying stratigraphy. However, the succession is highly ordered and organised into a hierarchy of depositional sequences arranged in a basinward stepping to landward stepping stacking pattern. This stacking pattern is reflected in the upward change from basal sand-rich intraslope lobes, through leveed sand-prone channel complexes to entrenched slope valley fills with low sandstone percentage. The system then aggrades a sand-prone channel complex, above which are backstepping distal lobe systems.

Within this framework it is possible to predict the stratigraphic position of key architectural styles and hence reservoir types at scales below seismic resolution, within the seismic-scale composite sequence set. The driving mechanism for sequence development is considered to be glacio-eustasy superimposed on a long term relatively low subsidence regime.

Chapter 4 – Stratigraphic evolution of a depositional sequence in an upper submarine slope setting: a case study of Unit F2

4.1 - Introduction

In Chapter 3, the stratigraphy of the upper Laingsburg Formation was presented and the architecture and lithofacies of five sand-prone units (D/E, E, F, G and H) intercalated with hemipelagic claystone units was documented. Some of these units (E, F G) are divided into sand-prone sub-units, each interpreted as the lowstand systems tract (LST) to a depositional sequence (Fig. 3.30). These are separated by metre-scale hemipelagic claystone units that are interpreted as the transgressive and highstand systems tracts to each depositional sequence. Depositional sequences were the smallest stratigraphic units identified and mapped at the regional scale of analysis used for the interpretation presented in chapter 3. In this chapter, one of these depositional sequences (Sub-unit F2) is broken down into its constituent slope valley/channel-fill (and overbank) elements.

In chapter 3, the main erosional/depositional feature highlighted in F2 is a slope valley that is filled by a distinctive depositional succession identified on the southern flank of the present day Heuningberg anticline. The valley-fill deposits are flanked by a 60 m thick succession of thin-bedded deposits that thin and fine away from the valley fill and are interpreted as levee deposits (Fig. 3.16; 3.1; Enclosure 2A). In this chapter, F2 is analysed in more detail along the same outcrop belt where the slope valley was identified, but farther to the west (up-dip), on the Doornfontein farm (Figs. 4.1; 4.2). At this location, other depositional elements were recognized. The integration of this dataset has enabled the stratigraphic evolution of Sub-unit F2 to be documented within a well-defined regional context.

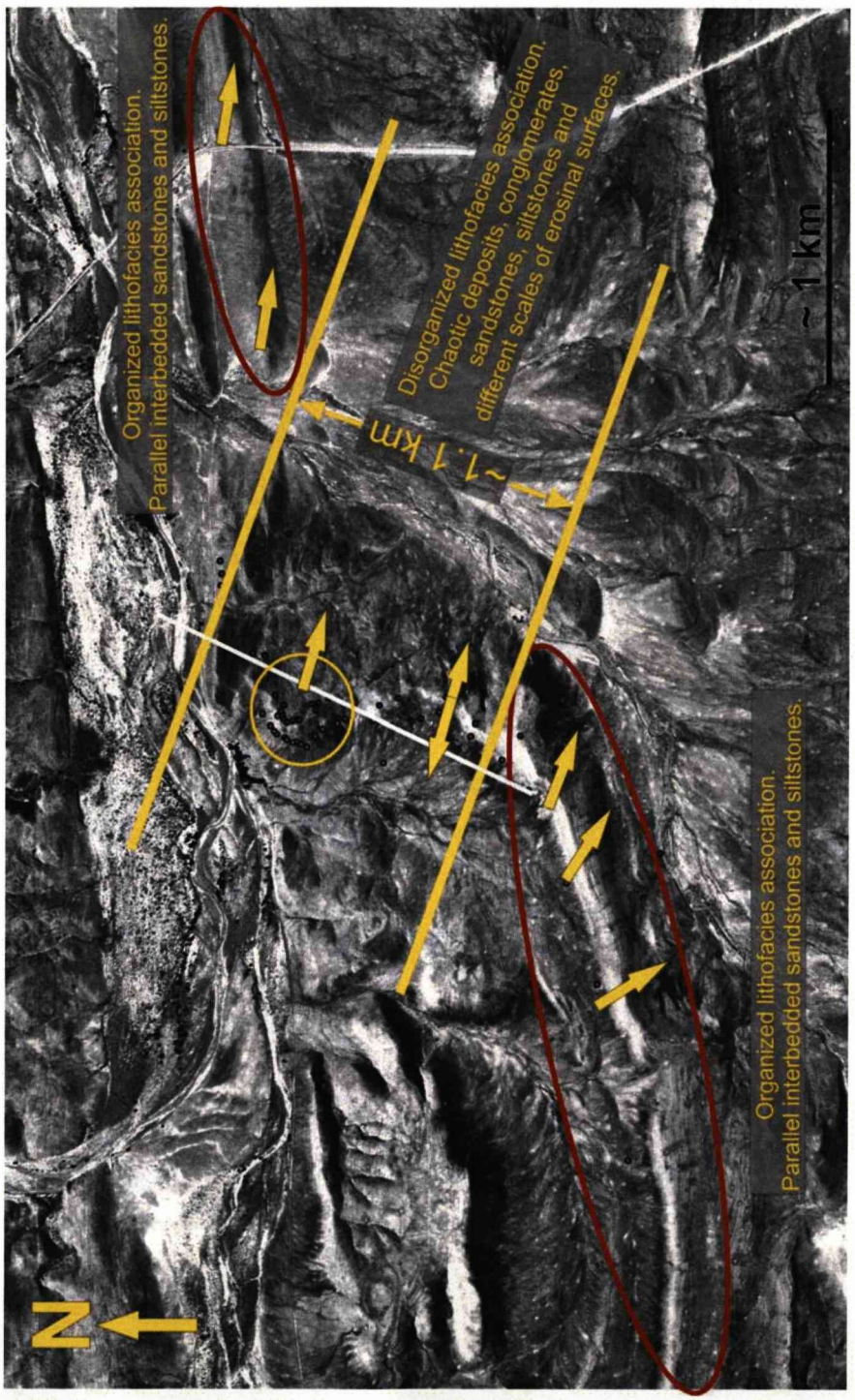

Figure 4.1 - Aerial photograph showing, between yellow parallel lines, the area occupied by several erosional surfaces and complex lithofacies associations (~ 1.1 km wide). Red ellipses show the areas where levee-overbank deposits (interpreted in chapter 3) crop out. The yellow circle shows the approximate area occupied by the case study in chapter 5. Yellow arrows represent main direction of palaeoflow. The double headed arrow represents azimuth data from primary current lineation and erosional surfaces. Small dots (see enlarged version in figure 4.2) are the GPS points for the base and top of the logged section. The white line perpendicular to the channel complex represents the approximate position of the stratigraphic panel shown in figure 4.3. The area shown in this photo is located on Doornfontein farm.

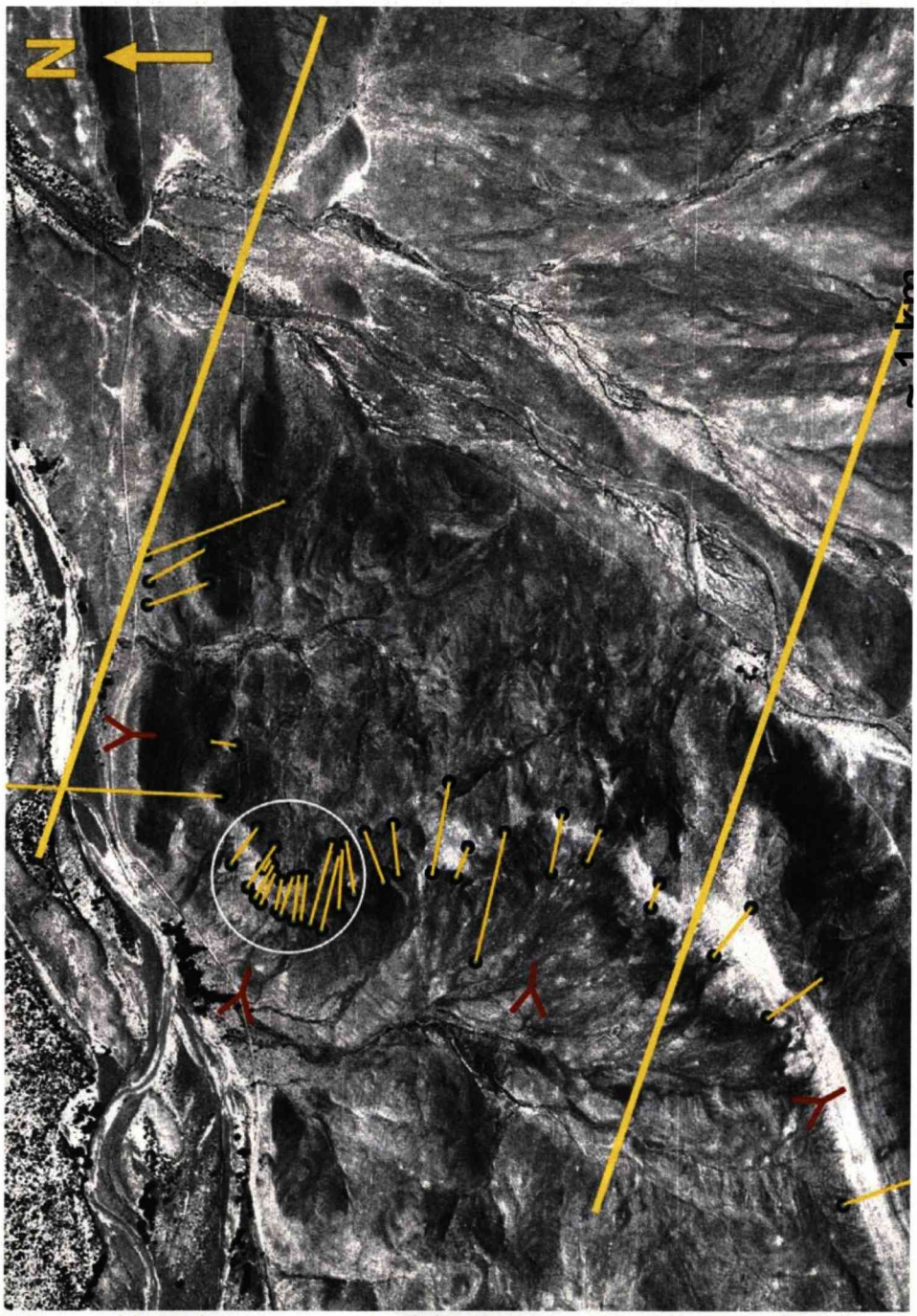

Figure 4.2 - Detail of the previous image highlighting: (1) logged section tracks depicted in as small yellow lines matching dots (GPS points of the base and top of the logs); (2) red symbols represent the stratigraphic younging direction; (3) Parallel large yellow lines represent boundaries between areas with different lithofacies associations as depicted in figure 4.1. White circle shows the chapter 5 study area.

4.2 - Anatomy of the F2 lowstand systems tract

On Doornfontein farm (Figs. 4.1; 4.2) a more than 1 km-wide, SW-NE oriented erosional feature is present. An area of complicated stratigraphy and variable lithofacies associations (LA 10, LA 9, LA 8, LA 7, LA 4, LA 2) that overlie a series of smaller scale erosional surfaces lie within the large erosional feature. Initially, this feature is referred to as a 'channel system'[2] due to the large amount of erosion at different scales within the kilometre-wide corridor. In the regional analysis presented in chapter 3, depositional elements identified in this site were not differentiated between unit F2 or F3 (Enclosure 2A). At the more detailed scale presented in this chapter, however, an attempt is made to discriminate between those elements that are of F2 age and those that belong to F3, although there remains some uncertainty in the stratigraphic relationship between axial (erosion-dominated) and marginal (deposition-dominated) parts of the stratigraphic succession.

4.2.1 - Hierarchy of incisional surfaces and classification of depositional systems

Observations

A hierarchy of erosion surfaces was established by mapping key surfaces between 26 logged sections (Fig. 4.3; Enclosure 5) and lithofacies association analysis of the sedimentary fill of the erosion surfaces within the channel system. The base of the entire channel system is identified as a first order surface[3]. However, it is not a single erosive surface but a composite surface of higher order surfaces, which can even belong to different stratigraphic units (i.e. sub-units F2 or F3).

The subsidiary erosional surfaces are termed second order surfaces and can also be composite. Second order surfaces bound erosional cuts that are usually greater than 300 m wide and 30 m deep, but truncation by

[2] The term 'channel system' is used in this work only to refer to a depositional system where more than one discrete channel is identified without any connotation of hierarchy of the erosional/depositional elements.

[3] This hierarchy is solely based on the scale of erosional features and has no sequence stratigraphic connotation.

younger erosion surfaces can reduce the preserved dimensions and complicate interpretation of hierarchical level. In these cases, lithofacies association analysis helped to clarify the hierarchical position of the erosional surface. Five possible second order erosion surfaces were identified (Fig. 4.3). One of them (the third in stratigraphic order from the base) has a fill that is sufficiently preserved to allow the recognition of third and fourth order erosion features within it, each type being marked by a characteristic filling style.

Interpretation

The interpreted geological setting (upper submarine slope – chapter 3), the characteristics of the erosion surfaces and the lithologies (discussed in detail in chapter 5) of the analysed succession lead to the identification of four orders of erosion surfaces, all formed by the action of erosive subaqueous gravity flows. The first order surface is in fact a composite of various second order surfaces which are interpreted (following Clark and Pickering, 1996) to have been carved by multiple discrete erosive flows that bypassed sand downdip. Ultimately, this leaves a negative concave up topographic feature on the contemporary sea floor in orthogonal section to the regional flow direction. This interpretation implies that along the flow direction, both down and up dip, the feature will have the three-dimensional shape of a channel, in this case a submarine channel (*sensu* Mutti and Normark, 1991). In a similar way, the third order erosional surfaces are also interpreted as the bases of submarine channels, being different only in their dimensions (width *vs.* depth). Fourth order erosional surfaces are smaller, localised and show more irregular geometry. Consequently, they are not interpreted as bounding channels, rather, as minor erosive features such as scour-fills (sub-channel elements).

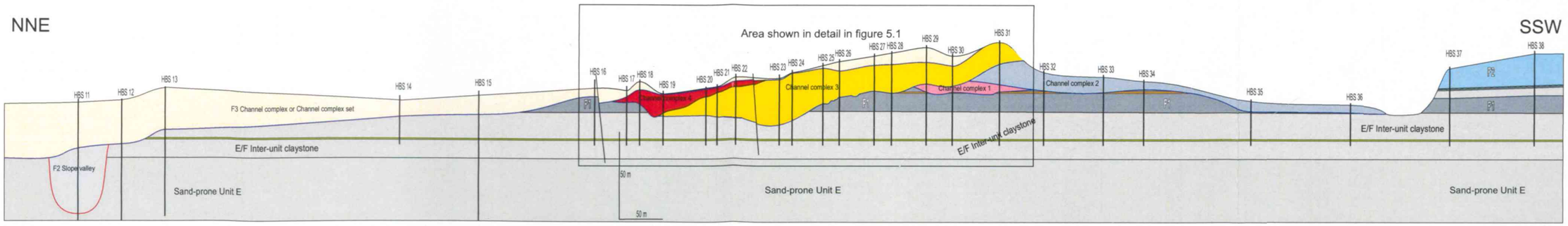

Unit	Sand-prone Unit E	E/F claystone unit	Local layer of siltstone	Sand-prone Unit F		
Sub-unit				F1	F2	F3 (?)
Depositional system	Interpreted in chapter 3	Interpreted in chapter 3	Not interpreted	Distal fringes of distributive systems *Interpreted in chapter 3*	F2 Slope valley *Interpreted in chapter 3* F2 Channel-levee complex set: Levee-overbank deposits *Interpreted in chapter 3*; Channel complex 4; Channel complex 3; Channel complex 2; Channel complex 1	F3 Channel complex or Channel complex set

Figure 4.3 - Stratigraphic panel based on correlation of logged sections (black vertical lines), mapping of key surfaces, and lithofacies association analysis. Different colours represent different depositional/stratigraphic unit labelled on the figure and/or identified in the colour code. Black square is the approximate area shown in enclosure 6. This panel is represented in figure 4.1 by the white line orthogonal to palaeoflow direction.

In this case the third order surfaces are interpreted as the bases to channel elements. The surface plus the fill represent a single cycle from incision to abandonment. These elements are, therefore, the building block of the depositional systems analysed here and so are classified as single cycle submarine channels. Following the hierarchical scheme presented by Sprague et al. (2003), it is proposed that the assemblage of single cycle submarine channels confined by the second order erosion surfaces are classified as submarine channel complexes, and the assemblage of channel complexes confined by the first order incision surface as submarine channel complex sets (Fig. 4.4). This being the case, the depositional system of the wide (> 1 km) corridor characterized by the large amount of erosive features and complicated facies associations is interpreted as at least one channel complex set. However, as previously stated, this channel complex set could represent an amalgamation of elements of different stratigraphic units (F2 and F3), and so, represent more than one channel complex set. Bearing in mind restrictions due the limited exposure an attempt is made to discriminate F2 and F3 elements in this study area.

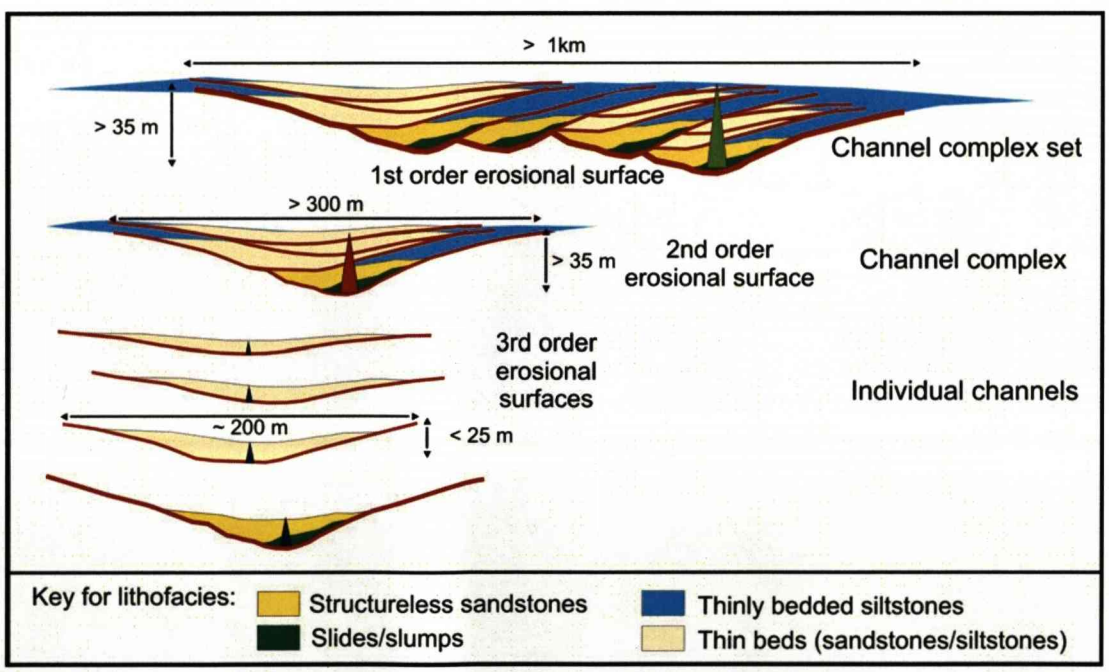

Figure 4.4 – Proposed hierarchy for the erosional/depositional elements (following Sprague et al., 2003).

4.2.2 - Discrimination between F2 and F3 aged erosional/depositional elements

Five second order erosion surfaces and their related fills have been identified within the study area on Doornfontein farm. However, the youngest surface and its fill do not share the same characteristics as the others. This is deeper (about 100 m) and wider (it is mapped for at least 500 m orthogonal to palaeoflow) than the others (Fig. 4.3; Enclosure 5) and its fill is much more sand-prone (Fig. 4.5). It shares a similar fill with a well characterised channel system identified in Sub-unit F3 further downdip (discussed in chapter 3). These data suggest a possible correlation of the fifth channel complex with the F3 channel system[4] further down dip to the east. In this case the youngest sandier channel-fill in the Doornfontein farm channel complex set would belong to the younger Sub-unit F3 and would represent a separate channel complex (or, maybe, a channel complex set) as it is part of a different sequence. This being the case the other four channel complexes in the Doornfontein farm area are interpreted to belong to F2. However, as no direct stratigraphic relationship is exposed between the axial (erosion-dominated) and marginal (deposition-dominated) deposits where the upper Unit F claystone are preserved, there remains some uncertainty concerning the exact ages of channel complexes 1-4.

[4] The term "channel system" is used here in the same way it was in section 4.2, i.e., only to refer to a depositional system where more than one discrete channel is identified without any connotation of hierarchy of the erosional/depositional elements.

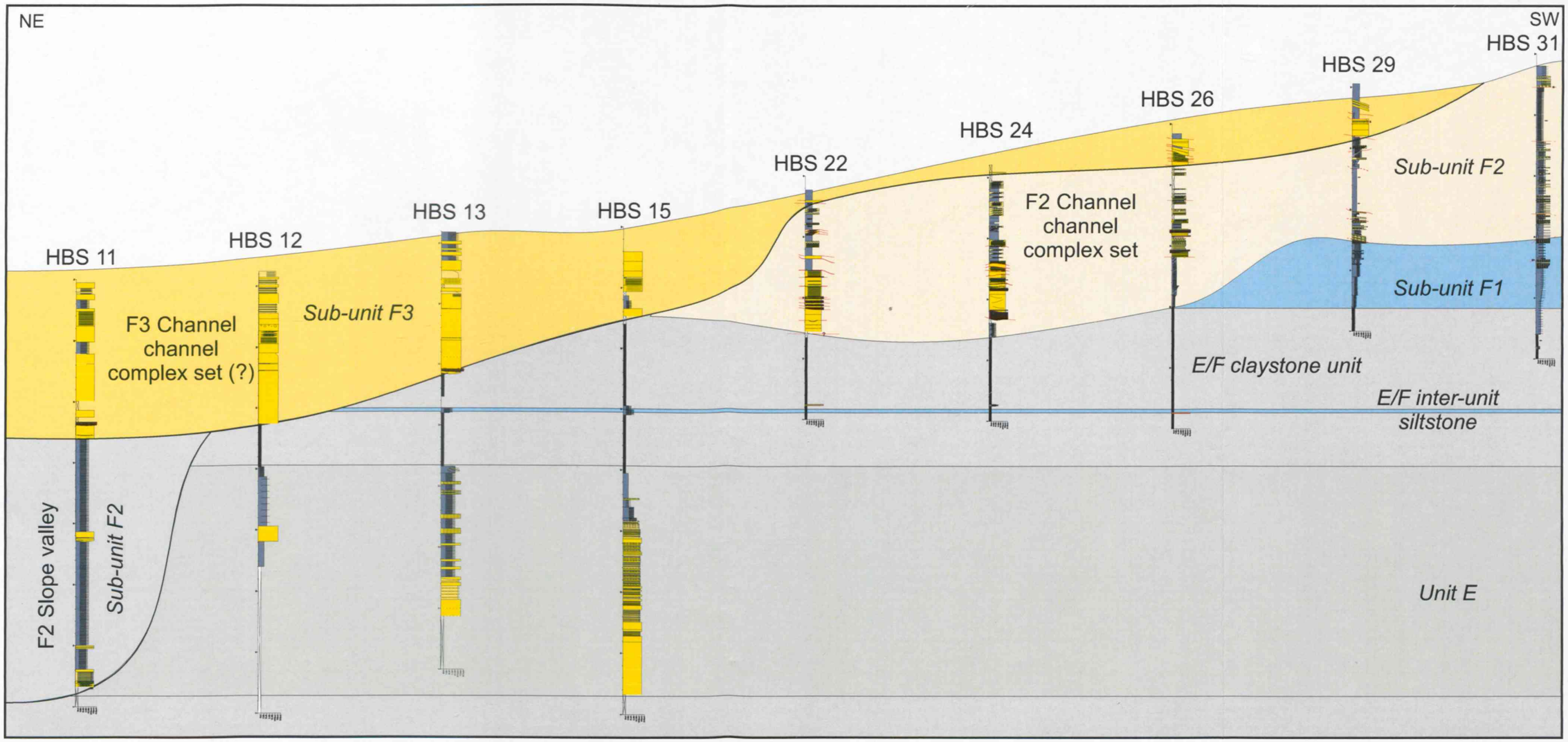

Figure 4.5 - Stratigraphic panel with logged sections highlighting the difference between lithofacies associations in the interpreted F2 Channel complex set (pale yellow) and the possible F3 Channel complex or Channel complex set (yellow). Logs HBS 11, 12,13 and 15 show higher content of structureless sandstones than those interpreted as belonging to F2 channel complex set. Also notice that the minimum incision in F3 is deeper than in F2. The panel is not at true horizontal scale. See figure 4.3 for location of the logged sections.

4.3 - Stratigraphic evolution of the F2 LST

4.3.1 - Physical stratigraphic data

The regional inter- and intra- unit claystone are the main physical stratigraphic constraints in this study. On Doornfontein farm the claystone unit between Units E and F is well exposed, allowing good control on the depth of the composite erosion in Unit F. An additional stratigraphic control in this area is a local thin (c.a. 1 m) unit of thin-bedded siltstone present within the claystone unit between Units E and F (the E/F inter-unit siltstone). This siltstone is exposed in almost all the area around the pericline on Doornfontein farm (Figs. 4.3; 4.5; Enclosure 5) and was used as a marker for the logged sections.

The intra-unit claystone between F1 and F2 is not present within the channel complex set due to the widespread erosion, but it is present in the thin-bedded deposits that flank the channel complex set that are interpreted as levee/overbank settings (Fig. 4.3; Enclosure 5). It is therefore possible to map sub-unit F1, and observe that it does not change lithofacies associations and architecture from "outside" of the channel complex set into the "inside" area, in contrast to the upper sub-units. This implies that despite the lower intra-unit claystone not being present in the channel complex set area, Sub-unit F1 is not part of this large erosive feature, supporting the interpretation in chapter 3 that F1 was deposited as an "apron-like" succession. Sub-unit F1 is, in fact, eroded by F2 and F3 in the channel complex set area.

4.3.2 - Stratigraphic evolution

The stratigraphic evolution of the lowstand systems tract (LST) of the F2 depositional sequence is directly related to the stratigraphic relationship between the slope valley (discussed in chapter 3) and the channel complex set (discussed in this chapter) both interpreted to belong to Sub-unit F2. Here, a model is presented for the evolution of the depositional system of a lowstand system tract in an upper slope submarine setting.

In chapter 3 it was shown that F2 is the thickest and most erosive sub-unit in Unit F. The levee and overbank deposits identified in Sub-unit F2 in the northern and central area (Enclosures 2A and 2B) can be up to 60 m thick. It was also discussed that such thick and sand-prone (in the lower parts of the succession) levees are, usually, not a product of deeply entrenched slope valleys as it is difficult for sand to spill out of that confinement. Consequently, it was proposed that prior to the entrenchment of the slope valley, an earlier non-entrenched channel system was present, and that supplied sediment to build and be confined by levees. The channel complex set identified on the Doornfontein farm could be interpreted as a remnant expression of the axial portion to an older F2-aged erosional/depositional channel-levee system (*sensu* Mutti and Normark 1991). Although there is a remnant of the entrenched siltstone-prone slope valley-fill on Doornfontein farm (Figs. 4.3; 4.5; Enclosure 5), no direct relationship between these two systems (the slope valley and the channel levee-complex set) is seen in the field, so it is not conclusive which system is older or younger. To elucidate this, a comparison is made with a model in the literature based on seismic data.

Deptuck et al. (2007) presented an example of a near surface canyon (Pleistocene in age) offshore of the Niger Delta (the Benin-major canyon) and discussed its stratigraphic evolution. The dimensions (depth *vs* width) and the depositional setting (upper slope) of the Benin-major canyon are similar to the interpreted slope valley in F2, suggesting that these two examples are appropriate for comparison. Deptuck et al. (2007) interpreted, from seismic data, levee-overbank deposits flanking the canyon and inferred that they were related to an "early incision of the canyon". The channel-fill deposits of this early incisional phase are interpreted to have been removed by later, deeper incisions. According to those authors the flows responsible for carving such a canyon would not have contributed, or only contributed little material to the levee-overbank construction (Fig. 4.6).

Using the Deptuck et al. (2007) model as an analogue, the channel-levee complex set in F2 would be older than the slope valley-fill (Fig. 4.7). The difference between the two examples is that in the Laingsburg case, parts of the early incisional/depositional elements (the channel complex set)

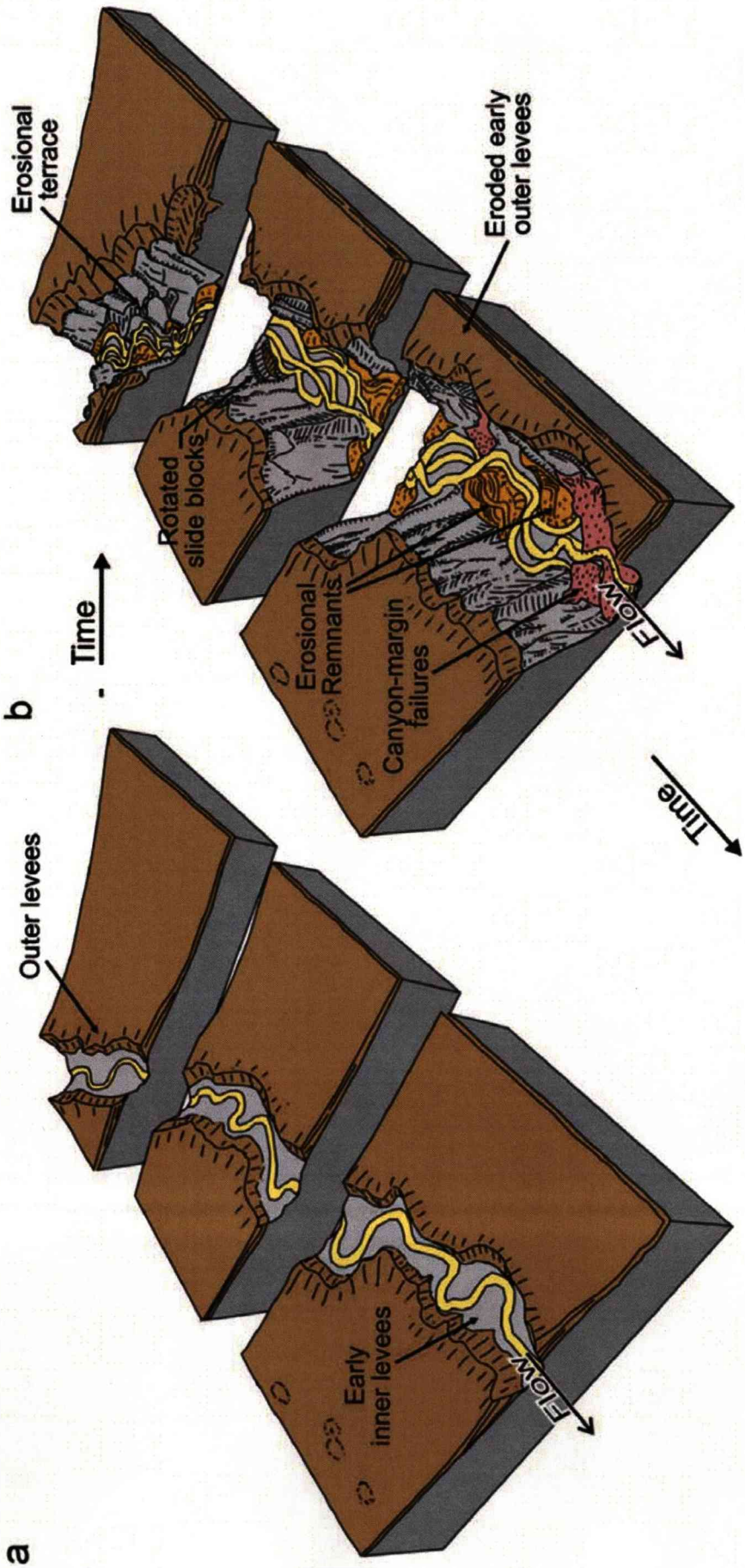

Figure 4.6 - Model for channel complex development (a) followed by deep incision of a canyon (b) proposed by Deptuck et al. (2007).

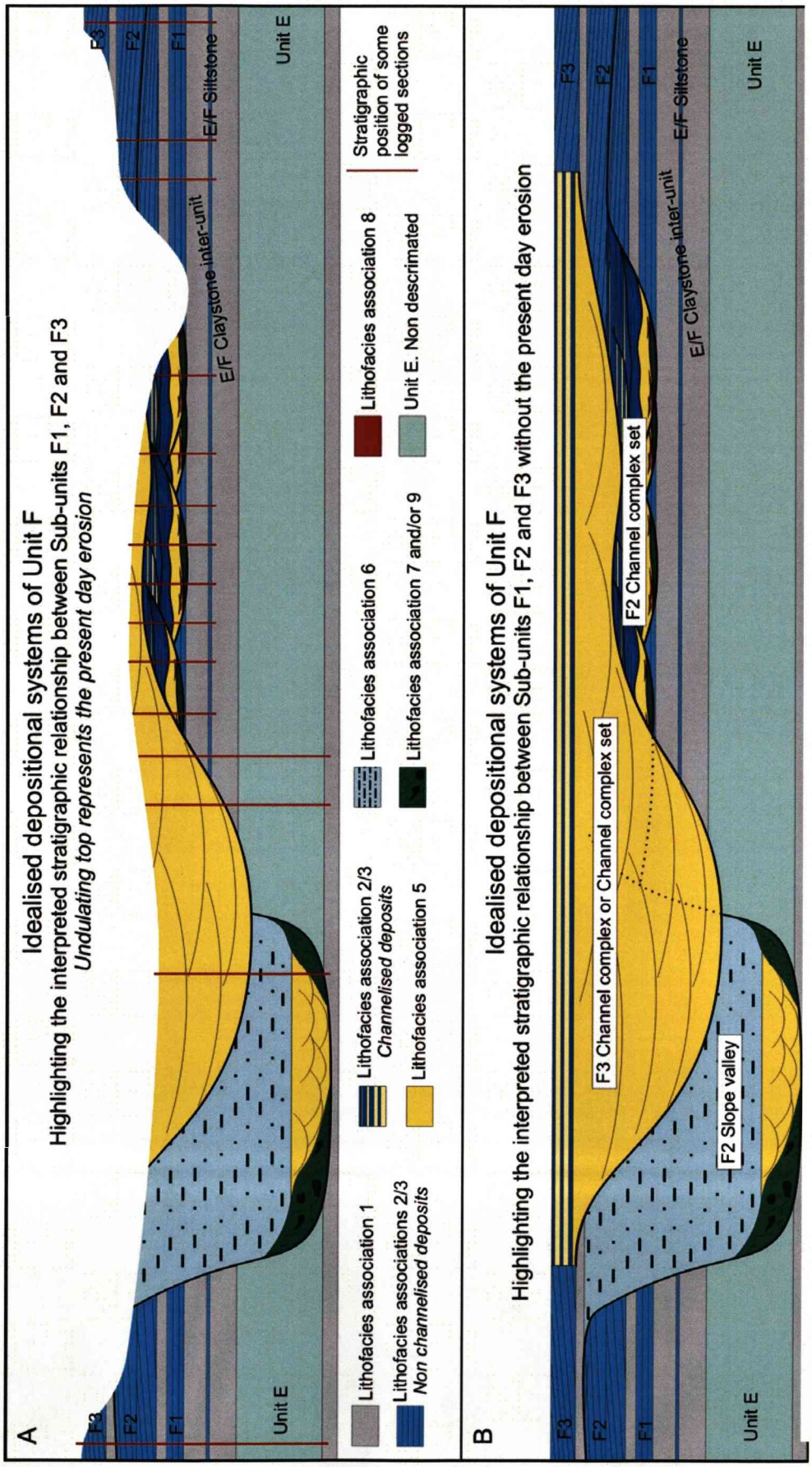

Figure 4.7 - Idealised across strike succession of the upper slope deposits in the Laingsburg Formation (from Unit E to Unit F) showing the interpreted stratigraphic relationship between Sub-units F1, F2 and F3. Dotted lines on the F3 system indicate the interpreted age relations between the slope valley and channel complex set.

are preserved, affording a more detailed interpretation of stratigraphic evolution than that presented by Deptuck et al. (2007).

The proposed model for the stratigraphic evolution of the LST of the F2 depositional sequence is that the channel-levee complex set would have developed as initial forced regressive deposits on the slope prior to the maximum rate of relative sea-level fall (the F inflection point). At this point, the cutting of the slope valley would have taken place at the time of maximum energy and it acted subsequently as the main conduit for gravity flows into the basin during early lowstand time. Filling of the valley then took place as the system backstepped later in the LST. This interpretation is summarised in figure 4.8.

This traditional interpretation, also reinforced by the example presented by Deptuck et al. (2007), is applicable for the development of F2. However as no direct physical relationship between the channel-levee complex set and the slope valley is seen in the field, alternative interpretations cannot be ruled out. Pratson et al. (2007) and references therein, present alternative possibilities such as earthquakes and spring sapping for the initiation and development of entrenched erosive features on submarine slopes. These processes are independent of the sequence stratigraphic evolution and in many cases are localised on the middle and lower submarine slope. Nevertheless they also can reach the shelf break and eventually capture a coarse-grained sediment feeder system. If this was the case in F2 the cutting of the valley and its landward evolution could be contemporary, or even older than the channel-levee complex set.

Within the whole analysed succession (chapter 3), Unit F is interpreted to have developed during the maximum progradation of the submarine slope. Therefore, this unit represents the most likely time at which the coarse-grained sediment source (possibly a river) reached the shelf break, favouring the development of the deeply incised slope valley. Similar scale erosive features are not found in the underlying units in this part of the depocentre. The coincidence of the location of the slope valley with the channel complex set suggests some level of genetic relationship. In the alternative model discussed above of a slope valley that initiated on the middle or lower submarine slope and reached the shelf edge by knickpoint

erosion, it is considered unlikely that this point should coincide exactly with an underlying upper slope channel system. These observations/ interpretations favour the sequence stratigraphic interpretation for the development of the channel complex set and the slope valley instead of the slope-initiated valley option.

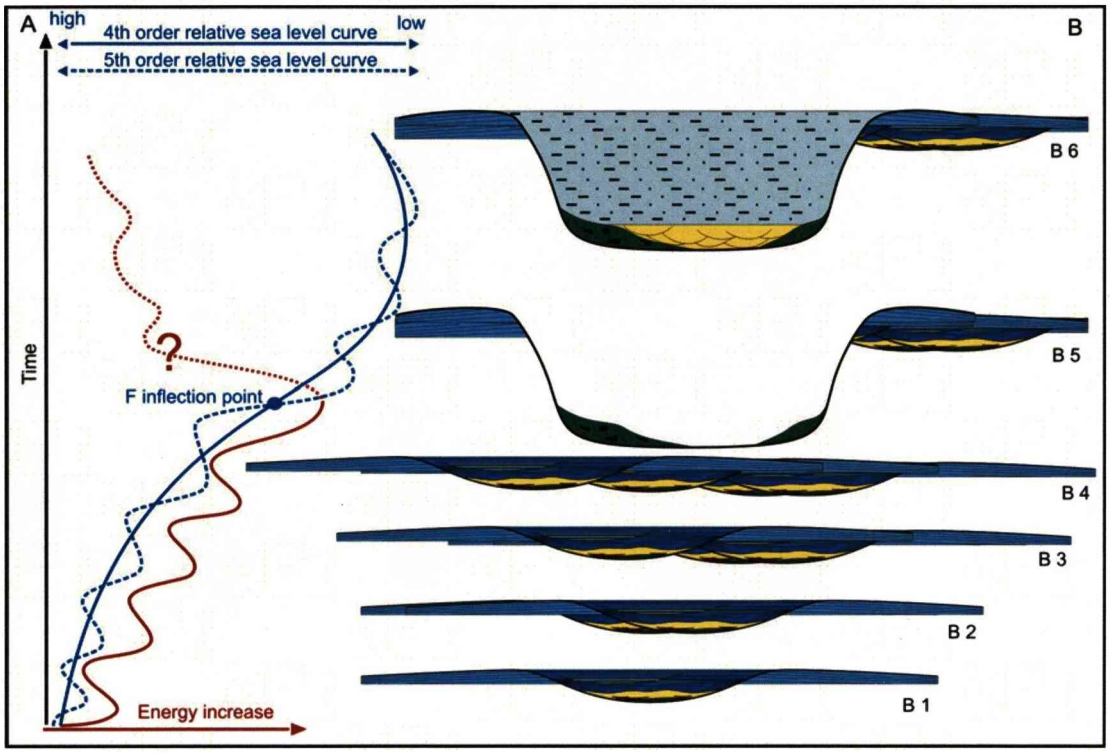

Figure 4.8 - Model for the stratigraphic evolution of the LST of the F2 based on the sequence stratigraphic principles. (A) Simplified interpreted energy profile through time during the F2 development. In the lower part the curve shows an overall increase in energy but punctuated by higher order decreases. In this lower portion the curve is a solid line because it was deduced from the geological record. In the upper part the curve shows an overall decrease in energy, however the acquired dataset does not enable a conclusive interpretation so this section of the curve is dotted. (B) Cartoons representing the stratigraphic development of the depositional systems in F2. B1 to B4 represent the evolution of the F2 Channel-levee complex set. B5 and B6 represent the development of the F2 Slope valley. B5 marks the highest interpreted energy of the depositional system and B6 represents the fill of the entrenched valley during an overall decrease in energy.

4.3.3 - Sequence stratigraphic controls on the development of F2

The absence of chronostratigraphic data precludes estimate of the duration of the F2 LST and its constituent erosional/depositional events and deposits. However the recognition of a hierarchy of elements allows a *relative* chronostratigraphic framework to be established. Further

comparisons with age constrained deep-water depositional examples presented in the literature can shed some light on the possible time involved for deposition of the case study sequence.

In the relative chronostratigraphic framework presented in chapter three, depositional sequence F2 lies within composite sequence F. Overlying Unit F is a thick claystone unit. This claystone unit can be compared to the thick hemipelagic unit overlying the Angola dataset presented by Mayall et al. (2006). Considering this as a reference, the whole composite sequence F could be interpreted as a response to a third order cycle of relative sea level change, representing 1-2 Ma (Mitchum and Van Wagoner, 1991). This being the case, the LST of depositional sequence F2 would be related to a 4^{th} order cycle of relative sea level change and its internal constituent channel complexes and single channels to higher order cycles of sediment supply to the slope (5^{th} and 6^{th} order).

In chapter 3 a repetitive organisation of stratigraphy was demonstrated at different scales (from depositional sequence to composite sequence set) in the erosional/depositional systems analysed in the entire research area, and this organisation was interpreted to reflect allocyclic control. In this chapter the internal development of erosional/depositional systems in the lowstand systems tract of a single depositional sequence has been presented. At this higher resolution analysis a similar hierarchical stratigraphic order is still evident in terms of the punctuated evolution of the channel complexes (possible 5^{th} order elements). At an even higher resolution (possible 6^{th} order elements), this order seems to break down, possibly as local processes started to dominate the architectural style.

Chapter 5 – Architectural hierarchy and anatomy of a submarine slope channel complex

5.1 – Introduction

There is an extensive literature on the morphology, dimensions and sedimentary fill of submarine channels based on both seismic data sets and outcrop studies (e.g. Mutti and Normark, 1991; Clark and Pickering 1996; Gardner and Borer, 2000; Mayall and Stewart, 2000; Abreu et al., 2003; Gardner et al., 2003; Mayall et al., 2006; Deptuck et al., 2007). These papers focus on classification, geometrical aspects, stacking patterns, depositional processes, and lithofacies distribution/prediction from individual elements up to whole systems. Outcrop examples are usually focussed on the coarse-grained fills (sandstones and coarser-grained lithologies) due to exposure problems with finer grained portions of fills. This biases the reported percentage of sandstone and commonly hinders identification of the extent of erosion surfaces and the stratigraphic relationship between the channel-fill and levee/overbank deposits. This chapter presents a detailed analysis of an upper slope submarine channel complex (following the hierarchical scheme of Sprague et al., 2003) in which the fine-grained content is well preserved, offering a rare opportunity to "walk-out" from the complex axis to complex margin through lithofacies transitions. The analysis includes description and interpretation of the stratigraphy of the channel complex-fill and the distribution and hierarchy of the erosional surfaces observed within the channel complex. The depositional processes and the stratigraphic evolution are also discussed, and a model is presented for channel complex infill and the nature of these features as reservoirs for hydrocarbons.

The channel complex analysed in this chapter is the third in the channel complex set of Sub-unit F2 and it was chosen because it has the most representative and complete stratigraphic record preserved, which allows a detailed interpretation of the lithofacies distribution and the hierarchy of the erosive features (Enclosure 6).

5.2 - Hierarchy of the incisional surfaces

In chapter 4 the basal erosive surface of the channel complex set was classified as a first order surface[5]. It was also seen that this first order surface is not a single surface, but forms a composite of several second order erosive surfaces, which represent the basal surfaces of channel complexes within the channel complex set.

The cross-section of the most completely exposed second order erosional surface crops out for about 300 m (SW-NE, roughly orthogonal to palaeoflow). It is truncated on one side by the present day topography and on the other side by younger second order erosional surface (Enclosure 6). Consequently, this surface was originally wider than 300 m. At the deepest point it incises 35 m cutting through an older second order erosion surface fill; sub-unit F1 (see chapter 3 for description and interpretation); and the claystone between Units E and F indicating that the erosion carved into the contemporary seabed (Enclosure 6). Hereafter this erosive surface will be called *erosional surface 3.1* (3 because this the third second order erosion surface, and 1 because it is the first fill of the case study; Enclosure 6).

Erosional surface 3.1 has a relatively steep concave up profile in the axial area (around the point of deepest incision) and a shallower profile at the margins (Enclosure 6). Within the fill three third order erosional surfaces show northeast sub-vertical offset. From the oldest upwards, these surfaces will be called *erosional surfaces 3.2, 3.3 and 3.4* (Enclosure 6). All of them are truncated to the NE by younger erosion surfaces. They are ~ 200 m wide and about 20/25 m deep (except for 3.4 that is considerably shallower, about 7 m), and they all show a shallower profile than erosion surface 3.1. On the southwestern margin, the second order erosional surface 3.1 and the third order erosional surface 3.2 merge to form the basal erosion surface of F2 (Enclosure 6). This suggests that surface 3.2 might have widened the previous cut but not deepened it, and that surface 3.1 is composite. Erosion surface 3.3, which is sub-vertically stacked above the sedimentary fill of 3.2,

[5] The terms first, second, third and fourth order used in this chapter are solely based on the scale of erosional features and have no sequence stratigraphic connotation.

also cuts down into it. Erosion surface 3.4 follows the same pattern in relation to 3.3, but with more lateral offset. In the axial area of second order erosional surface 3.1, the sedimentary succession between this surface and erosional surface 3.2 is incised by many minor erosion surfaces, randomly arranged (Enclosure 6). These minor erosional surfaces are interpreted as fourth order ones.

This description substantiates the hierarchy proposed in chapter 4 in which channels are grouped in channel complexes and these into channel complex sets. In this context the example discussed in this chapter is classified as a channel complex with the second and third order incisional surfaces bounding submarine channel-fills, hereafter called, from oldest to youngest, channels 3.1, 3.2, 3.3 and 3.4.

5.3 - Stacking patterns of the channel-fills

5.3.1 - Basal chaotic deposits (channel 3.1)

Observations

In the axial area of channel 3.1 the basal erosion surface is overlain by up to 4 m of tilted and slightly folded thinly bedded siltstones (Lithofacies L9; Enclosure 6). Grain-size and bed thickness are similar to the siltstones found laterally in Sub-unit F1 (Enclosure 6) and so it is difficult to map the erosion surface where it is adjacent to F1 since there is no abrupt change in lithofacies across it.

Interpretation / Depositional processes

The characteristics of these deposits suggest that they are slumps and slides sourced locally from the channel walls during the time the channel was being incised and acting as a conduit for the passage of erosive gravitational flows down dip.

5.3.2 - Sandstones and conglomerates (channel 3.1)

Observations

Most of erosion surface 3.1 is overlain by sharp based bodies of structureless/planar-laminated fine-grained sandstone and mudstone clast conglomerates. The sandstones are usually erosive based, between 0.3 m and 1 m thick (Lithofacies L6) and in some locations amalgamate to form bedsets more than 2 m thick (Fig. 5.1). Grooves and load structures are

Photo 5.1 – Basal chaotic deposits (L9) overlain by thick bed of structureless sandstone (L6; yellow notebook) which is eroded and overlain by mudstone clast conglomerate (L7). Overlying the conglomerate is a succession of about 2 m thick of amalgamated thick beds of structureless/planar-laminated fine-grained sandstone (L6). Axis of the channel. See photo location (photo 1) in Enclosure 6.

locally present at the bed bases. The sandstones vary from predominantly structureless in the axis to predominantly planar-laminated in lateral positions. However, even in the axis structureless sandstone is interlaminated vertically with planar-lamination.

Layers of mudstone clast conglomerate (L7), which can range from a few centimetres to more than one metre thick showing abrupt variation, commonly mantle erosional surfaces (Fig. 5.2). They are thicker in the axis and close to the base of the channel fill (Enclosure 6). Intraformational mudstone clasts are also present scattered within the sandstone beds, but concentrated toward bed bases.

The maximum preserved thickness of the whole sandstone/conglomerate succession within channel 3.1 is about 12 m (between logs HBS 20 and HBS 24 in Enclosure 6). Locally, an upward transition from planar-laminated fine-grained sandstone beds (L5) through climbing ripple laminated very fine-grained sandstone beds (L4a) into thin siltstone beds (L2) is observed (log HBS 21 in Enclosure 6). This indicates that the top of this succession is not significantly eroded at this point and provides a reliable thickness of 12 m. The sandstone-conglomerate succession represents the bulk of the fill.

Photo 5.3 – Mudclast conglomerates (L7) mantling scoured sandstone bed. Scale: 10 cm each division in logging pole. See photo location (photo 2) in Enclosure 6.

Palaeocurrent indicators from erosive features such as margins of erosion surface and sole marks show W-E and NW-SE bi-directional trends. Current ripple lamination palaeocurrents range from ENE to ESE (Fig 5.3A; Appendix 1).

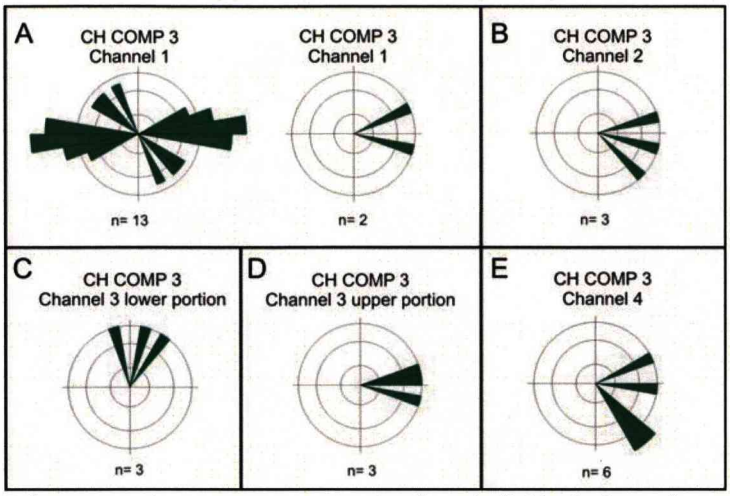

Figure 5.3 – Palaeocurrent measurement in the four individual channels comprised by channel complex 3. (A) channel 1; (B) channel 2; (C/D) channel 3; (E) channel 4. For palaeocurrent also see Appendix 1.

Interpretation / Depositional processes

The characteristics of the structureless-planar laminated sandstones intercalated with mudstone clast conglomerates suggest a mix of sediment bypass and deposition. The pattern of the conglomerates always overlying erosional surfaces leads to their interpretation as residual lags of energetic sediment gravity flows that eroded the channel floor and bypassed sand down dip leaving behind these deposits. By contrast, the sandstones show characteristics that suggest deposition from relatively less energetic sediment gravity flows. The vertical interchanging between structureless and faint planar lamination suggests deposition from long-lived flows with variation in momentum. Following Kneller and Branney (1995) this is interpreted as rapid deposition from prolonged, quasi-steady high-density turbidity currents due to non-uniformity in the flow. The occurrence of sandstones deposited from these kinds of currents does not mean terminal deposition, but implies some bypass of sand further down dip since only the near bed layer of the flow lost capacity and deposited (Allen, 1995). However the upward decrease in the residual lags within the succession suggests an overall decrease in the energy of the system and an increase in intra-channel deposition. Decreases of energy, volume and height of the sediment gravity flows would imply a decrease in the amount of spill and deposition outside of the channel, i.e. a reduction in external levee-overbank development

(following Clark and Pickering, 1996). However, this cannot be demonstrated in this work.

The non-erosive top of the sandstone-conglomerate succession with a thickness of about 12 m contrasts with the more than 35 m depth of erosional surface 3.1. This suggests that channel 3.1 was underfilled when channel 3.2 was cut.

5.3.3 - Thinly bedded/chaotic succession (channel 3.2)

Observations

The underlying unit is partially cut by channel 3.2, which is overlain by a distinctive siltstone-prone unit (LA 2). Toward the axis of channel 3.2 the erosional surface incises to its deepest point in a series of steps (at a scale of a few metres). Here, chaotic folded thin beds (L9) with some internal organization comprising folded rafts of sandstone beds within a siltstone matrix overlie the erosional surface (Fig. 5.4). These deposits are overlain by thin siltstones (L2) and discontinuous beds of fine-grained, planar- and current ripple-laminated sandstone (L4a), which locally directly overlie erosion surface 3.2. To the southwest, toward the channel margin, a subtle lateral change from this lithofacies to very thinly bedded siltstone with rare very thin beds of very fine-grained sandstone (LA 2) occurs (Fig. 5.5; Enclosure 6). The top of this succession is eroded by the younger erosion surface 3.3 so it is not possible to measure the true depositional thickness of channel-fill 3.2. The maximum apparent thickness of ~10 m was measured in log HBS28 (Enclosure 6) not in a channel axis position. Palaeocurrent measurements from current ripple lamination range from ENE to SE (Fig 5.3B; Appendix 1).

Interpretation / Depositional processes

The chaotic deposits in channel 3.2 are interpreted as locally derived slumps. The absence of claystone clasts at this site suggests that erosional surface 3.2 does not cut into the claystones below the base of Unit F up-dip. The undulating geometry of the erosional surface mantled by the slump deposits suggests high energy processes and so an increase in system

energy compared to the waning energy characteristics of the final stage of the underlying unit. Moreover, as the lithological record of this succession is predominantly fine-grained (silt-prone) and flows carrying only silt could not have cut the erosion surface, it is likely that the initial flows that incised the erosional surface bypassed sediment down dip, leaving behind only the localized slumps and possibly some contribution to the external levee-overbank deposits. The fine grained channel fill material would have been deposited from later weaker flows, which left siltstones and very fine grained sandstones in the channel axis and most siltstones in the channel margins.

The 3.2 erosional surface is stacked vertically over the axis of the underlying channel 3.1, which suggests that these two channel-fills are vertically or sub-vertically stacked, yet with very different fill types.

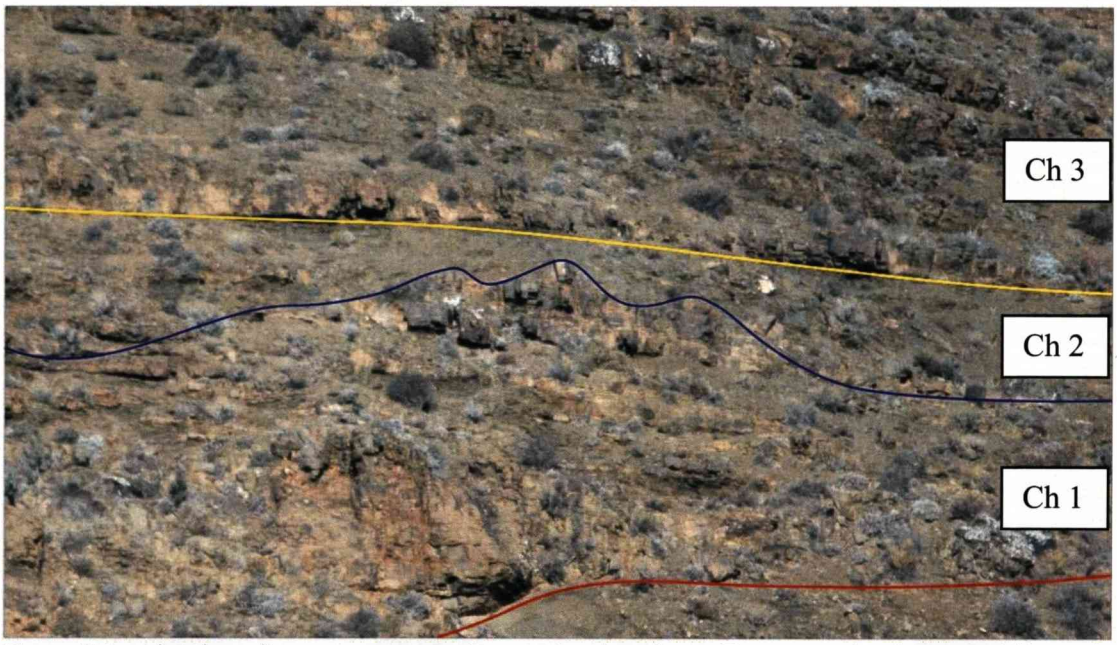

Figure 5.4 – The three lines represent major erosional surfaces. The succession between blue and yellow lines is dominated by lithofacies association 2 and 10 with some internal organization comprising, mainly, folded rafts of sandstone beds in a silt-prone matrix. See photo location (photo 3) in Enclosure 6.

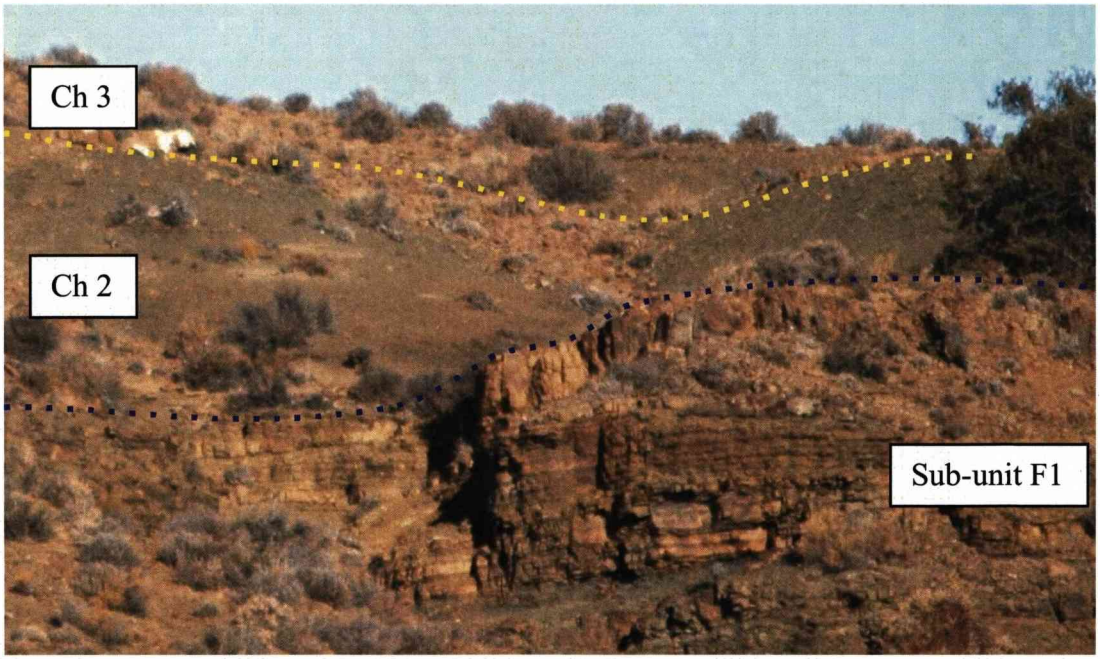

Figure 5.5 – Abrupt and irregular facies contrast at the base of the analysed stratigraphic succession showing fine-grained lithologies (LA 2) overlying sandstones (LA 4). The surface marked with the blue dotted line can be "walked out" up to the facies contrast showed in photo 1. Lithofacies change can be mapped from the point shown in photo 1 to the point shown in photo2. See photo location (photo 4) in Enclosure 6.

5.3.4 - Bedded succession (channel 3.3)

Observations

The basal erosional surface of channel-fill 3.3 is overlain at its southwestern margin by a succession of thick, medium and thin beds of very fine-grained sandstone and siltstone (LA 4). In the lower section, the beds are not parallel; rather multiple small-scale erosion surfaces result in irregular bedding patterns (Fig. 5.6). The beds preserve planar and incipient climbing ripple lamination and have erosive bases with locally thin layers (less than 10 cm) of mudclast conglomerates (Enclosure 6). Palaeocurrent measurements from ripple cross lamination show a preferential northward direction (Fig 5.4C; Appendix 1). In the upper portion of the channel-fill the beds are organized, into a thinning and fining upward trend with no minor erosion surfaces. Palaeocurrents from current ripples show a preferential eastward direction (Fig 5.4D; Appendix 1).

The maximum preserved thickness of channel-fill 3.3 is 11 m and it thins and fines away from the axis toward the southwestern margin where it intersects the present day topography (Enclosure 6).

Figure 5.6 – Interbedded sandstone and siltstone succession (LA 4) showing internal truncation. See photo location (photo 5) in Enclosure 6.

Interpretation / Depositional processes

The sedimentological characteristics and the geographical location of the lower section of channel-fill 3.3 indicate a channel margin environment of deposition. Palaeoflow orthogonal to the overall flow direction in the underlying channels supports this interpretation. The axis of the channel is interpreted to lie to the NNE, sub-vertically stacked on the underlying channel, and has been eroded away by the younger, overlying erosional surface 3.4. The upper portion of channel-fill 3.3 shows more organised characteristic that reflects deposition from dilute low density turbidity currents during later stages of the channel fill and abandonment.

5.3.5 - Bedded succession (channel 3.4)

Observations

Channel-fill 3.4 is laterally offset to the NNE in relation to channel-fill 3. The lower part of the fill is composed of thick beds of climbing ripple laminated very fine-grained sandstone interbedded with layers of siltstones that onlap the erosional surface (LA 4; Enclosure 6). The bed bases are sharp and locally erosive, and the tops are also sharp to weakly graded. The upper fill comprises interbedded medium and thin beds of current and incipient climbing ripple laminated very fine-grained sandstones interbedded with thin siltstones (LA 2). In this succession, beds can be mapped out beyond the boundary of underlying erosional surface 3.4 to the southwest. Palaeocurrent measurements from ripple lamination show a range from ENE to SE (Fig 5.3E; Appendix 1). Cut by young erosional surface the maximum measured thickness of the channel 3.4 is about 11 m (log HBS25, Enclosure 6).

Interpretation / Depositional processes

The onlap of the lower part of the fill onto erosional surface 3.4 indicates deposition after channel incision and initial sediment bypass. The more widespread distribution of the upper fill beyond the underlying margin of channel 3.4 suggests the formation of channel-scale overbank deposits. If this is the case, it is likely that the upper succession of channel 3.3 is actually the spill deposits of channel 3.4 age. The orthogonal palaeoflow directions reported between the lower and upper successions in channel 3.3 supports this interpretation. The implication of this interpretation is that the thickness of channel-fill 3.3 is less than the 11 m measured.

The fill of channel 3.4 shows an overall waning energy, starting with erosive flows, responsible for the channel incision, followed by depositional flows. The lower section show characteristics of deposition due to rapid deceleration of density sustained turbidity currents for the sandstone beds, and deposition from the flow tails for the overlying siltstones. The characteristics of the upper fill suggest deposition from less dense and more dilute turbidity currents.

5.4 - Channel complex 3: A model for channel complex development in upper submarine slope settings

The stratigraphy of the channels and channel complexes fills has been integrated to develop a generic model for the evolution of submarine channel complexes in upper slope settings. As previously interpreted, the energy of the depositional system at channel and channel complex scale presents a waning profile; therefore, although the cutting and filling processes are repetitive through the channel complex evolution the resultant records are different because they occur during a different period in the overall channel complex scale waning energy profile.

5.4.1 - Phase 1: Basal incision and sediment bypass

The basal incisional surface is carved during this phase by multi-event erosive sediment gravity flows. This is the most energetic phase at the channel complex scale and the deepest incision of the basal surface is expected during this phase. However, it is possible that some later enlarging of the channel complex took place especially if the individual channels are laterally offset. No deposition from the initial erosive flows is preserved inside the channel. It is possible that genetically related levee-overbank deposits developed during this time (Clark and Pickering, 1996; Peakall et al., 2000; and this study), and may have formed adjacent to channels that may have been entirely eroded away. The most likely deposits inside the channel during this phase are mass wasting deposits from the channel walls which can vary in scale.

5.4.2 - Phase 2: Channel fill: deposition and re-incisions

The initiation of this phase marks the point in the energy profile where deposition starts, although some sediment bypass should still be expected during this phase. The ratio between these two processes varies through the

channel complex evolution according to the position in the overall waning energy profile at channel complex scale.

The presence of sandstone intercalated with lags at the base of the channel complex fill indicates that periods of deposition took place between periods of bypass. Bypassing flows may enlarge the basal surface carved during the previous phase. The upward decrease of mudstone clast lag deposits demonstrates a progressive increase in the deposition/bypass ratio. This waning trend will continue until the eventual shutdown of the sand-supply system, or avulsion and development of the next channel re-incision. The first channel-fill should not be expected to fill the basal erosional surface since in upper submarine slope settings incision is usually relatively deep. Further cycles of re-incision and fill occur repeating these steps. However, an overall fining and thinning upward of the sedimentary fill should be expected as a function of the decreasing in energy at channel complex scale.

5.4.3 - Phase 3: Abandonment

In the upper slope setting, the abandonment of a channel complex can take place in an underfilled condition. Commonly, the last stage of deposition is marked by small channels, either erosive and/or levee-confined (Mayall and Stewart, 2000; Abreu et al., 2003; and this work). These small channels are typically of high sinuosity, confined by the margins of the larger channel complex. However if the channel complex is completely filled, such channels can spill and escape from the parent channel complex (an example of this situation, based on seismic data, is presented in chapter 6).

5.5 - Comparison with models in the literature

The model for the stratigraphic evolution of a channel complex presented above can be compared with different published models. In terms of processes, it has similarities with the "build-cut-fill-spill" model presented by Gardner and Borer (2000) and Gardner et al. (2003). The phases of "cut" and "fill" are well documented in this example but the "build" and "spill" phases are not. This is ascribed to the upper slope depositional setting. Gardner and Borer (2000) and Gardner et al., (2003) suggested that the "build" and "spill" phase should not be expected in an upper slope environment. The analysed channel complex lies within a channel complex set that is interpreted to be located on the upper submarine slope, which supports this suggestion. Although the Gardner and Borer (2000) and Gardner et al. (2003) model is derived from lower slope deposits it is suitable for comparison with the case study regarding the scale and hierarchy of the depositional elements.

The nature and stacking pattern of channel-fills in the channel complex in many aspects resembles the model presented by Mayall and Stewart (2000). This model, based on subsurface slope deposits offshore Angola, describes basal slumps overlain by a section of erosive based or amalgamated structureless and planar-laminated sandstones interbedded with mud clast conglomerates (mainly in the lower portion), and an upper succession dominated by finer lithologies (mainly siltstone). The Mayall and Stewart (2000) model interpreted a basal succession of sandstone and extraformational conglomerates underlying the slumps which was not documented in this work, but is explained by a wider availability of grain sizes in the Angola system. Apart from this, the two models are similar but differ in the scale of the depositional elements.

The size of channel complex in this case study (>300m wide *vs* 35m preserved thickness) is large enough to allow identification of smaller elements – channels- and scour-fills. However, if this example was imaged in seismic reflection data, even high resolution data, these elements could not be identified. The Mayall and Stewart (2000) channel complex model is 1 to

3 km wide and 50 m to 250 m thick – an order of magnitude larger than the channel complex analysed in this chapter, but similar to the channel complex set described in chapter 4. In the Laingsburg slope context, Mayall and Stewart's channel complex would be a channel complex set. This comparison shows that below the resolution of even 3D high resolution seismic data, smaller elements can be identified in channel complexes using outcrop datasets (Fig. 5.7).

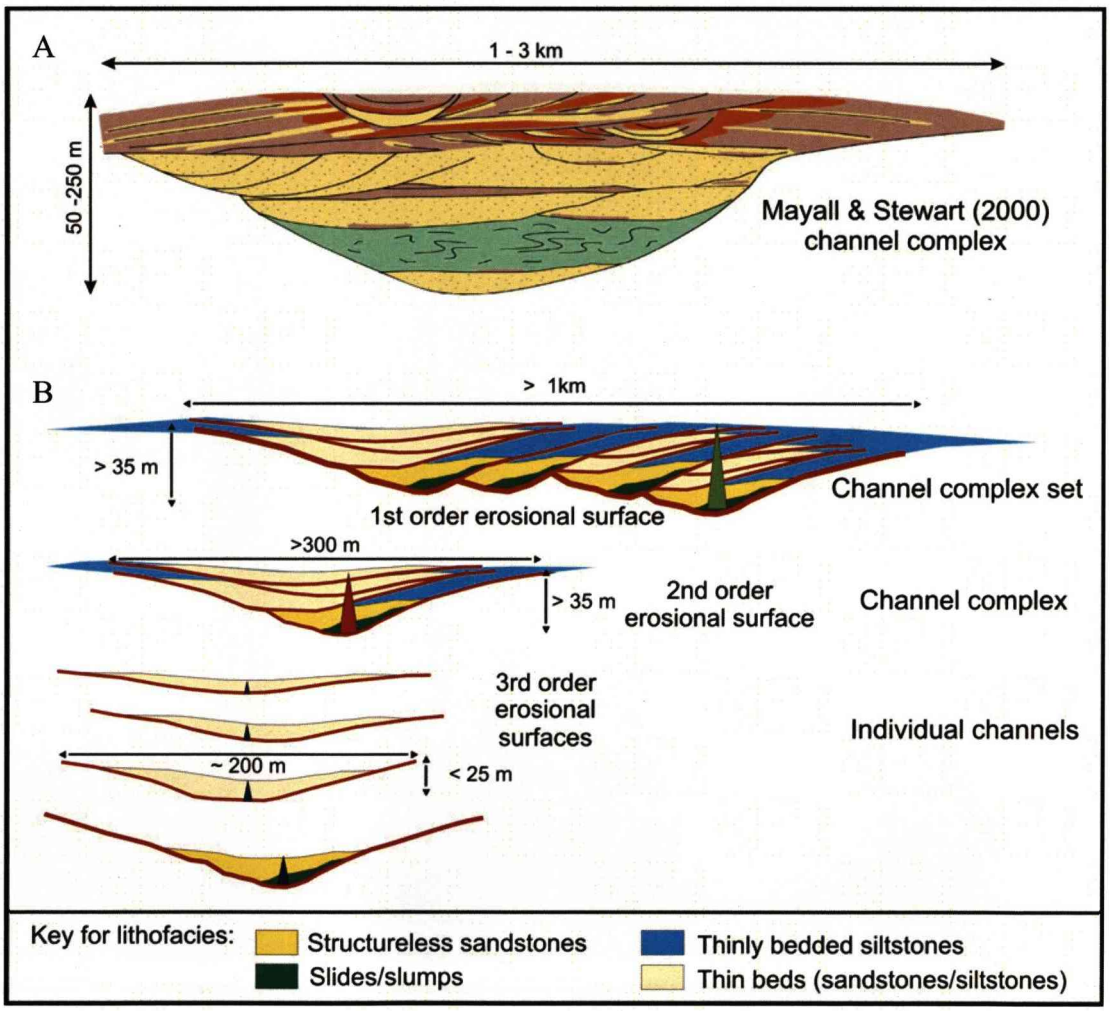

Figure 5.7 – Hierarchy of the erosional/depositional elements as interpreted in this work (B) compared with the model presented by Mayall and Stewart (2000) (A). Notice the difference of one order in the dimensions (width *vs* thickness) of those elements. What Mayall and Stewart (2000) interpreted as channel complex is interpreted in this work as channel complex set. This discrepancy is ascribed to the sub-seismic resolution afforded by the outcrop-based model constructed in this work.

5.6 - Implications for reservoir development within channel, channel complexes and channel complexes set in the upper submarine slope.

The above discussion strongly suggests that all 'channels' imaged in seismic data are at least channel complexes, and may display the levels of lithofacies complexity that has been demonstrated in this and previous chapters. The sedimentological implication is that more heterogeneities than those interpreted from the seismic data will be present in channel complexes. This can be a complicating factor in terms of the expected reservoir quality. The stratigraphic implication is that the order of events can be misinterpreted, since high order (allocyclic) events can be recorded in scales below the seismic resolution.

In the channel complex presented above, the sandiest section (highest net to gross) is the sandstone/conglomerate section deposited in the axis at the beginning of the backfill of the channel complex, i.e. the filling of the first individual channel. Therefore, this is the best reservoir interval for hydrocarbon within a channel complex. However, two factors can complicate the quality of reservoirs developed during this phase: (1) the volume of residual lags of non-reservoir mudclast conglomerate and (2) re-incision by later individual channel within a channel complex. Lags have a patchy distribution in the lower part of the first individual channel-fill. Therefore, although they represent local baffles to potential fluid flow they do not compromise the quality of the reservoir, mainly because the best quality reservoir is in the upper part of this high net to gross succession. The second factor, however, represents a major complication since later erosion by individual channels can remove the previously deposited sand-prone succession. This phenomenon is observed in channel complex 3, where the second individual channel, filled by a fine-grained succession, cuts down into the sandstones of channel-fill 1. It represents a major barrier for vertical reservoir connectivity (Enclosure 6). This can be enhanced in the case of laterally stacked channel-fills, where the lower net: gross channel margin successions would be preserved preferentially.

Nevertheless, at a larger scale (channel complex set), this problem can be mitigated since younger channel complexes can cut deeply into older fills removing such a barrier and connecting the basal high net to gross intervals of each complex to each other. Based this premise it is proposed that reservoir rocks in upper submarine slope settings are only economic in terms of hydrocarbon volumes, if they occur at the scale of a channel complex set. In a link with the sequence stratigraphic interpretation it can be said that high frequency allocyclic events, such those driven by the highest frequencies of the Milankovitch orbital band are not able to develop or preserve sufficient reservoir rocks in upper submarine slope setting.

Implications from this interpretation is that a predictive scheme for the presence of reservoir rocks in upper submarine slope settings can be developed once the hierarchy of the depositional elements and/or the chronostratigraphy of the analysed succession are known.

Chapter 6 – Slope channel systems of the Foz do Amazonas Basin, Brazilian Atlantic Equatorial margin: a seismic analogue case study

6.1 - Introduction and Objectives

In this chapter a comparison is made between the depositional environments, architecture and lithofacies distribution of the Laingsburg system and observations and interpretations from a similar depositional setting in a 3D seismic dataset from the Amazon Fan in the Foz do Amazonas basin.

The objectives of this chapter are:

- To apply the approach developed for the Laingsburg system to the deposits of a different mud-prone slope succession to identify generic similarities in deposits of a different age and in a different tectonic setting.
- To use the high resolution Laingsburg dataset to explore the issue of architectural hierarchy in a seismic dataset.
- To help assess up-dip and down-dip scenarios for the Laingsburg system within a larger-scale shelf to basin floor context, as provided by the seismic dataset.

6.2 - Geological setting of the seismic dataset

Deposition of the Amazon Fan in the Foz do Amazonas basin (Fig. 6.1) initiated around the boundary between the middle and upper Miocene (~11.6 Ma), when the Amazon river became a transcontinental river that connected the Andes to the Atlantic ocean. The fan developed through three main depositional phases with increasing sedimentation rate (Figueiredo et al., 2009).

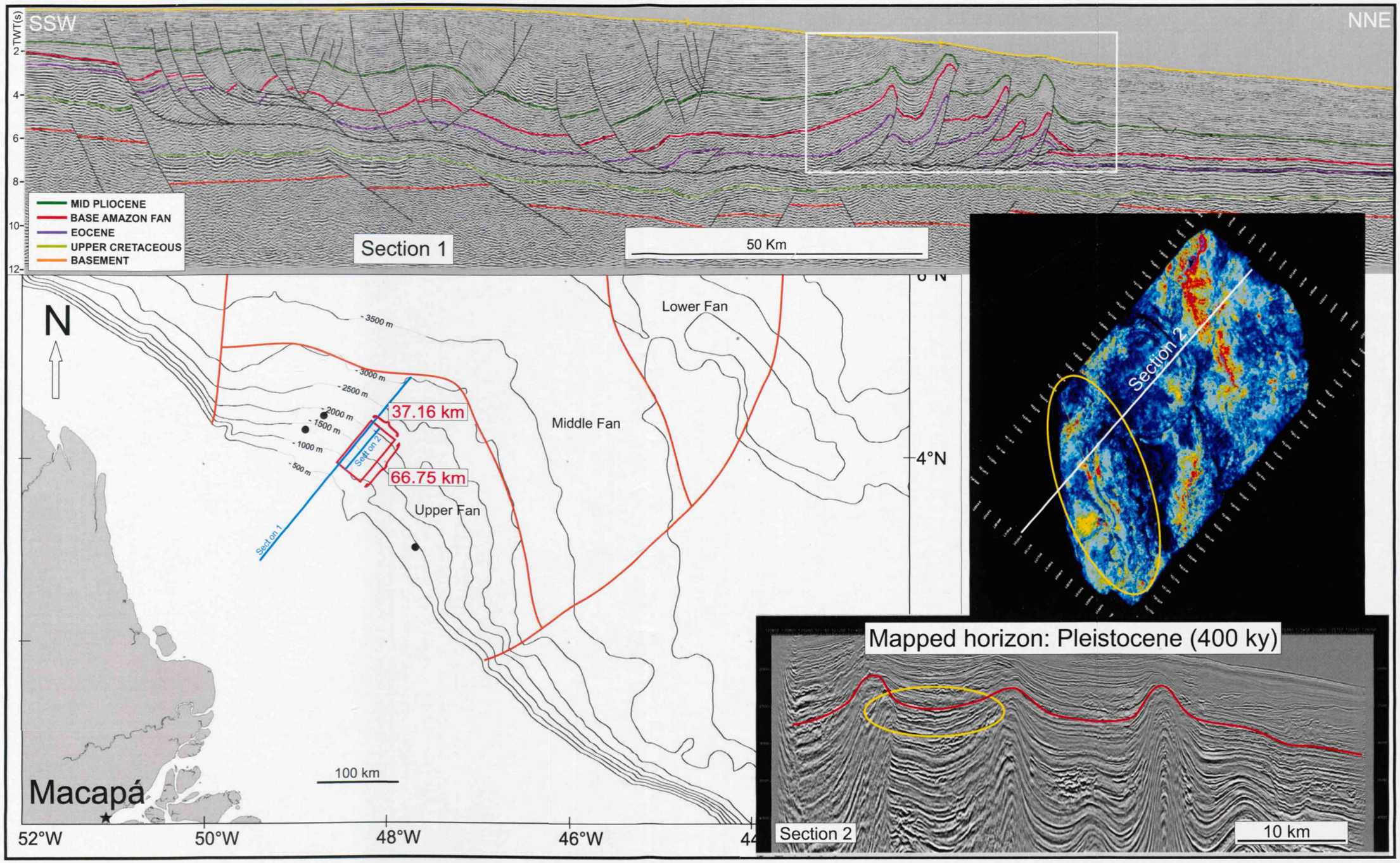

Figure 6.1 - Composite figure showing geographic location of the analysed 3D seismic data and other data. Red rectangle: area of the seismic project (~2,500 km2). Longer cyan line: regional 2D seismic section shown in the upper portion of the figure (white square on the section shows the approximate position of the 3D seismic data). Shorter cyan line: inline seismic section of the 3D data shown in lower right corner of the figure (red line is the mapped horizon; yellow ellipse shows the area analysed in this work). Also shown is an RMS amplitude map related to the red horizon of the whole seismic project area (white line: position of the inline seismic section shown below the map; yellow ellipse shows the area analysed in this work). The three black dots on the Amazon Fan represent wells. Base map of the Foz do Amazonas basin with shoreline and bathymetry (black lines) is from Petrobras data bank. Partial outline and internal divisions of the Amazon Fan (orange lines) are modified from Damuth et al. (1988). All other relevant information are in the figure.

The seismic data set analysed in this chapter is specific to Pleistocene deposits that belong to the third phase of Amazon Fan development (2.4 Ma to Present), when the average sedimentation rate was about 1.22 m/ky (with a peak of 11 m/ky) (Figueiredo et al., 2009).

The age of the interpreted seismic horizon from which the amplitude maps were generated is around 400 Ky. This age is constrained by biostratigraphic data from 3 deep-water wells (Fig. 6.1). The depositional setting of the analysed interval is interpreted as middle to upper slope and it is located on the compressional end of the gravitational tectonic cell of the Amazon Fan (Fig. 6.1).

6.3 - Geophysical analysis of the seismic data

The 3D seismic project in which the interpreted succession is located covers an area of approximately 2,500 km^2 on the middle/upper slope of the Amazon Fan (Fig 6.1). A seismic horizon located around 3.7 s (TWT, two way time) was mapped throughout the area (Fig. 6.1). Several amplitude extraction windows were created in order to obtain the best map view of the horizon and the stratigraphic succession. The best images were obtained in an RMS amplitude extraction window of 0.03 s (TWT) below the mapped horizon. The dominant frequency and the interval velocity at this horizon are about 30 Hz (Fig. 6.2) and 1727 m/s (Fig. 6.3) respectively. Applying these values to the formula $vr = iv/(4*df)$ (after Yilmaz, 2001), a vertical resolution of ~14.4 m is indicated for the seismic data at 3.7 s (TWT):

$$vr = iv/(4*df)$$

vr = *vertical resolution (m);*

iv = *interval velocity (m/s);*

df = *dominant frequency (Hz).*

$$vr = 1727/(4*30)$$

$$vr = 14.391m$$

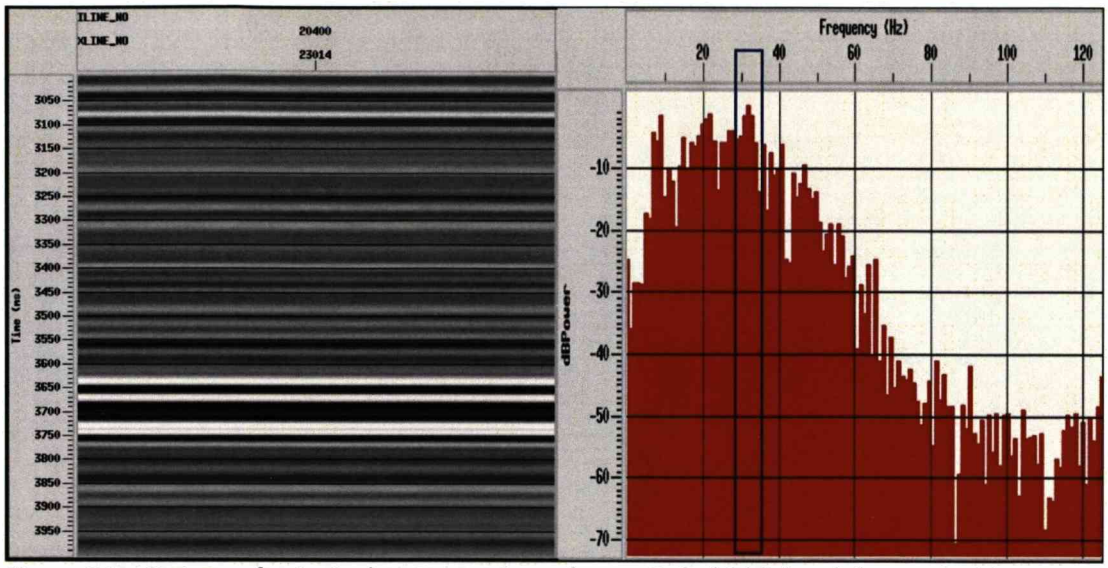

Figure 6.2 - Outputs of seismic data processing software. Left: highlight of the mapped horizon at ~3.7 s (TWT, two way time). Right upper: histogram of the frequencies at ~3.7 s (TWT).

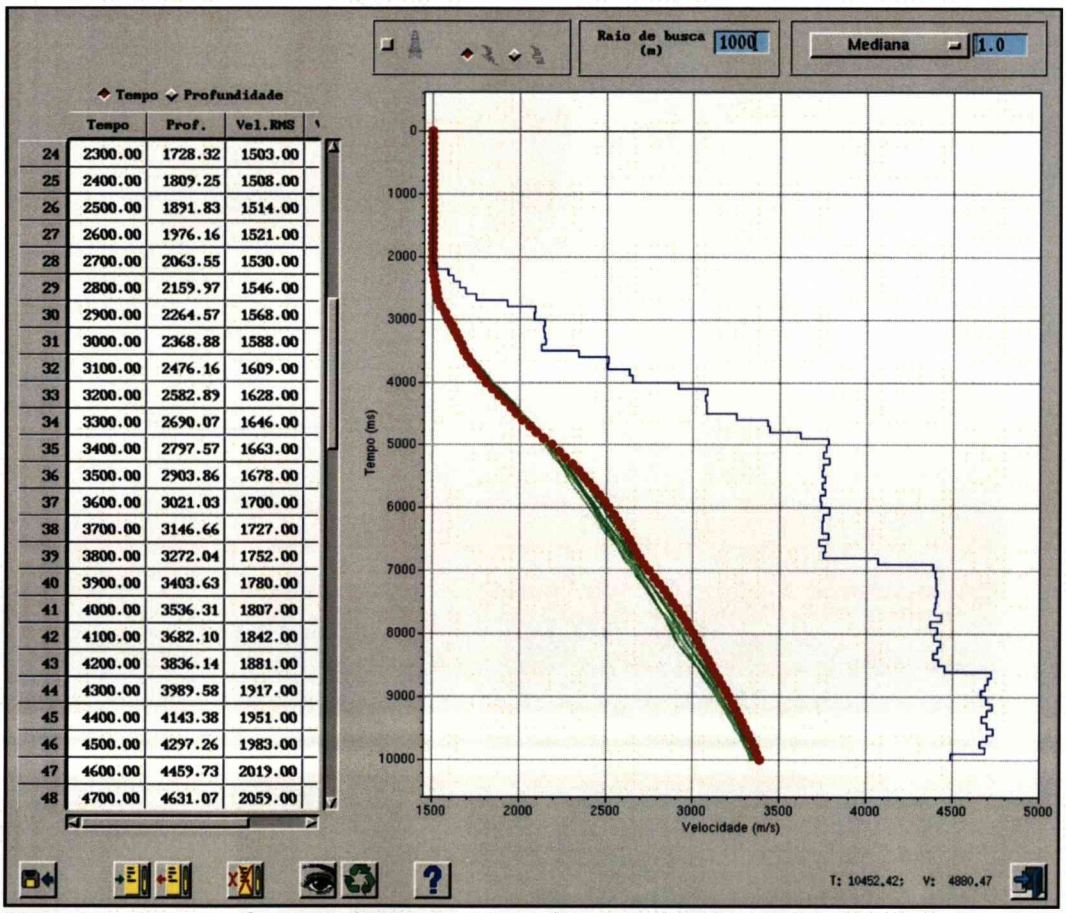

	Tempo	Prof.	Vel.RMS
24	2300.00	1728.32	1503.00
25	2400.00	1809.25	1508.00
26	2500.00	1891.83	1514.00
27	2600.00	1976.16	1521.00
28	2700.00	2063.55	1530.00
29	2800.00	2159.97	1546.00
30	2900.00	2264.57	1568.00
31	3000.00	2368.88	1588.00
32	3100.00	2476.16	1609.00
33	3200.00	2582.89	1628.00
34	3300.00	2690.07	1646.00
35	3400.00	2797.57	1663.00
36	3500.00	2903.86	1678.00
37	3600.00	3021.03	1700.00
38	3700.00	3146.66	1727.00
39	3800.00	3272.04	1752.00
40	3900.00	3403.63	1780.00
41	4000.00	3536.31	1807.00
42	4100.00	3682.10	1842.00
43	4200.00	3836.14	1881.00
44	4300.00	3989.58	1917.00
45	4400.00	4143.38	1951.00
46	4500.00	4297.26	1983.00
47	4600.00	4459.73	2019.00
48	4700.00	4631.07	2059.00

Figure 6.3 - Outputs of seismic data processing software. Left: numerical results of the time-velocity applied function. Right: in red is the graphic representation of the time-velocity function applied (other graphs are irrelevant for this work).

The RMS amplitude extraction window of 0.03 s converted to thickness (metres) by applying the following formula: $h = iv * (t/2)$.

$$h = iv * (t/2)$$

h = *thickness (m);*

iv = *interval velocity (m/s);*

t = *two way time (s)*

$$h = 1727 * (0.03/2)$$

$$h = 26m$$

resulted in a stratigraphic thickness of 26 metres.

These numbers show that the vertical resolution of the seismic data at the level of the interpreted horizon allows identification of sedimentary features thicker than 14 m. Therefore, the investigated 26 m-thick window is enough to avoid problems caused by sampling in a window below the vertical resolution (e.g., tuning effect). Geologically, this resolution limit means that the seismic dataset resolves channel complexes rather than their constituent channels, based on the hierarchy identified in the Laingsburg dataset (see chapter 5).

6.4 - Geological interpretation of the seismic data set.

The depositional features were interpreted based on seismic sections and RMS amplitude maps. In the seismic sections, discontinuous, bright or whitish horizons (hereafter called seismic facies 1) were interpreted to represent sand-prone deposits, and the background opaque grey or darker grading continuous horizons (hereafter called seismic facies 2) were interpreted as clay-prone deposits. In the amplitude maps, the sand-prone deposits are represented by grading from green (thin) to red (thicker) and the clay-prone deposits by blue to darker grading (Fig. 6.4). This pattern is widely accepted in seismic interpretation once it is supported by the integration of seismic and well datasets (wireline logs and ditch cuttings or cores). The logs based on the acoustic principle (sonic logs) share the same

physical medium as the seismic data, enabling the well logs to be tied to the seismic sections. Logs that reflect the lithological content of the succession (e.g. Gamma Ray log), integrated with ditch cuttings or cores, enable the construction of a lithological column which is matched with the seismic section and so the seismic facies are compared with the lithofacies (Fig. 6.5). In this case study, there is no well drilled within the seismic project analysed, however, there are three wells drilled in other seismic projects near to the study area (Fig. 6.1). The integration of seismic and wells at these points are extrapolated by seismic interpretation to the surrounding areas where the case study is located (Fig. 6.1).

The regional depositional dip of the Amazon Fan succession where the 3D seismic project is located is to the NE (Fig. 6.1); however, SE-NW trending palaeohighs formed by compressional folds caused local diversions in dip direction, which resulted in more complicated local palaeoflow directions (Pasley et al., 2004). The map view of the ~2,500 km^2 area shows a preferential SSE-NNW alignment of the erosional/depositional features (Fig. 6.1), which supports this interpretation. In the southwestern portion, geometric shapes suggest the presence of at least two roughly parallel, S-N oriented sinuous channel features flanked by adjacent deposits (Fig. 6.4). The combination of the regional dip and the apparent localized diversion of the channels around structural highs suggest that these two channel forms flowed from the south to the north (Fig. 6.1). They are between 26 m and 50 m thick, and between 200 m and 500 m wide. The western feature (ca. 500 m in width) appears wider than its eastern counterpart (ca. 300 m in width) (Figs. 6.9 - 6.18).

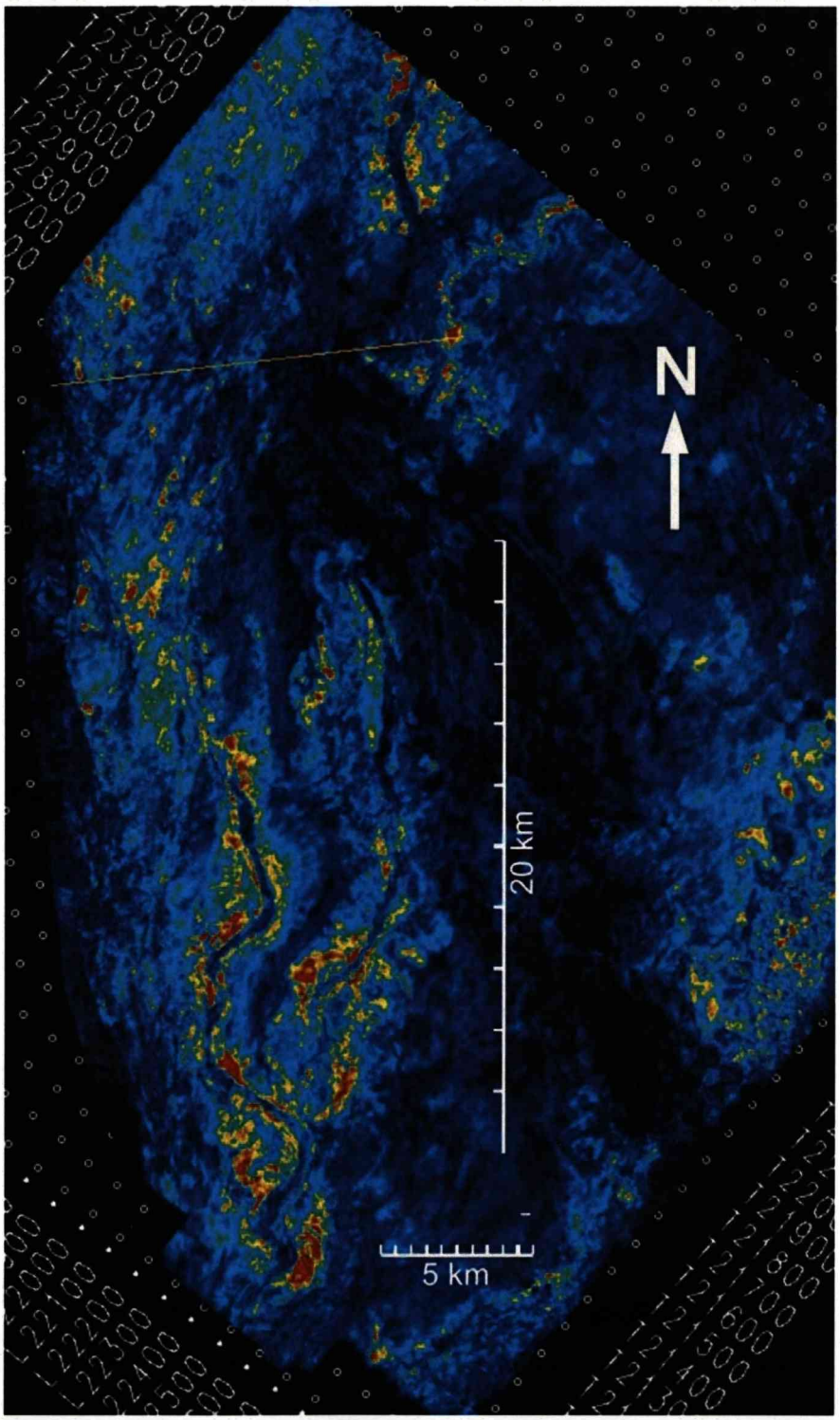

Figure 6.4 - RMS amplitude map to show the colour pattern that are assumed as seismic facies which are interpreted to represent the lithological content of the interval imaged in the map (~26m). Navy blue and darker grades are area where the seismic wave present low amplitude response which is a characteristic of shales, therefore, navy blue and darker grades represent shales. On the other end, red are areas with high amplitude response of the seismic wave, which is a characteristic of the sandstones (assuming that there is no carbonates in the analyses succession, what is the case in this example). Hence, red represents high sand content. The grading from red to navy blue represents variation on the sandstone/shale ratio. The same colour scheme applies to all subsequent amplitude maps shown in this chapter

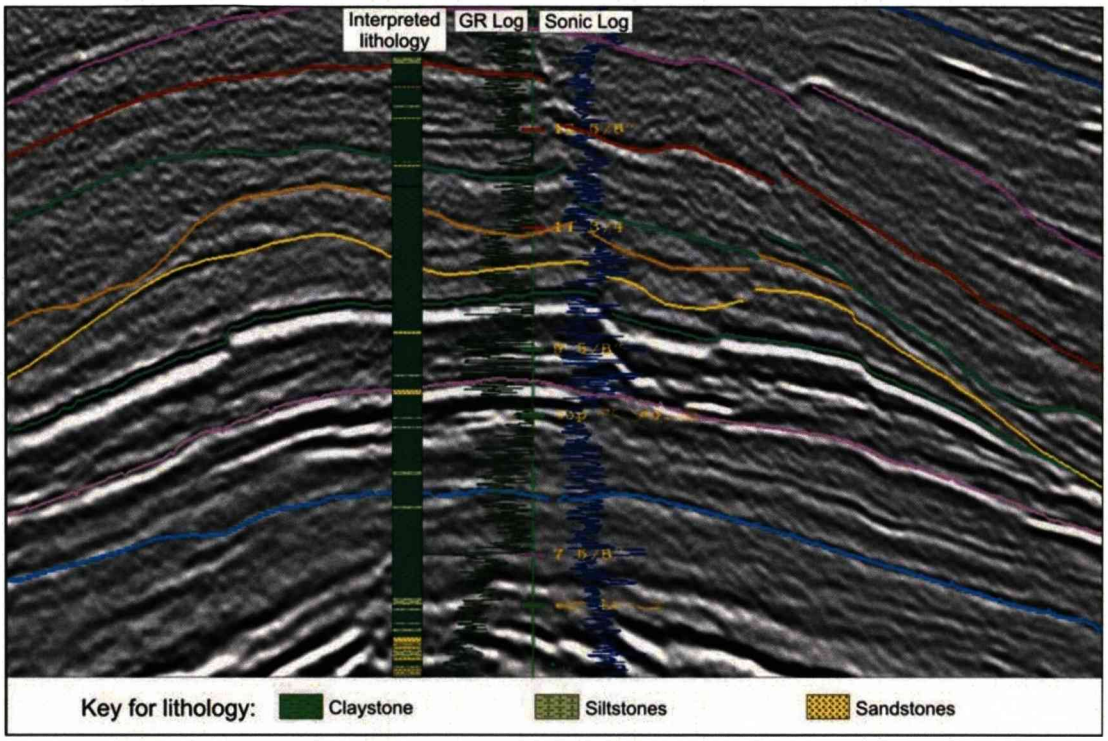

Figure 6.5 – Well to seismic tie diagram from one of the three wells drilled near to the area analysed in this chapter. The sonic log (based on the same acoustic principle as the seismic) is tied to the seismic section and the GR log accompanies it. These two logs integrated with the description of the recovered ditch cuttings enable the production of a vertical lithological column for the well. This column is compared with the visual pattern of the seismic section leading to the establishment of a range of seismic facies. In this example it is possible to see that opaque grey areas of the seismic section correspond to claystones in the well lithological column and the bright horizons are usually related to layers with more sand content.

6.5 - Architectural hierarchy and stratigraphical setting of the seismic dataset based on the approach developed in the high resolution Laingsburg study

Chapter five presented, at sub-seismic scale, the description and interpretation of a submarine slope channel complex in which the dimensions and hierarchy of the depositional elements are presented. Individual channel fills are ~200 m wide and <25 m thick, and channel complexes are wider than 300 m and thicker than 35 m. Comparing these dimensions with those channel-like features imaged in RMS amplitude maps from the Amazon Fan dataset it is most likely that these features are channel complexes. The smaller individual channels are interpreted to not be imaged due to the limits of the seismic resolution, however, in very high resolution image is possible to see within the channel complex some features which, considering the scale of the maps might be individual channel(s) (Fig. 6.6).

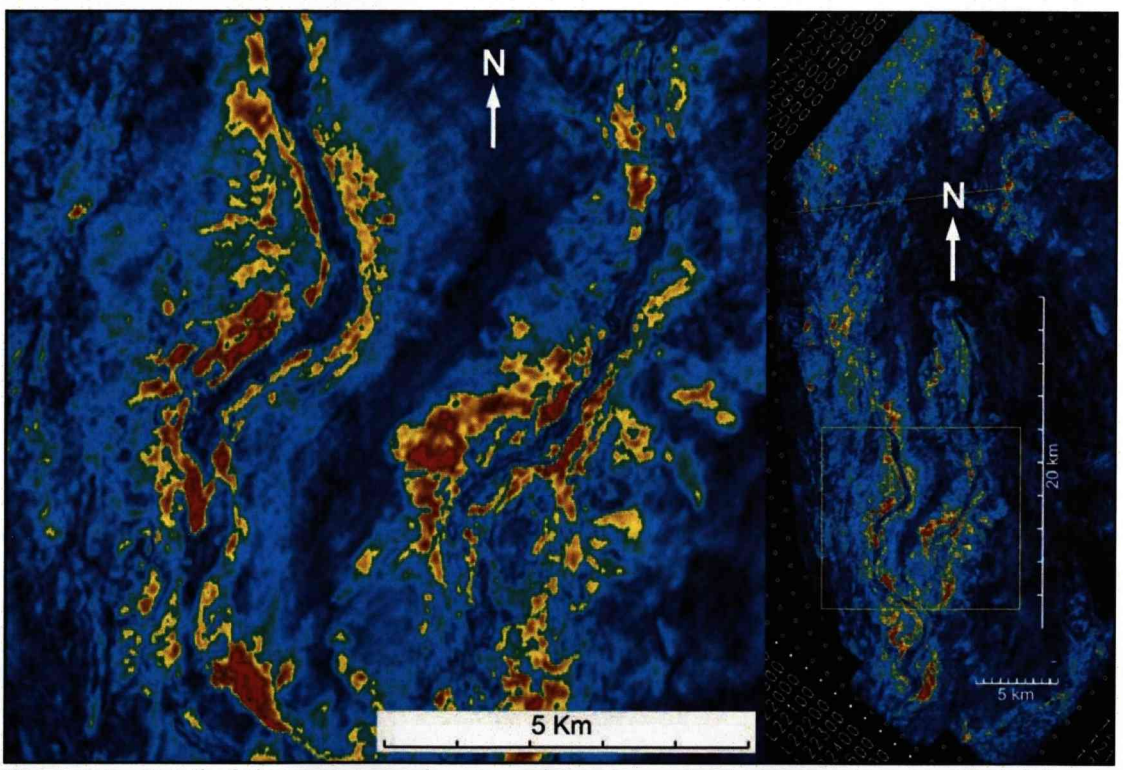

Figure 6.6 - Detail of the western and eastern channel complex-levee complexes. In the left hand very high resolution image, it is possible to see within the eastern channel complex some features which might be individual channel(s).

The channel complex analysed in chapter five is part of a larger channel complex set which together with the related adjacent levee and overbank deposits forms the LST of a depositional sequence. In the Amazon Fan seismic sections (Fig. 6.9 - 6.13), a larger concave up feature is seen (varying from 300 m to 400 m thick and ~1 km wide) that lies below the seismic horizon from which the two channel complexes were imaged. The scale of this feature and the seismic facies enclosed by it suggests a composite erosion surface filled with a disorganised assemblage of variable lithofacies associations. In comparison to the Laingsburg example discussed in chapters 4 and 5, this feature could be interpreted as a channel complex set (Figs. 6.7 and 6.8). Following this interpretation the two channel complexes imaged in the maps are part of the larger complex set, and represent the final phase of fill/abandonment of the larger feature. An approximately 300 m thick regional blanket of opaque grey seismic facies 2 overlies the channel complexes (Figs. 6.9 - 6.18) suggesting final abandonment and shutdown of the gravity driven depositional system.

The complex set is compared to two widely used models presented in the literature for the development and evolution of channels/channel complexes (Mayall and Stewart, 2000; Gardner and Borer, 2000 and Gardner et al., 2003). Considering only the well imaged upper complexes, the Mayall and Stewart (2000) model is more applicable since their abandonment phase is made up by smaller channel complexes rather than sheet-like deposits of a possible "spill" phase as advocated by Gardner and Borer (2000) and Gardner et al. (2003). Similarly to the Laingsburg example discussed in chapter five this is ascribed to the specific depositional setting, i.e., the upper submarine slope.

One observation about these late-stage channel complexes that emerged from the seismic data is that they do not necessarily follow the path of the underlying channel complex set. The seismic section in figures 6.9 to 6.15 show how one of these channel complexes (the western one) drifts away from underlying channel complexes. This indicates that the channel complexes are only partial confined by erosional or depositional topography of the underlying channel complex set.

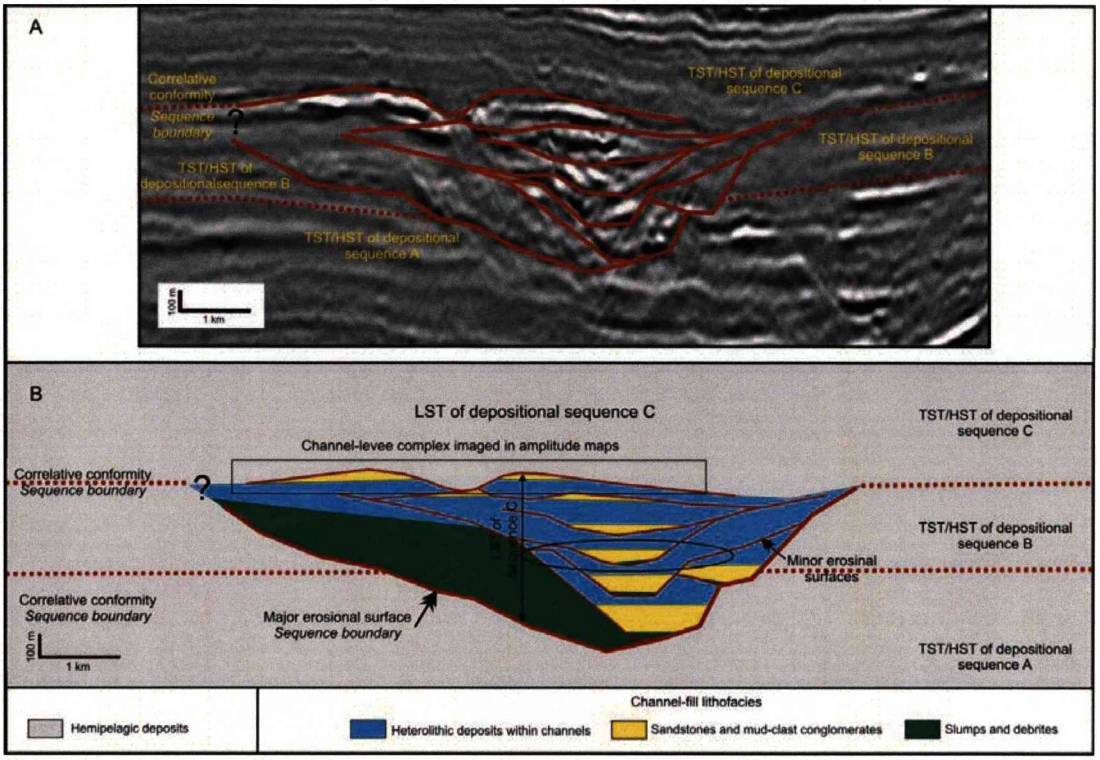

Figure 6.7 - (A) Detail of the seismic section shown in figure 6.9 with interpreted erosional surface of the channel complex set. (B) Cartoon with schematic interpretation of the erosional/depositional system of the upper slope of the Amazon Fan based on seismic section. At least three different successions of hemipelagic deposits are interpreted as transgressive and highstand system tracts of three different depositional sequences labelled from the oldest to the youngest, A, B and C. The major channel complex set is interpreted as the lowstand system tract of sequence C. Development of the major erosional surface and the emplacement of large slumps and/or debrite deposits are interpreted as the record of the early lowstand system tract on the upper slope. The channel complex set is broken down into smaller component channel complexes. Individual channels within these complexes are below the seismic resolution and cannot be identified from seismic interpretation. The black ellipse highlights one channel complex which is interpreted based on the model described in chapter 5 and shown in detail in figure 6.8.

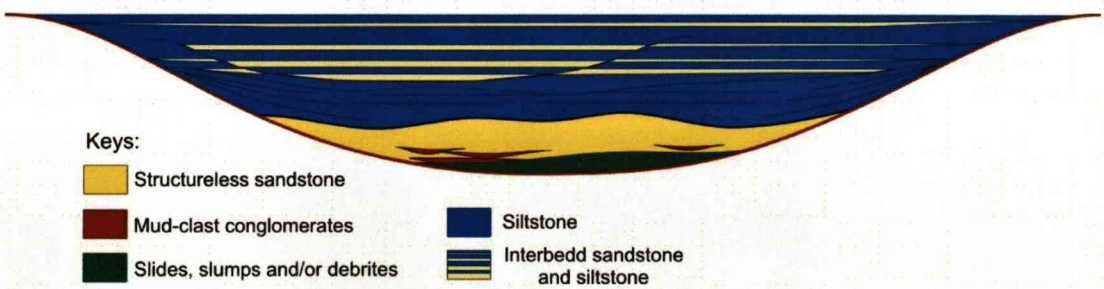

Figure 6.8 – Possible internal architecture of the channel complex highlighted in the black ellipse in figure 6.7. The sub-seismic scale interpretation is based on the example from Laingsburg Formation discussed in chapter 5.

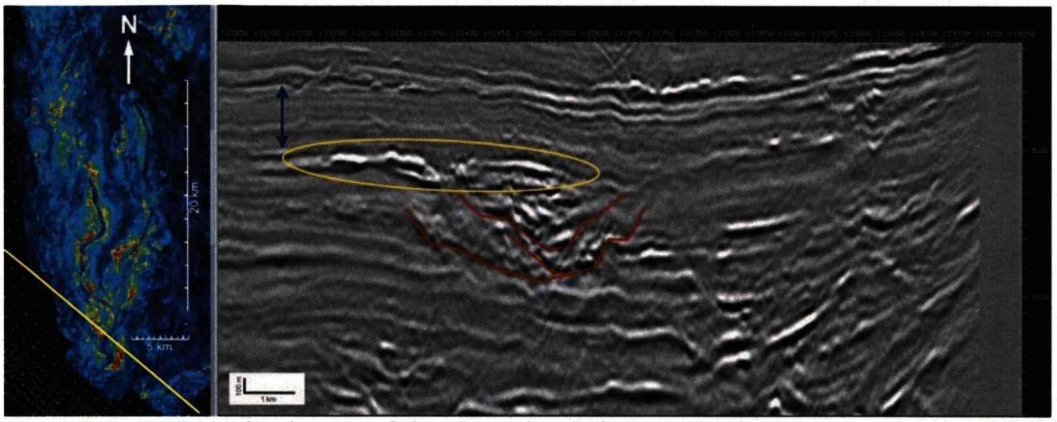

Figure 6.9 - RMS amplitude map of the channel complexes and seismic section showing: (1) Yellow ellipse: western channel complex flanked by levees. In this section the channel complex appears to have some degree of incision. (2) Red concave up lines: interpretation of a channel complex set. (3) Double head blue arrow: thickness of the blanket of clay-prone deposits overlying the channel complex. Thin yellow line on the map represents the position of the seismic section.

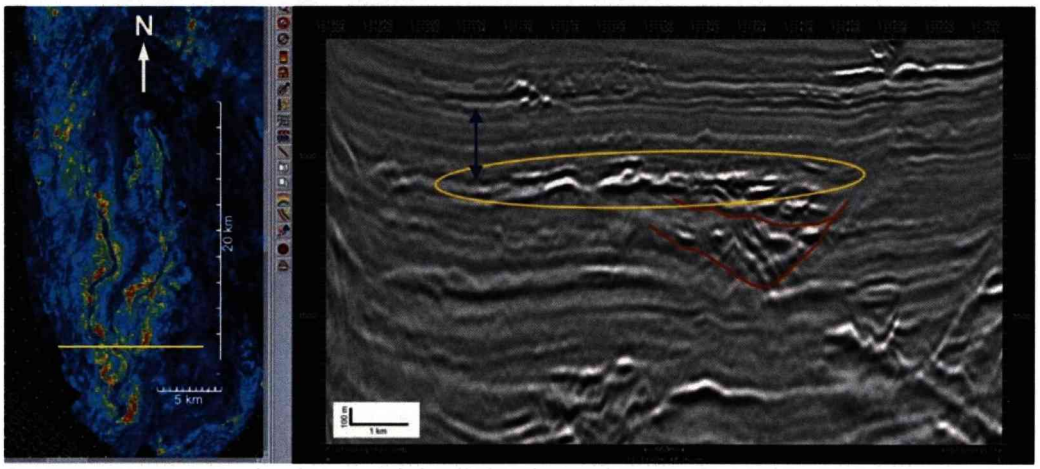

Figure 6.10 - RMS amplitude map of the channel complexes and seismic section showing: (1) Yellow ellipse: western channel complex flanked by levees. In this section the channel complex appears to be confined only by the levees. Even though it is not very clear, the eastern channel complex can be observed in this section. (2) Red concave up lines: interpretation of a channel complex set. (3) Double head blue arrow: thickness of the blanket of clay-prone deposits overlying the channel complex set. Thin yellow line on the map represents the position of the seismic section.

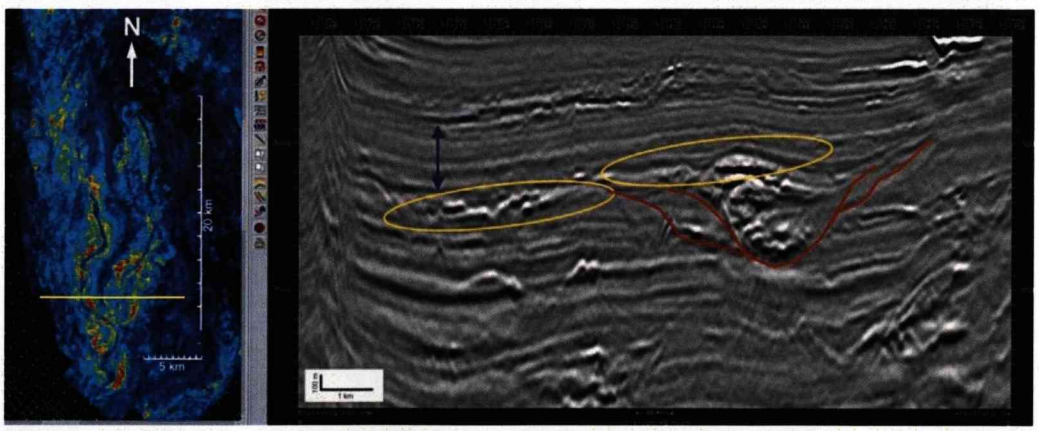

Figure 6.11 - RMS amplitude map of the channel complexes and seismic section showing: (1) Yellow ellipse: western and eastern channel complexes flanked by levees. (2) Red concave up lines: interpretation of a channel complex set. (3) Double head blue arrow: thickness of the blanket of clay-prone deposits overlying the channel complex set. Thin yellow line on the map represents the position of the seismic section.

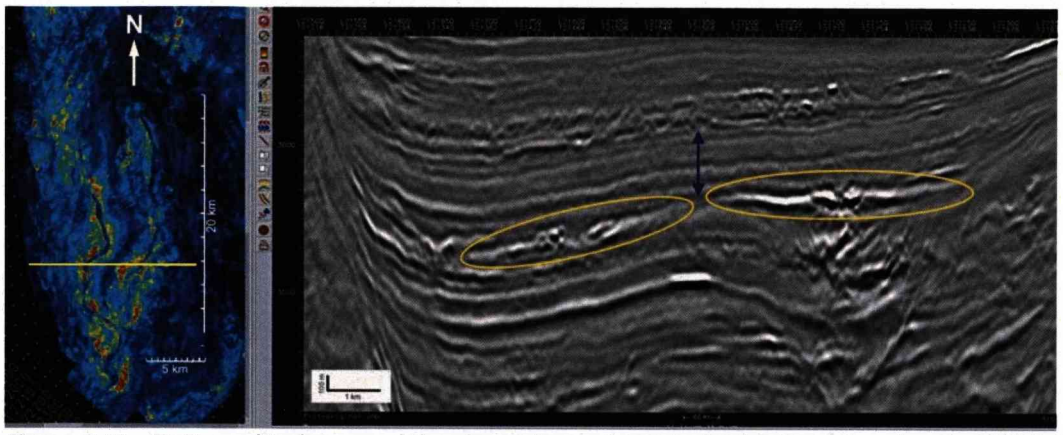

Figure 6.12 - RMS amplitude map of the channel complexes and seismic section showing: (1) Yellow ellipse: western and eastern channel complexes flanked by levees. In this section the eastern channel complex appears to be levee confined. (2) Double head blue arrow: thickness of the blanket of clay-prone deposits overlying the channel complex set. The channel complex set is poorly imaged in this section. Thin yellow line on the map represents the position of the seismic section.

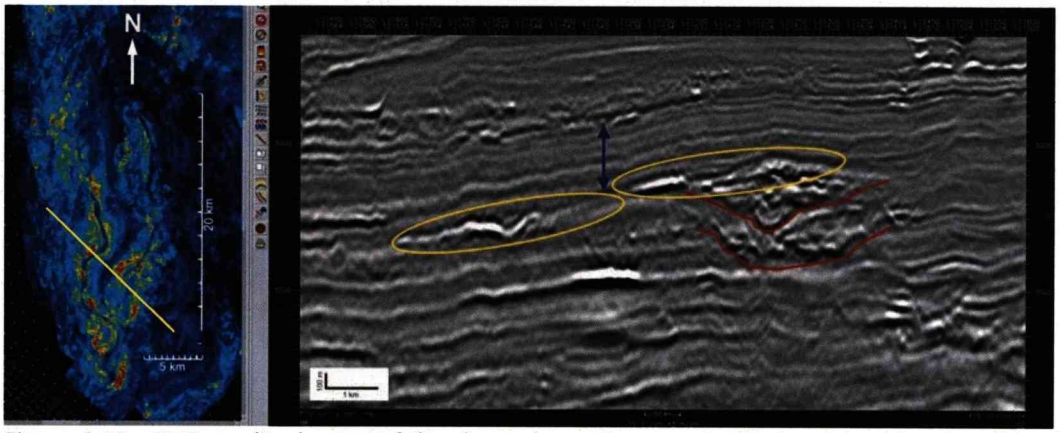

Figure 6.13 - RMS amplitude map of the channel complexes and seismic section showing: (1) Yellow ellipse: western and eastern channel complexes flanked by levees. (2) Red concave up lines: interpretation of a channel complex set. (3) Double head blue arrow: thickness of the blanket of clay-prone deposits overlying the channel complex set. Thin yellow line on the map represents the position of the seismic section.

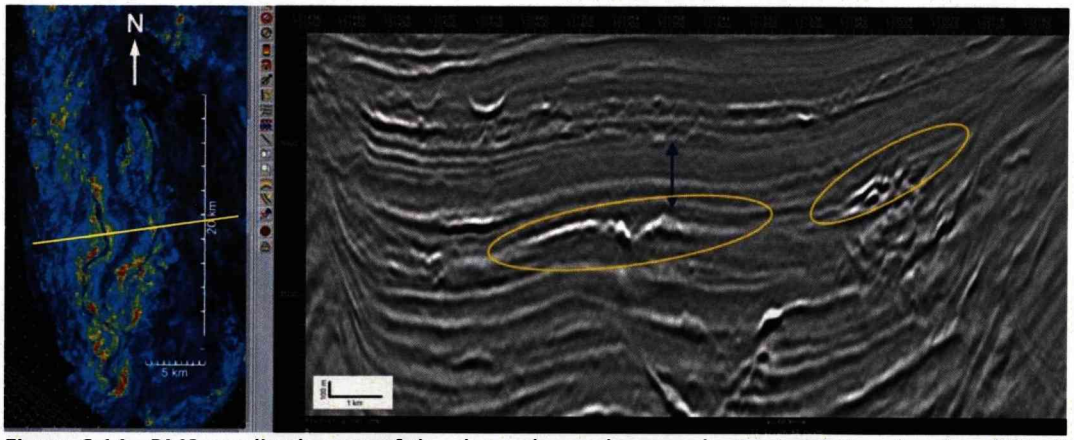

Figure 6.14 - RMS amplitude map of the channel complexes and seismic section showing: (1) Yellow ellipse: western and eastern channel complexes flanked by levees. (2) Double head blue arrow: thickness of the blanket of clay-prone deposits overlying the channel complex set. Thin yellow line on the map represents the position of the seismic section.

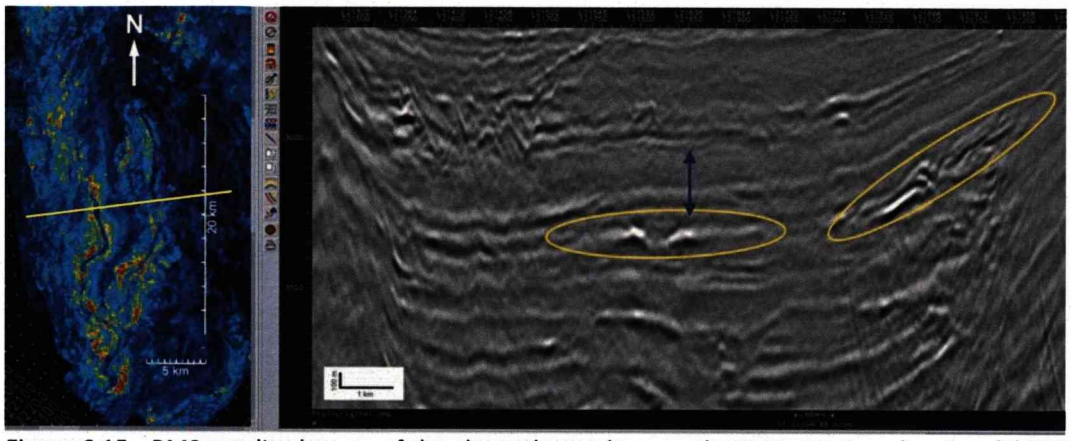

Figure 6.15 - RMS amplitude map of the channel complexes and seismic section showing: (1) Yellow ellipse: western and eastern channel complexes flanked by levees. (2) Double head blue arrow: thickness of the blanket of clay-prone deposits overlying the channel complex set. Thin yellow line on the map represents the position of the seismic section.

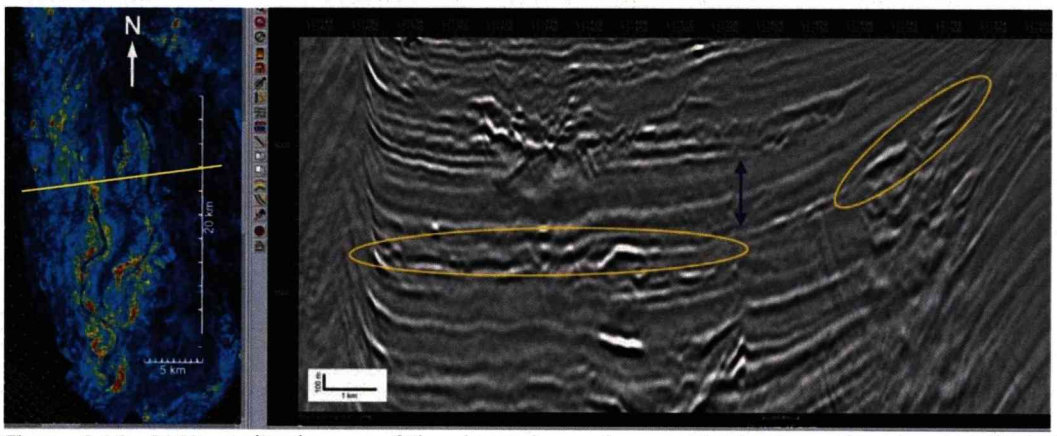

Figure 6.16 - RMS amplitude map of the channel complexes and seismic section showing: (1) Yellow ellipse: eastern channel complex appear flanked by levees; western channel complex does not present the characteristic geometric features of channel complex-levee system seen in previous section. In map view no channelised geometry is observed at the position of this section. (2) Double head blue arrow: thickness of the blanket of clay-prone deposits overlying the channel complex set. Thin yellow line on the map represents the position of the seismic section.

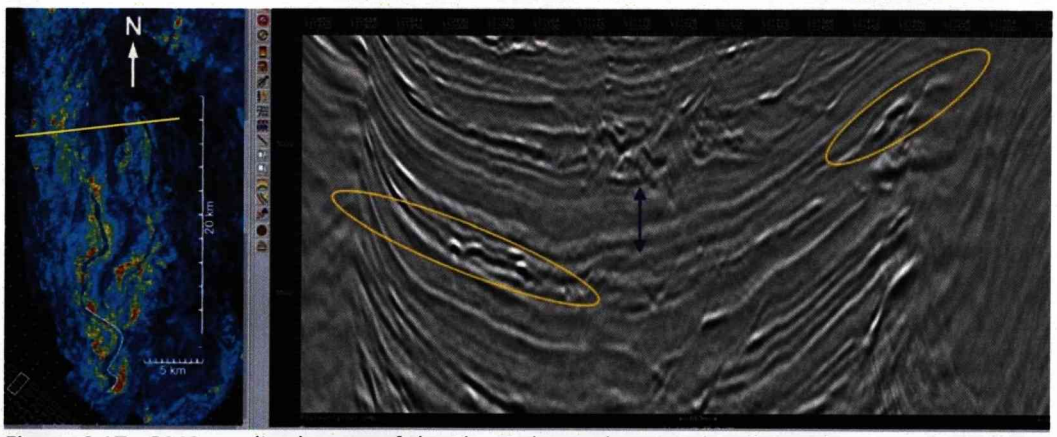

Figure 6.17 - RMS amplitude map of the channel complexes and seismic section showing: (1) Yellow ellipse: the eastern channel complex, which is still well imaged in this section; the western channel complex, conversely, presents slight variation in the vertical scale and shows an unconfined character. In map view no channelised geometry is observed. (2) Double head blue arrow: thickness of the blanket of clay-prone deposits overlying the channel complex set. Thin yellow line on the map represents the position of the seismic section.

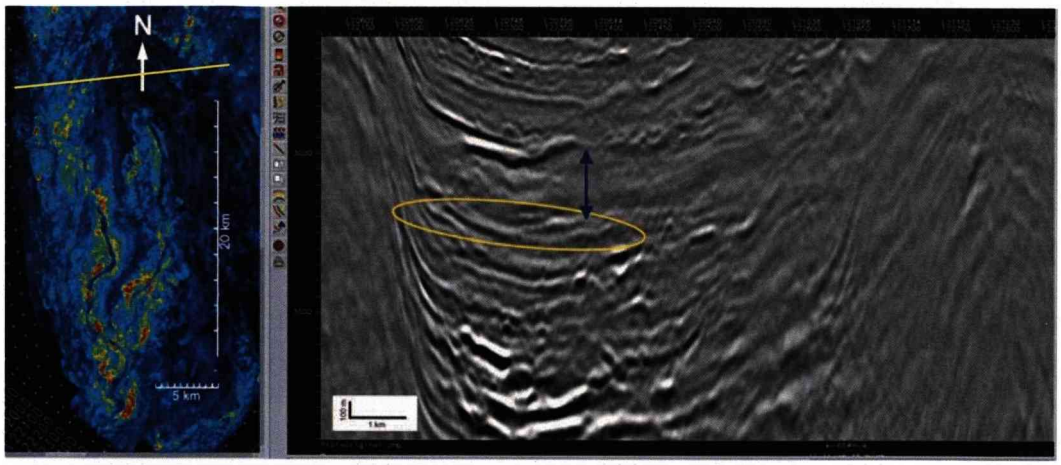

Figure 6.18 - RMS amplitude map of the channel complexes and seismic section showing: no imaging of the eastern channel complex and poor imaging of the western channel complex (yellow ellipse). Double head blue arrow: thickness of the blanket of clay-prone deposits overlying the channel complex set. Thin yellow line on the map represents the position of the seismic section.

6.6 - Stratigraphical hierarchy of the seismic dataset based on the approach developed in the high resolution Laingsburg dataset

As interpreted in chapter three, the studied stratigraphic succession of the upper Laingsburg Formation is built of depositional sequences that can be grouped in composite sequences within a composite sequence set. Chapters four and five broke down the LST of a single depositional sequence (a channel complex set/sets and related levee and overbank deposits) into smaller constituents channel complexes and individual channel-fills. Following this approach, the two channelised features imaged in RMS amplitude maps are interpreted as channel complexes within the upper, late stage part of a channel complex set. This complex set is interpreted to represent the LST of a single depositional sequence in the upper slope setting. The 300 m thick overlying clay-prone succession is interpreted as the TST/HST of the same depositional sequence. The physical limits of the analysed seismic dataset preclude an interpretation at a larger scale, consequently the direct comparison with the Laingsburg interpretation is made up to this stage. It is not possible to say if the 300m-thick clay-prone succession is the TST/HST deposits of a single or a composite depositional sequence or even a composite sequence set.

6.7 - Sub-seismic interpretation of the seismic dataset based on lithofacies association and architectural pattern of the sand-prone unit described and interpreted from the Laingsburg dataset.

6.7.1 - Relationship between the channel complexes imaged in RMS amplitude maps and adjacent deposits

One of the most difficult questions to answer with respect to submarine channel development, both from seismic and outcrop data sets, is the temporal relationship between the development of the channel and the adjacent deposits. Whether the adjacent deposits are younger, older, or coeval to the channel-fill is a difficult but important stratigraphic and reservoir production problem to solve. At outcrop, the passage from inside to outside of the channel deposits is commonly poorly exposed, or sometimes misinterpreted given the similarities of marginal within-channel facies to outside-channel thin-bedded deposits. In seismic data, on the other hand, geometries drive the interpretation. While resolution limitations and seismic quality can degrade imaging, in the example presented in this chapter the images are considered clear enough to offer a conclusive interpretation.

In both of the channel complexes imaged on the amplitude maps the geometries of the adjacent deposits track their sinuosity (Figs. 6.9-6.18). This is a good indication that the channel complexes and the adjacent deposits are genetically related. Consequently the proposed interpretation is that the adjacent deposits are levee and overbank deposits to the channel complexes. It could be argued that these levees are related to a possible older channel complex. However throughout the analysed seismic dataset (maps and sections) there is no indication of the presence of a possible older channel complex. The unique possibility in this case would be that the younger channel complex has followed the exact pathway of an older one which, given the complicated slope topography, is considered unlikely. Another alternative interpretation of such deposits is that they are older frontal lobes that the channels cut through during progradation. This would require the channel to cut through the axis of the lobe. A characteristic that

supports the levee/overbank interpretation is the lateral grading from red to blue (high to lower amplitude) with increasing distance from the channel complexes on both sides. This trend in seismic facies suggests that the reduction in amplitude corresponds with decreasing sandstone content with distance from the channel, a characteristic of levee-overbank deposits.

The width of each channel-levee complex is about 5 km and they are roughly symmetrical in cross-section. No preferable location for the thickest coarse-grained deposits on the levees is observed, i.e., they appear both on the outer and inner bends of the channel complexes. A possible driving mechanism for this is continuous overspill (Hiscott et al., 1997 and Peakall et al., 2000) rather than flow stripping (Pickering et al., 1989; Timbrell, 1993; Piper and Normark, 1983).

The scale of the channel complexes and the resolution of the seismic data preclude a precise interpretation as to whether the channel complexes were confined solely by aggradation of the levees or if some of the confinement was due to early incision. In some sections, e.g. figure 6.10, it appears they are entirely confined by the levees, conversely, in other sections, e.g. figure 6.9, it appears that they had some degree of incision beneath the base of adjacent levees.

In the Laingsburg Formation, characteristic channel-levee systems were interpreted in sub-units E2 and E3 in the northern area and F2 in the southern area (chapter 3). Medium and thin beds of climbing ripple laminated sandstones are intercalated with siltstones in overall thinning and fining upward successions that is characteristic of levee-overbank deposits. Although the grain-size and calibre of deposits in deep water are influenced by the sediment source area characteristics and transport processes across the shelf, the facies and geometry of levee-overbanks deposits should not vary significantly from those described in the Laingsburg Formation.

6.7.2 - Sand distribution from amplitude maps

6.7.2.1 - Eastern system

The eastern channel-levee system is not as well imaged as the western one and the imaging is interrupted for about 10 km in the centre-north portion (Figs. 6.9 - 6.19). However, down dip, beyond the non-imaged area, the characteristic geometry of a channel appears again. It is interpreted that this is the same channel complex (Fig. 6.19). In this case, within the area covered by the seismic project this channel complex is about 35 km long. It is also narrower and apparently thinner than the other channel complex (see below). According to the interpreted seismic facies, the channel complex is filled predominantly by clay-prone deposits and the levees are dominated by sand-prone deposits (Figs. 6.9-6.19). It suggests that the channel complex was backfilled by claystone deposits and that these are younger than the levees. Based upon the characteristic of the levees it can be predicted that sandy terminal or transient lobes can be found downdip from the imaged area.

6.7.2.1 - Western system

The western channel-levee system is better imaged than the eastern one. It is larger and shows well defined margins. The distal termination of the channel is imaged and down dip from this point the geometries suggest unconfined distributive deposits (Fig. 6.19). The distributive area is divided into two portions. The first, most proximal to the channel mouth is about 11 km long and 5 km wide. Here it is still possible to observe, both in map and cross- section view, a few small channel features cutting the interpreted unconfined deposits (Figs. 6.16; 6.17; and 6.19). The second portion, more

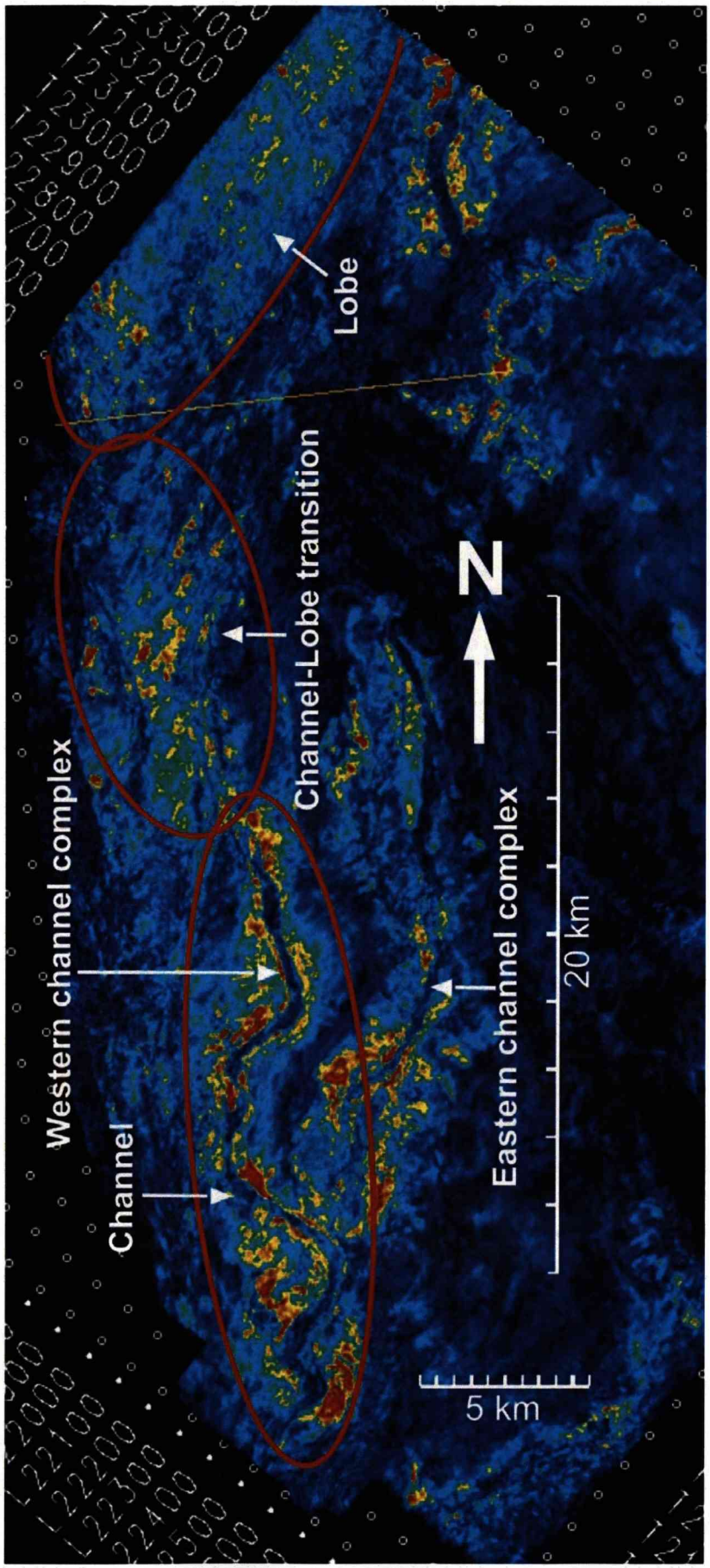

Figure 6.19 - RMS amplitude map showing the western channel-lobe system. On the map are indicated the areas of the channel, channel-lobe transition and lobe.

distal, shows more homogeneous distribution of seismic facies without channel features. Although the limits of the seismic project do not allow the imaging of this second portion entirely, it appears to be longer and wider than the first, more proximal distributive area. The geometry and the distribution of seismic facies within this area suggest the presence of lobe deposits (Fig. 6.19). This interpretation implies that the area between the lobes and the channel can be interpreted as a channel lobe transition zone. Based on the seismic facies analysis, geometries and well-understood regional context the whole depositional system is interpreted as a *linked slope channel-lobe system*.

The sand-prone Laingsburg Unit D/E is interpreted in chapter 3 as an intraslope lobe (Fig. 3.5 and 3.6) fed by channel(s) which are not exposed in the available outcrop. By analogy it also can be interpreted as a *linked slope channel-lobe system* similar to the western Amazon Fan system. Unit D/E has a high sandstone percentage (90%), however its maximum thickness is only about 8 m. The lobe interpreted in the seismic data does not seem to have a high net to gross, but to be imaged in amplitude maps it has to be thicker than the resolution limit (14 m), thicker than the D/E lobe. Even though these two systems have some differences their internal architecture, at a scale that cannot be seen in the seismic data, should not be very different, thus the description of the D/E lobe presented in chapter three is a thought to be a good example of the internal architecture of an intraslope lobe below seismic resolution.

6.8 - Generic similarities and differences between the Laingsburg slope succession and the Amazon Fan

A comparison of the Laingsburg and Amazon systems indicates that they are different in many parameters: scale, age and tectonic setting. The Amazon Fan is larger than 300,000 km^2 (Damuth et al., 1988) and at its thickest (on the submarine slope) it is about 9 km thick (compacted thickness; Silva et al., 1998). The submarine slope succession of the SW

Karoo basin during Laingsburg Formation time is about 1.2 km thick (compacted thickness; Grecula et al., 2003; Sixsmith et al., 2004; Flint et al., 2008; and this work) and the whole Permo-Triassic Karoo outcrop area is only about twice as large as the Amazon Fan (Visser, 1995) (Fig. 6.20). This shows that the Laingsburg submarine slope system is about one tenth the size of the Amazon Fan. The former is upper Permian in age and is non-tectonic, and the latter is upper Miocene to Present and is affected by gravitational tectonism. The Laingsburg is an exhumed system accessed by field work and the Amazon Fan is a buried system accessed only by seismic data or wells.

Mutti and Normark (1991) highlighted the caution for comparison between what they called *ancient* and *modern* turbidite systems taking account of differences such as those pointed out between the Laingsburg and the Amazon Fan systems. Nevertheless, these authors identified some elements (erosional features bigger than channels, overbank deposits, lobes, and channel-lobe transition deposits) they consider can be identified in both systems. In this field-based work all these elements, excepted channel-lobe transition, were identified and discussed in previous chapters. The attempt to compare the *ancient* Laingsburg system with the *modern* Amazon Fan system (sensu Mutti and Normark, 1991) made in this final chapter has shown that despite such considerable differences between depositional system some deepwater erosional/depositional elements can be expected in determining deepwater settings. Furthermore, this work has also shown that field-based study of exhumed *ancient* deepwater systems is a necessary complement (as demonstrated in chapters 4 and 5) to the understanding of buried *modern*, or *ancient* ones since these can only be accessed by indirected methods with limited resolution.

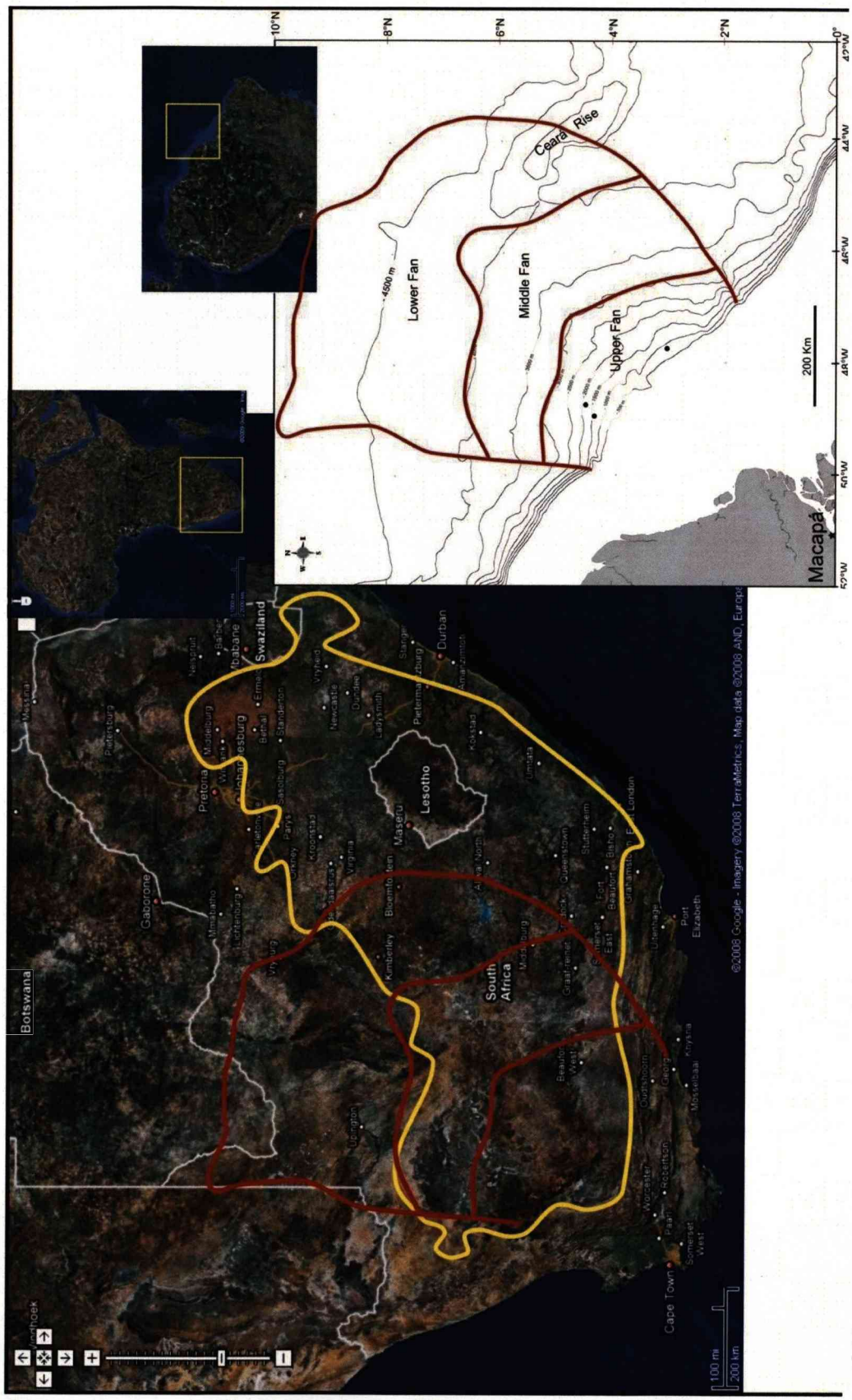

Figure 6.20 - Comparison between the area of the Amazon Fan (red outline modified from Damuth et al., 1988) and the Permo-Triassic Karoo outcrop area (yellow outline based on Visser, 1995).

Chapter 7 - Conclusions and recommendations for future work

7.1 – General Conclusions

Middle and upper submarine slope successions are usually not well preserved or exposed in the geological record due their typically fine grained character. The well exposed succession analysed in detail for the first time in this work enabled a novel interpretation for the stratigraphic evolution of the Laingsburg Formation. In addition, this research has developed exportable models to be used as analogues for middle and upper slope stratigraphic successions with no growth faulting, no salt or shale diapirism in seismic and outcrop-based investigations. Despite the apparent tectonic quiescence of the setting studied, a complicated spatial and temporal distribution of lithofacies and sedimentary environments was identified at outcrop. It was concluded that the storage and/or bypass of coarse-grained sediment through middle and upper submarine slopes is a function of seabed topography convolved with changes in usable accommodation and modulation in sediment supply caused by the temporal (stratigraphic) evolution of the submarine slope (progradation or retrogradation).

Variation in sea floor topography is interpreted to have been driven by differential compaction over underlying stratigraphy. Changes in the locus of deposition through time were documented across strike in the study area. Differential sand/clay depositional ratio on the slope led to differential compaction where mud-prone successions underwent more compaction than the sand-prone sections (Figs. 3.26 and 3.27). The characteristic of some deposits, such as Units D/E and E1 lobes (Figs. 3.5, 3.6, 3.8 and 3.9) also suggests down dip variation in seabed topography. Despite the lack of physical stratigraphic constraint down dip from the study area, it is speculated that such variation in sea floor relief is also caused by differential deposition/compaction due to accumulation of extensive sand-prone deposits on the basin floor and toe of slope (Fan A and Unit B; Grecula et al., 2003, Sixsmith et al., 2004).

Changes in usable accommodation and modulation in sediment supply caused by the temporal (stratigraphic) evolution of the submarine slope (progradation or retrogradation) are interpreted from the characteristics of the erosional/depositional features present through the analysed succession. Despite the complicated across-strike and down-dip distribution of the sand-prone deposits and their variable range of geometries, an organised and predictable stratigraphic pattern is identified. This pattern is characterized by an initial distributive system that was dominated by depositional processes and focussed in low relief areas (available accommodation) in the slope. These are overlain by channel-levee systems combining a mix of depositional and erosional processes, followed by entrenched slope valleys that are dominated by erosional processes at the most basinward stage of progradation. During subsequent retrogradation, distributive systems prevail again (Fig. 3.30).

A well organised temporal (stratigraphic) distribution was also identified. A consistent pattern of regional mappable claystone thicknesses enabled the establishment of a hierarchical scheme of these units, which group them in a range of thicknesses such as: (1) <5 m; (2) 20-40 m; and (3) 45-70 m. The first group divides sand-prone Units into Sub-units and the last two separate Units. Each claystone unit coupled with the underlying sand-prone deposits are interpreted to form a depositional sequence. The sequence boundaries are placed at the base of the sand-prone units, which are interpreted as the lowstand deposits. The overlying claystones are interpreted as the transgressive and highstand deposits). Eleven sequences were identified. Nine of them, based on the hierarchy of the thickness of the claystone units, can be grouped into three clusters of three sequences each that are interpreted as composite sequences. The three sequence sets plus one individual sequence, also based on the hierarchy of the thickness of the claystone units, are grouped into a composite sequence set. The remaining individual sequence, Unit H coupled with the overlying claystone unit, does not form part of the composite sequence set because the claystone unit broke a trend of thickening upward of these units (Fig. 7.1).

The lowstand deposits of the depositional sequences comprise a range of erosional/depositional elements. The lowstand depositional

succession of sequence F2 was broken down into a hierarchy of channel, channel complexes, channel complexes set, and slope valley, and their related levee-overbank deposits (Fig. 7.1). Despite the complicated stratigraphic relationship between these elements a model for the evolution of lowstand depositional succession on the upper submarine slope was proposed. It represents a series of events from the initiation, opening, and filling of channels/channel complexes/channel complex sets through the cut of an entrenched slope valley evidencing the main phase of down-dip bypass to the backfill of this large erosive feature with fine-grained sediments. Moreover, this model was integrated and tested with 3D high resolution seismic reflection data and the results revealed that it can resolve sedimentological and stratigraphic problems at a scale of individual channel-fills which is beyond the resolution afforded by 3D high resolution seismic.

These final general remarks are complemented with the answerers for the motivational questions posed in chapter 1 (Section 1.1.2) in order to scientifically evaluate the initial stated hypotheses to close the conclusions of this thesis.

7.2 – Responses to initial questions/hypotheses posed in this thesis

Questions 1 and 5: *What range of sedimentary processes act in middle and upper submarine continental slope settings (beyond the shelf edge)? What are the dominant depositional processes of the gravity driven flows?*

Complete Bouma sequences were not found in the slope succession of the upper Laingsburg Formation. Incomplete Bouma sequences are locally found in levee-overbank deposits (Tc; Tbc; Tcd; Tbcd from most to least common), distributive systems (Tab; Tb; Tbc; Tabc), and as parts of the late phase of channel fills (Tbc; Tbcd; Tcd). These specific lithofacies distributions are related to a combination of flow stripping over contemporaneous slope channel margins and across local subtle seabed topography. Volumetrically, tractional deposits make up the majority of the

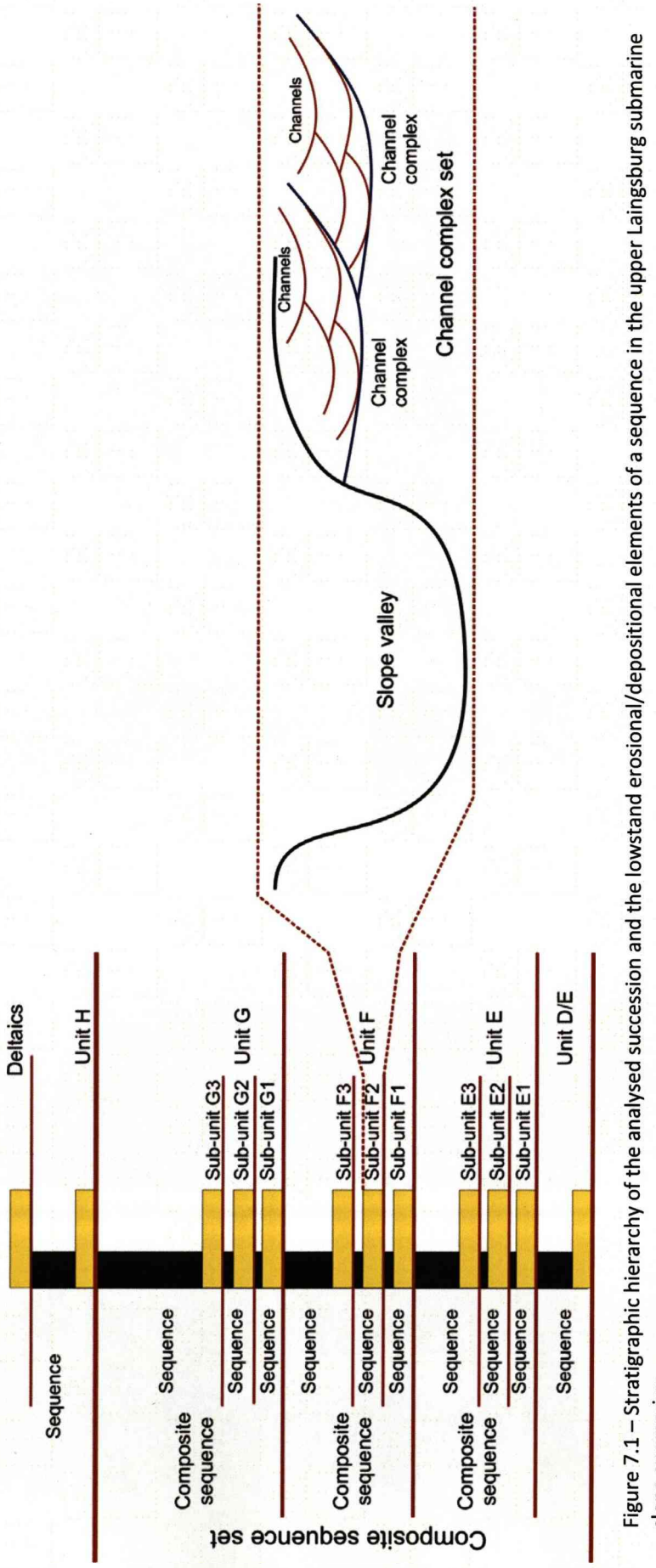

Figure 7.1 – Stratigraphic hierarchy of the analysed succession and the lowstand erosional/depositional elements of a sequence in the upper Laingsburg submarine slope succession.

sandstones deposited in the upper Laingsburg Formation. Thick sandstone beds of climbing ripple lamination indicate high rates of deposition from flows that are interpreted to have expanded upon leaving confinement (adjacent to or in front of channels).

Erosion surfaces mantled by mudstone clast conglomerates, and thin-bedded siltstone successions within channel-forms indicate periods when the dominant process was the bypass of coarse-grained sediment into the deeper basin. Within erosional features, thick bedsets of structureless sandstone are common. These non-Bouma-like sandy bodies are ascribed to deposition from prolonged, quasi-steady high-density turbidity currents (*sensu* Kneller, 1995).

Question 2: *What does fining-upward, muddy stratigraphy represent in submarine continental slope settings?*

The distribution of lithofacies associations and geometries of erosional/depositional elements show an organized pattern from distributive (base of the analysed succession) to incised and back to distributive again. This stacking pattern of depositional environments is interpreted to reflect an overall and long-term progradation (basinward-stepping) followed by retrogradation (landward-stepping) of the entire submarine slope (Fig. 3.30). In the progradational part of the succession, individual sand-prone packages (the Units) show an overall fining-upward profile, ascribed to an upward increase in the degree of down dip bypass of sand. The hierarchy of the stratigraphic elements identified (Fig. 3.29) combined with the down-dip evolution of the slope (Fig. 3.30) show that a long-term progradation followed by retrogradation comprises a composite sequence set. Therefore, fining-upward, muddy stratigraphy in submarine slope settings can be the result of a combination of down dip bypass of the coarse-grained content with the long term backstepping of the depositional feeder system.

Questions 3 and 4: *The upper and middle slope are settings where conduits for coarse-grained sediment bypass are regularly re-excavated and entrenched, however recent high resolution 3-D seismic data have suggested that a wider range of coarse grained deposits might occur in these*

settings. Can such deposits be also identified from outcrop dataset? What are the roles of subtle sea floor topography and the temporal evolution of the submarine slope (progradation or retrogradation) on the development of different types of sand-prone deposits on the middle and upper slope? How can subtle sea floor topography be reconstructed from outcrops in the absence of measurable onlap?

Integrated three dimensional stratigraphic and sedimentological analyses identified a range of sandbody types and geometries. The first two systems (Unit D/E and Sub-unit E1) were confined to a local depocentre in the north, possibly related to a down dip and/or across strike step in the gradient of the regional slope. The subsequent Sub-units E2 and E3 were still confined to the local northern depocentre. Sub-unit F1 healed the northern depocentre and then spilled laterally across the palaeoslope over the entire study area. Sub-unit F2 is divided into two phases. Early channel systems confined by genetically-related aggradational levees, both in the northern and southern areas, represent healed slope accommodation. A second phase is marked by entrenched valley systems where the composite erosion surface is lower and younger than the related levees, and represents periods of sediment bypass with final filling as the system started to backstep. Therefore, outcrop based studies can produce models at seismic scale but can also represent and explain complicated stratigraphic and process relationships that cannot be resolved with even high resolution 3D seismic data.

Two approaches are important to reconstruct subtle palaeo sea floor topography: (1) Physical stratigraphic correlation of depositional bodies and constrained by sedimentary logging and walking out key surfaces; and (2) analysis and mapping of lithofacies associations and architectural elements. The first provides understanding about the horizontal and vertical distribution of the depositional bodies (sand-prone or clay prone) which is useful to measure local to regional thickness variations in relation to underlying deposits. This delineates subtle topographic highs and lows at different times. The analysis of lithofacies associations and architectural elements within this framework, supplemented by palaeocurrent data, highlights process relationships between topography and sediment gravity flows. For

example, local distributive deposits on the upper slope indicate some sort of variation in the gradient of the sea floor and the presence of usable accommodation.

7.3 – Future Work

Recommendations for future work may involve testing the applicability of the models generated in this thesis to other datasets, to test their sensitivity to variables such as different sand/clay ratio, wider grain size range, different regime for generation of sea floor topography or even different scales of submarine slope. Such datasets can be provided from outcrop or seismic information. Specifically, it would be interesting to compare the stacking patterns identified in the Laingsburg slope succession with other datasets to investigate if other slope systems evolved through the punctuated accretion of sandy deposits at individual sequence scale and if sequences group into similar tripartite composite sequences. Is this a characteristic of slope systems in general, or just the late Palaeozoic icehouse world? The answer for this question, an interesting additional line of enquiry would be to compare a comparable slope succession deposited during a greenhouse period of earth history with this icehouse example. A testable hypothesis would be that the sequences are more easily identifiable in icehouse systems due to the larger variations in glacio-eustatic sea level (higher amplitude, same frequency) compared with greenhouse times.

Another question is whether the degree of stratigraphic organisation apparent here could be identified in mud-rich submarine slope successions that have a more dynamic substrate (mud- or salt-diapirism, or tectonically active settings)?

A worthwhile future research direction would be to test the high resolution outcrop-based models for slope systems generated in this work with ultra high resolution seismic data such as those from shallow seismic projects (e.g.150 Hz) since such datasets offer resolution at the same scale as that presented for the stratigraphic evolution and the pattern of channels and channel complexes in this work.

Comparisons with seismic models can also be made in order to predict the possible down dip extension of the erosional/depositional systems identified in this work, since the available outcrop of the coeval basin floor is limited. Comparison with ancient and modern slope successions could be made in order to test the role of differential compaction in driving the depositional locus and influencing the architectural pattern of the deposits.

References

Abbott, S.T. and Carter, R.M. (1994). The sequence architecture of mid-pleistocene (c.1.1-0.4 Ma) cyclothems from New Zealand: facies development during a period of orbital control on sea-level cyclicity. *In:* Boer, P.L. and Smith, D.G. (eds) *Orbital Forcing and Cyclic Sequences*, International Association of Sedimentologists, Special Publication 19, p. 367-394.

Abreu, V., Sullivan, M., Pirmez, C. and Mohrig, D. (2003). Lateral accretion packages (LAPs): an important reservoir element in deep water sinuous channels. *Marine and Petroleum Geology,* v. 20, p. 631-648.

Adams, E.W. and Schlager, W. (2000). Basic Types of submarine slope curvature. *Journal of Sedimentary Research*, v 20, p. 814-828.

Adeogba, A.A., McHargue, T.R. and Graham, S.A., (2005). Transient fan architecture and depositional controls from near-surface 3-D seismic data, Niger Delta continental slope. *American Association of Petroleum Geologists Bulletin*, v. 89, p. 627-643.

Allen, J.R.L. (1991). The Bouma division A and the possible duration of turbidity currents. *Journal of Sedimentary Petrology*, v. 61, p. 291-295.

Anderson, K.S., Graham, S.A. and Hubbard, S.M. (2006). Facies, Architecture, and origin of a reservoir-scale sand-rich succession within submarine canyon fill: Insights from wagon caves rock (Paleocene), Santa Lucia Range, California, U.S.A. *Journal of Sedimentary Research,* v. 76, p. 819-838.

Andersson, P.O.D., Worden, R.H., Hodgson, D.M. and Flint, S. (2004). Provenance evolution and chemostratigraphy of a Palaeozoic submarine fan-complex: Tanqua Karoo basin, South Africa. *Marine and Petroleum Geology*, v. 21, p. 555–577.

Baas, J.H. (2000). EZ-ROSE: a computer programme for equal-area circular histograms and statistical analysis of two-dimensional vectorial data: Computers and Geoscience, v. 26, p. 153-166.

Bailey, E.B. (1930). New light on sedimentation and tectonics. Geological Society of America, Bulletin 47, 1713-1726.

Bates, C.C. (1953). Rational Theory of delta formation. *American Association of Petroleum Geologist Bulletin*, v. 37, p. 2119-2162.

Beaubouef, R.T. (2004). Deep-water leveed-channel complexes of the Cerro Toro Formation, Upper Cretaceous, southern Chile. *American Association of Petroleum Geologists Bulletin,*. v. 88,, p. 1471-1500.

Beaubouef, R.T. and Friedmann, S.J. (2000). High Resolution Seismic/ Sequence Stratigraphic Framework for the Evolution of Pleistocene Intra Slope Basins, Western Gulf of Mexico: Depositional Models and Reservoir Analogs. *In:* Weimer, P., Slatt, R.M., Coleman J., Rosen N.C., Nelson H., Bouma A.H., Styzen, M.J. and D. T. Lawrence, D.T. (eds.) *Deep-water reservoir of the world, GCS-SEPM foundation, 20th Annual Bob F. Perkins conference*, p. 40-60.

Bouma, A.H. (1962). *Sedimentology of some flysch deposits*. Elsevier, Amsterdam. 168 p.

Bouma, A.H. (1979). Continental slopes. *In:* Doyle L.J. and Pilkey, O.H. (eds) *Geology of Continental Slopes*. Soc. Econ. Paleont. Mineral. Spec Publication 27, p. 1-15.

Bouma, A.H. (2000). Fine-grained, mud-rich turbidite systems: model and comparison with coarse-grained, sand-rich systems *In:* Bouma, A.H. and Stones, C.G. (eds), *Fine-grained turbidite systems*, American Association of Petroleum Geologists Memoir 72 / Society for Sedimentary Geology Special Publication 68, p. 9-20.

Campion, K.M., Sprague, A.R., Mohrig, D., Lovell, R.W., Drzewiecki, P.A., Sullivan, M.D., Ardill, J.A., Jensen, G.N. and Sickafoose, D.K. (2000). Outcrop expression of confined channel complexes. *In:* Weimer, P., Slatt, R.M., Coleman, J., Rosen, N.C., Nelson, H., Bouma, A.H.,

Styzen, M.J. and Lawrence, D.T. (eds) *Deep-water reservoir of the world, GCS-SEPM foundation, 20th Annual Bob F. Perkins conference*, p. 127-150.

Catuneanu, O. (2004). Basement control on flexural profiles and the distribution of foreland facies: the Dwyka Group of the Karoo Basin, South Africa. *Geology*, v. 32, p. 517-520.

Catuneanu, O., Hancox, P.J., and Rubidge, B.S. (1998). Reciprocal flexural behaviour and contrasting stratigraphies: a new basin development model for the Karoo retroarc foreland system, South Africa: *Basin Research*, v. 10, p. 417-439.

Catuneanu, O. , Wopfner H. and Eriksson P.G., Cairncross B, Rubidge B.S., Smith R.M.H., Hancox, P.J. (2005). The Karoo basins of south-central Africa. *Journal of African Earth Sciences,* v. 43, p. 211–253.

Clark, J.D. and Pickering, K.T. (1996). Architectural Elements and Growth Patterns of Submarine Channels: application to Hydrocarbon Exploration. *American Association of Petroleum Geologists Bulletin*, v. 80, p. 194-221.

Cole, D.I. (1992). Evolution and development of the Karoo Basin. *In*: De Wit, M.J. and Ransome, I.G.D. (eds),*Inversion Tectonics of the Cape Fold Belt, Karoo and Cretaceous Basins of Southern Africa*. Balkema, Rotterdam, p. 87-99.

Coleman, J.M., Prior, D.B. and Lindsay, J.F. (1983). Deltaic influences on shelf edge instability processes. *In*: Stanley, D.J. and Moore, G.T. (eds), *The Shelfbreak: Critical interface on Continental Margins*. Society. for Sedimentary Geology, Tulsa, p. 121-137.

Covault, J.A., Normark, W.R., Romans, B.W. and Graham, S.A. (2007). Highstand fans in California borderland: the overlooked deep-water depositional systems. *Geology*, v. 35, p. 783-786.

Cronin, B.T., Hurst, A., Celik, H. and Turkmen, I. (2000). Superb exposure of a channel, levee and overbank complex in an ancient deep-water slope environment. *Sedimentary Geology*, v 132, p 205-216.

Dailly, G.C. (1983). Slope readjustment during sedimentation of continental margins. *In:* Watkins, J.S. and Drake, C.L. (eds) *Studies in Continental Marine Geology*. American Association of Petroleum Geologists Memoir 34, p. 593-608.

Damuth, J.E. and Kumar, N. (1975). Amazon cone: Morphology, Sediments, Age and Growth Pattern. *Geological Society of America Bulletin*, v. 86, p. 863-878.

Damuth, J.E., Flood, R.D., Kowsmann, R.O., Belderson, R. H. and Gorini, M.A. (1988). Anatomy and growth pattern of Amazon Deep-Sea Fan as revealed by long-range side-scan sonar (GLORIA) and high-resolution seismic studies. *American Association of Petroleum Geologists Bulletin*. v. 72, p. 885-911.

Dean, W.E. and Gardner, J.V. (1986). Milankovitch cycles in the Neogene deep sea sediment. *Paleoceanography*, v. 1, p. 539-553.

Deptuck, M.E., Sylvester, Z., Pirmez, C. and O'Byrne C. (2007). Migration-aggradation history and 3-D seismic geomorphology of submarine channels in the Pleistocene Benin-major Canyon, western Niger Delta slope. *Marine and Petroleum Geology*, v. 24, p. 406-433.

De Wit, M. J. and Ransome, I. D. (1992). Regional inversion tectonics along the southern margin of Gondwana. *In:* DeWit, M. J. and Ransome, I. D. (eds) *Inversion tectonics of the Cape Fold Belt, Karoo and Cretaceous basins of Southern Africa*. Balkema, Rotterdam, p. 15–22.

Dietz, R.S. (1964). Origin of continental slopes: *American. Scientist*, v. 52, p. 50-69.

Droz, L., Kergoat, R., Cochonat, P. and Berne, S. (2001). Recent sedimentary events in the western Gulf of Lions (western Mediterranean). *Marine Geology*, v. 176, p. 23-37.

Emery, K.O. (1977). Stratigraphy and structure of pull-apart margins. *In:* McFarlan, E., Drake, C.L. and Pittman, L.S. (eds) *Geology of Continental Margins*. American Association of Petroleum Geologists, Continuing Education Course, Note Series n. 5, p. B1-B20.

Fairbridge, R.W. (1976) Effects of Holocene climatic change on some tropical geomorphic process. *Quaternary Research*, v. 6, p. 529-556.

Faure, K. and Cole, D. (1999). Geochemical evidence for lacustrine microbial blooms in the vast Permian Main Karoo, Parana, Falkland Islands and the Huab basins of southwestern Gondwana. *Palaeogeography, Palaeoclimatology, Palaeoecology*, v. 152, p. 189-213.

Fielding, C.R., Frank, T.D., Birgenheier, L.P., Rygel, M.C., Jones, A.T. and Roberts, J. (2008a) Stratigraphic imprint of the Late Paleozoic Ice Age in eastern Australia: a record of alternating glacial and nonglacial climate regime. *Journal of the Geological Society*, London, v. 165, p. 129-140.

Fielding, C.R., Frank, T.D., Birgenheier, L.P., Rygel, M.C., Jones, A.T., and Roberts, J. (2008b) Stratigraphic record and facies associations of the late Paleozoic ice age in eastern Australia (New South Wales and Queensland). *In:* Fielding, C.R., Frank, T.D., and Isbell, J.L. (eds) *Resolving the Late Paleozoic Ice Age in Time and Space*, The Geological Society of America, Special Paper 441, p. 41-57.

Figueiredo, J.J.P., Hoorn, C., Ven, P.H. vd., and Soares, E.F. (2009). Late Miocene onset of the Amazon River and the Amazon deep-sea fan: Evidence from the Foz do Amazonas Basin. *Geology*, v. 37, p. 619–622.

Fildani, A., Drinkwater, N.J., Weislogel, A., Mchargur, T., Hodgson, D.M. and Flint, S.S. (2007). Age control on the Tanqua and Laingsburg deep-water systems: New insight on the evolution and sedimentary fill of the Karoo Basin, South Africa. *Journal of Sedimentary Research*, v. 77, p. 901-908.

Flint, S.S. and Hodgson, D.M. (2005). Submarine slopes systems: processes and products. *In:* Hodgson, D.M. and Flint, S.S. (eds) *Submarine Slope Systems: Process and Products*. Geological Society, London, Special Publication 244, p. 1-6.

Flint, S.S., Hodgson, D.M., Sixsmith, P., Grecula, M., and Wickens, H. DeV. (2007). Deepwater basin floor/slope deposits of the Laingsburg Depocenter, Karoo Basin, South Africa *In:*: Nilsen, T., Shew, R., Stefans, G. and Studlick, J. (eds) *Atlas of Deepwater Outcrops*, American Association of Petroleum Geologists, ST56, p.326-329.

Fonesu, F. (2003). 3D Seismic images of a low-sinuosity slope channel and related depositional lobe (West Africa deep-offshore). *Marine and Petroleum Geology*, v. 20, p. 615-629.

Galloway, W.E. (1998). Siliciclastic slope and base-of-slope depositional systems: Component facies, Stratigraphic Architecture, and Classification. *American Association of Petroleum Geologists Bulletin*, v. 82, p. 627–643.

Gardner, M.H. and Borer, J. M. (2000). Submarine Channel Architecture along a Slope to Basin Profile, Permian Brushy Canyon Formation, West Texas. *In:* Bouma, A.H. and Stones, C.G. (eds) *Fine-Grained Turbidite Systems*. American Association of Petroleum Geologists Memoir 72 / Society for Sedimentary Geology, Special Publication 68, p. 195–215.

Gardner, M.H., Borer, J.M., Melick, J.J., Mavilla, N., Dechesne, M. and Wagerle, R.N. (2003). Stratigraphic process-response model for submarine channels and related features from studies of Permian Brushy Canyon outcrops, West Texas. *Marine and Petroleum Geology*, v. 20, p. 757-787.

Gee, M.J.R., and Gawthorpe, R.L. (2006). Submarine channels controlled by salt tectonics: Examples from 3D seismic data offshore Angola. *Marine and Petroleum Geology*, v. 23, p. 443-458.

Goldhammer, R.K., Oswald, E.J. and Dunn, P.A. (1994). High-frequency, glacio-eustatic cyclicity in the middle Pennsylvanian of the Paradox Basin: an evaluation of Milankovitch forcing. *In:* Boer, P.L. and Smith, D.G. (eds) *Orbital Forcing and Cyclic Sequences*, International Association of Sedimentologists, Special Publication 19, p. 243-283.

Goldhammer, R.K., Wickens, H.DeV., Bouma, A.H., and Wach, G. (2000). Sequence Stratigraphic Architecture of the Late Permian Tanqua Submarine Fan Complex, Karoo Basin, South Africa. *In:* Bouma, A.H. and Stone, C.G. (eds) *Fine-grained turbidite systems*, American Association of Petroleum Geologists Memoir 72 / Society for Sedimentary Geology Special Publication 68, p. 165-172.

Gilbert, G.K. (1885). The Topographic features of lake shores: *U.S. Geological Survey 5th Annual Report*, p.104-108.

Gilbert, G.K. (1890). Lake Bonneville: U.S. *Geological Survey Monograph* n. 1, 438p.

Grecula, M. (2000) *Stratigraphy and Architecture of Tectonically Controlled Turbidite Systems, Laingsburg Formation, Karoo Basin, South Africa* [unpublished PhD thesis]. University of Liverpool, 184 p.

Grecula, M, Flint, S., Wickens, D. and Potts, G.J. (2003). Partial Ponding of Turbidite Systems in a Basin with Subtle Growth-fold Topography: Laingsburg-Karoo, South Africa. *Journal of Sedimentary Research, v.* 73, p. 603-620.

Gresse, P.G., Theron, J.N., Fitch, F.J. and Miller, J.A. (1992). Tectonic inversion and radiometric resetting of the basement in the Cape Fold Belt. *In:* DeWit, M. J. and Ransome, I. D.(eds) *Inversion tectonics of the Cape Fold Belt, Karoo and Cretaceous basins of Southern Africa*: Balkema, Rotterdam, p. 217-228.

Hälbich, I.W. (1983) Tectonogenesis of the Cape Fold Belt (CFB), *In:* Söhnge, A.P.G. and Hälbich, I.W. (eds) Geodynamics of the Cape Fold Belt, Special Publication of the Geological Society of South Africa, v. 12, p.165-175.

Hedberg, H.D. (1970). Continental margins from viewpoint of the petroleum geologist. *American Association of Petroleum Geologists Bulletin*, v. 54, p. 3-43.

Herbert, T.D. and Fisher, A.G. (1986). Milankovitch climatic origin of the mid-Cretaceous black shale rhythms in central Italy. *Nature*, v. 321, p. 739-743.

Hodgson, D.M. and Haughton, P.D.W. (2004). Impact of syn-depositional faulting on gravity current behaviour and deep-water stratigraphy: Tabernas-Sorbas Basin, SE Spain *In:* Lomas, S.A. and Joseph, P. (eds) *Confined Turbidite Systems*, Geological Society, London, Special Publications, 222, p. 135-158.

Hodgson, D.M., Flint, S.S., Hodgetts, D., Drinkwater, N.J., Johannenssen, E.P. and Luthi, S.M. (2006). Stratigraphic evolution of fine-grained submarine fan systems, Tanqua depocentre, Karoo Basin, South Africa: *Journal of Sedimentary Research*, v. 76, p. 20-40.

Johnson, M.R. (1991). Sandstone petrography, provenance and plate tectonic setting in Gondwana context of the south-eastern Cape Karoo Basin. *South African Journal of Geology*, v. 94, p.137-154.

Kane, I.A., Kneller, B.C., Dykstra, A.K. and McCaffrey, W.D. (2007). Anatomy of a submarine channel-levee: An example from Upper Cretaceous slope sediments, Rosario Formation, Baja California, Mexico. *Marine and Petroleum Geology*, v. 24, p. 540-563.

Kenyon, P.M. and Turcotte, D.L. (1985). Morphology of a delta by bulk sediment transport. *Geological Society of America Bulletin*, v. 96, p. 1457-1465.

Keunen, Ph.H. (1963). Turbidites in South Africa. Trans. of the Geological Society of South Africa, v. 66, p. 191

Keunen, Ph.H., Migliorini, C.I. (1950). Turbidity currents as a cause of graded bedding. *The Journal of Geology*, v. 58, p. 91-127.

Kneller, B. C. (1995). Beyond the turbidite paradigm: physical models for deposition of turbidites and their implications for reservoir prediction. *In*: A.J. Hartley and D.J. Prosser (eds) Characterization of the Deep Marine Clastic Systems. Geological Society (London) Special Publications, v. 94, p. 31–49.

Kneller, B.C. and Branney, M.L. (1995). Sustained high-density turbidity currents and the deposition of thick massive sands. *Sedimentology*. v. 42, p. 607-616.

Kolla, V., Posamentier, H.W. and Wood, L.J. (2007). Deep-water and fluvial sinuous channels – Characteristics, similarities and dissimilarities, and modes of formation. *Marine and Petroleum Geology,* v. 24, p. 388-405.

Kolla, V., Bourges, Ph., Urruty, J.M. and Safa, P. (2001). Evolution of deep-water Tertiary sinuous channels offshore Angola (west Africa) and implications for reservoir architecture. *American Association of Petroleum Geologists Bulletin*, v. 85, p. 1373–1405.

Koša, E. (2007). Differential subsidence driving the formation of mounded stratigraphy in deep-water sediments; Palaeocene, central North Sea: *Marine and Petroleum Geology*, v. 24, p. 632–652.

Kuehl, S.A., Hariu, T.M. and Moore, W.S. (1989). Shelf sedimentation off the Ganges-Brahmaputra river system; evidence for sediment bypassing to the Bengal Fan. *Geology*, v. 17, p. 1132-1135.

López-Gamundí, O.R. and Rossello, E.A. (1998). Basin-fill evolution and paleotectonic patterns along the Samfrau geosyncline: the Sauce Grande basin - Ventana foldbelt (Argentina) and Karoo basin - Cape foldbelt (South Africa) revisited. *Geologische Rundschau*, v. 86, p. 819-834.

Matthews, M.D. and Perlmutter, M.A. (1994). Global cyclostratigraphy: an application to the Eocene Green River Basin *In:* Boer, P.L. and Smith, D.G. (eds), *Orbital Forcing and Cyclic Sequences*, International Association of Sedimentologists, Special Publication 19, p. 459-481.

Mayall, M. and Stewart, I. (2000). The Architecture of Turbidite Slope Channels. *In:* Weimer, P., Slatt, R.M., Coleman, J, Rosen, N.C., Nelson, H., Bouma. A.H., Styzen, M.J. and Lawrence D.T. (eds) *Deep-water reservoir of the world,* GCS-SEPM foundation, 20th Annual Bob F. Perkins conference, p. 578-586.

Mayall, M., Jones E. and Casey, M. (2006). Turbidite channel reservoir – Key elements in facies prediction and effective development. *Marine and Petroleum Geology*, v. 23, p. 821-841.

Mellere D., Plink-Bjorklund, P. and Steel, R.J. (2002). Anatomy of shelf-edgedeltas on a prograding Eocene shelf margin, Spitsbergen: *Sedimentology*, v. 49, p.1181–1206.

Mellere D., Breda, A. and Steel, R.J. (2003). Fluvially-incised shelf-edge deltas and linkage to upper-slope channels (Central Tertiary Basin, Spitsbergen). *In*: Roberts, H.H., Rosen, N.C., Fillon, R.H. and Anderson, J.B. *Shelf-Margin Deltas and Linked Downslope Petroleum Systems; Global Significance and Future Exploration Potential*, Gulf Coast Section: SEPM Foundation, 23rd Annual Research Conference Houston, Texas, p. 231–266.

Merwe, W.C. vd, Hodgson, D.M., Flint, S.S. (2009). Widespread syn-sedimentary deformation on a muddy deep-water basin-floor: the Vischkuil Formation (Permian), Karoo Basin, south Africa. Basin Research (in press).

Migliorini, C. (1943). On the mode of formation of Macigno-type complexes. Bollettino della Societa Geologica Italiana (translated by Ricci Lucchi). *Marine and Petroleum Geology*, v. 20, p. 527.

Mitchum Jr, R.M. (1977). Seismic stratigraphy and global changes of sea level, part 11: Glossary of terms used in Seismic Stratigraphy. *In:* Payton, C.E. (ed) *Seismic stratigraphy – applications to hydrocarbon exploration.* American Association of Petroleum Geologists Memoir 26, p. 205-212.

Mitchum Jr, R.M. and Vail, P.R. (1977). Seismic stratigraphy and global changes of sea level, part 7: Seismic stratigraphic interpretation procedure. *In:* Payton, C.E. (ed) *Seismic stratigraphy – applications to hydrocarbon exploration*. American Association of Petroleum Geologists Memoir 26, p. 135-143.

Mitchum Jr, R.M. and Van Wagoner, J.C. (1991). High-frequency sequences and their stacking patterns: sequence-stratigraphic evidence

of high-frequency eustatic cycles. *Sedimentary Geology*, v. 70, p. 131-160.

Mitchum Jr, R.M., Vail, P.R.and Sangree, J.B. (1977a). Seismic stratigraphy and global changes of sea level, part 6: Stratigraphic interpretation of seismic reflection patterns in depositional Sequences. *In:* Payton, C.E. (ed) *Seismic stratigraphy – applications to hydrocarbon exploration*. American Association of Petroleum Geologists Memoir 26, p. 117-133.

Mitchum Jr, R.M., Vail, P.R. and Thompson III, S. (1977b). Seismic stratigraphy and global changes of sea level, part 2: The depositional sequence as basic unit for stratigraphic analysis, *In:* Payton, C.E. (ed) *Seismic stratigraphy – applications to hydrocarbon exploration*. American Association of Petroleum Geologists Memoir 26, p. 53-62.

Moraes, M.A.S., Blaskovski, P.R. and Paraizo, P.L.B (2006). Arquitetura de reservatorios de aguas profundas. *Boletim de Geociencias da Petrobras*, v.14, p. 7-25.

Mulder, T., Migeon, S., Savoye, B. and Jouanneau, J.M. (2001). Twentieth century floods recorded in deep Maditerranean sediments. *Geology*, 29, 1011-1014.

Mutti, E. and Ricci Lucchi, F (1975). Turbidite facies and facies associations. In: Examples of Turbidite Facies and Facies associations from selected formations of the Northern Apennines (Eds. E. Mutti, G.C. Parea, F. Ricci Lucchi, M. Sagri, G. Zanzucchi, G. Ghibaudo, and S. Jacarino), p. 21-36. IX International Congress of Sedimentology, Nice, Field Trip A11.

Mutti, E. and Normark, W.R. (1991). An integrated approach to the study of turbidite systems. *In*: P. Weimer and M.H. Link (eds.), Seismic Facies and Sedimentary Processes of Submarine Fans and Turbidite Systems, p 75-125.

Mutti, E. (1992). Turbidite sandstones, Instituto di Geologia, Universit di Parma and Agip. 275 pp. book.

Nittrouer, C.A., Austin Jr, J.A., Field, M.E., Kravitz, J.H., Syvitsky, J.P.M. and Wiberg, P.L. (2007). Writing a Rosetta stone: insights into continental-margin sedimentary processes and strata *In:*, Nittrouer, C.A., Austin Jr, J.A., Field, M.E., Kravitz, J.H., Syvitsky, J.P.M. and Wiberg, P.L. (eds) *Continental Margin Sedimentation: from sediment transport to sequence stratigraphy.* Blackwell Publishing Ltd., 549p.

Normark, W.R., (1970). Growth patterns of deep sea fans. *American Association of Petroleum Geologists Bulletin*, v. 54, p. 2170-2195.

Pickering, K.T. and Corregidor, J. (2005). Mass transport complex and tectonics control on confined basin-floor submarine fans, Middle Eocene, south Spanish Pyrenees. *In:* Hodgson, D.M. and Flint, S.S. (eds) *Submarine Slope Systems: Process and Products*. Geological Society, London, Special Publication, 244, 51-74.

Pickering, K.T., Hiscott, R.N. and Hein, F.J. (1989). Deep marine environments – clastic sedimentation and tectonics. London, Unwin Hyman, 416 p.

Pickering, K.T., Clark, J.D., Smith, R.D., Hiscott, R.N., Ricci Lucchi, F.and Kenyon, N.H. (1995). Architectural elements analysis of turbidite systems, and selected topical problems for sandstone deep-water systems. *In:* Pickering, K.T., Hiscott, R.N., Kenyon, H.H., Ricci-Lucchi, F. and Smith, R.D.A. (eds) *Atlas of deep-water environments: architectural style in turbidite systems*, London, Chapman and Hill, p. 1-10.

Pirmez, C., Pratson, L.F. and Steckler, M. S. (1998). Clinoform development by advection-diffusion of suspended sediment: Modeling and comparison to natural systems. *Journal of Geophysical Research (solid Earth)*, v 103, n B10, 24,141 - 24,157.

Pirmez, C., Beauboeuf, R.T., Friedmann, S.J. and Mohrig D.C. (2000). Equilibrium profile and base level in submarine channels: example from Late Pleistocene systems and implication for the architecture of deep-water reservoir. *In:* Weimer, P., Slatt, R.M., Coleman, J., Rosen, N.C., Nelson, H., Bouma, A.H., Styzen, M.J., and Lawrence D.T. (eds.) *Deep-*

water reservoir of the world, GCS-SEPM foundation, 20th Annual Bob F. Perkins Conference, p. 782-805.

Plink-Björklund, P. and Steel, R.J., (2002). Sea-level fall below the shelf edge, without basin-floor fans. *Geology*, v. 30, p. 115–118.

Plink-Björklund, P. and Steel, R.J. (2004). Initiation of turbidity currents: outcrop evidence for Eocene hyperpycnal flow turbidites. *Sedimentary Geology*, v. 165, p. 29–52.

Porębski, S. J. and Steel, R. (2003). Shelf-margin deltas: their stratigraphic significance and relation to deep-water sands. *Earth-Science Reviews*, v. 62, p. 283–326.

Porębski, S. J. and Steel, R. (2006). Deltas and sea-level change. *Journal of Sedimentary Research*, v. 76, p. 390-403.

Posamentier, H.W. and Allen, G.P. (1999). Siliciclastic Sequence Stratigraphy – Concepts and Applications. SEPM Concepts in Sedimentology and Paleontology 7. Tulsa, 210 pp.

Posamentier, H. W. and Walker, R. G. (2006). Deep-water turbidites and submarine fans *In:* Posamentier, H. W., and Walker, R. G. (eds) *Facies Models Revisited*, SEPM Special Publication 84, p. 399–520.

Posamentier, H.W., Jervey, M.T. and Vail, P.R. (1988). Eustatic control on clastic deposition I – Conceptual framework. *In:* Wilgus, C.K., Hastings, B.S., Kendall C.G.St.C., Posamentier, H.W., Ross, C.A. and Van Wagoner, J.C.(eds), *Sea Level changes – An Integrated Approach*, Society for Sedimentary Geology, Special Publication 42, p. 110-124.

Prather, B.E. (2000). Calibration and visualization of depositional process models for above-grade slopes: a case study from Gulf of Mexico. *Marine and Petroleum Geology*, v. 17, p. 619-638.

Prather, B.E. (2003). Controls on reservoir distribution, architecture and stratigraphic trapping in slope settings. *Marine and Petroleum Geology,* v. 20, p. 529-545.

Prather, B.E., Booth, J.R., Steffens, G.S. and Craig, P.A. (1998). Classification, lithologic calibration, and stratigraphic succession of

seismic facies of intraslope basins, deep-water Gulf of Mexico. *American Association of Petroleum Geologists Bulletin*, v. 78, p. 701-728.

Pratson, I.A., Nittrouer, C.A., Wiberg, P.L., Steckler, M.S., Swenson, J.B., Cacchione, D.A., Karson, J.A., Murray, A.B., Wolinsky, M.A., Gerber, T.M., Mullenbach, B.L., Spinelli, G.A., Fulthorpe, C.S., O'Grady, D.B., Parker, G., Driscol, N.W., Burger, R.I., Paola, C., Orange, D. L., Field, M.E., Friedrichs, C.T. and Fedele, J.J. (2007). Seascape evolution on clastic continental shelves and slopes. *In:* Nittrouer, C.A., Austin Jr, J.A., Field, M.E., Kravitz, J.H., Syvitsky, J.P.M. and Wiberg, P.L. (eds) *Continental Margin Sedimentation: from sediment transport to sequence stratigraphy.* Blackwell Publishing Ltd, p. 339-380.

Prélat, A., Hodgson, D.M., and Flint, S.S., (2009) Evolution, architecture and hierarchy of distributary deep-water deposits: a high-resolution outcrop investigation from the Permian Karoo Basin, South Africa: Sedimentology (in press).

Reading, H.G. and Richards, M. (1994). Turbidite systems in deep-water basin margins classified by grain size and feeder system. *American Association of Petroleum Geologists Bulletin*, v. 78, p. 792-822.

Richards, M., Bowman, M. and Reading, H. (1998). Submarine-fan system I: characterization and stratigraphic prediction. *Marine and Petroleum Geology*, v. 15, p. 689-717.

Ross, W.C. (1990). Modeling base-level dynamics as a control on basin fill geometries and facies distribution: A conceptual framework *In:* Cross, T.A. (ed) *Quantitative dynamic stratigraphy*: Englewood Cliffs, New Jersey, Prentice-Hall, p. 387-399.

Ross, W.C., Halliwell, B.A., May, J.A., Watts, D.E. and Syvitsky, J.P.M. (1994). Slope readjustment: A new model for the development of submarine fans and aprons. *Geology*, v. 22, p. 511-514.

Rust, I.C. (1973). The evolution of the Paleozoic Cape Basin, southern margin of Africa. *In*: Nairn, A.E.M. and Stehli, F.G. (eds) *The Ocean*

Basins and Margins, The South Atlantic, Plenum Publishing Corp., New York, p. 247-276.

Rygel, M.C., Fielding, C., Frank, T.D. and Birgenheier, L.P. (2008). The magnitude of late Paleozoic glacioeustatic fluctuations: a synthesis. *Journal of Sedimentary Research*, v. 78, p. 500-511.

Sangree, J.B., and Widmier, J.M. (1977). Seismic stratigraphy and global changes of sea level, part 9: Seismic interpretation of clastic depositional facies. *In:* Payton, C.E. (ed) *Seismic stratigraphy – applications to hydrocarbon exploration*. American Association of Petroleum Geologists Memoir 26, p. 165-184.

Shanmugam, G. (2000). 50 years of the turbidite paradigm (1950s-1990s): deep-water processes and facies models – a critical perspective. *Marine and Petroleum Geology*, v. 17, p. 285-342.

Shultz, M.R., Fildani, A., Cope, T.D., and Graham, S.A. (2005). Deposition and stratigraphy architecture of an outcropping ancient slope system: Tres Pasos formation, Magallanes basin, southern Chile, *In:* Hodgson, D.M. and Flint, S.S. (eds) *Submarine Slope Systems: Process and Products*. Geological Society, London, Special Publications, 244, 27-50.

Silva, S.R.P., Maciel, R.R., and Severino, M.C.G. (1999). Cenozoic Tectonics of Amazon Mouth Basin. *Geo-Marine Letters*, v. 18 p. 256-262.

Sixsmith, P.J. (2000) *Stratigraphic development of a Permian turbidite system on a deforming basin floor: Laingsburg Formation, Karoo Basin, South Africa* [unpublished PhD thesis]. University of Liverpool, 229 p.

Sixsmith, P.J., Flint, S.S., Wickens, H.DeV., and Johnson, S.D. (2004) Anatomy and stratigraphic development of a basin floor turbidite system in the Laingsburg Formation, Main Karoo Basin, South Africa. *Journal of Sedimentary Research*, v. 74, p. 239-254.

Sprague, A.R.G., Sullivan, M.D., Campion, K.M., Jensen, G.N., Goulding, F.J., Sickafoose, D.K. and Jennette, D.C. (2002). The Physical Stratigraphy of Deep-Water Strata: a Hierarchical Approach to the

Analysis of Genetically related stratigraphic elemenys for improved reservoir prediction. *American Association of Petroleum Geologists Annual Meeting Abstracts*, Houston, Texas, p.10-13.

Sprague, A.R.G, Garfield, T.R., Goulding, F.J., Beaubouef, R.T., Sullivan, M.D., Rossen, C., Campion, K.M., Sickafoose, D.K., Abreu, V., Schellpeper, M.E., Jesen, G.N., Jennette, D.C., Pirmez, C. and B.T. Dixon (2003a). Integrated slope channel depositional models: the key to successful predition of reservoir presence and quality in offshore West Africa. *Conference Proceedings of Submarine Slope Systems: Processes, Products and Prediction*, University of Liverpool.

Sprague, A.R.G., Garfield, T.R., Goulding, F.J., Beaubouef, R.T., Sullivan, M.D., Rossen, C., Campion, K.M., Sickafoose, D.K., Abreu, V., Schellpeper, M.E., Jesen, G.N., Jennette, D.C., Pirmez, C., Dixon, B.T., Ying, D., Ardill, J., Mohrig, D.C., Poter, M.L., Farrell, M.E., and Mellere, D. (2003b). Integrated slope channel depositional models: the key to successful prediction of reservoir presence and quality in offshore West Africa. 4th E-Exitep, CIPM, Vera Cruz, Mexico.

Steel, R., Porębski, S. J., Mellere, D., Schellpeper, M. and Plink-Bjorklund, P. (2003). Shelf-edge delta types and their sequence-stratigraphic relationships. *In:* Roberts, H., Rose, N., Fillon, R.H. and Anderson, J.B., (eds) *Shelf Margin Deltas and Linked Down Slope Petroleum Systems: Global Significance and Future Exploration Potential.* Gulf Coast Section SEPM Foundation. 23rd Annual Research Conference, Deep-Water Reservoir of the World, Houston, Texas. p. 205-230.

Steel, R., Crabaugh, J., Schellpeper, M., Mellere, D., Plink-Bjorklund, P., Deibert, J. and Loeseth, T. (2000). Deltas vs. rivers on the shelf edge: their relative contribution to the growth of shelf-margins and basin-floor fans (Barremian and Eocene, Spitsbergen). *In:* Weimer, P., Slatt, R.M., Coleman J., Rosen N.C., Nelson H., Bouma A.H., Styzen, M.J. and D. T. Lawrence, D.T. (eds.) *Deep-water reservoir of the world, GCS-SEPM foundation, 20th Annual Bob F. Perkins conference*, Gulf Coast Section:

SEPM Foundation. 20th Annual Research Conference, Deep-Water Reservoir of the world, Houston, Texas. p. 981-1009.

Stow, D.A.V. (2005) Sedimentary *Rocks in the Field: A Colour guide*. Manson Publishing Ltd, London, 320p.

Stow, D.A.V., and Mayall, M. (2000). Deep-water sedimentary systems: New models for the 21st century. *Marine and Petroleum Geology*, v. 17, p. 125-135.

Stow, D.A.V., Reading, H.G. and Collinson, J.D. (2005). Deep seas. *In:* Reading, H.G. (ed) *Sedimentary Environments: Processes, Facies and Stratigraphy*, 3rd Edition, Blackwell Science Ltd., p. 395-453.

Swift, D.J.P. and Thorne, J.A. (1991). Sedimentation on continental margins, I, A general model for shelf sedimentation. *In:* Swift, D.J.P. (ed) *Shelf Sands and Sandstone Bodies: Geometry, Facies and Distribution*. Blackwell Sci., Cambridge, Mass., p. 3-31.

Syvitsky, J.P.M., Smith, J.N., Calabrese, E.A. and Boudreau, B.P. (1988). Basin sedimentation and the growth of prograding deltas, *Journal of Geophysics Research (oceans)*, v 93, n C6, p. 6895-6908.

Tankard, A., Welsink H., Aukes P., Newton R., and Stettler E. (2009). Tectonic evolution of the Cape and Karoo basins of South Africa. *Marine and Petroleum Geology* (*in press*).

Theron, A.C. (1967). *The sedimentology of the Koup Subgroup near Laingsburg* [unpublished M.Sc. thesis]. University of Stellenbosch. 25 p.

Thorne, J.A. and Swift, D.J.P. (1991). Sedimentation on continental margins, II, Application of the regime concept. *In:* Swift, D.J.P. (ed) *Shelf Sands and Sandstone Bodies: Geometry, Facies and Distribution*. Blackwell Sci., Cambridge, Mass, p. 33-58.

Todd, R.G. and Mitchum Jr, R.M. (1977). Seismic stratigraphy and global changes of sea level, part 8: Identification of upper Triassic, Jurassic, and Lower Cretaceous Seismic sequences in Gulf of Mexico an offshore West Africa. *In:* Payton, C.E. (ed) *Seismic stratigraphy* –

applications to hydrocarbon exploration. American Association of Petroleum Geologists Memoir 26, p. 145-163.

Truswell, J.F. and Ryan, P.J. (1969). A flysch facies in the lower Ecca Group of the Transkei. Trans. of the Geological Society of South Africa, v. 72, p. 151-158

Turner, B.R. (1999). Tectonostratigraphical development of the Upper Karoo foreland basin: orogenic unloading versus thermally-induced Gondwana rifting. *Journal of African Earth Sciences*, v. 28, p. 215-238.

Vail, P.R. and Mitchum Jr, R.M. (1977). Seismic stratigraphy and global changes of sea level, part 1: Overview. *In:* Payton, C.E. (ed) *Seismic stratigraphy – applications to hydrocarbon exploration*. American Association of Petroleum Geologists Mamoir 26, p. 51-52.

Vail, P.R., Mitchum Jr, R.M. and Thompson III, S. (1977a). Seismic stratigraphy and global changes of sea level, part 3: Relative changes of sea-level from coastal onlap. *In:* Payton, C.E. (ed) *Seismic stratigraphy – applications to hydrocarbon exploration*. American Association of Petroleum Geologists Memoir 26, p. 63-81.

Vail, P.R., Mitchum Jr, R.M. and Thompson III, S. (1977b). Seismic stratigraphy and global changes of sea level, part 4: Global cycles of Relative Changes of Sea Level. *In:* Payton, C.E. (ed) *Seismic stratigraphy – applications to hydrocarbon exploration*. American Association of Petroleum Geologists Memoir 26, p. 83-97.

Vail, P.R., Todd, R.G., and Sangree, J.B. (1977c). Seismic stratigraphy and global changes of sea level, part 5: Chronostratigraphic significance of seismic reflexions. *In:* Payton, C.E. (ed) *Seismic stratigraphy – applications to hydrocarbon exploration*. American Association of Petroleum Geologists Memoir 26,, p. 99-116.

Van Lente, B. (2004) *Chemostratigraphic trends and provenance of the Permian Tanqua and Laingsburg depocentres, southwestern Karoo Basin, South Africa* [unpublished PhD Thesis]. University of Stellenbosch, 339 p.

Van Wagoner, J.C., Posamentier, H.W., Mitchum, R.M., Vail, P.R., Sarg, J.F., Loutit, T.S. and Hardenbol, J. (1988). An overview of the fundamentals of sequence stratigraphy and key definitions. *In:* Wilgus, C.K., Hastings, B.S., Kendall C.G.St.C., Posamentier, H.W., Ross, C.A., Van Wagoner, J.C. (eds). *Sea Level changes – An Integrated Aproach*: Society for Sedimentary Geology, Special Publication 42, p. 39-45.

Veevers, J.J., Cole, D.I., and Cowan, E.J. (1994). Southern Africa: Karoo Basin and Cape Fold Belt. *In:* Veevers, J.J. and Powell, C.McA.(eds) *Permian-Triassic Pangean Basins and Foldbelts Along the Panthalassan Margin of Gondwanaland*, Geological Society of America, Memoirs 184, p. 223-280.

Viljoen, J.H.A. (1994). Sedimentology of the Collingham Formation, Karoo Supergroup, South Africa. *Journal of Geology*, v. 97, p. 167-183.

Visser, J.N.J. (1992). Basin tectonics in southwestern Gondwana during the Carboniferous and Permian. *In:* De Wit, M.J. and Ransome, I.G.D. (eds) *Inversion Tectonics of the Cape Fold Belt, Karoo and Cretaceous Basins of southern Africa*, Balkema, Rotterdam, p. 109-115.

Visser, J.N.J. (1993). Sea-level changes in a back-arc foreland transition: the late Carboniferous-Permian Karoo Basin of South Africa. *Sedimentary Geology*, v. 83, p. 115-131.

Visser, J.N.J. (1995). Post-glacial Permian stratigraphy and geography of southern and central Africa: boundary conditions for climatic modelling: *Palaeogeography, Palaeoclimatology, Palaeoecology*, v. 118, p. 213-243.

Visser, J.N.J. (1997). Deglaciation sequences in the Permo-Carboniferous Karoo and Kalahari basins of southern Africa: a tool in the analysis of cyclic glaciomarine basin fills. *Sedimentology*, v. 44, p. 507–521

Visser, J.N.J., and Praekelt, H.E. (1996). Subduction, mega-shear systems and Late Palaeozoic basin development in the African segment of Gondwana. *Geologische Rundschau*, v. 85, p. 632-646.

Walker, R.G. (1973). Mopping Up the Turbidite mess, in Ginsburg, R.N. (ed.) Evolving Concepts in Sedimentology, The John Hopkins University Press, Baltimore and London. 191p.

Walker, R.G. (1978). Deep-water sandstone facies and ancient submarine fans: models for exploration for stratigraphic traps. *American Association of Petroleum Geologists Bulletin*, v. 62, p. 932-966.

Weber, M.E., Wiedicke, M.H., Kudrass, H.R., Huebscher, C. and Erlenkeuser, H. (1997). Active growth of the Bengal Fan during sea-level rise and highstand. *Geology*, v. 25, p. 315-318.

Wild, R.J., Hodgson, D.M., and Flint, S.S. (2005). Architecture and stratigraphic evolution of multiple, vertically-stacked slope channel complexes, Tanqua depocentre, Karoo Basin, South Africa. *In:* Hodgson, D.M. and Flint, S.S. (eds) *Submarine Slope Systems: Process and Products.* Geological Society, London, Special Publications, 244, p. 89-111.

Wild, R., Flint, S., and Hodgson, D. (2009). Stratigraphic Evolution of the Upper Slope and Shelf Edge in the Karoo Basin, South Africa. *Basin Research* (in press).

Wickens, H. De V. (1994). *Basin Floor Fan building Turbidites of the Southwestern Karoo Basin, Permian Ecca Group South Africa*, [unpublished PhD thesis]. University of Port Elizabeth, 233 p.

Yang, C.S. and Baumfalk, Y.A. (1994). Milankovitch cyclicity in the Upper Rotliegend Group of The Netherlands offshore. *In:* Boer, P.L. and Smith, D.G. (eds) *Orbital Forcing and Cyclic Sequences*, International Association of Sedimentologists, Special Publication 19, p. 47-61.

Yilmaz, Ö. (2001). *Seismic Data Analysis, Processing, Inversion and Interpretation of Seismic Data*. Society of Exploration Geophysicists, Tulsa, OK, 2 vol., 2027p.

Appendix 1: Palaeo-flow measurements

This appendix present the palaeo-flow dataset acquired in this work. Most of the data are unidiretional measurements acquired from foresets of ripple cross lamination, but there are some bidiretional data, mainly from the orientation of erosional surfaces. This dataset was mostly obtained at/nearby to the logged sections, therefore the roses have a header with the identification of the logged section those data reffers to. Some data were acquired at sites other than logged sections, in which case they are identified by geographic location.

Some data from Sub-unit F2 are not identified by the logged section they belong to but by the depositional enviroment (channel complex or channel complex set, etc). It does not mean that they are new data, rather they are plotted according with the interpretation presented.

The roses are distributed in the following pattern:

1) Stratigraphic: from the base.

2) Geographic: from the north.

The identification of the logged section in the rose's caption follows the pattern:

1) The first two letters are the geographic location, always related to the structural features shown in figure 3.3. Therefore HB = Heuningberg anticline; Zk = Zoutkloof syncline; and BV = Baviaans syncline.

2) The third letter (only for Heuningberg anticline and Baviaans syncline) represents the flank of the structure: N for the northern and S for the southern. In Heuningberg there are some data acquired in the nose of the structure, in this case the third letter is a C that stand for "centre",

3) The number at the end of the header represents the sequential number of the logged sections.

The raw data was processed using the EZ-ROSE software (Baas, 2000).

Palaeocurrent in Unit D/E (Heuningberg)

Total of measuments: 11

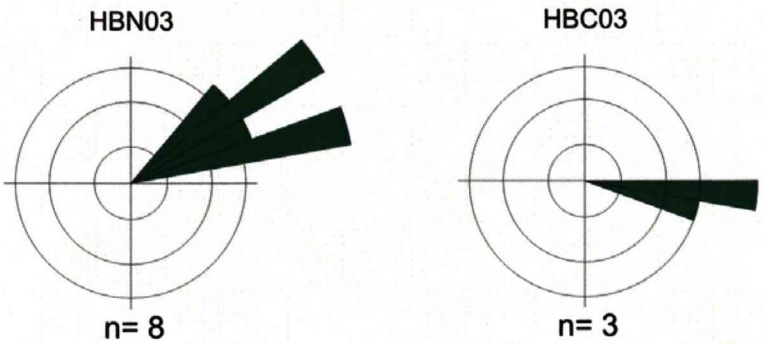

Palaeocurrent in Sub-unit E1

Total of measuments: 40

1- Heuningberg - north flank

HBN03

n= 2

HBN04

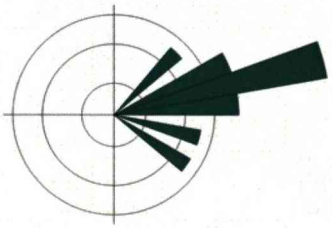

n= 13

2- Heuningberg - nose

HBC02

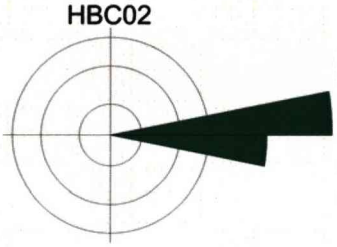

n= 9

3- Heuningberg - south flank

HBS02

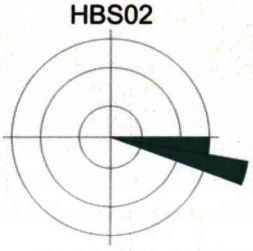

n= 3

HBS02/HBS03 (River)

n= 4

HBS03

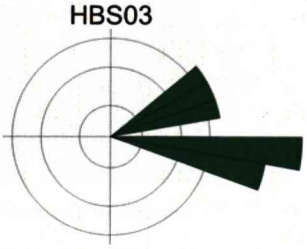

n= 8

HBS04

n= 1

Palaeocurrent in Sub-unit E2 (Heuningberg/Zoutkloof)

Total of measuments: 297

1- Heuningberg - north flank

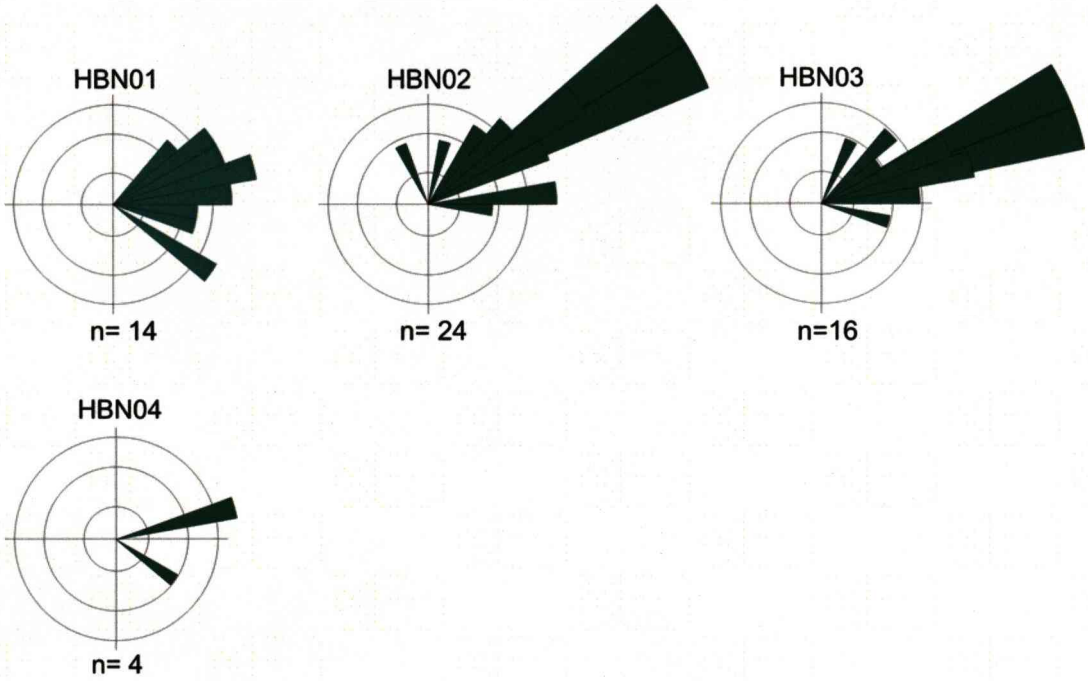

2- Heuningberg - nose

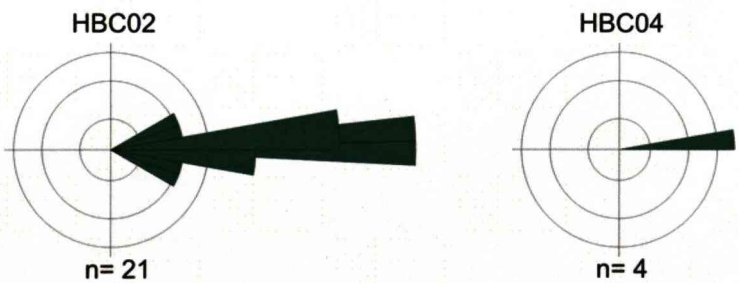

3- Heuningberg - south flank

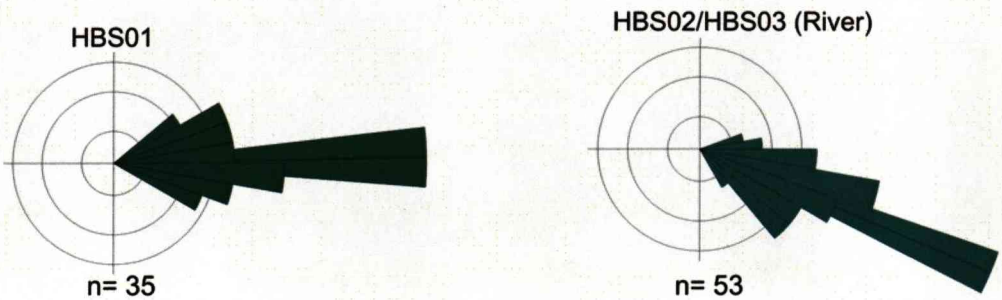

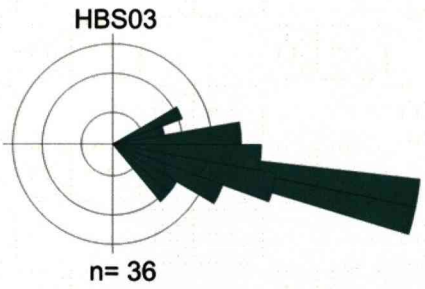
HBS03
n= 36

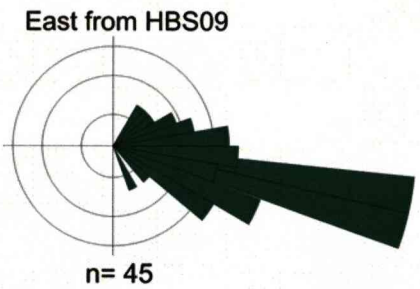
East from HBS09
n= 45

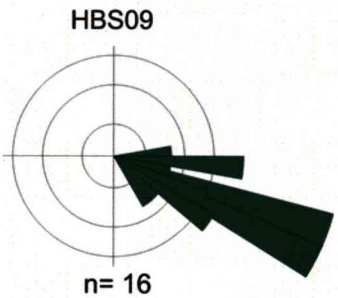
HBS09
n= 16

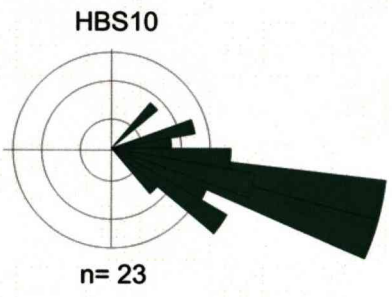
HBS10
n= 23

4- Zoutkloof

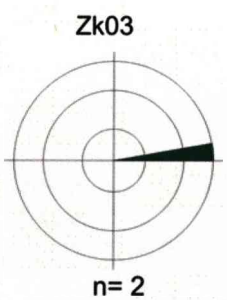
Zk03
n= 2

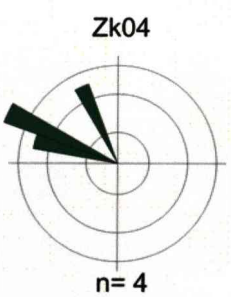
Zk04
n= 4

Palaeocurrent in Sub-unit F1 (Heuningberg / Baviaans)

Total of measuments: 102

1- Heuningberg - north flank

HBN02

n= 8

HBN03

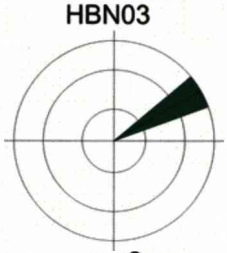

n= 2

HBN04

n= 3

2- Heuningberg - south flank

HBS10

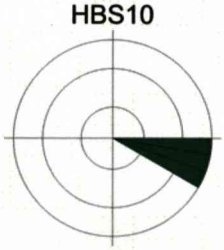

n= 3

HBS27

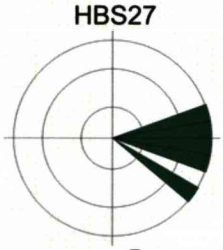

n= 5

HBS29

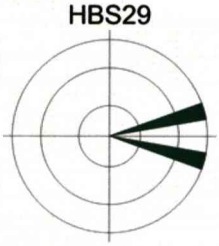

n= 2

HBS30

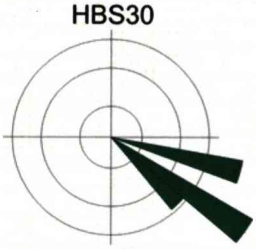

n= 7

HBS31

n= 2

HBS32

n= 1

HBS34

n= 1

HBS37

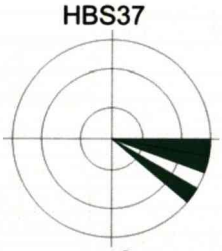

n= 3

HBS31

n= 5

HBS32

n= 1

3- Baviaans syncline - south flank

Baviaans South eastest point (flutes)

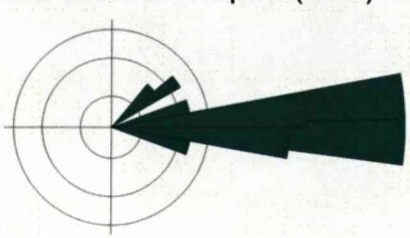

n= 31

Baviaans South eastest point (ripples)

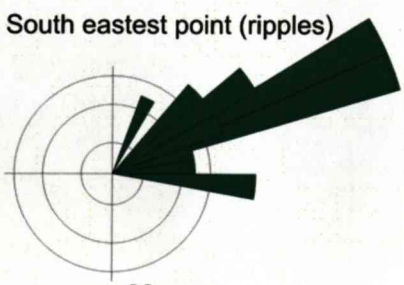

n= 28

Palaeocurrent in Sub-unit F2 (Heuningberg)

Total of measuments: 420

1- Heuningberg - north flank

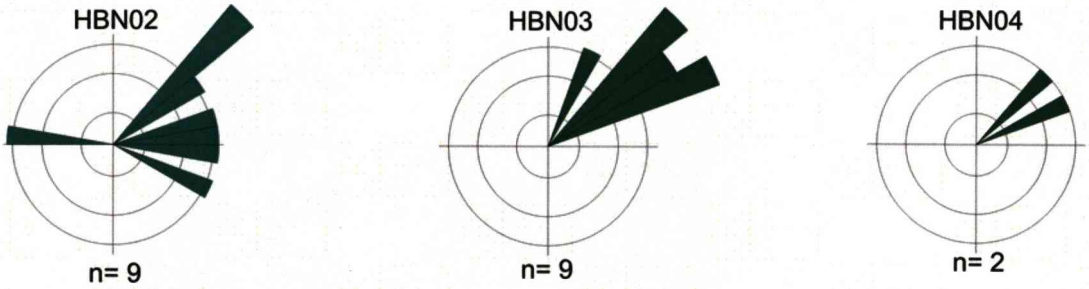

2- Heuningberg - nose

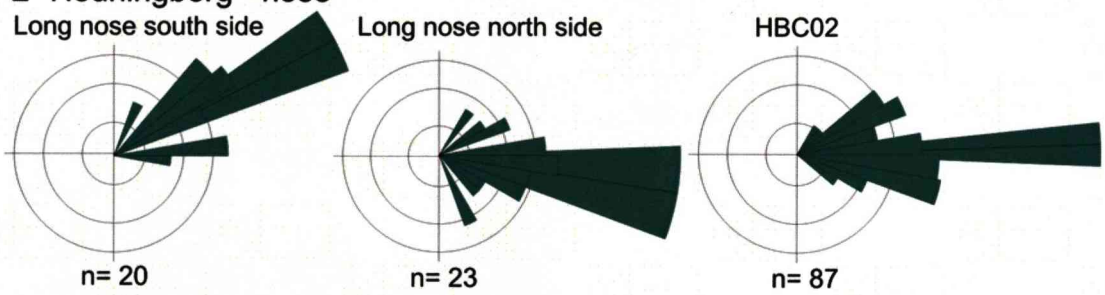

3- Heuningberg - south flank

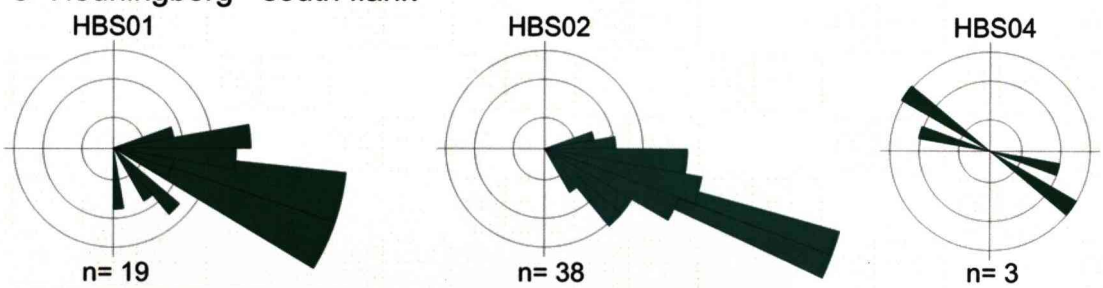

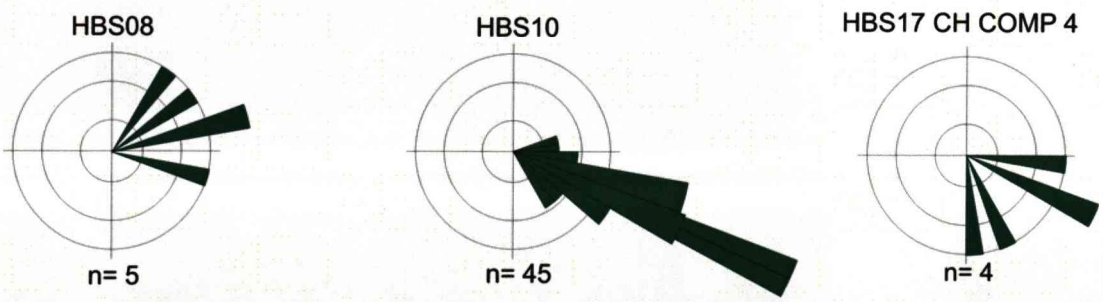

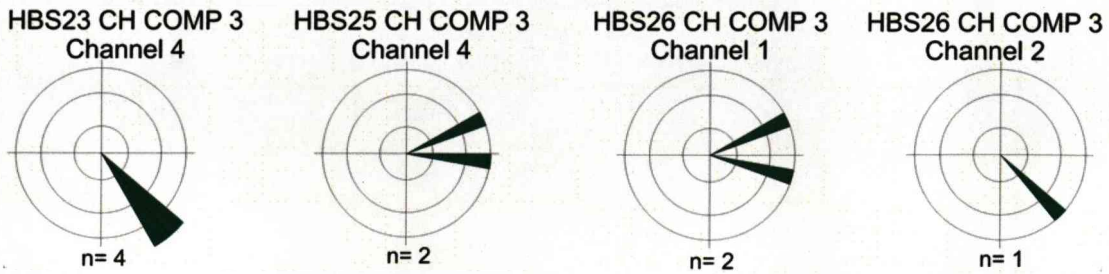

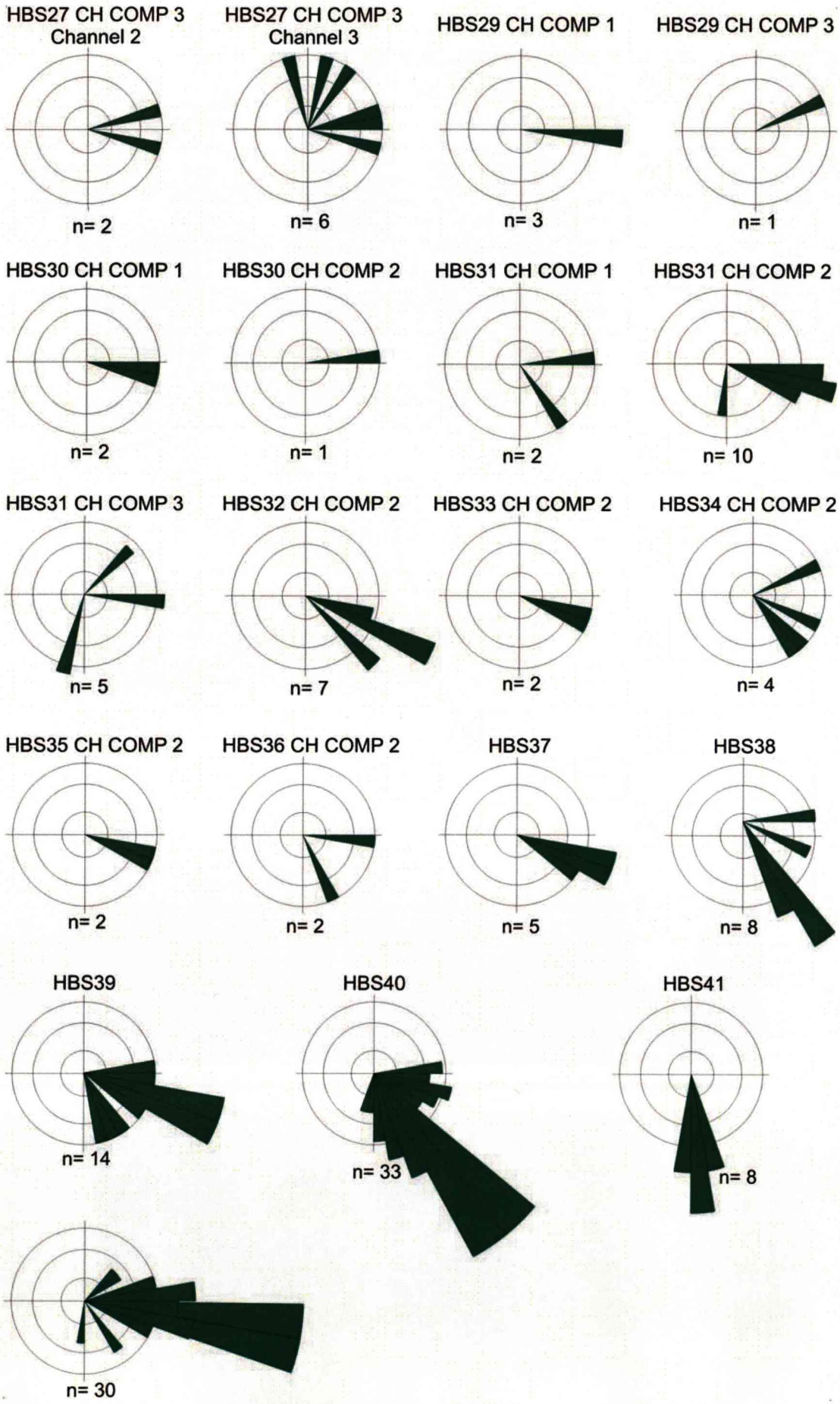
HBS27 CH COMP 3
Channel 2
n= 2
HBS27 CH COMP 3
Channel 3
n= 6
HBS29 CH COMP 1
n= 3
HBS29 CH COMP 3
n= 1
HBS30 CH COMP 1
n= 2
HBS30 CH COMP 2
n= 1
HBS31 CH COMP 1
n= 2
HBS31 CH COMP 2
n= 10
HBS31 CH COMP 3
n= 5
HBS32 CH COMP 2
n= 7
HBS33 CH COMP 2
n= 2
HBS34 CH COMP 2
n= 4
HBS35 CH COMP 2
n= 2
HBS36 CH COMP 2
n= 2
HBS37
n= 5
HBS38
n= 8
HBS39
n= 14
HBS40
n= 33
HBS41
n= 8
n= 30

Palaeocurrent in Sub-unit F2 (Zoutkloof)

Total of measuments: 103

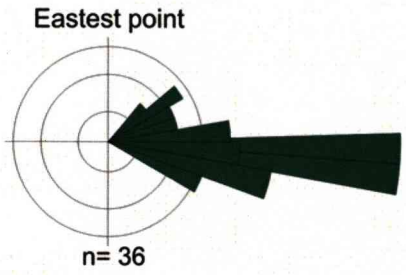

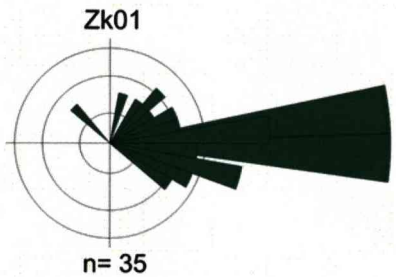

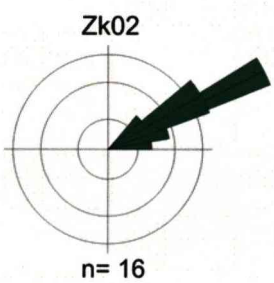

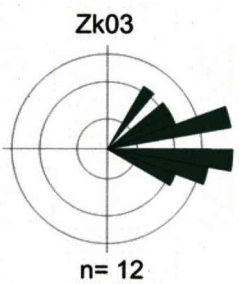

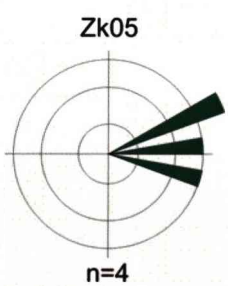

Palaeocurrent in Sub-unit F2 (Baviaans)

Total of measuments: 103

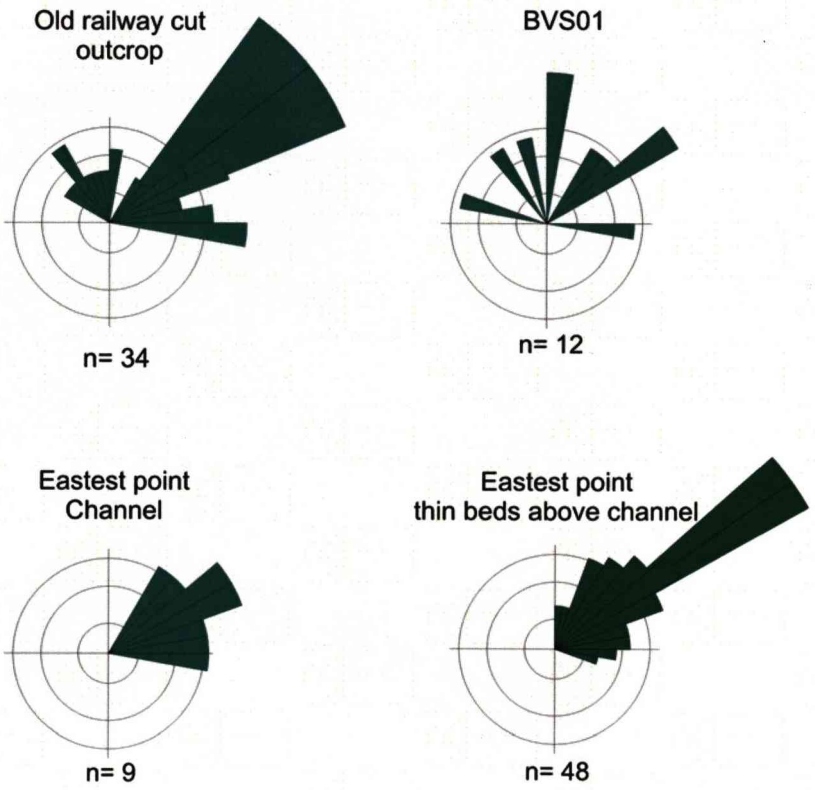

Channel complex 1

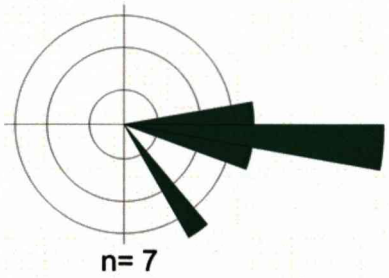

Channel complex 2

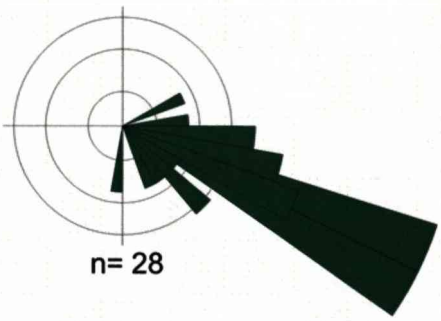

Channel complex 3

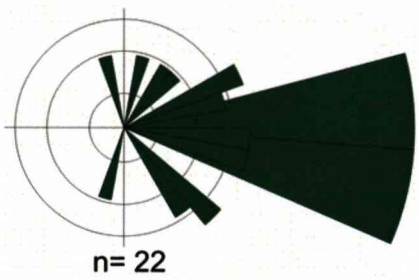

Channel complex 3
Erosional surfaces

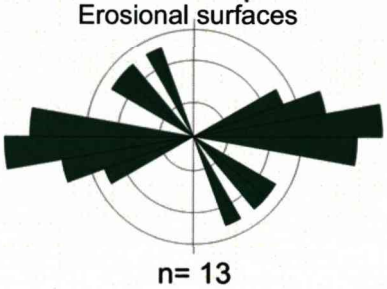

Channel complex 4

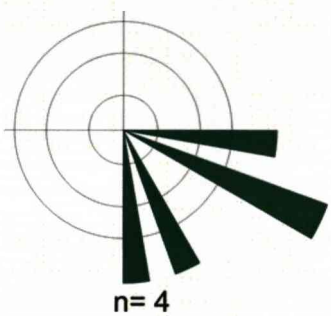

Channel complex set

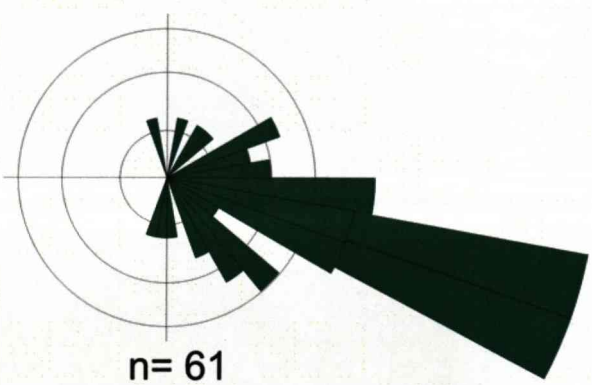

Channel-levee complex set

Northern levee

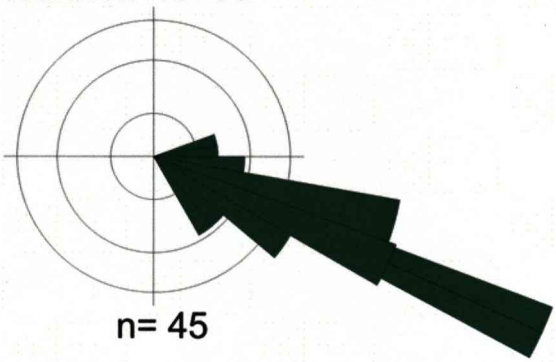

n= 45

Channel complex set

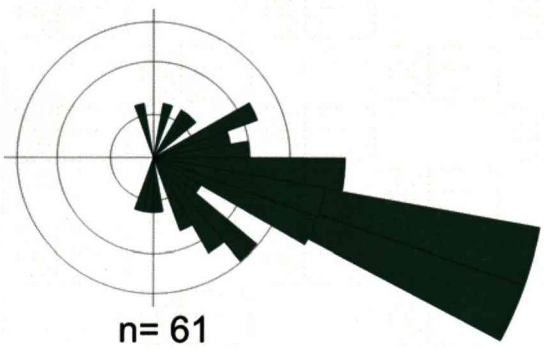

n= 61

Southern levee

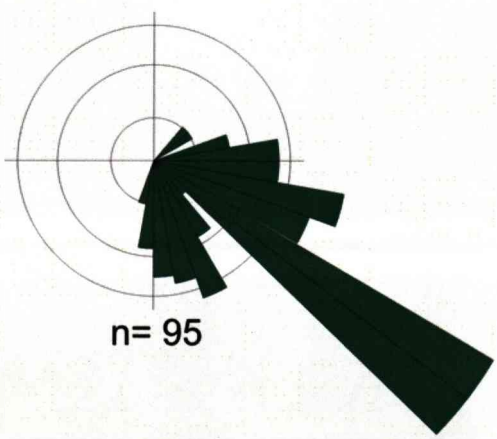

n= 95

Palaeocurrent in Sub-unit F2 (Heuningberg / Zoutkloof)

Total of measuments: 103

1- Heuningberg - north flank

HBN02

n= 3

2- Heuningberg - nose

HBC02

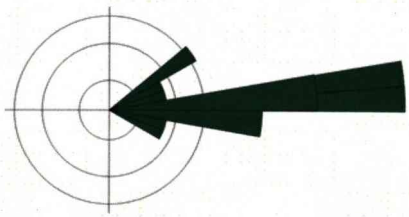

n= 27

3- Heuningberg - south flank

HBS03

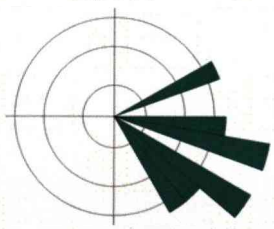

n= 8

HBS04-05-06-07

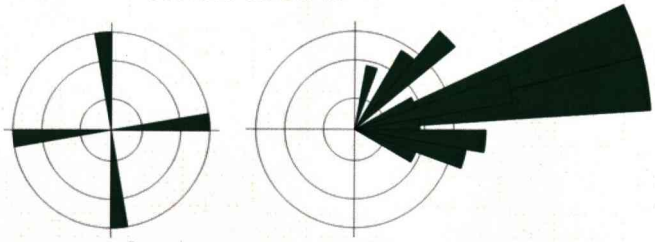

n= 2 n= 22

HBS40

n= 2

HBS41

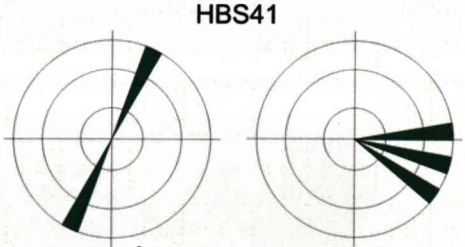

n= 1 n= 3

3- Zoutkloof

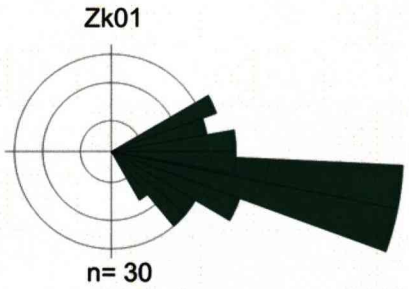

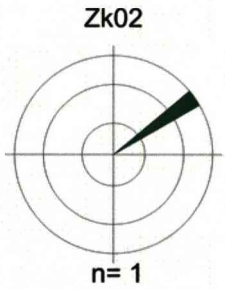

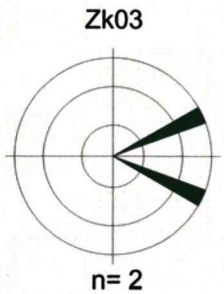

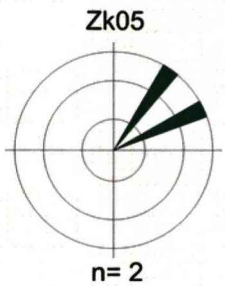

Palaeocurrent in Unit H (Heuningberg)

Total of measuments: 04

1- Heuningberg - north flank

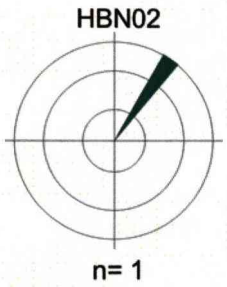

2- Heuningberg - south flank

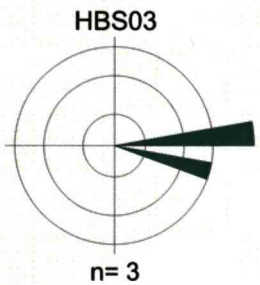

Appendix 2: Key for the logged sections

Sandstones

Bed shape


Rippled top and planar base


Rippled top and amalgamated base


Rippled top and loaded base


Rippled top and erosive base


Planar top and base


Planar top and loaded base


Planar top and erosive base


Planar top and amalgamated base


Normal grading


Inverse grading

Symbols


Organics


Lags

Rip-up clasts


Current-ripples lamination

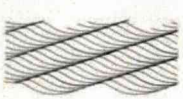
Climbing-ripples lamination


Planar lamination

Siltstones

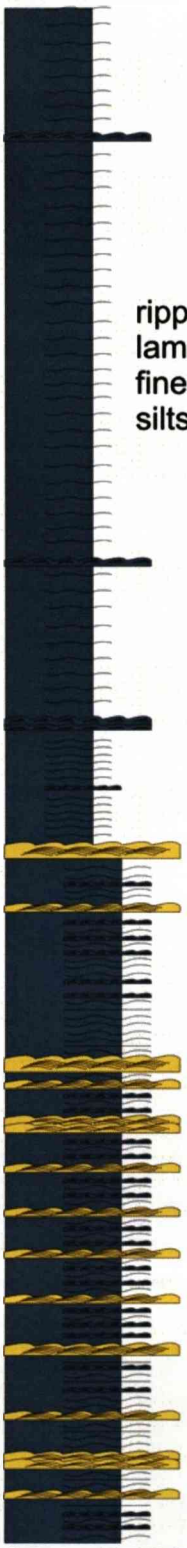

ripple- and wavy-laminated interbedded fine and medium siltstones

ripple- and wavy-laminated interbedded medium and coarse siltstones, and very fine-grained sandstone

Hemipelagic claystone

Non-exposure

Appendix 3: Coordinates (GPS) of the sedimentary log

HEUNINGBERG ANTICLINE					
Log name	**Base**		**Top**		
	X	**Y**	**X**	**Y**	
NB NORTH					
HBN 02	0477565	6340120	0477582	6340411	
HBN 02 shift	0477698	6340408	0477689	6340929	Shift
HBN 01	0479683	6340233	0479671	6340662	
HB N 01 shift	0479545	6340678	0479459	6340890	Shift
HBN 03	0475800	6340522	0475705	6340930	
HBN 04	0470892	6339787	0470935	6340296	
HBN 05	0468367	6339680	0468583	6340217	
NB NOSE					
HBC 01 (support log)	0480602	6338896	0480747	6338699	Not edited
HBC 02	0480775	6339016	0482164	6337950	
HBC 03 (support log)	0481125	6338935	0481444	6338772	Not edited
HBC 04	0480561	6337496	0481182	6337432	
NB SOUTH					
HBS 01	0479526	6337178	0481165	6336413	
HB South 1.1 (Support log)	0479958	6336906	0480013	6336872	Not Scanned
HBS 02	0479707	6336258	0480069	6335053	
HBS 03	0477905	6335974	0478111	6335200	
HBS 03 shift	0478184	6335231	0478299	6334925	
HBS 04	0477035	6335296	0477175	6334902	
HBS 05	0476942	6335263	0477072	6334849	
HBS 06	0476848	6335231	0476992	6334810	
HBS 07	0476734	6335145	0476962	6334792	
HBS 08	0476285	6335054	0476374	6334605	
HBS 09	0474025	6335913	0473976	6334045	
HBS 09 (support log)	0473673	6334347	0473679	6334253	Not edited
HBS 10	0473114	6334258	0473075	6333826	
HBS 10_20m (support log)	0473090	6334260	0473073	6334187	Not Scanned
HBS 10_60m (support log)	0473075	6334261	0473088	6334188	Not Scanned
HBS 10_40m (support log)	0473057	6334260	0473067	6334186	Not Scanned
HBS 11	0472065	6334132	0472082	6334025	
HBS 12	0472017	6334126	0472163	6333881	
HBS 13	0471975	6334129	0472014	6334018	
HBS 14	0471725	6334011	0471718	6333967	
HBS 15	0471712	6334727	0481616	6334002	
HBS 16	0471501	6333976	0471569	6333829	
HBS 17	0471494	6333920	0471512	6333908	
HBS 18	0471459	6333946	0471533	6333897	
HBS 19	0471440	6333932	0471499	6333902	
HBS 20	0471429	6333923	0471483	6333898	

HEUNINGBERG ANTICLINE (Continuation)					
Log name	Base		Top		
	X	Y	X	Y	
NB SOUTH					
HBS 21	0471416	6333894	0471485	6333345	
HBS 22	0471409	6333886	0471472	6333886	
HBS 23	0471398	6333863	0471477	6333864	
HBS 24	0471400	6333850	0471480	6333847	
HBS 25	0471392	6333833	0471479	6333840	
HBS 27	0471421	6333781	0471514	6333781	
HBS 28	0471447	6333754	0471538	6333795	
HBS 29	0471468	6333701	0471711	6333748	
HBS 30	0471483	6333673	0471559	6333734	
HBS 31	0471487	6333619	0471663	6333586	
HBS 32	0471477	6333568	0471532	6333547	
HBS 33					
HBS 34	0471323	6333533	0471559	6333481	
HBS 35	0471507	6333329	0471564	6333304	
HBS 36	0471422	6333214	0471467	6333198	
HBS 37	0471335	6333100	0471423	6333033	
HBS 38	0471224	6333003	0471295	6332906	
HBS 39	0470882	6332865	0470992	6332519	
HBS 40	0470509	6332750	0470621	6332306	
HBS 41	0469862	6332635	0469921	6332117	
HBS 42	0468991	6332675	0468889	6332231	

ZOUTKLOOF SYNCLINE					
Log name	Base		Top		
	X	Y	X	Y	
ZK 01	0482760	6332676	0482724	6332889	
ZK 01 shift	0482785	6332871	0482768	6333368	Shift
ZK 02	0479198	6332178	0479180	6332629	
ZK 02 shift	0479345	6332674	0478978	6333216	Shift
ZK 03	0475913	6331358	0475904	6331758	
ZK 04	0474681	6331243	0474658	6331379	
ZK 05	0473554	6331054	0473503	6331456	

BAVIAANS SYNCLINE					
Log name	Base		Top		
	X	Y	X	Y	
SSD07	0483855	6323713	0483853	6323756	Not scaned
SSD06	0483834	6323712	0483885	6323770	Not scaned
SSD05	0483928	6323718	0483924	6323785	Not scaned
SSD04	0483981	6323719	0483977	6323772	Not scaned
SSD03	0484020	6323724	0484018	6323772	Not scaned
SSD02	0484061	6323726	0484057	6323788	Not scaned
SSD01	0484101	6323728	0484091	6323789	Not scaned
1001	0484137	6323730	0484139	6323803	
1002	0484176	6323735	0484182	6323792	
1103	0484219	6323735	0484213	632379	
1104	0484260	6323737	0484259	6323783	
1105	0484301	6323742	0484294	6323791	
1206	0484339	6323742	0484337	6323791	
1407	0484378	6323749	0484330	6323793	
1408	0484419	6323748	0484411	6323799	
1409	0484462	6323753	0484456	6323807	
1510	0484504	6323756	0484494	6323813	
1511	0484525	6323762	0484521	6323813	
1612	0484618	6323778	0484617	6323817	
1613	0484661	6323778	0484661	6323828	
1614	0484707	6323776	0484703	6323833	
1615	0484748	6323779	0484749	6323848	
1616	0484787	6323786	0484778	6323835	
1717	0484828	6323785	0484827	6323842	
1718	0484868	6323788	0484870	6323843	
1719	0484908	6323786	0484911	6323844	
1720	0484950	6323791	0484949	6323842	
BVS 01	0479946	6323615	0479895	6324077	
BVS 01.1 (support log)	0480174	6323611	0480202	6323327	
BVS 02	0478844	6323648	0478865	6323892	
BVS 02.1 (support log)	0476837	6323868	0477018	6324245	
BVS 03	0474479	6324788	0474779	6325395	
BVS 04	0473503	6325148	0473764	6325692	
BVN 01	0477088	6326738	0477069	6326442	
BVN 02	0478224	6326802	0478193	6326500	
BVN 02 (continuation)	0478251	6326701	0478353	6326179	
BNV 03 (1st part)	0475487	6326647	0475556	6326485	
BNV 03 (2nd part)	0475041	6326485	0475082	6326254	
BVN 03 (continuation)	0475056	6326475	0475146	6326014	

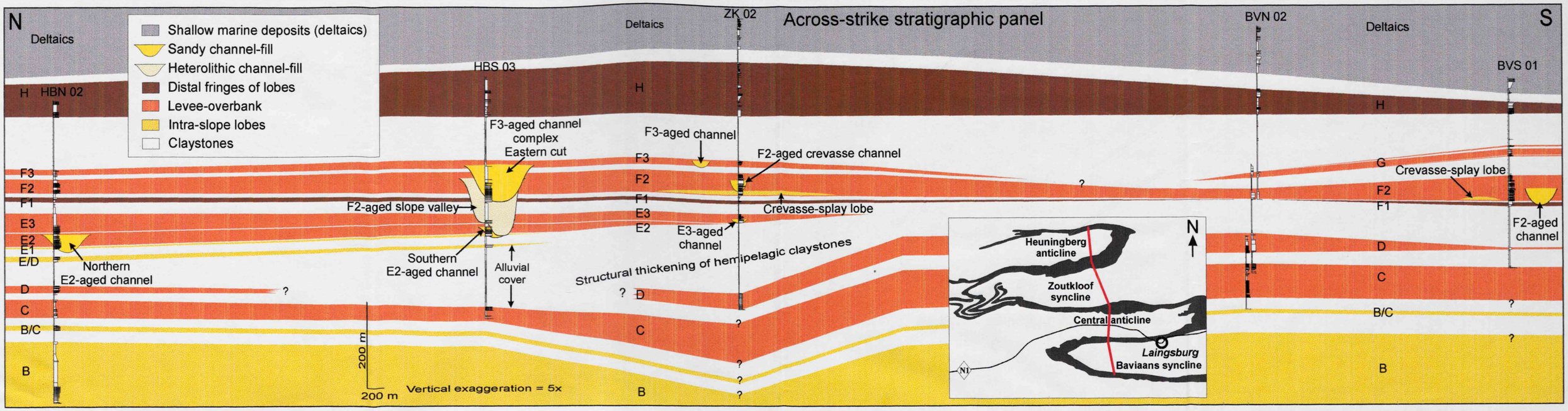

Enclosure 1A: across-strike stratigraphic panel. Insets: key for colours and map with location of the panel (red line).

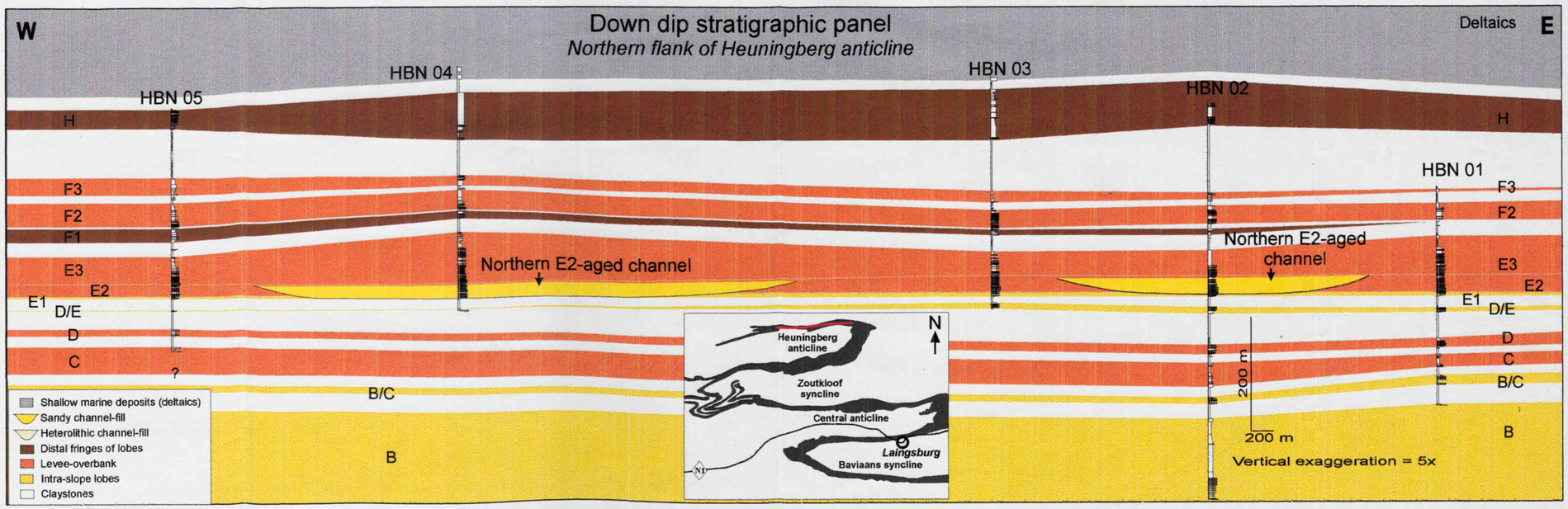

Enclosure 1B: down-dip stratigraphic panel. Insets: key for colours and map with location of the panel (red line).

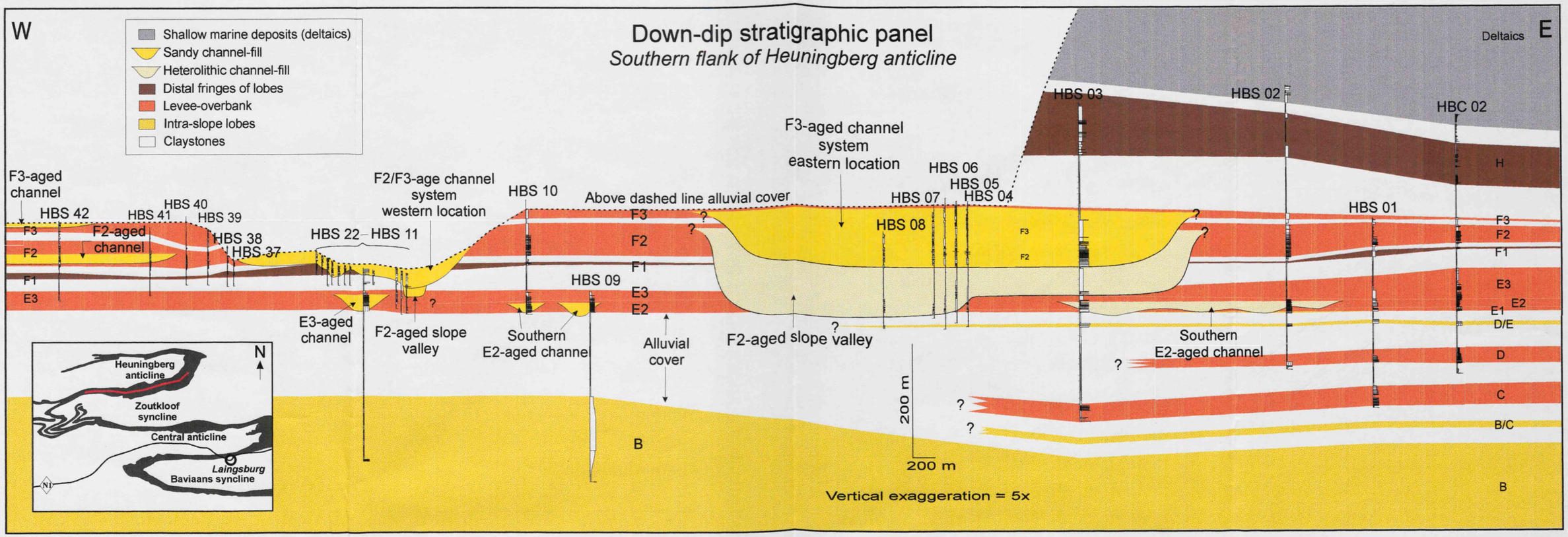

Enclosure 2A: down-dip stratigraphic panel. Insets: key for colours and map with location of the panel (red line).

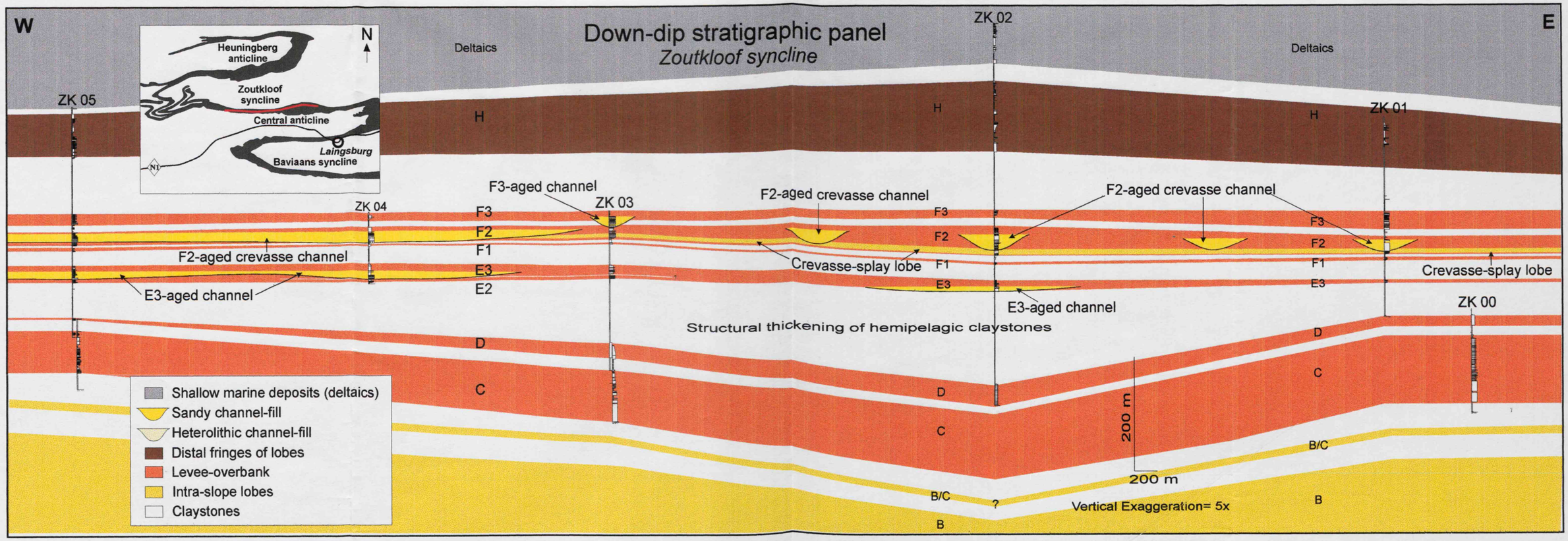

Enclosure 2B: down-dip stratigraphic panel. Insets: key for colours and map with location of the panel (red line).

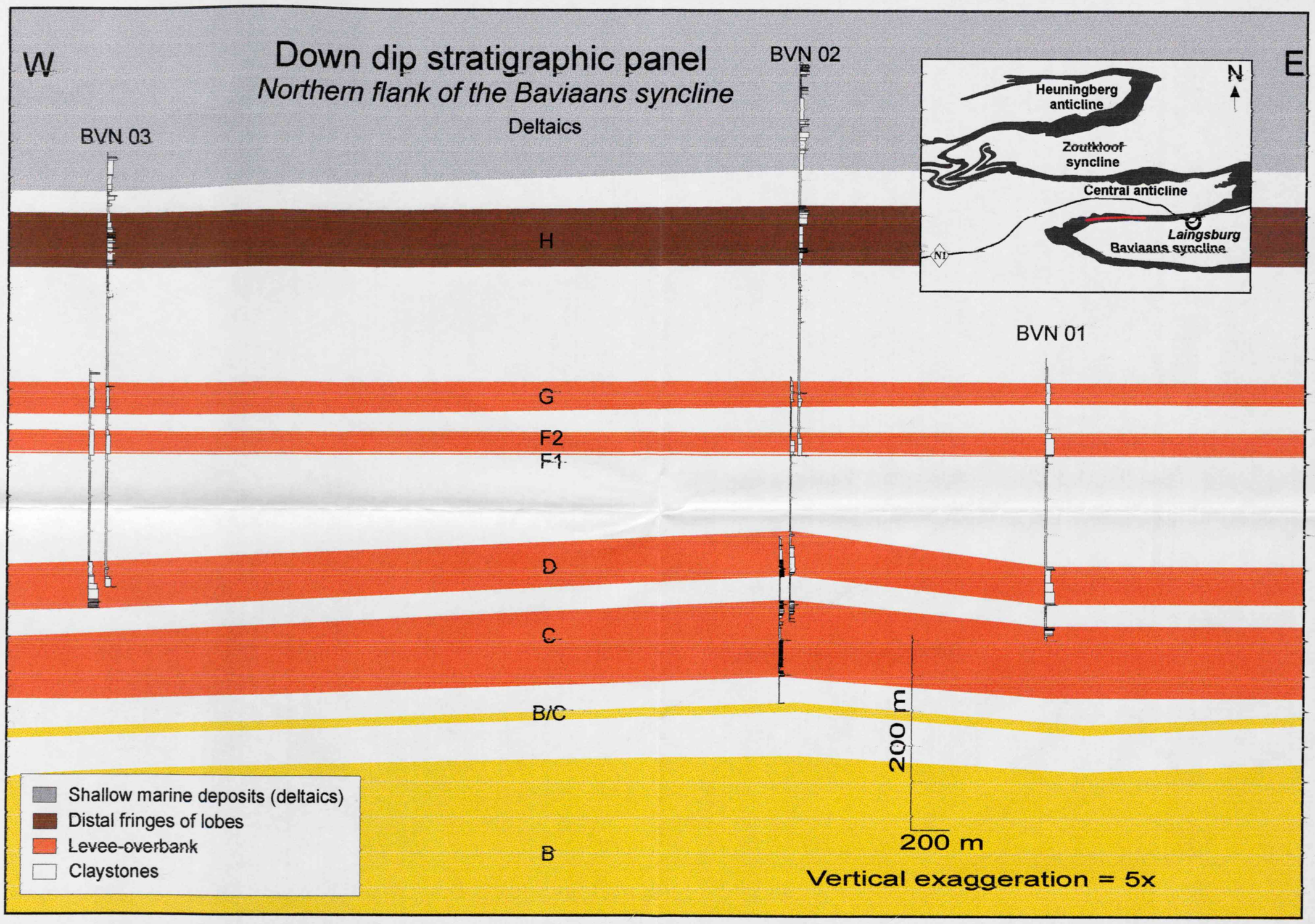

Enclosure 3A: down-dip stratigraphic panel. Insets: key for colours and map with location of the panel (red line).

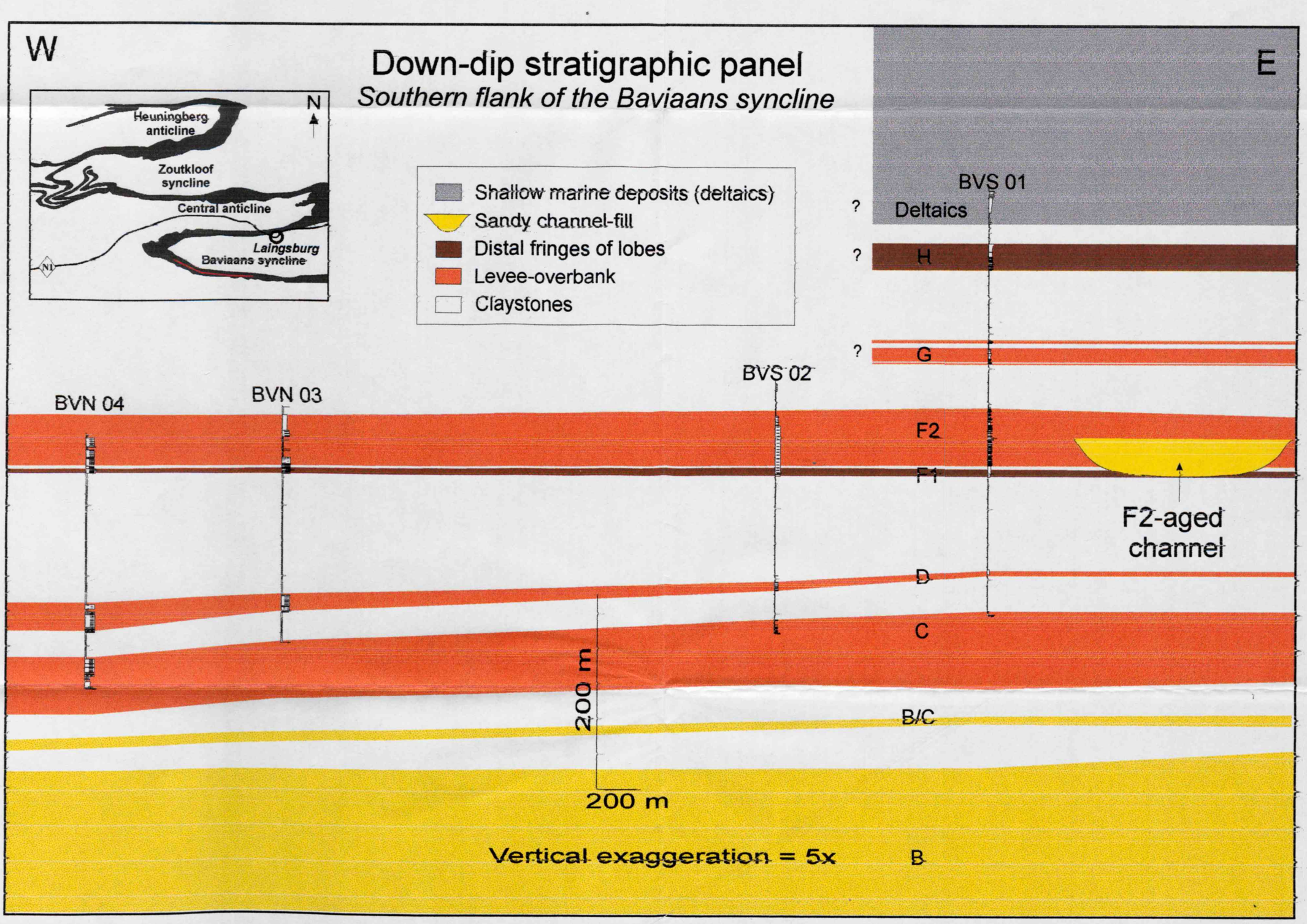

Enclosure 3B: down-dip stratigraphic panel. Insets: key for colours and map with location of the panel (red line).

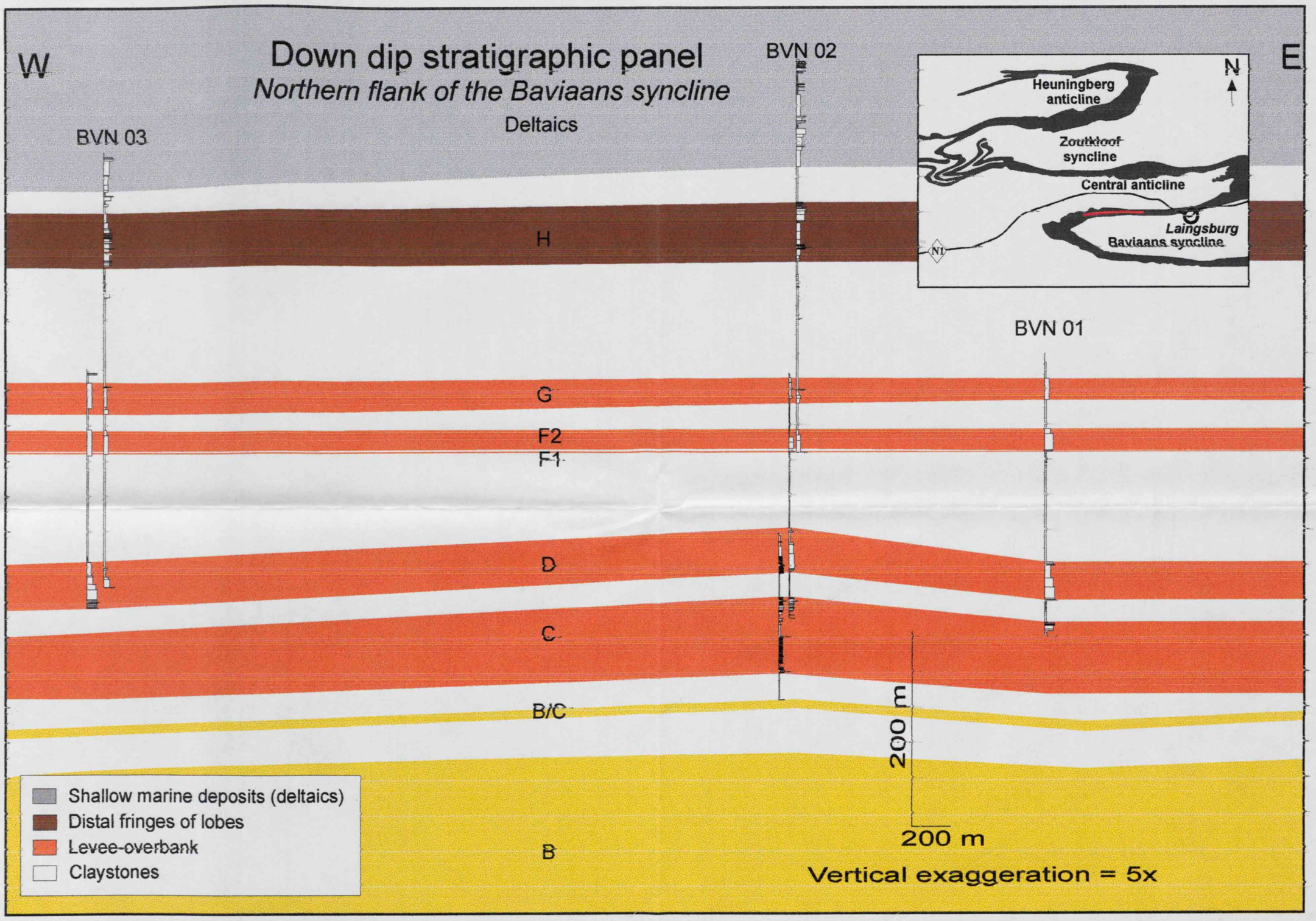

Enclosure 3A: down-dip stratigraphic panel. Insets: key for colours and map with location of the panel (red line).

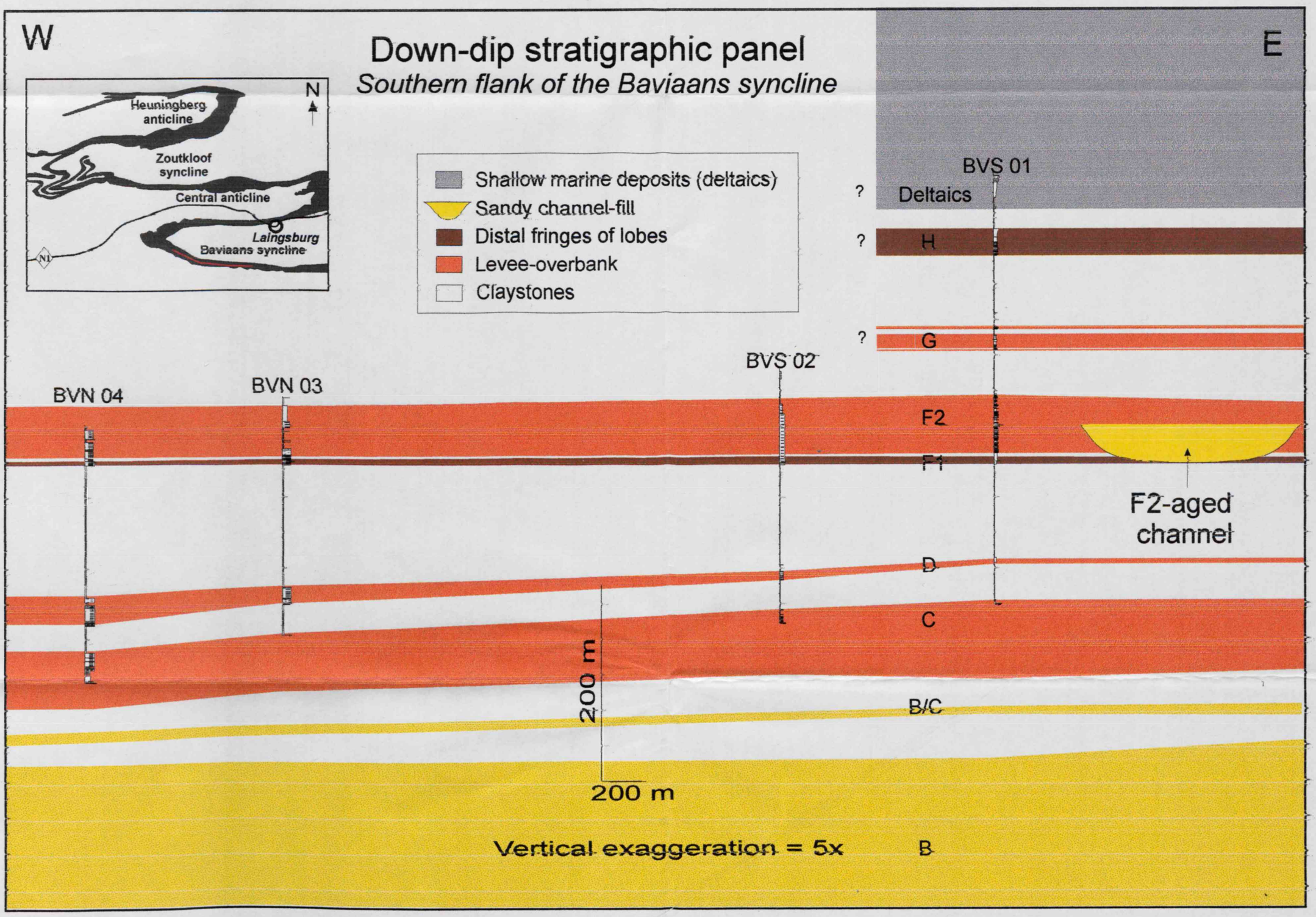

Enclosure 3B: down-dip stratigraphic panel. Insets: key for colours and map with location of the panel (red line).

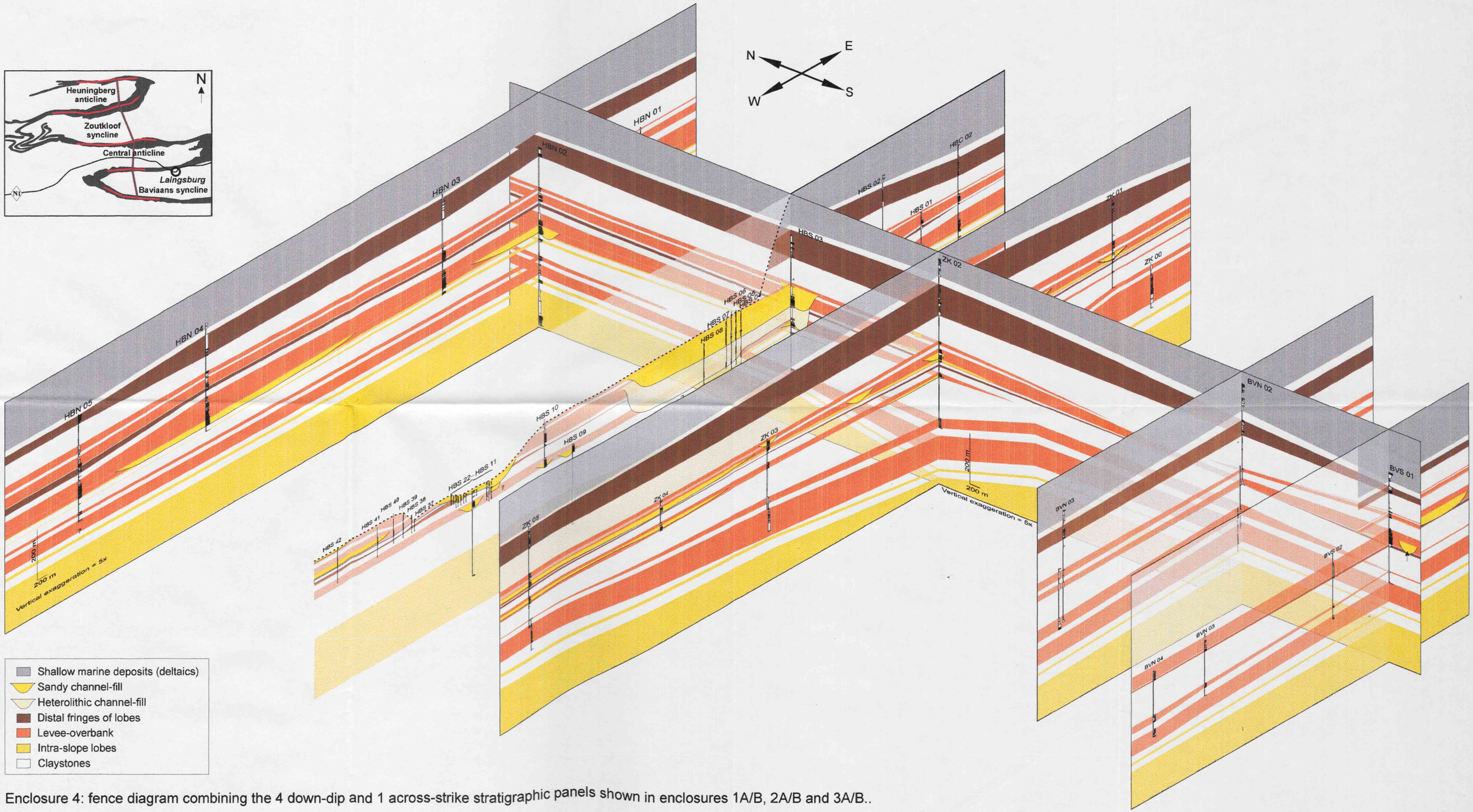

Enclosure 4: fence diagram combining the 4 down-dip and 1 across-strike stratigraphic panels shown in enclosures 1A/B, 2A/B and 3A/B..

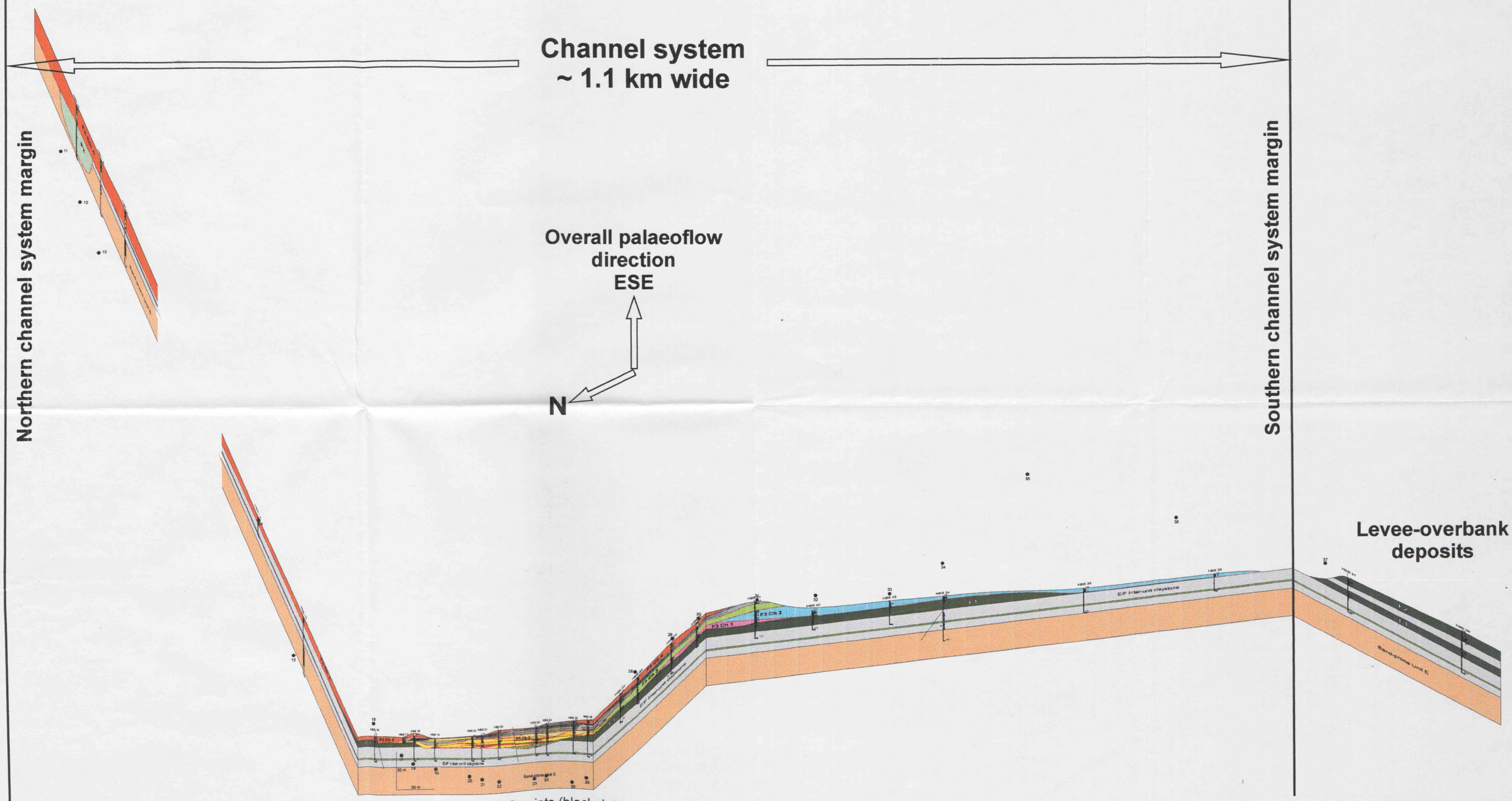

Enclosure 5: composite diagram combining stratigraphic panels with map of the GPS points (black dots numbered from 11 to 38) for the base of each log.
The term Channel system is used in this figure according to the notation in footnote 1 in chapter 4.

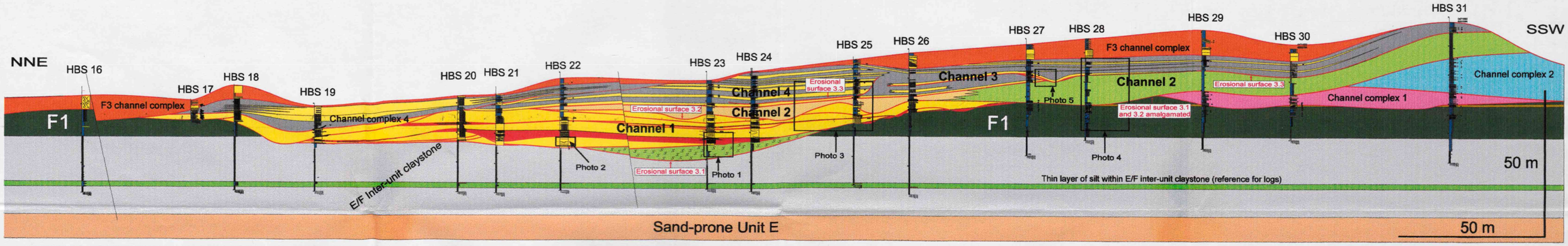

Keys for lithofacies distribution in chanel complex 3			
Channel 1	Channel 2	Channel 3	Channel 4
Structureless/planar-laminated fine sandstones	Siltstones *Channel margin*	Siltstones	Siltstones
Mudstone clast comglomerates *Lag deposits*	Slumps, siltstones and rippled laminated sandstones. *Channel axis*	Planar and/or climbing rippled very fine sandstones	Planar and/or climbing rippled very fine sandstones
Slumps and/or Slides			

Enclosure 6 - Detailed stratigraphic panel (located in figure 4.3) showing the main lithofacies associations and erosional surfaces (red lines) of channel complex 3. Black squares on the panel show position of the photos called in the text. For colour code see keys for lithofacies distribution in channel 3.